PhD Dissertation

International Doctoral School in Information and Communication Technology

DISI - University of Trento

CORRESPONDENCE AMONG CONNECTOMES AS COMBINATORIAL OPTIMIZATION

Nusrat Sharmin

Advisor:

Dr. Paolo Avesani

Co-advisor:

Dr. Emanuele Olivetti

Bruno Kessler Foundation, Trento, Italy.

University of Trento, Italy.

Thesis Reviewed By:

Dr. Descoteaux Maxime

University of Sherbrooke, Canada.

Dr. Gloria Menegaz

University of Verona, Italy.

October 2017

Final Examination Committee Members:

Dr. Gloria Menegaz
Associate Professor
University of Verona, Italy.

Dr. Med. Elke Gizewski
Professor
Medical University of Innsbruck, Austria.

Dr. Enrico Blanzieri
Associate Professor
University of Trento, Italy.

Abstract

Diffusion magnetic resonance imaging (dMRI) data allows the reconstruction of the neural pathways of the white matter of the brain as a set of 3D polylines, by means of tractography algorithms. The neuronal axons within the white matter form the anatomical links between regions of the brain, which are referred to as anatomical connectivity, or structural connectivity. The complete collection of structural connectivity is referred to the structural connectome, which helps to understand the human brain functionality. The 3D polylines are called *streamlines* and the set of all streamlines is called *tractogram*, which represents the structural connectome of the brain. In neurological studies, it is often important to identify the group of streamlines belonging to the same anatomical structure, called *tract* or *bundle*, like the cortico-spinal tract or the arcuate fasciculus. The statistical analysis of the diffusion data of tracts is used in multiple applications, for example, to study gender differences , to observe the changes in age and to correlate with diseases. This kind of studies requires the analysis of groups of subjects, which creates two important problems: aligning tractography data across subjects, a problem called **tractogram alignment**, and the extraction of tracts of interest, named **tract segmentation problem**. Due to the anatomical variability across subjects, these two problems are difficult to solve. In this thesis, we investigate those two problems and propose a novel approach and efficient algorithms for their solution.

Typically, the alignment of two tractograms is obtained with registration methods. Registration methods transform the tractograms in order to increase their mutual similarity. In the literature, the best practice for tractogram registration is based on finding one global affine transformation that minimizes their differences. Unfortunately, this approach fails to reconcile local differences between the tractograms. In contrast to transformation-based registration methods, we propose the concept of tractogram correspondence, whose aim is to find which streamline of one tractogram corresponds to which streamline in another tractogram, i.e., a map from one tractogram to another. As a further contribution, we propose to use the relational information of each streamline, i.e., its distances from the other streamlines in its own tractogram, as the building block to define the optimal correspondence. We provide an operational procedure to find the optimal correspondence through a combinatorial optimization problem and we discuss its similarity to the *graph matching* problem. Finally, we adapted an approximate solution of the graph matching to solve the correspondence.

Several automatic tract segmentation methods have been developed over the last years. Segmentation approaches can be categorized into *unsupervised* and *supervised*. A common criticism to unsupervised methods, like clustering, is that there is no guarantee to obtain anatomically meaningful tracts. For this reason, in this thesis, we focus on supervised tract segmentation, which is based on prior knowledge. We propose a novel supervised tract segmentation method, that segments the tract of interest, e.g. the arcuate fasciculus, by exploiting a set of example tracts from different subjects. In analogy to tractogram alignment, our proposed supervised segmentation approach is based on the concept of the streamline correspondence, i.e. on finding which streamline in one tractogram corresponds to which streamline in the other tractogram. We showed that streamline correspondence can be a powerful principle to transfer the anatomical knowledge of a given bundle from one subject to another one. In the literature of supervised segmentation, streamline correspondence has been addressed with a nearest neighbour strategy. We observed that segmenting tracts with a nearest neighbour strategy has a number of limitations. Conversely, in this thesis we address the tract segmentation problem as a *linear assignment problem* (LAP), a cornerstone of combinatorial optimization. With respect to nearest neighbor, the LAP introduces a constraint of one-to-one correspondence that substantially improves the quality of segmentation. We draw from the literature of algorithms for solving the LAP and adopt one of the most efficient solutions available. To this, we add a strategy for merging correspondences coming from different examples, i.e. from different subjects, in order to account for the anatomical variability across the population.

In order to implement graph matching and LAP for alignment and segmentation of tractograms, we needed to address the very large computational cost due to the large number of streamlines involved. To reduce the amounts of computations, in both cases we represented streamlines as vectors through a Euclidean embedding technique called *dissimilarity representation*. With such representation, we obtained fast nearest neighbor queries through the use of *k*d-trees, which were instrumental to dramatically reduce the amount of computations: from months to minutes.

Keywords
Brain Connectivity, Diffusion magnetic resonance imaging (dMRI), Tract Segmentation, Tractogram Alignment, Neuroimaging, Machine Learning, Combinatorial Optimization Problem, Linear Assignment Problem, Graph Matching

Acknowledgements

The journey of my PhD is a life changing experience for me and it may be not possible without continuous supports, encouragements, and motivations offered by many wonderful people that I met during the time period.

First and foremost I would like to take this opportunity to thank my supervisor Dr. Paolo Avesani, for his excellent guidance and advice during my PhD. He guides me in every step of the journey. He not only guides me for technical stuff but also give me motivation and encouragement during the period. Without his proper and careful mentorship, my PhD would be very difficult. Special thanks to my co-advisor Dr. Emanuele Olivetti; he has been helping me in every detail. He is such a person that I can ask for any kind of help; from helping me to understand technical things to assist me to write thesis or scientific papers. Actually, without his support, the success of the thesis would be limited. Both of them are very kind to me, and without them, the journey would not be that easy.

I would like to thank Professor Maxime Descoteaux and Professor Gloria Menegaz for providing the valuable feedback that enriches my thesis. I would like to thank Dr. Gloria Menegaz, Dr. Med Elke Gizewski and Dr. Enrico Blanzieri for agreeing to be committee members of my PhD examination.

I take this opportunity to thank Dr. Diana Porro and Dr. Thien Bao for being helpful initially, when it was very difficult for me to adapt in a new and challenging field. Their supports make it easy to settle down in our lab. I am really grateful to Dr Sandro Vega Pons and Dr. Vittorio Iacovella for their suggestions about the research problem.

I would like to thank Dr. Eleftherios Garyfallidis and Dr. Fabian Pedregosa for their valuable suggestions and opinions about my scientific papers.

I would love to thank all of my colleagues, who are very gentle and polite to me. I have started my PhD in a foreign country; but their friendliness made me feel that I am one of them. They have been always by my side in difficult moments during my PhD. I would like to thank Dr. Danilo Benozzo for his continuous support and motivation throughout my PhD period. I thank my fellow PhD student Giulia Bertò for helping me to proofreading my thesis.

Finally, I would like to thanks my parents and parents-in-law for giving me the opportunity to chase my dream. I also thank to my husband for his endless and essential support.

Nusrat Sharmin
Trento, 30 September 2017

Publications

Journal Papers

[1] Emanuele Olivetti, **Nusrat Sharmin**, and Paolo Avesani. *Alignment of Tractograms As Graph Matching*. Frontiers in Neuroscience, 2016.

[2] Diana Porro-Munoz, Emanuele Olivetti, **Nusrat Sharmin**, Thien Bao Nguyen, Eleftherios Garyfallidis, and Paolo Avesani. *Tractome: A Visual Data Mining Too for Brain Connectivity Analysis*. International Journal of Data Mining and Knowledge Discovery (DAMI), 2014.

Manuscripts Under Review

[1] **Nusrat Sharmin**, Emanuele Olivetti, and Paolo Avesani. *White Matter Tract Segmentation as Multiple Linear Assignment Problems*

Conference Paper

[1] **Nusrat Sharmin**, Emanuele Olivetti, and Paolo Avesani. *Alignment of Tractograms as Linear Assignment Problem*. Computational Diffusion MRI (CDMRI), Mathematics and Visualization, pages 109-120. Springer International Publishing, 2016.

[2] Emanuele Olivetti, Giulia Bertò, Pietro Gori, **Nusrat Sharmin**, Paolo Avesani. *Comparison of Distances for Supervised Segmentation of White Matter Tractography*. 7th International Workshop on Pattern Recognition in NeuroImaging, 2017.

Posters

[1] **Nusrat Sharmin**, Emanuele Olivetti, and Paolo Avesani. *White Matter Tract Segmentation By Means of Streamlines Correspondence*. Annual Meeting of the Organization for Human Brain Mapping (OHBM 2017)

[2] **Nusrat Sharmin**, Paolo Avesani, and Emanuele Olivetti. *Aligning Tractograms: a Linear Assignment Problem*. Italian Chapter of International Society of Magnetic Resonance in Medicine (ISMRM, 2016).

[3] Paolo Avesani, Emanuele Olivetti, Thien Bao Nguyen, **Nusrat Sharmin**, and Nivedita Agarwal. *White-Matter Alignment Across Subjects by Tractography Mapping*. In 21th Annual Meeting of the Organization for Human Brain Mapping (OHBM 2015).

Software

[1] Tractome: A Visual Data Mining Tool for Brain Connectivity Analysis

`http://tractome.org/`

`https://github.com/FBK-NILab/tractome`

[2] Alignment of Tractograms As Graph Matching: Graph-based alignment using the Doubly Stochastic Projected Fixed-Point (DSPFP) algorithm

`https://github.com/emanuele/DSPFP`.

[3] Automatic segmentation of tract/bundles from tractography data based on the linear assignment problem (LAP)

`https://github.com/FBK-NILab/LAP_tract_segmentation`

Contents

List of Tables

List of Figures

List of Algorithms

List of Acronyms

3D	3-dimensional
ADC	Apparent Diffusivity Coefficient
AF	Arcuate Fascicle
AUC	Area Under Curve
CB	Cingulum Bundle
CC	Corpus Callosum
CG	Cingulum
CNS	Central Nervous System
CSD	Constrained Spherical Deconvolution
CSF	Cerebro Spinal Fluid
dMRI	Diffusion Magnetic Resonance Imaging
dODF	Diffusion Orientation Distribution Function
DR	Dissimilarity Representation
DSC	Dice Similarity Coefficient
DSPFP	Doubly Stochastic Projected Fixed-Point
DTI	Diffusion Tensor Imaging
DW-MRI	Diffusion-Weighted Magnetic Resonance Imaging
DWI	Diffusion-Weighted Imaging
EuDX	Euler integration Delta function fiber crossing
FA	Fractional Anisotropy
FACT	Fiber Assignment by Continuous Tracking
FN	False Negative

fODF fiber Orientation Distribution Function

FP False Positive

FPR False Positive Rate

GM Graph Matching

GPU Graphics Processing Unit

HARDI High Angular Resolution Diffusion Imaging

HCP Human Connectome Project

ICF Interactive Closest Feature point

ILF Inferior Longitudinal Fascicle

IOFF Inferior Occipito-Frontal Fascicle

LAP Linear Assignment Problem

LAPJV Jonker-Volgenant algorithm for Linear Assignment Problem

MAM Minimum Average Distance

MD Mean Diffusivity

MDF Minimum average flip Distance

MdLF Middle Longitudinal Fascicle

NN Nearest Neighbor

ODF Orientation Distribution Functions

PDF Probability Density Function

ROC Receiver Operating Characteristic

ROI Region of Interest

SFF Subset Farthest First

SLR Streamline Linear Registration

TN True Negative

TP True Positive

TPR True Positive Rate

UF Uncinate Fascicle

WM White Matter

WMQL White Matter Query Language

Part I

Dissertation

Chapter 1

Introduction

In this chapter, we outline the problems and solutions described in the dissertation. We also provide some necessary context to make the presentation accessible to a wide audience.

1.1 Research Context and Motivation

The human brain regulates all human activities by controlling the central nervous system (CNS). The CNS is composed of two types of tissue: *gray matter*, known as cerebral cortex, and *white matter*. The core part of CNS comprises the neurons, that is the nerve cells, which consist of three main parts: cell body, dendrites and axons. Gray matter is composed of cell bodies and dendrites and serves the processing in the brain, while white matter mainly contains the neuronal axons that are responsible for transferring the signal among different regions of the brain [45]. The axons transfer the electrical impulse to other neurons through the axonal ending and dendrites. For this reason, the neuronal axons within the white matter form the anatomical links between regions of the brain, which are referred to as *anatomical connectivity*, or *structural connectivity* [78] [31]. The complete collection of structural connectivity is referred to the structural connectome, which helps to understand the human brain functionality [134]. The study of anatomical connectivity is crucial to understanding how the brain works. Such study also helps characterize neurological diseases and supports pre-surgical planning. Therefore, research on methods to investigate the white matter becomes essential in neuroscience and clinical applications.

Diffusion Magnetic Resonance Imaging (dMRI) [8] is a widely used technique for analysing human brain white matter. DMRI provides information about the local orientation of white matter axons in each voxel of a brain image. Reconstruction and tracking algorithms estimate the local orientation of axons at voxel-level and reconstruct the approximate trajectories of the neural pathway as 3D polylines called *streamlines*. Thus, a streamline is a vectorial representation of approximately 10,000 neuronal axons following the same path. The whole set of streamlines is called *tractogram* and it represents the structural connectome of the brain. Moreover, streamlines belonging to the same anatomical structure are called *tract* or *bundle*, such as the cortico-spinal tract or the arcuate fasciculus.

Statistical analysis of white matter tracts helps to study brain alterations related to diseases, aging, disorders and language deficits [86]. The common approach to statistical analysis is to extract local diffusion properties, for example fractional anisotropy (FA) or mean diffusivity (MD), from the tract and to perform quantitative analysis [100]. Such tract-based quantitative analysis is valuable as it takes into account the information from a set of streamlines that belong to the same anatomical area. It is also valuable to observe the differences in the properties of the specific tracts over a group of subjects. Dealing with a group of subjects generates two issues: how to

align the subjects, called **tractogram alignment problem**, and how to extract the desired bundles, called **tract segmentation problem**.

Tractograms of different brains need to be aligned for various purposes, such as group-analysis, segmentation, and atlas construction [102]. Due to the variability of the human brain, the aligning of tractograms helps to determine which anatomical locations correspond across subjects. One of the main goals of this thesis is to investigate the *tractogram alignment problem*.

In order to benefit from the quantitative analysis over the tracts, automatic extraction of the tract from the whole brain tractogram is an important task [86]. In principle, grouping or organizing the streamlines into anatomically meaningful tracts is known as *tract segmentation problem*. The task entails extracting a tract of interest from the tractogram of a given subject in a way that is consistent with those of other subjects. In this thesis, we propose a new method to address the tract segmentation problem.

In a healthy brain, it is expected that homologous anatomical structures are present across all subjects. Based on this idea, the alignment of tractograms can be seen as the procedure after which homologous anatomical structures match. In the same way, segmenting tracts by transferring anatomical knowledge from the example tract of one subject to the tractogram of a new subject can be seen as a procedure after which the desired tract in the new subject matches the example. In this thesis, we exploit the recent idea of *correspondence* to implement the procedure of matching. The idea of correspondence is in contrast to that of *transformation*, typical of standard registration methods, where streamlines undergo geometrical changes to increase similarity between subjects. With correspondence, the tractogram (or tract) is divided in units, for example, streamlines, and the goal is to find which units correspond across tractograms by optimizing some quantity of interest. With this map of correspondences, it is possible to obtain accurate alignment and to segment tracts of interest from examples.

The correspondence problem can be defined as finding which element of a set matches the element of another set [123]. The correspondence problem can be formalized as a *combinatorial optimization problem* [85]. Given a loss function that measures the degree of mismatch of correspondence, the task is to explore the discrete combinatorial space of all possible correspondences to find the one that minimizes loss. The problem of finding the minimum is extremely demanding, in terms of computations.

1.2 Problem Statement

In recent years, a large amount of research has been done to study white matter tractograms and tracts. This research involves reconstructing the tractogram in a more accurate way, improving the alignment of the tractogram, finding an efficient way to extract the tract, and developing tools to analyze the diffusion properties of the tract. The thesis focuses on two of those problems: *tractogram alignment* and *tract segmentation*. In addition, we also discuss the computational issues that arise when dealing with large tractogram datasets.

1.2.1 Tractogram Alignment

In multiple applications, such as group-analysis, segmentation, and atlasing, tractograms of different subjects need to be aligned. The main purpose of the alignment is to match corresponding anatomical structures across tractograms. The common approach to align the tractograms is registration, which means applying geometrical transformation/deformation to the data. Current literature on tractogram registration can be divided into two groups: voxel-based tractogram registration and streamline-based tractogram registration. Typically, in voxel-based tractogram registration, two tractograms can be aligned by first estimating a transformation between the corresponding

volumetric images, such as T1, fractional anisotropy (FA, see [8]), or orientation distribution functions (ODFs, see [116, 29]), and then by applying the transformation to the streamlines of the tractograms. Both linear and non-linear methods have been proposed to register volumetric data, see [30]. In linear methods, an affine transformation is usually estimated, for example with FSL/FLIRT, see [68], and then applied to the coordinates of the streamlines. In non-linear volumetric transformations, the tractogram needs to be re-created after transforming the dMRI data. The streamline-based approach has the advantage of directly using the streamline information of the tractograms, instead of the volumetric image. Also, streamline-based approaches can be classified in linear and non-linear registration. Linear methods have been proposed to directly register whole tractograms by finding an affine transformation that minimizes a given loss function computed only from the streamlines [102, 55]. However, the non-linear transformation of streamlines is currently very limited due to the high computational cost and, for this reason, it is focused only on the tract/bundle alignment [168]. A comprehensive review of the literature on tractogram alignment can be found in Chapter 2.

In the case of linear registration, both voxel-based and streamline-based, the results are often non satisfactory. A single affine transformation can reconcile only part of the difference between the tractograms of two subjects. Many differences remain at the local level, for example the systematic displacement of entire tracts, and thinner/thicker or longer/shorter tracts. We demonstrate the limitation of linear registration methods with an example in Figure 1.1, where the two tractograms, represented with 10000 streamlines each, are depicted in green and white (see subfigure A). We registered the two tractograms with affine registration (see subfigure B), showing good overlap. In contrast, at the local level, the overlap may not be as good. Subfigures C and D show section 7 of Corpus Callosum, before and after affine registration. In subfigure D, it is clearly visible that the overlap is still poor.

Even when using non-linear registration techniques at voxel-level or at streamline-level, we cannot find the desired match due to two main drawbacks. First, with non-linear registration at voxel-level, it is mandatory to re-create the tractogram from scratch, which entails a cost both computational and of expertise. Moreover, by creating a new tractogram, we would lose the expert-made segmentations obtained on the old tractogram. Finally, there are strong technical concerns about re-orienting the ODFs when applying the transformation, see [29]. Second, with non-linear registration of streamlines, we cannot address full tractograms but only bundles, due to the excessive computational cost, see [47].

In this work, we propose to avoid the transformations and to directly find the correspondence between streamlines between two tractograms, that is, to find which streamline correspond across two tractograms. We illustrate the idea of correspondence with both simulated streamlines and real streamlines in Figure 1.2 and Figure 1.3 respectively. In Figure 1.2, two sets of five simulated streamlines are depicted in blue and red without any alignment (see subfigure A). After registration, (see subfigure B), the two sets match at the global level, even though differences at the local level are still strong. In subfigure C, we show the concept of tractogram correspondence. The two sets of streamlines are displayed with arbitrary displacement, and black straight lines show the correctly identified corresponding streamlines across the sets. Figure 1.3 illustrates section 7 of Corpus Callosum, before and after affine registration (see subfigures A and B), and correctly aligned with the correspondence as computed by our proposed algorithm.

The algorithmic problem of finding the correspondence between streamlines of different tractograms can be framed as a combinatorial optimization problem. In this regard, it requires both the definition of a loss function, that is, a function that scores the correspondence, and the exploration of the combinatorial space to find the correspondence with the best score. The problem of defining the loss function is not straightforward, and the huge dimensionality of the combinatorial search space, due to the large tractogram dataset, makes this problem computationally very demanding.

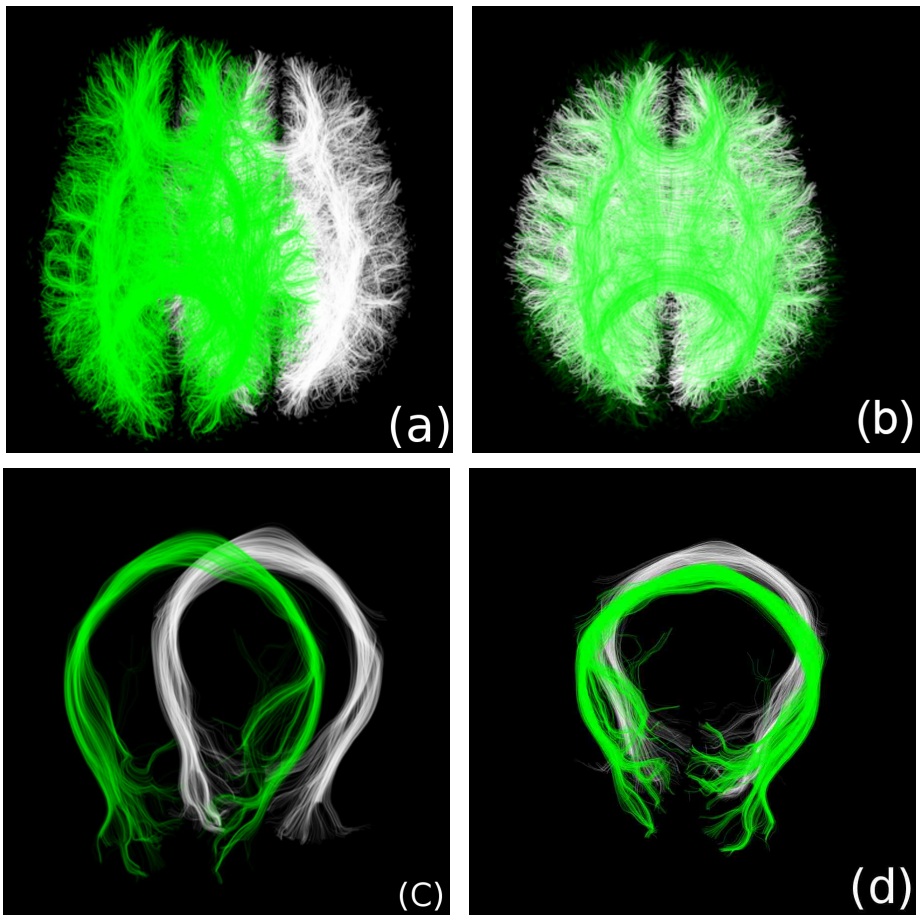

Figure 1.1: Two tractograms from two different subjects before (A) and after affine registration (B). Segmented Corpus Callosum, section 7, from two tractograms before registration (C) and after registration (D).

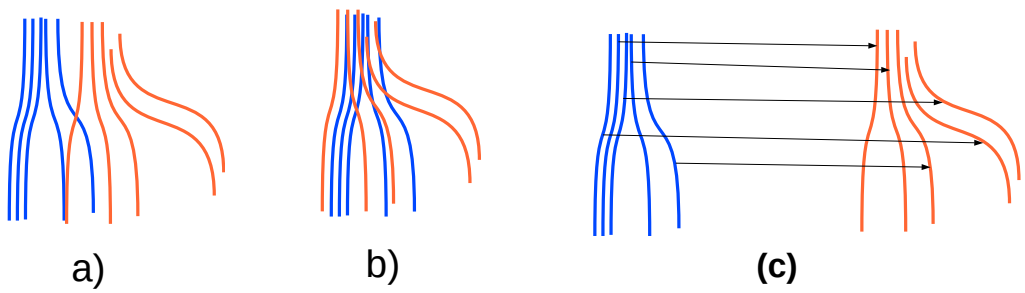

Figure 1.2: Simplified sketch of affine registration vs. our proposed correspondence approach. We show two tractograms of 5 streamlines each before registration (A), after affine registration (B) and the correspondence (C), i.e. each streamline of one tractogram corresponds to one streamline of another tractogram. Connection are shown with black arrow line.

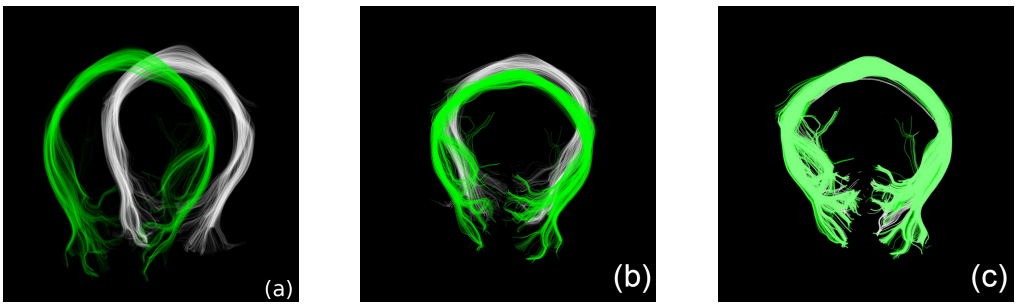

Figure 1.3: Our proposed correspondence problem with real data: Corpus Callosum section 7 of two subjects before registration (A), after whole-brain affine registration (B), after whole-brain alignment through correspondence.

1.2.2 Tract Segmentation

Several *manual* and *automatic* tract segmentation methods have been developed over the last few years. The manual approach [96, 154], also known as*virtual dissection*, is time demanding and limited to manual selection of Region of Interest (ROIs). Automatic tract segmentation can be divided into three different groups: *ROI-based* also known as *parcellation-based*, *unsupervised clustering approach* and *supervised segmentation approach*. Automatic ROI-based tract segmentation requires linear or non-linear registration, which can cause loss of the information present in the diffusion images [1, 167]. The unsupervised approach, also known as *fiber clustering*, is one of the most widely used tractogram segmentation techniques in the literature [128, 54, 146, 118]. Clustering methods mostly address the single-subject. Moreover, with clustering, there is no guarantee to obtain anatomically meaningful tracts [138]. A comprehensive summary of the existing tract segmentation methods are discussed in Chapter 2.

Supervised segmentation is an approach based on prior knowledge. Such knowledge can come from the models or features of tracts/bundles [32]. In particular, models are built to describe tracts/bundles and not the whole tractogram. Prior knowledge can also come from expert labelling of an anatomical atlas or from labelling clusters of streamlines from multiple subjects, in a process of atlas creation, see [103, 152, 62, 162, 77]. Once the atlas is available, the segmentation of the tract of interest in a new subject can be carried out. We present a detailed methodology of the supervised segmentation approaches in Chapter 2.

Existing methods of supervised segmentation have some limitations, the main ones being the high computational cost [103, 152], the need to segment a large number of subjects to construct the atlas in case of multiple atlases [62], and the dependency on the definition of threshold values [162, 77]. Moreover, a recently proposed approach requires the labelling of individual streamlines, which is time consuming and depends on a very demanding preprocessing [77]. In this literature, given a tract from one subject, the problem of finding the corresponding streamlines in the tractogram of another subject has been addressed with a nearest neighbor (NN) strategy [162].

With the NN strategy, after co-registering the two tractograms, for each streamline of one tractogram the corresponding one in the other tractogram is the geometrically nearest one, see [162]. This strategy is greedy, because it aims to minimize the distance of each streamline individually, without taking into account the whole anatomical structure the streamlines belong to. This is one of the reasons why we have observed that the NN strategy provides poor results in many cases. In Figure 1.4, we show an example of this issue, where two segmented tracts from two different (coregistered) tractograms, marked in white and green (subfigure A), are compared. In subfigure B, the corresponding NN streamlines of the white tract are shown in blue. It is clearly visible that the segmentation is poor, with a visibly inferior number of streamlines between the blue tract (NN) and the green tract

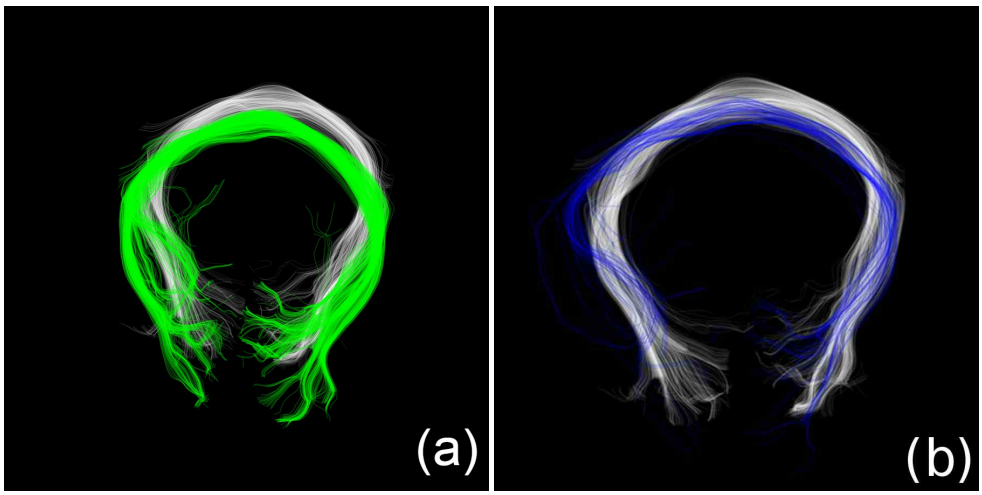

Figure 1.4: Two segmented Corpus Callosum section 7 from two different tractograms in white and green (left) and the nearest streamlines of the tract (in white).

(ground truth). This is another issue of the NN strategy: by always greedily selecting the closest streamline in the new tractogram, multiple streamlines of the example tract frequently end up corresponding to the same streamline in the target tractogram. For this reason, the number of streamlines of the estimated tract in the target tractogram is always inferior or at most equal to that of the example tract, leading to a systematic and unrealistic thinning.

In this thesis, we address the problem of segmenting a single specific tract from the whole tractogram of a new subject, using the prior information of the previous segmentation of the same tract/bundle from the tractogram of multiple subjects. In essence, instead of creating an explicit mathematical model of the tract, our proposal is to find which streamlines of the new tractogram belong to the desired tract using previous examples. Differently from the NN strategy, we propose a non-greedy strategy that aims at finding corresponding streamlines by taking into account the whole example tract when choosing each correspondence. In Section 1.3, we provide an intuitive description of our solution.

1.2.3 Scalability Issues

The computation of NN has multiple applications in tractogram alignment and segmentation. In general, given two co-registered tractograms and one streamline in the first tractogram, retrieving its closest streamlines in the second tractogram has a high computational cost. The straightforward solution entails computing the distances from the given streamline to all other streamlines in the second tractogram and then selecting the closest one. The approaches currently adopted in the literature are more efficient than the straightforward solution and are based on several pre-processing steps that may involve clustering, the definition of thresholds and the use of fast graphics processing units (GPUs), see [162, 77].

When implementing efficient solutions for the NN strategy, streamlines are often transformed into vector with a fixed dimension. Due to the different lengths and number of points, streamlines cannot be directly represented as vectors all of the same dimension. Current solutions of the NN strategy re-sample all streamlines to a given number of ($3D$) points, for example $N = 20$, thus creating an approximate representation in a vectorial space of $3 \times N$ dimensions, for example 60 dimensions. Unfortunately, re-sampling causes loss of information (see Figure 1.5 for an example). In the figure, the tract is shown before (subfigure A) and after re-sampling by applying

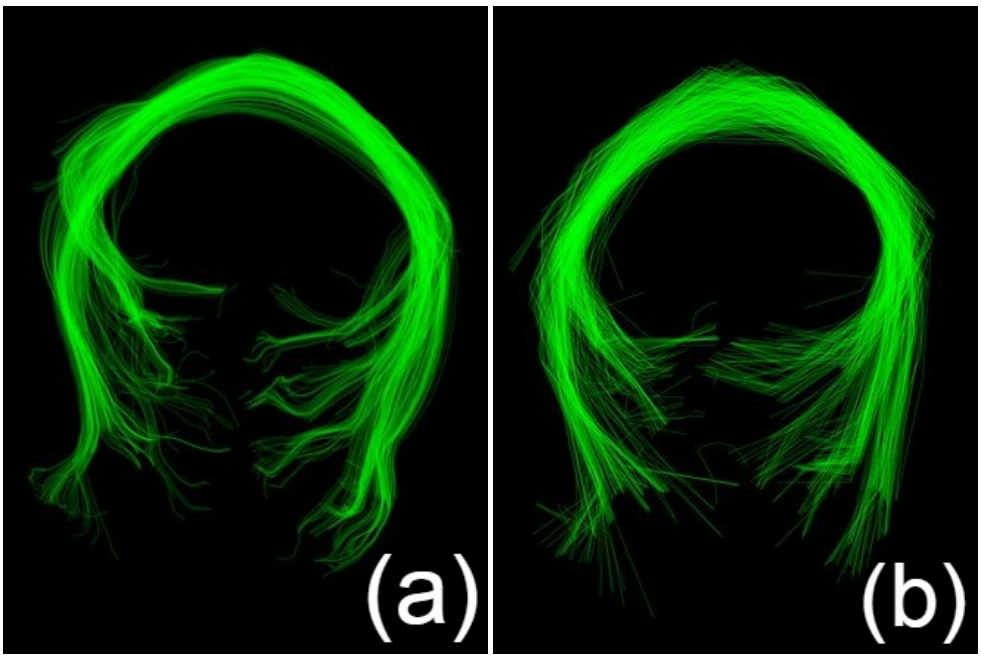

Figure 1.5: (left) Corpus Callosum section 7 tract before resampling and (right) after resampling

the re-sampling with $N = 10$ points (subfigure B).

1.3 The Solution

In this section, we provide an intuitive description of our solutions for the problem of tractogram alignment and supervised tract segmentation that are the main contributions of this dissertation.

1.3.1 Tractogram Alignment as Graph Matching

Contrary to the registration methods, we propose to solve the tractogram alignment problem as the tractogram correspondence problem. When designing a strategy for alignment, defining the loss function is one of the crucial aspects. To define the loss function, we propose to encode each tractogram as a large, fully-connected weighted graph, where each node/vertex corresponds to a streamline and the weights of the graph's edges are the distances between streamlines within the same set. Given two tractograms, that is, two graphs, the original problem of finding the correspondence between two sets of streamlines can be recast as the problem of finding corresponding nodes/vertices between the two graphs, a famous combinatorial optimization problem called *graph matching*. In this work, we provide an operational procedure to compute tractogram alignment based on a recent approximate graph matching algorithm, specifically the doubly stochastic projected fixed-point (DSPFP) algorithm [84].

1.3.2 Tract Segmentation as Linear Assignment Problem

We address the tract segmentation problem as a streamline correspondence problem. We cast the problem of finding corresponding streamlines as a Linear Assignment Problem (LAP). The LAP is a combinatorial optimization problem that finds corresponding streamlines imposing a one-to-one constraint while minimizing the distances

between corresponding streamlines. We adopted a variant of the well-known Jonker-Volgenant algorithm for Linear Assignment Problem (LAPJV) [12] to efficiently get the optimal solution of the LAP. Based on that, we also propose a novel supervised tract segmentation method that segments the tract of interest in a new subject using a set of examples (tracts) as prior information. Corresponding streamlines for each example are found through LAP and combined into one desired segmented tract within the new tractogram using a ranking scheme.

1.3.3 Scalable Nearest Neighbour (NN) for the Tractogram

In this thesis, we also propose an efficient way to compute the NN of given streamlines. Such implementation is needed to obtain an efficient implementation of graph matching and LAP, that is, for tractogram alignment and tract segmentation. Our proposed procedure to compute the NN greatly simplify the computation both in terms of time and the number of logical steps. Our procedure includes a vectorial representation of the streamlines of the tractogram, based on the Dissimilarity Representation (DR) [106], and the construction of kd-trees from the obtained vectors of the streamlines. Finally, by applying the efficient NN query of the kd-tree, we can quickly retrieve the closest streamlines.

The DR is a technique to embed all streamlines in the same Euclidean space. The DR maps each streamline in the vector of its distances with respect to a selected set of representative streamlines, called prototypes. This leads to a vectorial representation of the streamlines, where the domain information is taken into account, provided that an informative streamline-to-streamline distance function is available. A crucial step in the DR procedure is the selection of the prototypes. Thus, given the large number of streamlines, a fast prototype selection algorithm is also needed. For this purpose, we propose a domain-based heuristic that improves the general prototype selection policy. This policy is a stochastic approximation of an effective algorithm for prototype selection that scales well with the large collection of streamlines, see [106].

1.4 Innovative Aspects

This research is meant to improve the quantitative analysis over the tracts by exploiting the concept of tractogram correspondence and by proposing efficient implementations to the resulting algorithmic problems. The main contributions of the thesis are as follows.

1. **Tractogram Alignment as Correspondence Problem:** We introduce a different perspective on the tractogram alignment problem. In contrast to transformation-based registration methods, in this work we propose the novel concept of correspondence, the aim of which is to find which streamlines correspond tractograms. We provide an operational procedure to find the optimal correspondence through a combinatorial optimization problem.

2. **Correspondence Problem as Graph Matching:** We formulate the problem of tractogram correspondence as a graph matching problem. We have shown that this kind of formulation dramatically improves the results of the state-of-the-art algorithms. We propose to represent tractograms as graphs and we adopt a recent inexact sub-graph matching algorithm to approximate the solution of the tractogram correspondence problem.

3. **Tract Segmentation as LAP:** We propose a novel supervised tract segmentation method, that segments the tract of interest in a new subject using a set of tracts as prior information. We show that streamline correspondence is a powerful principle to transfer the anatomical knowledge of a given bundle from one

subject to another. The computation of streamline correspondence is formulated as a LAP, a combinatorial optimization problem that minimizes the distances between corresponding streamlines with a one-to-one constraint. Our proposed supervised tract segmentation method is accurate, simple, efficient and faster than other solutions in the literature.

4. **Efficient Scalable Solution for NN:** We propose an efficient and fast way to compute the NN of the given streamline of one tractogram to another tractogram. Our proposed procedure to compute the NN greatly simplifies the computation both in logical steps and time.

1.5 Thesis Outline

We have organized this thesis into two parts. The first part focuses on the goal of the thesis, background study, problem statement, proposed methods, experimental results, and discussions, in seven chapters. The second part, which consists of three chapters, includes the published works and the work done in preparation throughout the period of the Ph.D. program.

Chapter 2 provides a background study focusing on five different topics: i) diffusion magnetic resonance imaging (dMRI) ii) diffusion Models, iii) tractography algorithm, iv) tractogram alignment, and v) tract segmentation. The chapter is organized as follows. Section 2.1 introduces the human brain anatomical connectivity, the basic principle of diffusion MRI. The various techniques for diffusion model estimation are presented in Section 2.2. In Section 2.3, we describe different tractography algorithms. We introduce tractogram registration and discuss the SOA of the registration techniques and their limitations in Section 2.4. Subsequently, in Section 2.5 we discuss the existing tract segmentation approaches in the literature. In Section 2.6 we summarize the contents of this chapter.

Chapter 3 presents the mathematical formulation of the tratcogram registration problem and the tract segmentation problem. There, we also present the formulation of the correspondence problem. For this purpose, first we introduce the notation for representing streamlines, tractograms and streamline distance functions in Section 3.1. Then, we give a general formulation of the tractogram registration problem and provide the basic terminology for the formulation of the tractogram correspondence problem in Section 3.2. Finally, we provide the formulation of the tract segmentation problem in Section 3.3.

Chapter 4 presents our major contributions for tractogram alignment and the tract segmentation problem. This chapter is organized into three sections based on each of the contributions. We formulated the tractogram alignment problem as the graph matching problem. In Section 4.1, first, we introduce the basic terminology of the graph matching problem, including the properties of the graph. Then, we discuss the similarity of the correspondence problem with the graph matching problem and the formulation of the tractogram alignment as graph matching. We briefly discuss the existing methods for the approximate solutions of the graph matching problem. We present the details of the efficient solution that we adopted from the recent literature, that is, the Doubly Stochastic Projected Fixed-Point (DSPFP) algorithm. In Section 4.2, we introduce the linear assignment problem (LAP) and present the formulation of the tract segmentation as linear assignment problem. We present a brief summary of the existing solutions of the LAP and a detail description of the adapted Jonker-Volgenant algorithm (LAPJV) algorithm. To conclude, in Section 4.3 of this chapter, we present our contribution about the efficient, scalable solution for the nearest neighbour computation for the tractogram. In this case, the proposed method uses the dissimilarity representation (DR) and the k-d tree structure which we introduce at the beginning of the section.

Chapter 5 presents the description of the dataset used for the experiments, as well as the method for generating the ground truth data. We use the Human Connectome Project (HCP, see [150]) dMRI dataset, which is publicly

available. Details of the dataset along with the methods used for the tractogram generation are provided in Section 5.1. We use the White Matter Query Language (WMQL, see [157]) for the ground truth tracts labelling. We briefly discuss the use of the WMQL and the anatomical background of the segmented tract with the WMQL in Section 5.2.

Chapter 6 presents the experimental results conducted to prove our proposed methodologies, for example tractogram alignment as graph matching and tract segmentation as the linear assignment problem. A large amount of experimental analysis was conducted for validating our proposed concepts and is fully reported in the papers of Part II. In this chapter, we report a meaningful subset of the Experiments. We describe in detail how the experiments were conducted for alignment and segmentation. In both cases, we compare our proposed methods with the state-of-the-art methods. In Section 6.1 and Section 6.2, we report the experimental results of the tractogram correspondence and tract segmentation, respectively. In Section 6.3 we demonstrate the running time for our proposed scalable NN solution.

Chapter 7 summarizes the thesis by discussing the results presented in Chapter 6 and presenting the conclusion of the contributions and some potential future directions of our proposed methods. Additionally, we discuss the limitations of our proposed methods.

Part II: Published and Submitted Work

Chapter 8: The work described in this chapter is based on our contributions on tract segmentation. We propose a novel supervised tract segmentation method which comprises a manuscript of the segmentation method. This manuscript is under review. The details of the manuscript are as follows: **Nusrat Sharmin**, Emanuele Olivetti, and Paolo Avesani. *White Matter Tract Segmentation as Multiple Linear Assignment Problems*.

Chapter 9: The work described in this chapter is based on our contributions to the tractogram alignment problem. The work is published in Frontiers in Neuroscience, 2016. The details of the publication are as follows: Emanuele Olivetti, **Nusrat Sharmin**, and Paolo Avesani. *Alignment of Tractograms As Graph Matching*. Frontiers in Neuroscience, 2016.

Chapter 10: The work described in this chapter is published in the Computational Diffusion MRI (CDMRI), MICCAI Workshop. This work is based on the tract segmentation with the concept of the corresponding streamlines. This work showed a powerful principle to transfer the anatomical information from one brain to another through the streamlines correspondence. In addition, the streamline correspondence proves our claim that alignment can not only align tractograms but also provide useful information. The details of the publication are as follows: **Nusrat Sharmin**, Emanuele Olivetti, and Paolo Avesani. *Alignment of Tractograms as Linear Assignment Problem*. Computational Diffusion MRI (CDMRI), Mathematics and Visualization, pages 109-120. Springer International Publishing, 2016.

Appendix A: This appendix contains the supplementary material of the article in Chapter 9.

Appendix B: This appendix contains the experimental results for the prototype selection of the dissimilarity representation as a part of a scalable solution for the nearest streamline computation. It is part of the following publication: "Diana Porro-Munoz, Emanuele Olivetti, **Nusrat Sharmin**, Thien Bao Nguyen, Eleftherios Garyfallidis, and Paolo Avesani. *Tractome: A Visual Data Mining Tool for Brain Connectivity Analysis*. International Journal of Data Mining and Knowledge Discovery (DAMI), 2014."

Chapter 2

Background

Overview

This chapter provides a background study focusing on five different topics: i) diffusion magnetic resonance imaging (dMRI), ii) diffusion models, iii) tractography algorithms, iv) tractogram alignment, and v) tract segmentation.

Diffusion magnetic resonance imaging (dMRI) is a unique, noninvasive technique for analysing human brain white matter. We first present the fundamental theory of the human brain anatomical structure and the basic principles of the diffusion, followed by a brief description of the diffusion imaging. From the diffusion imaging, it is possible to measure the local orientation of the neural axons of the white matter into the voxel. We continue the discussion with a review of the techniques used to model the diffusion signal into the voxel. We start the discussion with the diffusion tensor model (DTI), followed by the high angular resolution diffusion imaging (HARDI).

Next, we introduce the *tractography algorithm* or the *tracking algorithm*, a technique that integrates the diffusion signal within each voxel. By integrating the diffusion signal, the tractography algorithm reconstructs the three-dimensional trajectories of white matter axons, known as *streamlines*. A set of streamlines is called *Tractogram*, which is the input dataset of this thesis. However, the tractography algorithm can be categorized as the local and global approaches, where the local approaches can be deterministic and probabilistic.

The tractography algorithm generates the number false-positive streamlines. Hence the post-processing of the tractogram has been developed recently. We briefly discuss the tractogram post-processing methods.

In this chapter, we also present the state-of-the-art (SOA) of two main research problems of tractogram data analysis: *tractogram alignment* and *tract segmentation*. We aim to investigate these two problems in this thesis. In order to perform the investigation thoroughly, we review the existing methods of *tractogram registration* (also known as *tractography registration*), which is a common approach to align the tractogram. For the discussion of the registration techniques, we divide the existing methods into two large categories: *voxel-based* and *streamline-based* registration. With each category of registration, we also discuss the advantages and limitations of the methods.

Next, we discuss the existing techniques of *tract segmentation* by dividing it into three different categories: *region of interest (ROI) based segmentation*, *unsupervised clustering techniques* and *supervised tract segmentation*. The pros and cons of each type of segmentation method are presented in the review of the methods.

Organization of the Chapter

The chapter is organized as follows. Section 2.1 introduces the human brain anatomical connectivity, the basic principle of dMRI. The various techniques for diffusion model estimation are presented in Section 2.2. In Section 2.3, we describe different tractography algorithms. We introduce tractogram registration and discuss the SOA of the registration techniques and their limitations in Section 2.4. Subsequently, in Section 2.5, we discuss the existing tract segmentation approaches in the literature. In Section 2.6, we summarize the contents of this chapter.

2.1 Diffusion Magnetic Resonance Imaging (dMRI)

In the following Subsections, we describe brain anatomical connectivity, the basic principle of diffusion imaging. Before starting the discussion in detail, it is worth noting that the terms dMRI, diffusion imaging, diffusion-weighted magnetic resonance imaging (DW-MRI), and diffusion-weighted imaging (DWI) all refer to diffusion-weighted magnetic resonance imaging.

2.1.1 Brain Anatomical Connectivity

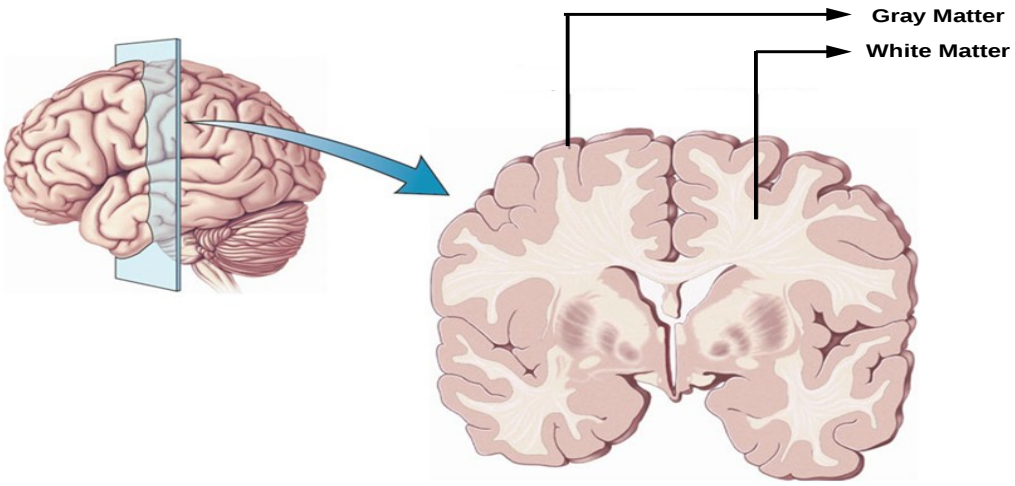

Figure 2.1: White Matter and Gray Matter of the brain. Image is adapted from NIH Medline [1]

The most important and complex part of the human body is the brain, which can be divided into three parts: telencephalon (composed of two cerebral hemispheres), diencephalon (a group of structures located deep within the cerebrum) and brain stem [63]. The human brain regulates all human activity by controlling the central nervous system (CNS). It contains different elements, such as blood, cerebrospinal fluid (CSF), white matter (WM), and gray matter (also known as cerebral cortex). White matter and gray matter [45] (see Figure 2.1) are the two tissue elements of the CNS. In Figure 2.1, gray matter is the pinkish-grey color in the living brain, or the cortex, the various parts of which are connected by the white matter. Magnetic Resonance Imaging (MRI) [8] of a brain reveals

[1] http://multiple-sclerosis-research.blogspot.com/2015/01/education-whats-mri.html

information about the gray and white matter structures, and diffusion-weighted magnetic resonance imaging (DW-MRI) provides the anatomical information about the white matter structure.

The core component of the CNS is the neurons (nerve cells), which are responsible for communication and information processing within the brain [60]. A neuron is composed of three parts: the cell body or soma and two processes: the *dendrites* and the *axon* (see Figure 2.2). The processing of the brain takes place in the gray matter, which is composed of cell bodies and dendrites, while white matter is composed of billions of myelinated axons which connect various gray matter areas of the brain to each other. The axons transfer the electrical impulse to the other neurons through axonal endings and dendrites. In this way, axons create a wiring system, which is referred to as a brain connecting cable, to transfer signals to different regions of the brain. This wiring system is known as the white matter architecture or *the anatomical connectivity* [135]. More precisely, the complete collection of the white matter neural axon in a large volume is called the *connectome* [134]. The anatomical connectivity varies across subjects and plays an important role in identifying mental diseases, and neurological or neuropsychiatric diseases. Research on white matter structure and organization is therefore essential for neuroscience.

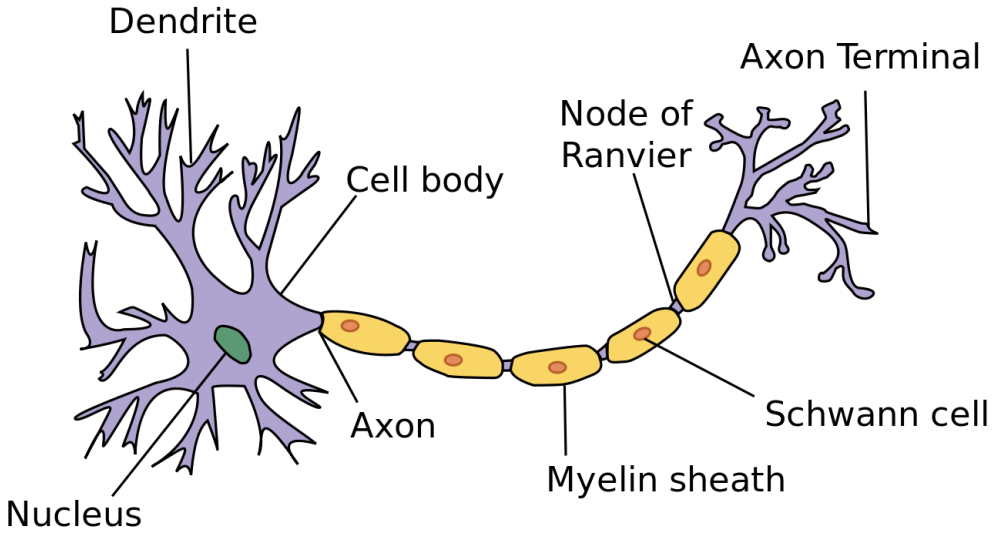

Figure 2.2: Structure of the neuron: basic components of the neuron, including the nerve cell body, dendrite, nucleus, axon, myelin sheath, node of ranvier and axon terminal. Figure is adapted from *Wikimedia Commons*

2.1.2 Principles of Diffusion Imaging

Diffusion Basics

Due to the internal thermal energy, water molecules present the random translational motion, called *the Brownian Motion* [8]. On a macroscopic scale, this motion can be interpreted as the *diffusion phenomena*, which is a physical process essential for the normal functioning of living systems. The diffusion of molecules can be free or restricted, and can be categorized as isotropic or anisotropy. In the case of fluids and some homogeneous solid materials, the diffusion can be the same in every direction, which is known as *isotropic*, while in the case of biological tissue, molecules can move in a specific manner in a given direction, which is referred to as *anisotropic* diffusion.

The amount of diffusion depends on the size of the molecules and the temperature. In 1905, Einstein proposed to use a probabilistic framework for demonstrating the description of diffusion motion [63]. According to Einstein's

diffusion equations, the mean square displacement (r) of the molecule during observation time (t) can be derived as follows:

$$r^2 = 6Dt \tag{2.1}$$

where D is the *diffusion coefficient* and the unit of measurement of D is mm^2s (meters squared per second).

In the case of free diffusion, the probability distribution function of the mean square displacements (r) is the Gaussian distribution, which can be represented by the following equation:

$$p(r,t) = \frac{1}{\sqrt{(4\pi t)^3 D}} e^{-\frac{r^T r}{4tD}} \tag{2.2}$$

where $p(r,t)$ is the probability function of the motion of particle, which is also known as the *diffusion propagator* [42].

In the case of the human brain, the motion of the water molecules strongly depends on the surrounding membranes. Membranes from the boundaries restrict the motion of the water molecules, which leads to lower diffusion coefficients than free diffusion coefficients in an unbounded area.

Diffusion Imaging

In DW-MRI, the diffusion coefficient is not compute directly; instead, the average square displacement is measured within each voxel, that is, the three-dimensional volume element. However, as mentioned above, due to the presence of cell membranes, inclusions, and macromolecules in the tissue, the mean displacement of molecules computed (computed by Equation 2.1) appears to be low. This is referred to as the *apparent diffusion coefficient (ADC)* [52]. Moreover, the average displacement of molecules within the voxel (due to the fact that a very large number of molecules are present in each voxel) is measured by a *diffusion displacement probability function*, which is referred to as an *ensemble-average propagator (EAP)* of water molecules [63].

DW-MRI [8] acquisition is very challenging as it needs high-quality raw dMRI. Measuring diffusion using magnetic resonance imaging (MRI), therefore, is about the physics of the acquisition and dealing with the imperfections of the diffusion sequence. It is beyond the scope of this thesis to present the physics of the diffusion MRI, rather we will present an intuitive process to capture the diffusion signal with the MRI.

A current standard method for computing the diffusion with MRI is the pulsed gradient spin echo (PGSE) sequence which was introduced by Stejskal-Tanner in 1965 [63]. It measures the diffusion by estimating the displacement of particles during different phases of the acquisition process. Diffusion signal can be defined by the Stejskal-Tanner formula under the assumption of the Brownian Motion as follows:

$$S_b = S_0 e^{-bD} \tag{2.3}$$

where S_0 is the baseline image without any diffusion weighting, D is the ADC and b-value is the diffusion weighting parameter to tune the diffusion attenuation of the DWI. b-value is the key parameter in the DWI and is required to acquire the images properly and is measured in s/mm^2.

In order to estimate the EAP, q-space imaging has been proposed by Callaghan [22]. q-space imaging is a DW-MRI technique to study the diffusion distribution which has the Fourier relation with the EAP.

2.2 Diffusion Models

DMRI allows for the investigation of the microscopic diffusion of water molecules in *vivo* which reveals the microstructure properties of the underlying tissue. In order to acquire these images, we need different diffusion images with magnetic field gradients applied in various directions. Then, a reconstruction step is used to measure the 3-*D diffusion probability density function (PDF)* from the sequence of acquired images with different gradients. Hence the main purpose of the reconstruction is to compute the information about the spatial distribution of the diffusion signal within each voxel [52].

A reference method for computing the diffusion signal is diffusion tensor imaging (DTI) [8]. However, the evolution of MRI techniques introduces an acquisition method based on high angular resolution diffusion imaging (HARDI) [42], which is now the central part of a large number of neuroscientific studies. We will briefly present the review of the reconstruction models in the following subsection. A more detailed overview of the diffusion model can be found in [63, 42, 6, 41].

2.2.1 Diffusion Tensor Model

The Diffusion tensor (DT) model has rapidly grown and is a promising method for the diffusion signal reconstruction [52]. The DT used by the diffusion modality is known as the diffusion tensor MRI,Diffusion Tensor Imaging (DTI) or Diffusion Tensor-Magnetic Resonance Imaging (DT-MRI) [8].

In the human brain, particularly in white matter, the apparent diffusion is not isotropic, but anisotropic [41]. In the case of anisotropic, water molecules cannot be characterized by a single ADC, meaning that a scalar D is not sufficient to describe the diffusion. The anisotropy nature of the diffusion can be handled by using three diffusion images along three orthogonal diffusion directions (x, y, z) and a baseline image without diffusion. Thereby, diffusion images can be represented by the S_x, S_y, S_z and S_0. With these images, by solving the equation 2.3 three times and then by computing the geometric average, the ADC is estimated. Based on this fundamental concept of the ADC, in 1994, the diffusion tensor was proposed to model the diffusion properties of the biological tissues.

Mathematically, the DT can be represented by a 3×3 symmetric, positive-definite matrix. The DT is defined as follows [8]:

$$DT = \begin{pmatrix} D_{xx} & D_{xy} & D_{xz} \\ D_{yx} & D_{yy} & D_{yz} \\ D_{zx} & D_{zy} & D_{zz} \end{pmatrix} \tag{2.4}$$

Due to the symmetric nature of the diffusion tensor, six tensor coefficients (three diagonal and three non-diagonal) are sufficient to represent the diffusion properties of the water molecules. Moreover, by using these six coefficients, the displacement distribution of water molecules can be shaped as an ellipsoid [52]. The three eigenvalues of the diffusion tensor, denoted as λ_1, λ_2, λ_3, describe the diffusion rate along with the three principal axes of the ellipsoid. The main eigenvector indicates the fiber's direction. However, the DT model has an assumption that the probability distribution of the water molecules follows the Gaussian distribution with its three orthogonal eigenvectors [8].

Parameters Derived From the Diffusion Tensor:

Several diffusion properties can be derived from the DTI. Two important and commonly used properties derived from the DTI are the mean diffusivity (MD) or ADC and the fractional anisotropy (FA) [52]. The MD [8] is

the average diffusion rate in all directions, defined as the average of the eigenvalues. MD can be represented as follows:

$$MD = \frac{trace(DT)}{3} = \frac{(\lambda_1 + \lambda_2 + \lambda_3)}{3} \tag{2.5}$$

where $trace(DT)$ is the trace of the tensor.

The most used parameter for the anisotropy in DTI is FA. The FA [8] is the scalar metric used to characterize the presence and absence of a preferred direction of diffusion in diffusion imaging. FA can be defined as follows:

$$FA = \sqrt{\frac{3}{2}}\sqrt{\frac{((\lambda_1 - MD) + (\lambda_2 - MD) + (\lambda_3 - MD))}{(\lambda_1 + \lambda_2 + \lambda_3)}} \tag{2.6}$$

FA values vary between 0 and 1. The 1 implies very anisotropic and 0 means completely isotropic [52].

Both FA and MD are used for statistical analysis of white matter structure in clinical studies, for example, alterations related to diseases, aging, disorders, and language deficits [86].

DTI Limitations

Although neuroscientists and clinicians commonly use the DTI model, it has some limitations in practice.

DTI is limited in addressing the diffusion characteristic of the white matter structure in the proper way [42]. More precisely, the Gaussian diffusion model assumption is the most important limitation of DTI. Under this assumption, every imaging voxel can contain a single-fiber population, which is not sufficient, as most of the voxels (over 90% of the white matter voxels) contain multiple crossing fibers [117]. Hence, DTI has the limitations of imaging voxels of multiple fibers, for example, fanning and crossing (see Figure 2.3). Moreover, for multiple fiber crossings and high curvature, the DTI model is no longer Gaussian and violates the assumption of the DTI model [42].

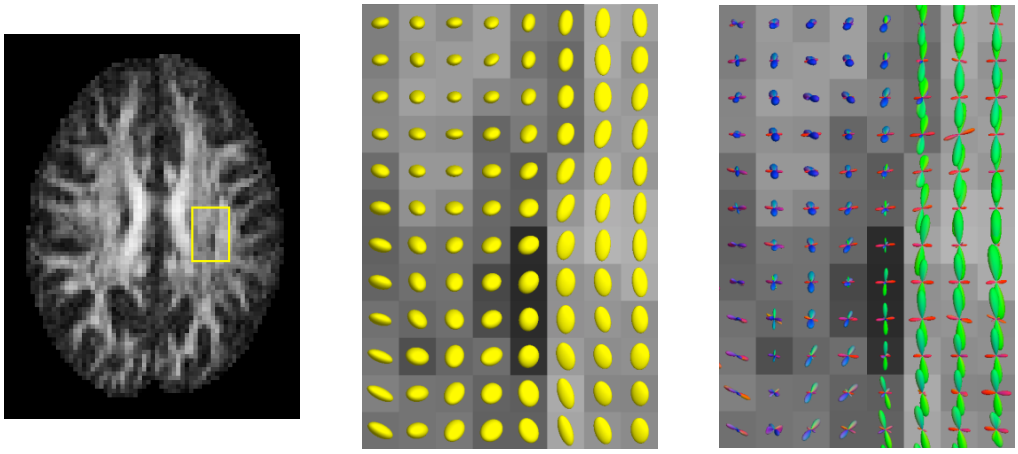

Figure 2.3: An example of crossing fibers (left) A ROI is shown in the axial FA map (middle) Results obtained after diffusion tensor model (right) Results obtained using spherical deconvolution [144]. Images are adapted from *CDMRI invited talk by J-Donald Tournier* [2]

Figure 2.3 (left) shows a ROI (rectangular with yellow) located in the axial FA map, the reconstruction of the ROI by applying the diffusion tensor model (middle), and the spherical deconvolution (right), see Section 2.2.2.

The figure clearly shows that the diffusion tensor model is unable to recognize the presence of the multiple fiber orientations.

2.2.2 High Angular Resolution Diffusion Imaging (HARDI)

To overcome the limitations of the DTI model, high angular resolution diffusion imaging (HARDI) has been developed. The goal of HARDI is to solve the crossing fibers problem of DTI and provide new anisotropy measures beyond the classical FA derived from the DTI. To fulfill this purpose, HARDI acquires more information about the diffusion weighted images by capturing the higher angular frequency features of the diffusion weighted signal. In this way, reconstruction models based on HARDI acquisition allow for better representation of the complex fiber geometry.

A number of reconstruction methods have been proposed based on the HARDI acquisition protocol. Proposed methods can be model-free (nonparametric) and model-based (parametric) [42]. In principle, model-based methods take into account the biological assumption. Based on such assumptions, they build the diffusion model of the water molecule, while model-free methods work without any physical assumptions about the tissue properties.

Following, we will present the existing reconstruction methods based on HARDI techniques in the literature. Note that we do not intend to provide the mathematical details of the model; instead, we will discuss the features and limitations of the model.

Diffusion Spectrum Imaging (DSI)(Model-free Approach): In the context of HARDI imaging, the most important aspect is the Fourier transform relationship between the q-space (diffusion space) and the real space probability distribution function that describes the diffusion process of the water molecules [42]. However, one of the most important features of the diffusion propagator is the diffusion Orientation Distribution Function (dODF) [63]. Diffusion spectrum imaging (DSI) aims to reconstruct the dODF [63].

In principle, the ODF is a function on the sphere that can be represented with evenly distributed points and gives the idea for the dominated direction [52]. With regards to the diffusion data, ODF gives the probability diffusion of the water molecules in a given direction. Accordingly, dODF is a function on the solid sphere describing the average probability of the diffusion of the water molecules into any solid angle. dODF consists of the full angular information of the diffusion probability displacement function [52].

DSI is one of the most accurate methods of estimating the dODF, but a long acquisition time makes this method incompatible for medical applications [6]. To overcome DSI limitations, single-shell HARDI techniques [41] have been developed to efficiently extract the diffusion PDF and ODF.

Single-shell HARDI Techniques:

To overcome the fiber crossing problem, single-shell HARDI techniques were proposed with the aim of requiring less scan time without major hardware requirements [42]. Typically, the diffusion signal is acquired through uniformly distributed gradient directions on a single-shell of b-value (or a single-shell of q-space). Based on the single shell acquisition, the aim of HARDI reconstruction is to have an angular function which maxima is aligned with the fiber structure.

Moreover, compared to DSI, the single-shell HARDI requires less time due to the fact that samples are taken on a single sphere in diffusion space [42]. In general, single-shell HARDI reconstruction can be categorized into two groups: model-free and mixture model-based techniques.

Mixture Model-based Approach: In mixture model-based approaches, distinct fiber populations are modeled separately.

The multi-tensor or multi-Gaussian model is the simple natural extension of the DTI method with more than one tensor per voxel [63]. It assumes that mixtures of Gaussians can describe the diffusion PDF. Several methods proposed based on the multi-tensor model can be found in [92, 71]. Another important mixture model is the Ball-and-Stick model [63]. This method is based on the assumption that water molecules in an imaging voxel belong to two types of population: a restricted population and a free population. Gaussian distributions and isotropic Gaussian distribution are used for the restricted and free population, respectively. The approach extends to a mixture of restricted compartments, which are able to recover multi-fiber compartments. The ball-and-stick model is available in FSL, `http://fsl.fmrib.ox.ac.uk/fsl/fslwiki`.

Although mixture models lead to a more complex computation, it extracts the accurate diffusion features from diffusion MRI, which doesn't require any additional post-processing [6]. Nevertheless, all of these methods suffer from a priori selection about the number of compartments and also sensitive to the noise [6].

Spherical Deconvolution (SD) (Model-based): The Spherical Deconvolution (SD) [144] methods generalized the mixture model-based method by assuming a orientation of fiber distribution, instead of distinct fiber orientation.

The original SD method was proposed in 2004. It assumes that a diffusion signal can be generated by a single-fiber response function, which is convoluted with a distribution of fiber orientations. The main idea is to measure the response function of a single fiber and view the HARDI signal as the convolution of the response function. It proposes using spherical harmonics and rotational harmonics to parametrize the signal and fiber response function, respectively. The response function used as the deconvolution kernel, which is estimated from the data [42]. This method can consider as a model-based method, as it requires a deconvolution kernel. However, the SD method estimate the fiber orientation distribution function (fODF) [144], which is a variant of the ODF function.

The basis of the SD estimation is linear and very fast to compute. As a limitation, the choice of deconvolution kernel is empirical and based on prior assumptions of the data [42]. Moreover, SD methods are very sensitive to noise.

Due to the linear solution of the SD estimation, it suffers several limitations, including the negative fiber ODF values. The original SD improves with nonlinear methods that can deal with the negative diffusion signal values during the deconvolution process. Therefore, to ensure the positivity, a constrained regularization needs to be added. In this way, the Constrained Spherical Deconvolution (CSD) [142] method has been proposed. The CSD method is used to obtain high-quality fODF from the HARDI data, and it has become one of the most widely used methods for obtaining the fiber orientation of white matter. The implementation of CSD is available in MRtrix [3] and Dipy [4]. In this thesis, we used the CSD to reconstruct the diffusion signal.

To conclude, Figure 2.4 illustrates crossing fiber reconstruction through different reconstruction techniques. It shows the diffusion tensor is flat and limited. We also observe that the crossing fibers can be reconstructed efficiently with ODF and fODF.

Peak extraction from the ODF: In order to approximate the direction of the fibers, the principle directions of the fiber ODF or peaks (local maxima) are extracted from the ODFs. The peaks extracted from the ODFs are interpreted as the principle direction of the underlying fiber direction. In general, the local maxima of the ODFs are computed by selecting a large number of points on the sphere and searching the neighbors within a fixed

[3] http://www.mrtrix.org/
[4] http://nipy.org/dipy/

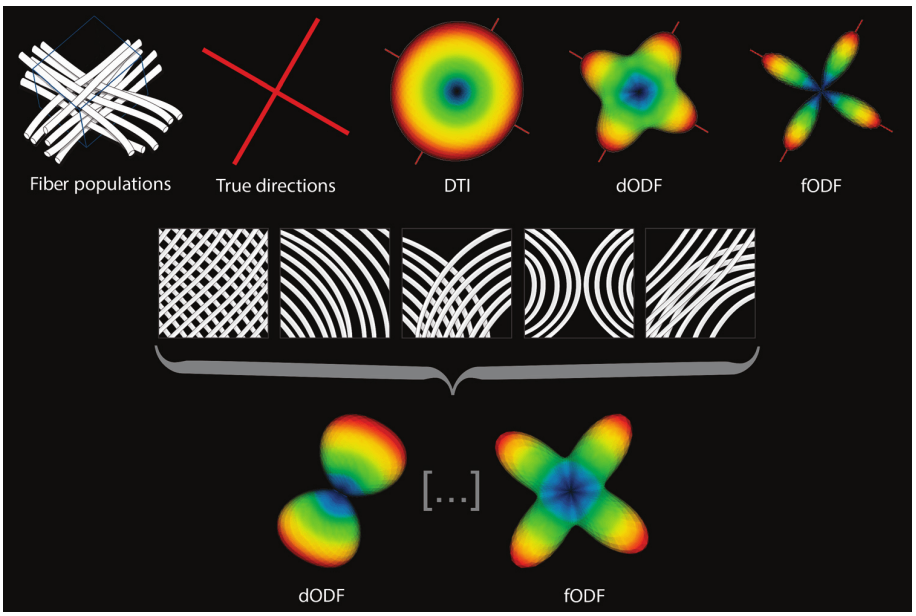

Figure 2.4: Crossing fiber reconstruction with different reconstruction methods [from [42]]

radius [48]. Based on this basic approach, several methods have been proposed to compute the peaks [40, 71, 98]. However, finding the peaks is crucial when the ODFs are noisy and many local maxima present in there.

Multi-shell HARDI

In order to improve the ODF angular estimation, the extra amount of diffusion-weighted images need to be included. Therefore, several methods have been proposed based on multi-shell HARDI acquisition.

Multi-shell Constrained Spherical Deconvolution: Increased interest in acquisition of the HARDI has lead to the extension of the single-shell CSD method to handle the multi-shell data [70]. The multi-shell data incorporates into the CSD by estimating the multi-tissue ODFs. The resulting approach is referred to as the multi-tissue CSD (MSMT-CSD). In contrast with the single-shell CSD, MSMT-CSD can provide information about WM, gray matter (GM) and CSF through the fODF estimates in the voxel. MSMT-CSD increases the precision of the fODF fiber orientations of the WM and decreases the presence of the fODF containing the GM/CSF. Thus MSMT-CSD has the advantage in estimating the high-quality fODF in each voxel.

3*D* **Simple Harmonic Oscillator Based Reconstruction (3*D*-SHORE):** In 2013, the 3*D* Simple Harmonic Oscillator based reconstruction (3*D* SHORE) [93], was proposed, in the class of multi-shell HARDI techniques. With the 3*D*-SHORE method, it is possible to continuously represent the diffusion signal. However, it allows to estimate the diffusion properties, such as EAP and ODF. Additionally, it shows a good perspective to measure the diffusion signal within a clinically feasible acquisition time.

HARDI Limitations

Although the estimation of diffusion signal with HARDI reconstruction is very promising, it is far from being used in clinical purposes. In other words, HARDI-based measures are yet to make a significant mark in clinical

applications, where DTI is mostly used.

HARDI requires longer acquisition time compared to the DTI, which needs to be justified before it can be used in clinical applications. Besides the longer acquisition time, HARDI techniques also cannot differentiate between the crossing, kissing and branching fiber configuration within an imaging voxel [42] (see Figure 2.4). However, the new multiplex MRI scanner is shortening the acquisition time, which give a strong motivation for the HARDI reconstruction.

2.3 Tractography Algorithm

Tractography algorithms or tracking approximate the white matter pathway, by using the directional information from diffusion measurements. The polylines, as representations of the trajectories of the white matter pathway, are known as *streamlines* or *tracks*. A streamline, in this context, is a vectorial representation of thousands of neuronal axons. The whole set of streamlines from the full brain is called *tractogram*. Hence the output of the tractography algorithm is the set of sreamlines in 3-*D* space. In Figure 2.5, an example of generating the streamline from the orientation of the signal within voxels is presented.

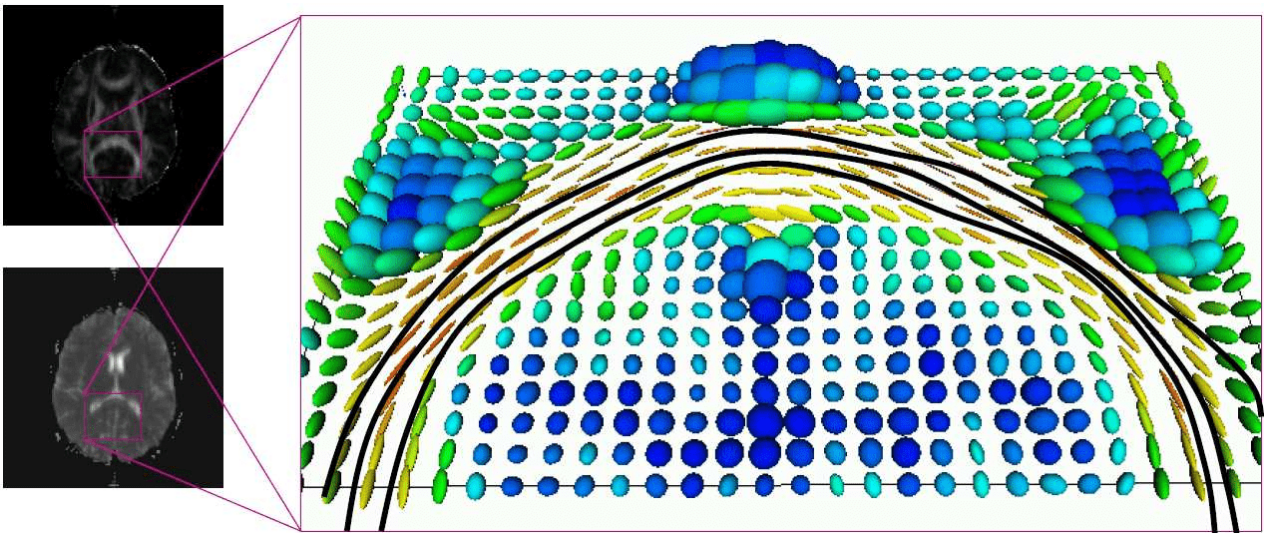

Figure 2.5: Tracking from the diffusion tensor direction information: visualization of the orientation of each voxel from tensor direction information, color encoded from the FA image. The trajectories show the streamline reconstructed by connecting the set of voxels based on the direction in DTI [from [63]]

In recent years, a large number of tracking algorithms have been proposed in the literature. Tractography algorithms can be categorized as local (further subdivided into deterministic and probabilistic) and global [135]. In the following Subsection, we discuss the tractography algorithm based on the local and global approach.

2.3.1 Local Approaches for Tractography Algorithm

Local tracking algorithm uses the local diffusion orientation at each voxel to determine the white matter pathway [63]. It adapts the local greedy criteria to propagate a streamline. According to the local greedy criteria, the

[4] http://cmic.cs.ucl.ac.uk/cdmri10/invited_tournier.pdf

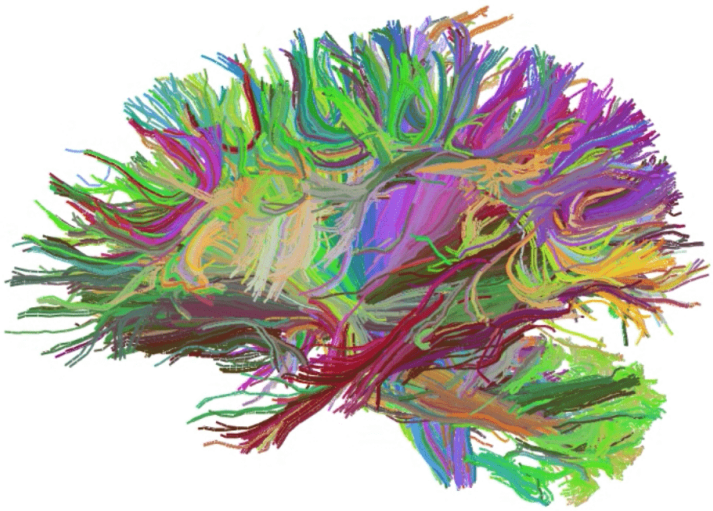

Figure 2.6: Whole brain tractogram with deterministic tractography algorithm based on the EuDX [from [52]]

streamline reconstruction starts from an initial starting (seed) point and sequentially follows with the local diffusion orientation in adjacent voxels.

In general, a local tractography algorithm includes key parameters such as seed selection, maximum and minimum streamline length, masking or stopping criteria for terminating a streamline, and the minimum radius of curvature allowed for building each streamline [36]. Of these, the two most important parameters are the seeding and the stopping criteria. These two parameters have a huge impact on the number of streamlines and the density of the streamline per voxel.

Seeding: Local tracking algorithms require a starting point, which is referred to as seeding, to initially start the propagation of the streamline. In general, seeding can be ROI seeding or white matter mask [63]. In both cases, a defined number of seeds are placed in each voxel to reconstruct the polyline and from each seed point, a streamline is propagated.

Stopping Criteria: Stopping criteria gives an intuition of when the streamline propagation needs to stop [63]. Two different approaches are primarily used in the tracking algorithm as stopping criteria: i) based on white matter mask, (ii) based on the maximum curvature threshold. The stopping criterion based on white matter mask is mainly the threshold mask of FA. With the white matter mask, in the case of low anisotropy, the tracking stopped due to the fact that uncertainty of the principal diffusion direction is high at that point. Nevertheless, low anisotropy sometimes occurs due to the crossing fiber per voxel. In that case, many true positive pathways may not be revealed with the stopping criteria. A second common stopping criterion is the maximum curvature threshold. The curvature threshold aims to avoid fast change in the streamline direction as the white matter fibers do not represent high curvature. In addition, another stopping criteria proposed in [129] uses anatomical information from the anatomical-contrast images to determine where the streamline needs to terminate. The presence of the anatomical information can exploit the seeding for tracking from the gray matter and white matter interface. The tractogram generated with this anatomical constraint is known as the anatomical-constrained tractography (ACT).

The local tractography algorithm can be divided into two subcategories: the deterministic streamline tractography and the probabilistic streamline tractography [135]. Following, we present the algorithms proposed in the

literature in both categories.

Deterministic Streamline Tracking algorithm

The deterministic tracking algorithm [9] is a simple and fast algorithm to propagate the streamline. In general, the *deterministic tracking algorithm* uses the most probable direction of diffusion model to integrate the trajectories and propagates streamlines by making a series of discrete local optimum decisions. Deterministic tracking initially was applied with the DTI reconstruction model but was later extended to utilize the multiple orientations estimated in single voxel by the HARDI reconstruction.

Following we discuss different deterministic tracking algorithms by underlying whether they work with the tensor or the HARDI methods.

In the case of DTI-based deterministic tracking, tensors are computed through the diffusion tensor reconstruction models, then the tractography algorithm takes the direction from the tensor to generate the streamline. One of the earliest algorithms in the class of deterministic tracking algorithms is the Fiber Assignment by Continuous Tracking (FACT) [94], which is based on the DTI reconstruction. The FACT algorithm starts from an arbitrary point in the white matter and propagates in both backward and forward directions. Like the DTI reconstruction, FACT tracking has the limitation for tracking the cross fiber in the voxel. Other methods that have also been proposed in this class by differentiating between different tracking algorithm parameters can be found in [34, 95].

As the HARDI reconstruction method can overcome the limitation of the crossing fiber within a voxel, an extension of the deterministic streamline tractography algorithms has also been proposed based on the HARDI reconstruction in the literature. In that case, tracking algorithms utilize the multiple fiber orientations in a single voxel. The proposed deterministic tracking algorithms were based on the classical diffusion ODF reconstruction from q-ball imaging (QBI), the principle direction of the dODF was computed from the DSI, and the fODF from the spherical deconvolution, etc [23].

In 2012, the EuDX (Euler integration Delta function fiber crossings) algorithm [52] was proposed. The EuDX algorithm can be applied with both the DT and the ODF model reconstruction from the HARDI. In the case of HARDI reconstruction, any number of crossing fibers can be used for the tracking, depending on the reconstruction methods. As the EuDX algorithm places more emphasis on the reconstruction model, it becomes a robust algorithm to inspect the different reconstruction results using the streamlines. EuDx algorithm is available in Dipy `http://nipy.org/dipy/`. Figure 2.6 shows the tractogram generated with the deterministic EuDX algorithm.

Another deterministic streamline tracking algorithm with the HARDI reconstruction was proposed in [140]. The fiber orientation was estimated from the FOD and tracking was processed with the orientation of the nearest FOD peaks. This algorithm is available in `http://www.mrtrix.org/` and is referred to as the *SD_STREAM* or *iODF*1 in MRtrix.

Limitations: Although the deterministic algorithm is simple and very fast, it has some limitations. Deterministic algorithms have a conservative strategy in choosing directions at each step of streamline generation. The consistent choice of the maximum peak of the reconstructed model of voxel diffusivity neglects the uncertainty of its estimation process. It should be worthwhile to explore directions that are close to the maximum peak. A less restrictive strategy in choosing the direction of a streamline may reduce the consequences of the error in reconstructing the model of voxel diffusivity.

To overcome the limitation of the deterministic algorithm, probabilistic tractography algorithms have also been proposed.

Probabilistic Streamline Tractography algorithm

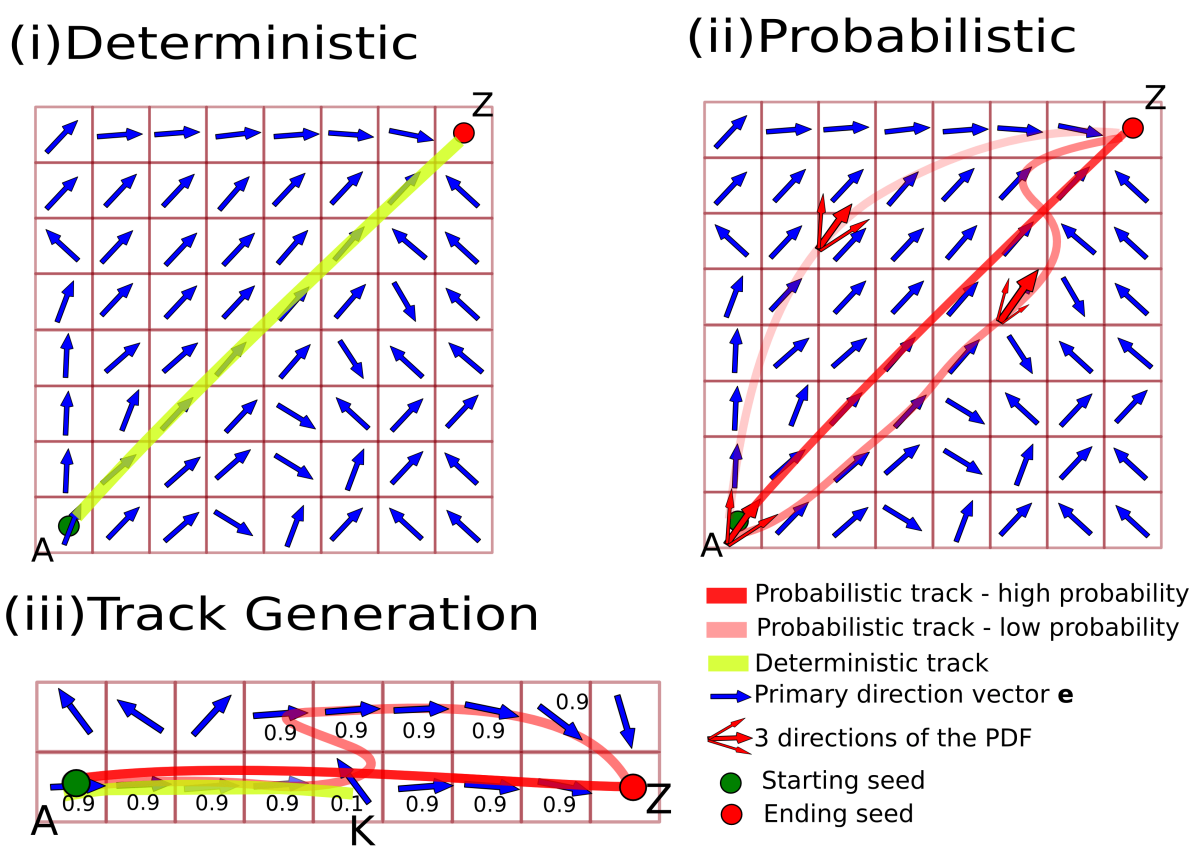

Figure 2.7: A simplified 2D example to distinguish between the deterministic and probabilistic tracking algorithm: (i) the yellow line depicted a single trajectory generated by the deterministic tracking algorithm, (ii) three possible pathways, generated by the probabilistic tracking algorithm, (iii) probabilistic and deterministic tracking with a very simple example with weights of the direction, shown by a given example. Image taken from [52].

The probabilistic tracking approach [10] is currently one of the most promising streamline tracking algorithms to generate the tractogram. It mostly uses the orientation distribution function and its variants, for example, diffusion Orientation Distribution Function (dODF), fiber orientation distribution function (fODF), and 2nd order integration over fiber orientation distribution (iODF2) from each voxel in order to propagate the tracking. The aim of the probabilistic tracking algorithm is to generate the multiple pathways estimated from the seed point and to assign the probability to the reconstructed pathway. Then, the set of all possible paths are traced and connected. Additionally, it can propagate the streamlines even when the direction is unclear. The output tractogram, reconstructing from the probabilistic tracking algorithm, contains a large number of streamlines.

In Figure 2.7, we have shown a simplified 2D example to distinguish between the deterministic and probabilistic tracking algorithm. Subfigure (i) shows one local direction in each pixel in blue and the generated trajectory with deterministic tracking algorithm in yellow. The deterministic tracking takes into account the only one direction in each pixel and propagates the track. In Subfigure (ii), in each pixel, the orientation of the blue vector can be represented by a PDF. The three combined red arrows represent the three directions of the PDF, among many directions that are possible for each pixel. With the simple toy example, in Subfigure (ii), we have shown three

possible trajectories generated by the probabilistic tracking algorithms, i.e. two possible one in light red and the diagonal one in deep red. In Subfigure (iii), a simple example is shown only with two rows of the pixel, in order to understand the value of the more probable trajectory. In the rows, we kept two values 0.9 and 0.1 which represent two directions. We referred to the discontinuous position with 0.1 as K. The figure shows that the deterministic tracking has stopped in position K (in yellow) and the probabilistic tracking generated two possible trajectories in light and deep red.

A number of different approaches have been developed for the probabilistic tracking algorithm. Proposed methods differ in the orientation function and how to assess the uncertainty of the orientation.

Although the probabilistic tracking algorithm mostly uses the ODF information, some methods also propose using the tensor information [74]. In [74], the proposed technique utilized the tensor information and the bootstrap technique was used to derive the uncertainty of the data, that is, it was used as a prior assumption to assign the probability. This algorithm is available in `http://www.mrtrix.org/` and referred to as the *Tensor_Prob* in MRtrix.

In [40], the author proposed a probabilistic tracking algorithm to generate the tractogram based on the ODF from the HARDI. They used a fiber ODF estimation obtained from the SD reconstruction model of the dODF from QBI. This method can accurately produce a set of fibers but failed to reflect the continuity of the fibers between the cortical and subcortical regions. In [25], another probabilistic algorithm for the QBI is proposed. This algorithm was an extension of the FACT deterministic algorithm, named as modified fiber assignment using the continuous tracking (MFACT). This algorithm used the diffusion model reconstruction from QBI and was able to handle the multi-fiber directions within each voxel. This method lacks validation and comparison with other methods.

In [141], another probabilistic tracking algorithm was proposed based on the probability density function (PDF). This method was based on the 2nd order integration over fiber orientation distribution (denoted as iFOD2) and the probability was approximated by computing the product of the amplitude of the FOD. The proposed tracking algorithm has the capability to track accurately in the crossing fiber regions and generate less invalid streamlines. This algorithm is available in `http://www.mrtrix.org/` and referred to as the *iODF*2 in MRtrix.

Limitations: Although the streamlines produced by the probabilistic tracking algorithms can cover more anatomical bundles or tracts compared to deterministic tracking, it has the limitation of producing invalid streamlines. In this context, streamlines can be considered invalid if i) they are connected with ROIs that are not expected to connect, or ii) their connections exit from the expected fiber bundle mask [36]. It also contains the streamlines which have no connection between two ROIs. Hence producing a large number of invalid streamlines limits the probabilistic tracking algorithms.

2.3.2 Global Approaches for Tractography Algorithm

Unlike the step-by-step fitting of the pathway by the local tracking algorithm, the global tractography algorithm fits the entire pathway by using the diffusion orientation of all voxels along the pathway length. It tries to address the limitations of the probabilistic algorithm by increasing the resistance of the noise during tracking. Moreover, to handle the connectivity issue of the probabilistic algorithm, the global approach proposes the distance independent tracking method.

Global approaches identify the best path between two endpoints of a region by identifying an optimal path, according to some optimization criteria. To do that, the approach takes into account the global properties along the entire curve to generate fiber trajectories.

In the literature, several global tractography algorithms have been proposed. A global Bayesian model is proposed in [67]. In regions with low uncertainty, the trajectories are represented by splines, which are compatible with the local fiber orientations. Consequently, with high uncertainty, the global connectivity constrains the local parameter estimation to reconstruct the fiber trajectories. In [99], another method is proposed based on the front evolution and it computes the path for the maximum diffusivity between two points. The maximization of the global diffusivity is done by the minimization of the integral path. This approach is fast and less sensitive to noise. Other interesting and promising global tractography approaches can be found in [110, 143].

Limitations: Global tractography algorithms need to search a large solution space that is composed of all the connections between two regions. Searching in large solution space requires a high computational time and a large amount of memory [131]. This is considered as a limitation of the global tractography algorithm.

Tractography Cleaning:

Tractograms generated through the tractography algorithm contain a number of invalid or false-positive streamlines due to several reasons, such as, noise of the diffusion data, improper integrals of the reconstruction, and tracking methods. Thus the postprocessing steps of the tractogram have also been introduced to filter out the invalid streamlines. Tractogram filtering is also referred to as tractography cleaning, which is still an open problem due to the criteria needed to filter the streamlines. Nevertheless, a few promising methods, such as COMMIT [38] and LiFE [112], SIFT [130] have been proposed in the literature as part of the active research in this topic.

In 2013, a tractogram filtering method called Spherical-deconvolution informed filtering of tractograms (SIFT) [130] was proposed. The method proposed improving the accuracy of the reconstruction technique by fitting the streamline distribution along with the diffusion signals in each voxel. In that case, the diffusion signal was generated from the SD methods and then the streamlines were generated. Hence a better measure of the diffusion signal can be obtained from the streamlines generated by SIFT algorithm.

In 2014, another method, called Linear fascicle evaluation (LiFE) [112], was proposed to evaluate the result of the tractography algorithm. Instead of generating the streamlines like the previous method (SIFT), the LiFE method takes the tractogram as input and predicts the diffusion signal. The prediction error, that is, the difference between the predicted and measured diffusion signals, is then computed in order to evaluate the tractogram. Although it is a very promising method, it has the limitation to address all the streamlines from the whole brain tractogram.

In 2015, another method, named the Convex Optimization Modeling for Microstructure Informed Tractography (COMMIT) [38], was proposed to enrich the tractogram data. It proposed to combine the estimation of local microstructure properties of the tissue with the tractography algorithms, in order to make the tractogram more related to the anatomy. From a set of streamlines, the diffusion signal in each voxel was modeled and globally fitted the signal through a global weight which was measured by solving the convex optimization problem. COMMIT is a fast, accurate and widely used method for tractogram filtering.

2.4 Tractogram Registration

In neurological studies, it is important to study the diffusion properties among a group of subjects. In order to study the across subject diffusion properties, it is necessary to find a correspondence between the anatomical structure of different subjects. For this purpose, tractograms from different brains need to be aligned.

The most common approach to aligning the tractograms is registration (known as *tractography registration*). Theoretically, registration is the method of spatial adjustment of the images by applying a geometric transformation or the deformation to the images. In the context of dMRI, registration techniques can be applied to both the voxel of the diffusion image and the streamline of the tractogram [64]. Hence we divide the discussion of the existing tractogram registration into two groups: *voxel-based* and *streamline-based* registration.

Both the voxel-based and streamline-based registration can be linear or nonlinear. Linear registration applies the global translation, rotation, scaling and shears on the input images for aligning with the reference images. In contrast, nonlinear registration applies the local wraps instead of using global transformations. We divide both the voxel-based and streamline-based registration into two subcategories: linear and nonlinear registration.

2.4.1 Voxel-based Tractogram Registration

Voxel-based registration is applied on the voxel of the diffusion images. In this case, the input images could be the diffusion image from one subject (or brain), and the reference image could be the diffusion image from the same brain, a different brain, or the image made by averaging images from the different brains, referred as normalized image. A widely used normalized image is the Montreal Neurological Institute (MNI) template, which is a standard brain image based on the averaging of 58 people [52].

The images used in the voxel-based registration can be diffusion images with different modalities. Three different modalities were used so far: *scalar-based*, *tensor-based* and *the spherical harmonics* based [55]. Voxel-based registration can be categorized into the linear and nonlinear approaches. Linear approaches transform all the voxels by applying a single linear function or linear transformation, while nonlinear approaches [28, 27, 30] provide a deformation field that assigns a displacement vector to each voxel [55].

Voxel-based Linear Registration

Voxel-based linear registration approaches applied to the scalar images, for example, fractional anisotropy (FA) images, non-diffusion-weighted $(b0)$ images, the $T1$ weighted images (sequence from the MRI).

The most widely used scalar volume for the linear transformation is the FA image or the non-diffusion-weighted $(b0)$ images. By using the FA or $b0$ images, the transformation matrix is recovered through various registration techniques and then the transformation matrix is applied to the diffusion tensor images in order to align two diffusion images [86, 136]. The proposed registration techniques for voxel-based linear registration are as follows: the rigid registration method, which is based on the normalized mutual information [136], the multiresolution elastic matching algorithm [3], multiresolution B-spline method [125], B-spline registration based on the sum-of-squared-differences (known as the FSL/FLIRT) [68], and affine image co-registration techniques.

Advantages and limitations: The main advantage of linear registration with scalar images is that it can use any intensity-based medical image registration technique to register the diffusion images. Moreover, the computational complexity of linear registration is very low. Nevertheless, registration on scalar images does not take into account the directional information of the DTI images which limits this type of registration technique.

To overcome the limitation of registration with scalar images, a number of approaches have been proposed to utilize the orientation information by using the diffusion tensor [57, 108, 66, 161]. Registration using the tensor images is more complex due to the multidimensionality of the diffusion tensor data. Moreover, tensor orientation needs to maintain consistency with the anatomical structure before and after registration. Several tensor-based registration techniques have been proposed in the literature. In [108], the author uses an iterative process to register

the diffusion tensor images by using various features of the tensor. In [165], the author proposes diffeomorphic deformable tensor registration by explicitly exploring the tensor orientation from the whole brain. This method is known as the Diffusion Tensor Imaging Toolkit (DTI-TK). In addition, other approaches have been proposed based on different techniques, including finite-strain diffeomorphic registration, elastic registration [161], and tensor orientation features with neighborhood interpolation [66].

Advantages and limitations: As mentioned before, the DTI-TK method requires tensor reorientation steps to maintain the consistency between the anatomical structure and tensor direction. In this way, it ensures that the tensor orientation will remain consistent before and after the registration, which is an advantage of the tensor-based methods. The resulting computational cost for the reorientation is considered as the limitation of this kind of approach.

Voxel-based Nonlinear Registration

At present, the nonlinear registration approaches are the most accepted registration techniques in the neuroimaging community. Like linear registration, nonlinear registration can be applied to the FA or T1 image, or to the tensor or fiber orientation distribution functions (ODF) [116]. In the case of nonlinear registration, deformation fields are extracted from the images and applied locally to each of the voxels of the diffusion images. More precisely, the deformation fields [151] are being optimized using the cost functions of each voxel. However, most of the nonlinear methods initially applied a linear registration to match the images globally before applying the nonlinear registration.

Among the voxel-based nonlinear registration techniques, one of the well-known algorithms is the FSL/FNIRT (FMRIB's nonlinear image registration tool) [69]. This method works only with volumetric or scalar images, that is, FA or b0 images. In principle, it registered the FA or b0 images from a subject to a popular FA template, generated by averaging the FA images from the different brains. By optimizing the registration, it extracted a small deformation field which applied back on the FA image of the subject to be registered. Another high-performing nonlinear registration is the Advanced Normalization Tools (ANTs) [7], which is based on the symmetric normalization algorithm (denotes as SyN) and the optimization is done with the Euler-Lagrange equation. This method is applied on the FA or T1 weighted images. In [117], the authors proposed a nonlinear method that register the FOD images including appropriate reorientation and modulation.

Advantages and limitations: Nonlinear registration based on the volumetric images is now a widely used technique. It also outperforms linear registration techniques. Nevertheless, this kind of technique has the limitation to re-generate the tractogram after transforming the dMRI data accordingly. The cost of regenerating tractograms may be high, in terms of computation time and required knowledge to operate the full pipelines of preprocessing, reconstruction, tracking, and filtering.

2.4.2 Streamline-based Tractogram Registration

Streamline-based registration techniques, also known as direct registration, use the streamline information from the tractogram [55]. Besides the streamlines, no other information from dMRI data is used for the streamline-based registration. Therefore, this kind of method can avoid the registration error of diffusion images and can improve the accuracy of the registration technique.

The streamline-based approach is a recent approach and, therefore, very few publications are available [55]. In this thesis, we are also interested in methods for tractogram alignment that directly operate on streamlines.

Streamline-based Linear Registration

In the case of streamline-based linear registration, an affine transformation is computed and then applied to the coordinates of the streamline. In principle, affine transformation can be computed from the voxel-based linear registration, for example with FSL/FLIRT, or from the streamlines.

One of the first works in this category is proposed in [79]. There, curvature and torsion features were used to represent each streamline in a multi-scale framework. A mean square difference was used to measure the similarity between streamlines at different scale levels. The method tried to match each streamline individually, making the method computationally expensive. Point-based registration [90] have also been proposed to register the tractograms. In a point-based approach, each streamline was represented by a spatial coordinate sequence and projected into a high dimensional feature space. The registration problem was then treated as a point set alignment problem. The problem was resolved by efficient Interactive Closest Feature point (ICF). The computational complexity of the high dimensional search was handled by implementing approximate NN techniques. This method was limited by inter-subject registration and was demonstrated only with the pre-selected tracts (bundles of interest). Another type of linear registration was proposed in [170], where the streamlines were projected onto high dimensional feature space with a 3-D coordinate sequence. A fiber model was extracted by the adaptive mean shift (AMS) clustering and the weight of each fiber model was assigned by the Gaussian Mixture Model (GMM). The registration was performed as the alignment of two GMMs by maximizing the correlation ratio.

Recently, new linear methods have been proposed to directly register whole tractograms, see [102, 55], without the intermediate step of registering volumetric images. These methods find an affine transformation that minimizes a given loss function computed only from streamlines. In [55], the loss function is based on a streamline-streamline distance of a subset of all streamlines. Another unbiased multi-subject registration is proposed in [102]. There the registrations are done by minimizing the entropy-based objective function. The distance between the streamlines is calculated and the kernel density estimation is used to transform the distances into probabilities. Then the Shannon entropy of the distribution of streamlines are computed. Note that the Shannon entropy is considered as the objective function, which is minimized over the set of affine transformations and the final transformation matrix is retrieved. Although this work showed the advantages of group-wise registration, it has the limitation to resolve the affine transformation.

Limitations: Streamline-based linear registration is promising as it doesn't require the diffusion MRI information. However, a single affine transformation can reconcile the part of the differences of the tractograms of two subjects; it cannot address the difference at the local level, that is, the systematic displacements of entire tracts, longer or shorter tracts, and tracts with more or fewer streamlines.

Streamline-based Nonlinear Registration

The literature on streamline-based nonlinear registration is mainly focused on the bundles or tracts alignment.

In [169], the authors developed the log-Euclidean polyaffine framework for the nonlinear registration algorithm. Corresponding tracts were aligned across subjects by warping their spatial probability maps computed from the coordinates of the streamlines. In [168], consistency clustering is used to label streamlines in an iterative process with polyaffine transformations. In [159], a diffeomorphic registration algorithm is used on the Gaussian

process representation of streamline density maps. In [47] streamlines were represented as current and the distance defined based on the spatial distribution of the mean local tract direction. Moreover, the framework of *currents* is proposed to warp the streamlines of tracts for registration, atlasing and variability analysis. This literature addresses nonlinear bundle alignment but not whole tractogram alignment, also for the high computational cost of the algorithms. Another approach to nonlinear registration of streamlines is to use deformation fields, computed from nonlinear volume registration, directly on streamlines. This approach is mentioned in [29], but without a quantitative evaluation of its effect.

Limitations: Nonlinear streamline-based registration algorithms have a high computational complexity. Moreover, these techniques limited to apply on the tract alignment, not on the whole brain tractogram.

2.5 Tract Segmentation

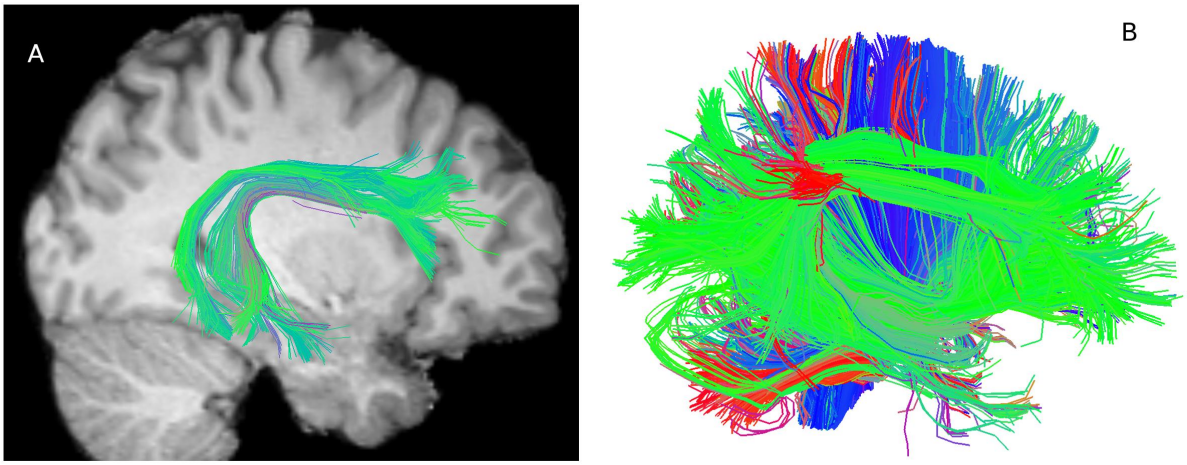

Figure 2.8: Tract segmentation: (A) a segmented right arcuate fasciculus (AF) tract from the whole brain tractogram and segmented by the expert neuroanatomists. T_1 weighted image slice is visualized along with the tract (B) The whole brain tractogram generated with EuDX [Image taken from [52]]

All of the streamlines from a whole brain tractogram are not immediately useful for clinical purposes [103]. Therefore, they need to be organized into anatomical meaningful structures. Streamlines belonging to the same anatomical area are called *tracts* or *bundles*. Grouping or organizing the whole brain tractogram into an anatomical meaningful tract is known as the *tract segmentation problem* [103] (see Figure 2.8). In Figure 2.8, we have shown an example of the tract segmentation. Subfigure A showed the segmented arcuate fasciculus (AF) tract along with the $T1$ weighted image slice. The AF tract is segmented from the whole brain tractogram (see Subfigure B) by the expert. However, once the segmentation is done, the statistical analysis over the tract is used in multiple applications, for example, to study gender differences [65], and to observe changes in age [122] and to correlate it with diseases [14, 109].

Several tract segmentation approaches developed over the last few years can be divided into manual and automatic tract segmentation approaches. The manual approach, also known as *virtual dissection* [96, 154, 24], extracts the tract using the ROIs defined by neuroanatomical expertise. Even though manual ROI-based methods give very

impressive tract segmentation results, these methods still have big constraints to involve neuroanatomical expertise and also require a great amount of time.

Automatic tract segmentation methods can be categorized into three difference large groups: ROI-based segmentation, unsupervised tractogram clustering, and supervised tract segmentation.

2.5.1 ROI-based Segmentation Technique

In the automatic ROI-based approach, as for the manual approach, tracts are excluded by applying a set of ROIs. In this case, instead of involving the neuroanatomist directly, an anatomical atlas was used with expert provided ROIs. Automatic ROI-based tract segmentation is required to perform the linear or nonlinear registration to an anatomical atlas in advance [1, 167]. In [167], the author proposed using large deformation metric mapping (LDDMM) for nonlinear warping an atlas with ROIs to segment the tracts from an individual subject. However, it has to be noted that the registration to the atlas can cause loss of information present in the diffusion images [146]. Automatic ROI-based methods are known to provide remarkable results [62], meaning they are sometimes used as ground truth to validate the result of other segmentation methods.

Another automatic segmentation technique also proposed utilizing the additional information from the ROIs, that is, cortical parcellation into ROIs. This method is also referred to as the automatic parcellation-based segmentation approach [157] which draws the attention nowadays. Parcellation-based methods take advantage of the cortical parcellation and address the question of which part of the streamline may be connected [17, 139] in order to segment the tract. Moreover, it divides the tract according to the cortical regions or nodes that they connected and enables the study of the brain as a network. A good review of parcellation based segmentation methods can be found in [101]. Among the parcellation-based automatic segmentation methods, the white matter query language (WMQL) [157] is one of the most adopted. Tracts are extracted by the anatomical position based on a cortical parcellation from the Freesurfer. In this work, we used the WMQL to generate the ground truth label for the tracts.

Limitations: The automatic ROI-based approach requires the registration of the subject to an atlas. By doing the registration, there is a chance to lose the information present in the diffusion images. In the parcellation-based approach, segmentation techniques only focus on the parcellation without considering all the streamlines from the whole brain tractogram.

2.5.2 Unsupervised Clustering Technique

The unsupervised approach, also known as *fiber clustering*, is one of the most widely used tractogram segmentation techniques in the literature [128, 54, 146, 118]. The purpose of clustering is to group the streamlines according to their mutual similarity (or distance), in an anatomical sense. Clustering methods mostly address the single-subject and are unable to address the problem across subjects. The main challenge of clustering methods is to incorporate the human anatomy into a clustering result.

During the last few years, various clustering based segmentation methods have been proposed. A detailed survey of clustering methods used in the literature can be found in [101, 138].

In unsupervised clustering methods, there are two main aspects: i) a well-defined similarity measure and ii) the clustering technique [138]. Similarity measures, proposed in the literature, are mostly based on different streamline distance functions. Various streamline distances have been proposed in the literature, for example, Hausdorff distance [35, 100], Minimum Average Direct Flip Metric (MDF) distance [54], average point distance along with the dot product of the tangent [128], the closest point distance and mean of closest point [35], and Euclidean

distance [44]. Besides the distance, streamline properties are also used for the similarity measure, for example, a 9-D shape descriptor for the streamline including the main coordinate (three numbers) and its covariance matrix (six numbers) [16], and the curvature of the streamline [87].

Both the spectral [128, 16, 73, 44, 54, 100, 118] and hierarchical clustering [166, 61, 153, 120, 146] approaches have been applied to cluster fiber tracts in the literature. In the case of spectral clusterings, the following methods have been proposed: Fuzzy C clustering [128], K-nearest neighbors [44], normalized cut [16], and K-means [100], mini batch k-means [113].

Limitations: The main challenges of the clustering method are twofold: i) handling a large amount of data and ii) incorporating the human anatomy into a clustering result, that is, automatic labelling of the cluster. Clustering techniques require the computation of the pairwise similarities between streamlines which grow quadratically with a number of streamlines. Hence it suffers high computational complexity. However, to extract the anatomical meaningful tracts from the clusters, it has the obligation to incorporate the clusters with an atlas. It is not clear how this incorporation is performed as the clusters are in streamline-level and the atlas is in voxel-level. Hence the projection from the voxel to streamline level is still questionable and limited the clustering technique.

2.5.3 Supervised Tract Segmentation

As clustering methods suffer the problem of automatic labelling of tracts, several *supervised segmentation* methods have been proposed to deal with this limitation [54]. In supervised learning, the main perception is to learn about the tract in advance by adopting prior knowledge. After learning or training, the task is to segment the tract from a new subject. Based on the two kinds of prior knowledge, we divide the proposed supervised tract segmentation approaches into two different categories: i) *Atlas-based supervised segmentation* and ii) *Model-based supervised segmentation*.

Atlas-based Supervised Segmentation

In atlas-based supervised segmentation, prior knowledge can come from expert labelling of an anatomical atlas, see [87], or from labelling clusters of streamlines from multiple subjects in a process of atlas creation, see [103, 152, 62, 162, 77]. Once the atlas is available, the segmentation of the tract of interest in a new subject can be carried out.

In the case of an anatomical atlas, a set of ROIs specified by the expert were provided as the prior knowledge and tracts were extracted by generating the streamlines from the ROIs [87]. Furthermore, in order to segment the new subject, streamlines from the new subject were represented by B-spline representation and k-nearest neighbor (KNN) was computed in order to assign the anatomical label to the most similar streamline.

Atlas can be created from multiple subjects and used as prior knowledge for the supervised segmentation method. In [103], a high dimensional atlas was reconstructed from multiple tractograms. Initially, a subset of streamlines from the whole brain tractogram was selected from each subject and embedded with the spectral embedding. In order to group the streamlines, unsupervised k-means clustering was applied in the embedding space and obtained clusters were labelled by the expert to create an anatomical atlas of white matter tracts. Then the tracts of the test subject were aligned with the atlas and the closest cluster centroids were computed to assign the anatomical label. Instead of unsupervised clustering, linear Support Vector Machine (SVM) was used in [152] to classify the tracts. Both of these above-mentioned methods are computationally demanding.

In [62], a single atlas-based approach was proposed, based on the expert provided tracts from multiple subjects. A single atlas was constructed in advance by applying the intra-subject clustering, followed by the inter-subject clustering. The inter-subject clustering first extracted the tracts and then merged the tracts based on the pairwise distance between the centroid from each subject. The test subject was labelled by finding the closest centroids from the single subject to inherit the anatomical label. This method highly depends on the number of subjects involved in constructing the atlas and suffers from high computational complexity. Moreover, merging various clustering (intra-subject and inter-subject clustering) techniques made this approach complex and complicated.

Recently, a faster version of the method in [62] was presented in [77]. There, they proposed to accelerate the automatic labelling of the test subject by filtering the streamlines. Filtering was done based on the streamline distances from the single atlas. An extensive investigation on the Euclidean distance between streamlines was performed to find the streamlines to filter. Although this method is very impressive in terms of time, the method needs to specify a *segmentation threshold* for each tract which is crucial to select.

In [162], another supervised segmentation method was proposed based on multiple atlas. In contrast to the construction of the single atlas by combining multiple subjects (like in [62]), here each subject is treated as a single atlas and in this way a multiple atlas was created. In principle, to create the multiple atlas, agglomerative clustering is applied to each subject and then with the help of the expert, the label of the cluster is assigned. For automatic labelling of the new subject, a voting scheme has been proposed which includes two thresholds, a distance threshold, and a vote threshold. Additionally, they implemented a GPU to execute the experiment. This method is indeed based on a very simple concept, and is also efficient and very flexible about the number of multi-atlas datasets. However, agglomerative clustering and strong dependency of threshold values are the main limitations of the method.

In summary, existing atlas-based segmentation has some limitations, the main ones being the high computational cost [103, 152], a dependency on the number of subjects to construct the atlas in the case of a multiple atlas [62], and a dependency on the definition of threshold values [162, 77].

Model-based Supervised Segmentation

In supervised segmentation, besides atlases, other kinds of prior information can be used as prior knowledge, such as models or features of tracts/bundles. Models are built to describe tracts/bundles and not the whole tractogram. We referred to these segmentation techniques as *model based supervised tract segmentation*.

One of the very first methods in this class is proposed in [32]. Here, the authors proposed segmentation based on a parametric tract model. A parametric model, based on the beta mixture model of similarity cosines of the tract was computed by learning the angular continuity and inter-fiber directional similarity of the probability distributions. Afterwards, the parametric model was matched with the new subject in order to extract the tract. Various parametric models of tracts have also been proposed in the literature, for example, the Gamma Mixture model of the distance [89], the Gaussian process of the tract probability map [156], and the hierarchical Dirichlet process mixture model [155].

Whether model-based supervised segmentation gives the benefit of finding the specific tract of interest from the test subject, it has the limitation of using a limited number of tract segmentation, depending on the availability of the tract model.

Supervised Tract Segmentation: Key Aspects

In this section, we give a comprehensive summary of the supervised tract segmentation literature. In order to organize the body of work in this field, we articulate the discussion along these five topics: alignment, embedding space, similarity/distance, correspondence techniques and refinement step.

Alignment

In supervised tract segmentation, tractograms are initially aligned to an atlas. Both voxel-based and streamline-based atlases have been used in literature, e.g. white matter ROI-based anatomical atlas [87], high dimensional atlas [103, 152], example-based single atlas [62, 77], example-based multi-atlas [162]. To the best of our knowledge, the specific step of alignment has been conducted with standard methods: in most of the cases with voxel-based linear registration [103, 62, 162] and in the others with nonlinear voxel-based registration [152].

Embedding space

Streamlines are complex geometrical objects with a different number of points one from another. They are unfit to be directly given as input to many efficient data analysis algorithms which, instead, require vectors all with the same number of dimensions. Tractograms are large collections of streamlines, from hundreds of thousands to millions of streamlines, and their analysis is often limited by the required computational cost. A common preprocessing step before using algorithms like clustering, or nearest neighbor, is to transform streamlines into vectors, a process called *Euclidean embedding*. Different authors opted for different embedding approaches, like the spectral embedding [103], the re-sampling of all streamlines to the same number of points [162, 62, 77], the use of B-splines with re-sampling [87] and the dissimilarity representation [105]. Re-sampling all streamlines to a fixed number of points is the most common approach to obtain the embedding. In principle, up-sampling/down-sampling to a particular number of points may cause the loss of information. On the other hand, spectral embedding has high computation cost. The dissimilarity representation has shown remarkable results in terms of machine learning applications [104] and exploration of tractograms [113], at a moderate computational cost.

Streamline Distance

In order to find corresponding streamlines from one tractogram to another one, the definition of the streamline distance plays a crucial role. Most commonly, the corresponding streamline in the new tractogram is defined as the closest one, for the given streamline distance function. Similarly, when doing clustering for tract segmentation, the streamline distance function is a fundamental building block. Different streamline distance functions have been used in the supervised tract segmentation literature, e.g. minimum closest point (MCP) [103], symmetric minimum average distance (MAM) [105], minimum average flip distance (MDF) [162], Hausdorff distance [87], normalized Euclidean distances [77], Mahalanobis distance [162].

Correspondence technique

One crucial aspect of supervised tract segmentation is the mechanism to find the corresponding streamline between the tractograms of different subjects, in order to transfer anatomical knowledge. A common approach for addressing such problem is to use the nearest neighbor strategy, i.e. finding the nearest streamline or centroid in the atlas and labelling the streamlines of the new subject based on that. In [103], a high dimensional atlas was reconstructed from multiple tractograms. Then the new subject was aligned with the atlas and the closest cluster

centroids from atlas were computed to assign the anatomical label. In [62], nearest centroids of the new subject were computed from a single atlas from multiple subjects, with the normalized Euclidean distance. Recently, a faster implementation has been proposed in [77]. There, they proposed to label each single streamline instead of cluster centroids and to accelerate the computation time by filtering the streamlines in advance, using properties of the normalized Euclidean distance. A limitation is that an appropriate threshold has to be defined for each tract to be segmented. Similarly, in [162], the nearest neighbor strategy is used to find corresponding streamlines between those of the tractogram of a new subject, with those of multiple example-subjects (12, in their experiments). Again, two thresholds, i.e. a distance threshold and a voting threshold, are required to be set in order to obtain the segmentation. The proposed implementation requires a GPU.

Refinement

After segmentation, in order to improve the accuracy of the segmented tract, a few authors propose a refinement step, for example, to identify and remove outliers. In [91], a tree based refinement step was introduced. Initially, they padded the segmented tract with the nearest neighbors and then used a probabilistic boosting tree classifier to identify the outliers.

Another common approach used for the purpose of refinement is referred to as the *majority voting* [119]. In [162], authors proposed a voting scheme in order to label the tract. Every example subjects vote the tract of the test subject, based on the similarity of that tract with the example subjects. After collecting the votes from every example subjects, the majority of votes is computed, in order to label the tract. In [152], authors used the majority voting for validating their segmentation method with the k-means algorithms. In [72], authors proposed to use the majority voting, in order to accurate the segmentation result. Here the Hausdorff distance metric used in the clustering approach in order to select the similar shape streamline and if the streamline appeared twice out of four clustering result, they consider that streamline as the true streamline.

2.6 Conclusions

In this chapter, we studied the theoretical background of dMRI and tractogram. We presented a brief description of the dMRI, a non-invasive technique for studying the brain anatomical connectivity. dMRI measures the translational displacement (diffusion) of water molecules in the brain tissue, which is mechanically constrained by the myelinated axons. Thereby, it provides information about the local orientation of white matter axons and able to capture the local diffusion phenomena of water molecules. Next, we reviewed the techniques to locally model the diffusion signal. We started the discussion with DTI, a simple method for the diffusion signal reconstruction and continued with the HARDI reconstruction methods.

From the local orientation of the diffusion, tractography algorithms reconstruct the approximate trajectories of the axons as polylines or streamlines, so they resemble the white matter anatomical structures. Several tracking algorithms exists in the literature and in this chapter, we presented the local and global approaches of the streamline-based tractography algorithms. We have discussed the pons and cons of every tracking algorithm and observed that finding the optimal tracking algorithm is really crucial, for example, the probabilistic and deterministic tracking algorithm have the trade-off between valid/invalid streamlines connections.

Next, we also presented a very brief overview of the tractography cleaning, which is a post-processing step to filter the invalid streamlines generated by the tracking algorithm.

In neurological studies, it is important to study the diffusion properties among the group of subjects. Hence tractogram need to be aligned in order to find the correspondence between the anatomical structure of different

subjects. One of the common approaches for aligning the tractograms is the tractogram registration. We reviewed the literature on tractogram registration methods by dividing it into two categories, i.e. voxel-based and streamline-based registration. We discussed the pros and cons of both categories.

Streamline belongs to the same anatomical structure are called tract or bundle. The statistical analysis of the diffusion properties over the tract(s) helps to study different neurological applications. To extract the tract from the whole brain tractogram is known as the tract segmentation problem. In this chapter, we reviewed the three different segmentation approaches: ROI-based segmentation, unsupervised clustering approaches and supervised tract segmentation algorithms. However, in this thesis, we aim to investigate the supervised approach of tract segmentation. Hence we focused on the supervised segmentation approach literature and presented the five key aspects of the supervised segmentation, i.e. alignment, embedding space, similarity/distance, correspondence techniques and refinement step.

In the next chapter, we will present the mathematical terminologies to formulate the problem of tractogram registration and tract segmentation.

Chapter 3

Problem Statement

Overview

In the previous chapter, we studied the theoretical background of dMRI and tractogram. We also reviewed the literature on tractogram registration and tract segmentation. In this chapter, we present the mathematical terminologies to formulate the problem of tractogram registration and tract segmentation.

We first introduce the notation to represent the streamline, tractogram, and a brief summary of streamline distance functions. Then we present a general formulation of tractogram registration and open issues of tractogram registration techniques. In contrast to the registration method, in this thesis, we propose the concept of tractogram correspondence. Hence, in this chapter, we introduce the basic formulation of the tractogram correspondence problem.

We also present the generic formulation of the automatic tract segmentation problem. We propose a novel supervised tract segmentation approach based on the concept of streamline correspondence. Therefore, we present the formulation of tract segmentation as a streamline correspondence problem. In the current literature of tract segmentation, streamline correspondence is addressed by the nearest neighbor (NN) strategy. We present the formulation of streamline correspondence as NN, and conclude this chapter by discussing the limitations of supervised tract segmentation methods.

Organization of the Chapter

Basic notation and terminology of tractogram and streamline distance are presented in Section 3.1. In Section 3.2 we introduce the basic notation and formulation of tractogram registration and tractogram correspondence. Subsequently, in Section 3.3, we present the generic formulation of tract segmentation.

3.1 Basic Notation and Terminology

In this thesis, a trajectory resulting from the tractography algorithm is referred to as "streamline" or "track". Thus,"tractogram" is a set of streamlines from the whole brain, and "tract" or "bundle" is a subset of the tractogram which have an anatomical meaning.

Streamline and Tractogram Let the polyline $s = \{\mathbf{x}_1, \mathbf{x}_2, \ldots\}$, where $\mathbf{x}_i \in \mathbb{R}^3$, be a *streamline*, reconstructed from dMRI data through reconstruction and tractography algorithms. Let the *tractogram*, $T = \{s_1, s_2, \ldots, s_M\}$ be

defined as a set of M streamlines, where $M \approx 10^6$. Let $t = \{s_1, s_2, \ldots, s_k\} \subset T$, be a subset of the tractogram, called *tract*, usually with a specific anatomical meaning, for example, the cortico-spinal tract (CST).

Streamline Distance In order to measure the distance between two streamlines, numerous streamline distance functions have been proposed in the literature [44] [166] [88]. Some of the proposed distance functions are as follows: minimum closest point (MCP) [103], symmetric minimum average distance (MAM) [54], minimum average flip distance (MDF) [162], Hausdorff distance [87], normalized Euclidean distances [77], mahalanobis distance [162]. Among them, the most commonly used streamline distance is the Hausdorff distance [35]. The Hausdorff distance treats the streamlines as a cloud of points and compares each point of one streamline with each point of a second streamline. However, it doesn't take into account the sequential nature of the streamline points, and is computationally costly due to the inter-point distances. Hence the modified versions of the Hausdorff distance have also been adopted in the literature, denoted as Minimum (or Maximum or Mean) Average Minimum (MAM) distance [54]. A simpler version of the symmetric distance function is also used to measure streamline distance, called the minimum average direct flip (MDF) distance [54]. We present these two distance functions, MAM and MDF, in detail.

MAM Distance The symmetric minimum average (MAM) distance belongs to the Hausdorff-type distance function. It is a widely used distance function for the streamline distance computation. MAM distance takes into account all points of the streamline, and the set of minimum distances are computed between each point of one streamline to each point of another streamline (see Figure 3.1). MAM distance has three different versions, Mean, Maximum and Minimum. Among these three versions of MAM distance, we used the Mean version of MAM distance for streamline distance computation.

Given two streamlines s_A and s_B, the formulation of the three versions of MAM distances can be defined as follows:

$$d_{MAM_{avg}}(s_A, s_B) = \frac{1}{2}(D_{mean}(s_A, s_B) + D_{mean}(s_B, s_A)) \tag{3.1}$$

$$d_{MAM_{min}}(s_A, s_B) = \min(D_{mean}(s_A, s_B), D_{mean}(s_B, s_A)) \tag{3.2}$$

$$d_{MAM_{max}}(s_A, s_B) = \max(D_{mean}(s_A, s_B), D_{mean}(s_B, s_A)) \tag{3.3}$$

where

$$D_{mean}(s_A, s_B) = \frac{1}{|s_A|}\sum_{i=1}^{|s_A|} d(\mathbf{x}_i^a, s_B) \tag{3.4}$$

and

$$d(\mathbf{x}, s_B) = \min_{j=1,\ldots,|s_b|} ||\mathbf{x} - \mathbf{x}'_j||_2 \tag{3.5}$$

$$D_{min}(s_A, s_B) = \min_{i=1,\ldots,|s_b|} d(\mathbf{x}_i^a, s_B) \tag{3.6}$$

$$D_{max}(s_A, s_B) = \max_{i=1,\ldots,|s_b|} d(\mathbf{x}_i^a, s_B) \tag{3.7}$$

where $\mathbf{x}_i^a$ and $\mathbf{x}'_j$ are the points of the streamline s_A and s_B, respectively.

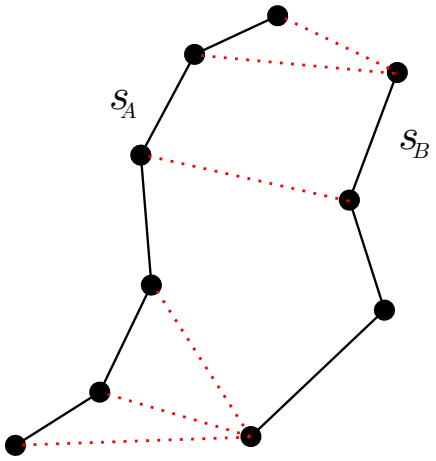

Figure 3.1: Distance between two streamlines S_A and S_B (solid lines): the set of minimum distances between each point of two streamlines are labelled with dotted lines.

MDF Distance The MDF distance has the constraint to have the same number of points of two streamlines. This distance function also takes into account the streamline direction in both ways: the direct and the flipped streamline. The MDF distance is computationally very fast, which is its main advantage.

Given two streamlines s_A and s_B, the MDF distance can be defined as follows:

$$d_{MDF}(s_A, s_B) = min(d_{direct}(s_A, s_B), d_{flipped}(s_A, s_B)) \tag{3.8}$$

where $d_{direct}(s_A, s_B) = d_{direct}(s_B, s_A) = \frac{1}{n_s}\sum_{i=1}^{n_s} ||\mathbf{x}_i^a - \mathbf{x}_i^b||_2$ and $d_{flipped}(s_A, s_B) = d_{flipped}(s_B, s_A) = \frac{1}{n_s}\sum_{i=1}^{n_s} ||\mathbf{x}_i^a - \mathbf{x}_{n_s-i+1}^b||_2$, n_s is the number of points of two streamlines s_A and s_B, and $\mathbf{x}_i^a$ and $\mathbf{x}_{n_s-i+1}^b$ are the points of streamlines s_A and s_B, respectively.

3.2 Tractogram Alignment

In this section, we introduce the notation of tractogram registration, that is, a common approach for tractogram alignment. Then, we describe our proposed methodology to align the tractograms, named *tractogram correspondence*.

3.2.1 Tractogram Registration

Let T_A and T_B be the two tractograms reconstructed from two volumetric images, I_A and I_B respectively. I_A and I_B could be either FA, tensor images or the spherical harmonics. The goal of registration is to align the tractogram T_A to T_B by applying the transformation matrix, g. The transformation matrix g can be computed by linear or nonlinear function by using either images I_A and I_B (voxel-based Registration) or tractograms T_A and T_B (streamline-based registration).

Voxel-based Linear Registration:

As mentioned in the previous chapter (see Section 2.4.1), in the case of voxel-based linear [86, 3, 125, 68] registration, the final transformation matrix (g) is calculated by maximizing the similarity between images I_A and I_B.

We formulate the voxel-based linear registration as follows:

$$g = \underset{\theta \in \psi}{\operatorname{argmax}}\, sim(\theta(I_A), I_B) \tag{3.9}$$

where ψ is the set of all possible transformations, θ represents the affine transformation, $\theta \in \mathbb{R}^{3X3}$, and *sim* means the similarity measure. In the literature, similarity measures are performed in various ways, such as mutual information [136], sum of square difference [68] and correlation coefficient [121].

The matrix representation of affine transformation (g) can be stated as:

$$\begin{pmatrix} a' \\ b' \\ c' \\ 1 \end{pmatrix} = \begin{pmatrix} x_{1,1} & x_{1,2} & x_{1,3} & y_a \\ x_{2,1} & x_{2,2} & x_{2,3} & y_b \\ x_{3,1} & x_{3,2} & x_{3,3} & y_c \\ 0 & 0 & 0 & 1 \end{pmatrix} \begin{pmatrix} a \\ b \\ c \\ 1 \end{pmatrix} \tag{3.10}$$

where $X = [x_{i,j}]; i, j = 1,2,3$ is a matrix of a linear transformation representing the rotation, scaling and shearing; $Y = (y_a, y_b, y_c)$ is a vector representing the translation or shift.

Finally, the transformation matrix (g) from equation (3.9) is applied on source tractogram T_A, in order to register with T_B:

$$T_A^{'} = g \bullet T_A \tag{3.11}$$

where $T_A^{'}$ is the transformed tractogram of T_A.

Note that in the case of registration with the tensor information, different methods also involve the interpolation, i.e. utilized the tensor orientation features with the interpolation [64]. The common method for interpolation is the interpolation with the nearest neighbour.

Voxel-based Nonlinear Registration:

In contrast to the linear methods, the voxel-based nonlinear registration [69, 7, 117] computes a deformation field from the diffusion images and then applies it to every voxel of the image. Then the tractogram is reconstructed from the transformed image.

Given two images $I_A, I_B : \Omega \mapsto \mathbb{R}$, where $\Omega \subset \mathbb{R}^3$, and a deformation field, $\phi : \Omega \mapsto \mathbb{R}^3$, needs to determine. The deformation maps the image I_A to the image I_B by applying the deformation field ϕ on each voxel of the image I_A. In such a way, the corresponding structures of I_A and I_B are mapped onto each other. Finally, from the transformed image of I_A, the tractogram is generated and tractogram T_A is registered with tractogram T_B.

Streamline-based Linear Registration:

In the case of a streamline-based linear approach [79, 90, 170, 102, 55], the registration is performed directly on the tractograms T_A and T_B. In contrast to the voxel-based registration, instead of the voxel from the volumetric image, streamlines are considered for registration.

For the computational complexity, registration of the whole brain tractogram with streamline information is quite difficult. Therefore, streamline-based registration has been demonstrated between a randomly selected subset of whole tractograms, T_A and T_B or only between the tracts of two subjects. Let $T_a \subset T_A$, $T_b \subset T_B$ and T_a and T_b represent either the small subset or the anatomical meaningful tract. The linear streamline-based registration can

be defined as follows:

$$g = \underset{\theta \in \psi}{\operatorname{argmin}} \sum_{\substack{T_a \in T_A \\ T_b \in T_B}} sim(\theta(T_a), T_b) \tag{3.12}$$

The symbols θ, ψ, *sim* in equation 3.12 carry the same meanings as stated before. *sim* can be measured by minimizing a given loss function computed from streamlines [55] or by minimizing the entropy-based objective function [102]. Now the final transformation (g) applies on the source tractogram, T_A.

$$T_A^{'} = g \bullet T_A \tag{3.13}$$

where $T_A^{'}$ is the transformed tractogram of T_A.

Streamline-based Nonlinear Registration:

Nonlinear streamline-based registration [169, 168, 159, 47, 29] is mainly focused on the alignment of the tracts.

Let two tracts t_a and t_b be taken from the tractogram T_A and T_B, respectively. As for the voxel-based nonlinear registration, the deformation field ϕ is computed from the subset of tractogram T_a and T_b and afterward, the ϕ is applied to each point of each streamline of the tract, t_a, in order to align with t_b.

3.2.2 Open issues: Tractogram Registration

Tractogram registration is indeed a commonly used approach to align the tractograms. Nevertheless, current literature on tractogram registration techniques suffers some limitations, which are discussed in Section 2.4 of Chapter 2. Here we summarize the limitations of tractogram registration.

In the case of linear registration, both voxel-based and streamline-based, a single affine transformation can reconcile only part of the difference between the tractograms of two subjects. Many differences remain at the local level, for example systematic displacement of entire tracts, and thinner/thicker or longer/shorter tracts. We demonstrate the limitation of linear registration methods with an example in Figure 1.1 of Chapter 1. Moreover, addressing the full brain tractogram with streamline-based linear registration is not straightforward. In that case, registration is performed on a subset of the streamlines from the whole tractogram [102] or on the clusters of the whole tractogram (by applying the clustering algorithm on the whole brain tractogram) [55]. None of them consider all the streamlines from the whole tractogram.

The nonlinear registration techniques at voxel-level or at streamline-level also have some drawbacks. With the nonlinear registration at voxel-level, there is a constraint to re-generate the tractograms after the registration which makes this method computationally costly. Moreover, there are strong technical concerns about re-orienting the ODFs when applying the transformation, see [29]. With nonlinear registration of streamlines, due to the excessive computational cost, full tractograms cannot be addressed, see [47].

Several tracking algorithms are available in the literature and every tracking algorithm has its own bias. For example, probabilistic tracking algorithm generates a larger number of streamlines compared to the deterministic tracking. The optimal choice of the tracking method and of the tracking parameters is still an open challenge. Moreover, in the context of the tractogram alignment, aligning tractograms generated with two different tracking algorithms, might be even harder.

3.2.3 Tractogram Correspondence

As in [102] and in [55], in this thesis, we are interested in methods for tractogram alignment that directly operate on streamlines, without resorting to volume-based registration. This is due to two main reasons: first, in many practical cases, tractogram alignment is based on registration of images that either do not contain diffusion MRI information at all, such as T1 images, or contain just a portion of it, such as FA images, which is clearly suboptimal. In the case that full ODFs are considered (see for example [116]), the effects of re-orientation may create problems when re-generating the tractogram, see [29]. The second reason is that the cost of re-generating tractograms, after registering volumes, may be high, in terms of computational time and required knowledge to operate the full pipelines of preprocessing, reconstruction, tracking and filtering, see [112].

In contrast with transformation-based registration methods, in this thesis we propose the concept of tractogram correspondence, whose aim is to find which streamline of one tractogram corresponds to which streamline in another tractogram, i.e. a map from one tractogram to another.

Tractogram Alignment as Tractogram Correspondence

We cast the problem of aligning two tractograms, T_A and T_B, as the problem of finding the corresponding streamlines between them. Once such correspondence has been established, T_A will be aligned to T_B by transforming each streamline $s^A \in T_A$ into the corresponding streamline $s^B \in T_B$, as if to perfectly match it. Notice that such transformation is not explicit, that is, no deformation field is computed. Knowing the coordinates of s^B is enough obtain the aligned s^A.

In order to solve the correspondence problem, we define the binary matrix $Q = [q_{ik}]_{ik} \in \{0,1\}^{N_B \times N_A}$, that we call *correspondence matrix*, such that q_{ik} is 1 streamline i of T_A corresponds to streamline k of T_B and 0 vice versa. We require that $\sum_k q_{ik} = 1$, that is each streamline in T_A, must have a corresponding streamline in T_B, while the reverse is not necessarily true. This last case, for example, occurs when $N_A \neq N_B$, that is, the one-to-one correspondence, cannot be made. In particular, when $N_A > N_B$ multiple streamlines of T_A may correspond to the same streamline of T_B.

We notice that the discrete space on which the loss function needs to be minimized is extremely large, that is, there are $N_B^{N_A}$ different possible correspondences. Given the typical size of tractograms, in the order of 10^6 streamlines, it is apparent that the combinatorial optimization problem is difficult to solve and that approximations should be introduced.

Correspondence based on Relational Information

Finding the best correspondence between two tractograms requires two ingredients: the definition of a loss function, that is a function that scores the correspondence, and the exploration of the combinatorial space in order to find the best correspondence. Notice that the definition of a loss function for tractogram correspondence should not be based on the direct distance between streamlines across different tractograms, because such a distance becomes anatomically meaningful only *after* the alignment is done. For this reason, as the building block of the loss function, we propose that two streamlines of different tractograms should correspond when their respective set of distances, and those of other streamlines in their own tractograms, are similar. This idea is motivated by our results in [106], where it is shown that representing a streamline as the set of distances from the other streamlines in its own tractogram is indeed an accurate Euclidean embedding, that is, the geometrical information of the streamlines is preserved.

Formally, let $A = [a_{ij}]_{ij} \in \mathbb{R}^{|T_A|\times|T_A|}$ be the matrix of distances of each streamline from all other streamlines in T_A, i.e., $a_{ij} = d(s_i^A, s_j^A)$. If Q is a correspondence matrix of T_A to T_B, then the matrix $QAQ^\top \in \mathbb{R}^{N_B\times N_B}$ represents A after applying such correspondence. To better understand this step, consider that, in the special case where $N_A = N_B$ and Q is a one-to-one correspondence, then Q is a permutation matrix and $QAQ^\top$ is a matrix where rows and columns are obtained just by permuting those of A according to Q. As a consequence, a meaningful definition of distance, that is a loss L, between T_A and T_B is the matrix distance (Frobenius norm, $||\cdot||_F$) between the mapped A and B: $L = ||B - QAQ^\top||_F^2$. Then, the problem of finding the best possible correspondence Q^* between T_A and T_B becomes the combinatorial optimization problem

$$Q^* = \underset{Q\in\mathcal{Q}}{\operatorname{argmin}} ||B - QAQ^\top||_F^2 \tag{3.14}$$

where $\mathcal{Q}$ is the space of all possible correspondences. As noted before, $\mathcal{Q}$ is extremely large and, clearly, this problem is extremely hard to solve.

3.3 Tract Segmentation

In this section, we provide a general formulation of various automatic tract segmentation techniques, including ROI-based segmentation, unsupervised clustering and supervised segmentation.

Extracting the tract (t) from the whole brain tractogram (T) is known as a tract segmentation problem which can be defined as follows:

$$t = seg(T), t \subset T \tag{3.15}$$

where *seg* function refers to the tract segmentation function. It is worth noting that we define the *seg* function in a generic manner in order to explicitly explain the inputs and outputs of different tract segmentation techniques. Our intention is not to give a proper mathematical formulation of the segmentation techniques. However, in equation 3.15, the input of the *seg* function is the whole brain tractogram, T and the output is the segmented tract, t from the tractogram. Some additional parameters (depending on the kind of segmentation technique) can also be included as input, for example, Atlas or regions of interest (ROIs). The segmentation can be performed directly on the voxel-level or the streamline-level, and, therefore, the input and the output of the segmentation approach, in general, can be the voxels or the streamlines. As an example, in the case of ROI-based segmentation, the additional inputs of the *seg* function are Atlas and ROIs (in voxel space) along with the tractogram (in streamline space).

In the following, we present the formalization of the different segmentation methods by explicitly mentioning their inputs and outputs.

ROI-based Tract Segmentation

In principle, the inputs of the *seg* function for the automatic ROI-based tract segmentation [1, 167, 157] are the whole brain tractogram (T), the Atlas, $atlas_v$ and the ROIs, roi_v. The $atlas_v$ can be an anatomical Atlas or the parcellation-based Atlas and is in voxel space. The tractogram and ROIs are in streamline and voxel space, respectively. However, initially, the tractogram needs to register with the Atlas and tracts are extracted by computing the streamlines passing through the ROIs. Hence the final output of *seg* function is the tracts in streamline space. The ROI-based tract segmentation can be defined as follows:

$$seg(T, Atlas_v, roi_v) : t \subset T \tag{3.16}$$

Unsupervised Clustering Technique

In the case of the unsupervised clustering based approach [128, 44, 16, 100, 113], the main goal is to cluster the whole brain tractogram into groups or clusters. The input of the *seg* function is the whole brain tractogram, T, in streamline space. However, two important aspects of the clustering approach are as follows: i) a well-defined similarity or distance measure and ii) the clustering algorithm. The clustering approaches initially measure the similarity or the distance matrix among the streamlines and then apply the clustering algorithms on that matrix. We refer to Section 2.5.2, where we mentioned the various distance functions and clustering algorithms used in clustering approaches.

Clustering attempts to partition T into p groups, $K = \{K_1, \ldots, K_p\}$,$K_i = \{s_1, \ldots, s_j\}$, with $p \leq N$, such that

$$seg(T) : \{K_1, \ldots, K_p\} \tag{3.17}$$

and

$$K_i \neq \varnothing, i = 1, \ldots, p \text{ and } \cup_{i=1}^{p} K_i = T \tag{3.18}$$

Note that the cluster K is a set of streamlines, not the anatomical meaning tract t. The clusters need to be incorporated with the anatomical Atlas ($atlas_v$) in order to assign the anatomical label to the clusters. However, as the Atlas is in voxel space, the final extracted tract (by assigning the label to the cluster) is also in voxel space.

Supervised Tract Segmentation

Supervised tract segmentation uses prior knowledge in order to segment the tract. This prior knowledge can be the model of the tract, the expert segmented tract of interest or an Atlas with expert labeled tract.

Atlas-based Supervised Segmentation

In the case of Atlas-bases segmentation [103, 152, 162, 77, 62] prior knowledge can be expert labeling anatomical Atlas in voxel space ($atlas_v$) or multi-atlas, that is, created from multiple subjects in streamline space ($atlas_s$).

Given the tractogram in streamline space and the Atlas in voxel space, $atlas_v$, we can define the Atlas-based supervised segmentation as follows:

$$seg(T, atlas_v) : \{t_1, \ldots, t_N\} \subset T \tag{3.19}$$

In the case of Atlas in streamline space, supervised segmentation can be defined as follows:

$$seg(T, atlas_s) : \{t_1, \ldots, t_N\} \subset T \tag{3.20}$$

where $t_1, \ldots, t_N$ are the segmented tracts from the tractogram T.

An important aspect of Atlas-based supervised segmentation is to incorporate the prior knowledge (from the Atlas) to the tractogram. In order to do that, for a given streamline of a tractogram T, the closest streamline from the Atlas ($atlas_s$) is retrieved and then assigned the same label of the streamline from the Atlas ($atlas_s$). In such a way, we can state that given a set of streamlines of one subject, the problem of finding the corresponding streamlines in the tractogram of another subject has been addressed with the NN strategy [162]. We explicitly describe streamline correspondence in Subsection 3.3.1 and streamline correspondence as NN in Subsection 3.3.2.

Model-based Supervised Segmentation

The input of the *seg* function for the model-based supervised segmentation technique is the parametric model of the tract and the tractogram. The parametric model can be built based on the following parameters: the Gamma mixture model of the distance [89], the Gaussian process of tract probability map [156], and the hierarchical dirichlet process mixture model [155]. The model-based segmentation technique can be defined as follows:

$$seg(T, t_m) : t \subset T \tag{3.21}$$

where t_m is the parametric model of the tract.

3.3.1 Tract Segmentation as Streamline Correspondence Problem

We address the problem of tract segmentation as the streamline correspondence problem, that is, on finding which streamline in the new tractogram corresponds to a given streamline in the example tract. Given one example of the tract of interest, $t_A = \{s_1^A, \ldots, s_k^A\}$, for example the segmented CST from subject A, finding the correspondence set of streamlines of subject B, can be defined as t_A: $t_{A \to B} \subset T_B$. The extracted tract, $t_{A \mapsto B}$, is an approximation of the actual tract/bundle of interest in subject B, i.e. t_B.

The problem of finding the correspondence is combinatorial one and its solution is a correspondence map between the two sets. We denote the map as a binary matrix $P = [p_{ij}]_{ij} \in \{0,1\}^{|T_A| \times |T_B|}$, that we call *mapping* matrix, such that p_{ij} is 1 when streamline $s_i^A \in T_A$ corresponds to streamline $s_j^B \in T_B$, and 0 otherwise. In practical cases, it is common to observe that different tractograms have a different number of streamlines, i.e. $|T_A| \neq |T_B|$. Moreover, corresponding tracts across different subjects may have different sizes, meaning that different streamlines of one tractogram may correspond to the same streamline in another tractogram. For these reasons, in general, the correspondence between streamlines cannot be a bijective or an injective map but a many-to-one or many-to-many map.

3.3.2 Streamline Correspondence as Nearest Neighbor

As mentioned above (see Section 3.3), streamline correspondence can be addressed with the NN technique. The straightforward solution of retrieving neighboring streamlines is to compute the distance from the given streamline to all other streamlines in the new/target tractogram and then getting the minimum streamline.

Assuming that the tractograms of the two subjects are registered in the same space (e.g. see [55]), a simple supervised segmentation method is based on the NN algorithm: we define the segmented bundle as the set of streamlines of the target subject that are NN of the streamlines of the example bundle.

More formally, let T^A_{example} and T^B_{target} be the tractograms of two different subjects, A and B. Let $b^A_{\text{example}} \subset T^A_{\text{example}}$ be an example of the bundle of interest, segmented by an expert. Let $b^B_{\text{target}} \subset T^B_{\text{target}}$ be the (unknown) corresponding bundle we want to approximate using automatic supervised segmentation, via NN. Under the assumptions that T^A_{example} and T^B_{target} are co-registered, the approximate bundle $\hat{b}^B_{\text{target}} \subset T^B_{\text{target}}$ is such that

$$\hat{b}^B_{\text{target}} = \{\text{NN}(s_e^A, T^B_{\text{target}}), \forall s_e^A \in b^A_{\text{example}}\} \tag{3.22}$$

where s_e^A is a streamline of the example tract of subject A and $\text{NN}(s_e^A, T^B_{\text{target}}) = \text{argmin}_{s^B \in T^B_{\text{target}}} d(s_e^A, s^B)$ its NN streamline in T^B_{target}, i.e. the one having minimum distance from s_e^A.

3.3.3 Open issues: Supervised Tract Segmentation

We intend to investigate the supervised tract segmentation approach as it has the guarantee to segment the anatomically meaningful tract.

Existing methods of supervised segmentation have some limitations, the main ones being the high computational cost [103, 152], the requirement of a large number of segmented tractograms to construct the Atlas in the case of multiple Atlases [62], and the dependency on the definition of threshold values [162, 77]. Moreover, a recently proposed approach requires the labelling of individual streamlines, which is time consuming and depends on demanding preprocessing [77].

As mentioned in Section 3.3.2, in the literature, given a tract from one subject, the problem of finding the corresponding streamlines in the tractogram of another subject has been addressed with a NN strategy [162]. The approaches currently adopted to compute the NN are based on several pre-processing steps that may involve clustering, the definition of thresholds and the use of fast graphics processing units (GPUs), see [162, 77].

Furthermore, we observed that finding corresponding streamlines with the NN strategy is suboptimal. A typical problem with NN is that homologous anatomical structures of two different subjects may have a systematic displacement even after the initial affine registration. In those cases, the NN strategy would be too greedy and would fail to retrieve the correct corresponding streamlines because of the systematic displacement, selecting instead the closest ones. We illustrate this issue in Figure 1.4 of Chapter 1.

This is another issue of the NN strategy: by always greedily selecting the closest streamline in the new tractogram, frequently, multiple streamlines of the example tract end up corresponding to the same streamline in the target tractogram. For this reason, the number of streamlines of the estimated tract in the target tractogram is always inferior, or at most equal to that of the example tract, leading to systematic and unrealistic thinning (see Figure 1.4).

In this work, differently from the NN strategy, we propose a non-greedy strategy to segment the tract. We claim that introducing the further constraint of *one-to-one* correspondence between streamlines forces the correspondence to follow the local displacements that may occur due to the initial affine registration. Additionally, our proposal is to find which streamlines of the new tractogram belong to the desired tract using previous examples.

Chapter 4

Methods

Overview

In the previous chapter, we presented the formulation of the tractogram alignment and the tract segmentation problem. Besides that, we also presented our proposed concept of aligning two tractograms, called *tractogram correspondence*. In the case of tract segmentation, we showed the mathematical formulation of streamline correspondence as nearest neighbor (NN) strategy.

In this chapter, we mainly discuss the proposed solutions of tractogram correspondence problem and tract segmentation problem. Regarding the solution of tractogram correspondence, we provide an operational procedure to find the optimal correspondence through the graph matching (GM) problem. For this purpose, we first introduce the basic definition and formulation of the GM problem and these will be followed by a review of GM solutions. We also elaborately describe the adapted doubly stochastic projected fixed-point (DSPFP) algorithm to solve the GM problem.

In this thesis, in contrast with the NN formulation, the streamline correspondence problem formulated as the linear assignment problem (LAP). To adopt the appropriate solution of the LAP, we have studied the literature of existing LAP solutions and adopted the Jonker-Volgenant Algorithm for Linear Assignment Problem (LAPJV) algorithm. By adapting the solution of the LAP, we also provide a complete framework for supervised tract segmentation. The LAP formulation of the tract segmentation, adapted algorithm for the LAP and detail procedure of the segmentation framework will be reported in this chapter.

In order to implement the GM and the LAP solutions efficiently, we proposed a scalable procedure to address the NN solutions, which we also describe at the end of this chapter.

Organization of the Chapter

We divide this chapter into three different sections based on tractogram correspondence, tract segmentation and scalable solution for the nearest neighbor computation. The chapter is organized as follows. Section 4.1 discusses the tractogram correspondence, GM problem and solutions. Section 4.2 provides the formulation of LAP and its solution, and details of the proposed tract segmentation mechanism. Subsequently, in Section 4.3, we present the scalable solution of NN technique.

4.1 Tractogram Correspondence

In this section, we will present the formulation of tractogram correspondence problem as GM problem. The first initial step is to encode the tractogram as a graph. We introduce the basic notation for graphs, followed by the formulation of the GM problem.

4.1.1 Basic Notation and Terminology

Graph construction is the first important step of the application of the GM techniques [137]. Therefore, a good and effective representation of the graph is necessary.

A *graph* $G = (V,E)$ is composed of vertices and edges. V is a finite set of vertices or nodes, and $E \subset V \times V$ is a set of connections (edges) between the vertices. Edges are said to be undirected when they have no direction and a graph G containing only such types of edges is called undirected. Otherwise, it is called directed graph.

A *weighted graph* is an order triple $G = (V,E,f)$ which made of a finite set of vertices V, the corresponding set of edges E and a weighting function $f : E \mapsto \mathbb{R}$, which gives a real non-negative value to each edge.

An *adjacency matrix* is a way to represent a graph as a matrix. Each graph can be represented by a square adjacency matrix A of size $|V| \times |V|$, where a_{ij} is equal to one if there is an edge between vertex i and vertex j, and zero otherwise. The adjacency matrix of a weighted graph is defined by the weights of their edges. In this case, the entries of the main diagonal of the adjacency matrix is zero.

Encode Tractogram as Graph

For a given tractogram, T, the creation of the corresponding graph G is composed of three steps: the construct of the nodes, the edges and the weights.

Nodes: each vertex of G corresponds[1] to one streamline of T

Edges: we consider the connection between two streamlines as an edge, E.

Weights: the weight of each edge is the distance between the related streamlines.

Given a Tractogram, T, a graph G, can be encoded as follows: $G = (id(T),E,d)$, where $id(T) = \{id(s_1),\ldots,id(s_N)\}$ and $id(s_i) = i$, s_i is the streamline from the tractogram and $id(s_i)$ is the index of the streamline, $E \subseteq id(T) \times id(T)$ and $f((i,j)) = d(s_i,s_j)$, where $d(s_i,s_j)$ is the distance function to compute the distance between the streamlines s_i and s_j. Note that the distance is considered here as the weight of each edge.

Figure 4.1 demonstrates a small set of streamlines which contains 5 streamlines (left) and the constructed graph from those streamlines (right). The graph is constructed using the Networkx `http://networkx.github.io//`. The graph shows five nodes (in red) constructed from five streamlines and edges represented by the black lines along with the weights (numerical values) computed by the distance between the streamlines. Note that to visualize the graph encoding clearly, we choose to show only a small number of streamlines encoding, instead of the whole brain tractogram.

4.1.2 Tractogram Correspondence as Graph Matching

A combinatorial optimization problem, that is strongly related to the tractogram correspondence problem, is the GM problem (see [33, 163]).

[1] Technically, each vertex is an object whose property is the identifier of the streamline to which it is associated.

[2] `http://networkx.github.io//`

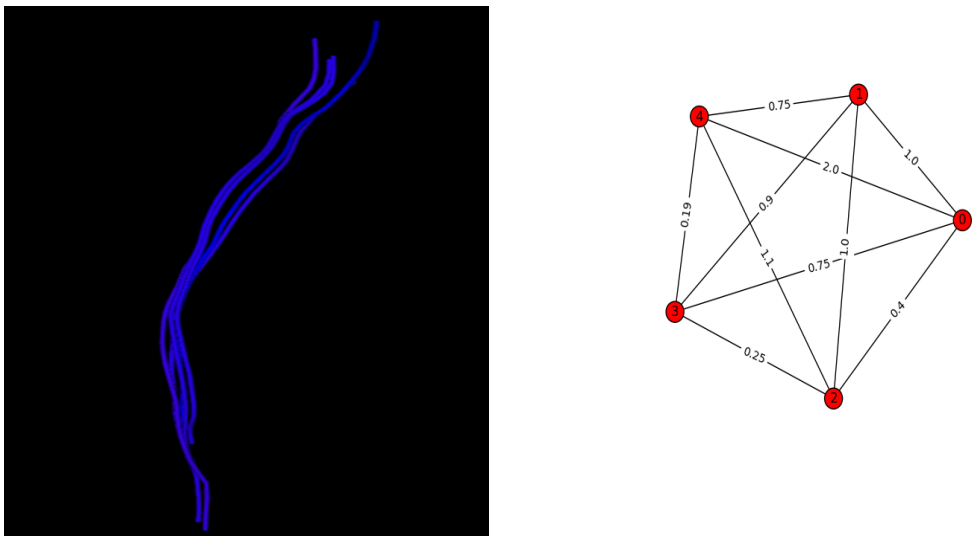

Figure 4.1: Tract encoded by graph: (left) a small set of streamlines which contains 5 streamlines (right) encoded graph with five nodes from a small set of streamlines. Graph visualized by the *NetworkX* [2]

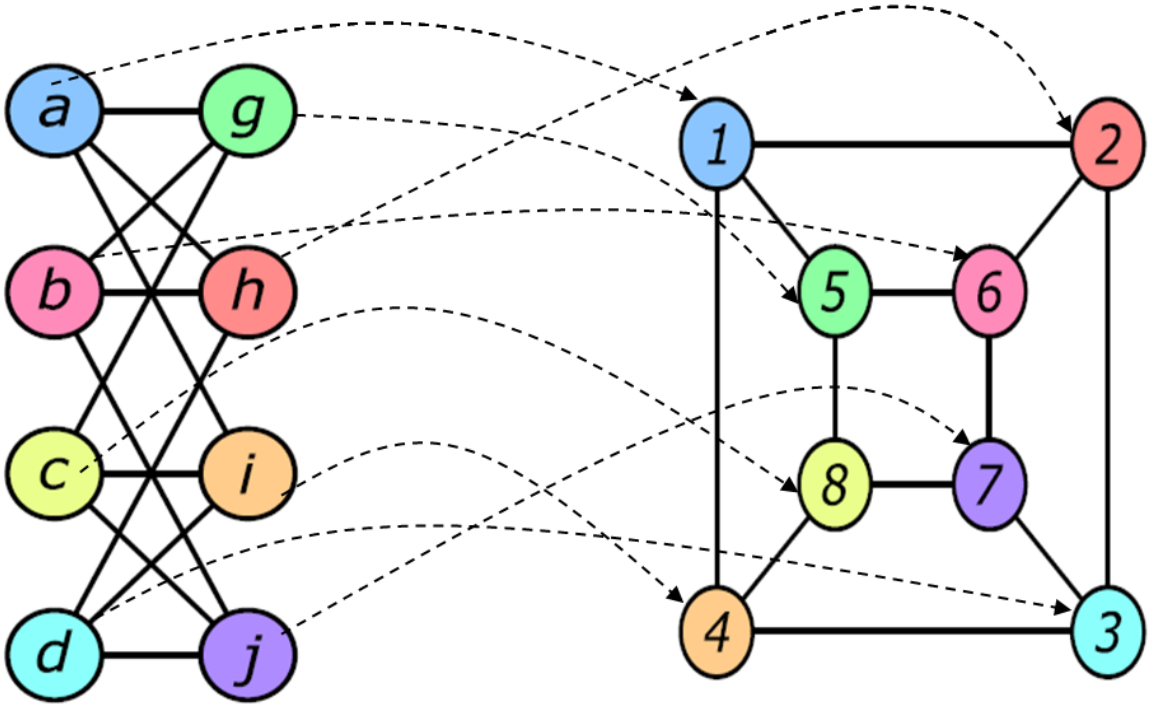

Figure 4.2: Graph matching example: two graphs with eight nodes are matched. Dotted lines represent the match between the nodes of the graph [from [137]

Let two different tractograms T_A and T_B are represented by two different graphs, G_A and G_B. We denote as $A \in \mathbb{R}^{N_A \times N_A}$ and $B \in \mathbb{R}^{N_B \times N_B}$ the adjacency matrices of the weighted graphs G_A and G_B with $|V_A| = N_A$ and $|V_B| = N_B$, respectively. The GM [137] problem aims at finding the corresponding vertices in two graphs, G_A and G_B, of equal size ($N_A = N_B$), with adjacency matrices A and B (see Figure 4.2). Differently from the correspondence of

streamlines described in Section 3.2.3, the correspondence of GM is a one-to-one (bijection). Formally, the GM problem is formulated as

$$P^* = \underset{P \in \mathcal{P}}{\operatorname{argmin}} ||A - PBP^\top||_F^2 \tag{4.1}$$

where $||.||_F$ is the Frobenius matrix norm. It is worth noting that Equation 4.1 is very similar[3] to the correspondence problem of Equation 3.14. Specifically, when the correspondence between streamlines is a permutation of indices, then the matrix Q is a permutation matrix and the correspondence problem of Equation 3.14 becomes identical to the graph matching problem of Equation 4.1: $||A - PBP^\top||_F^2 = ||B - QAQ^\top||_F^2$ when $P = Q$, so $Q^* = P^*$.

When the two graphs have different sizes ($N_A \neq N_B$), the GM problem is called *sub-graph matching* (sub-GM) problem and the goal is to find the corresponding vertices from the smaller graph to the larger graph. The GM and sub-GM problems are known to be non-deterministic polynomial-time hard (NP-hard) [33], in general, and only approximate solutions can be obtained in most of the practical cases, i.e., when the number of vertices is more than twenty. Notice that a matching P can also be considered a correspondence, i.e. $P \in \mathcal{P} \subseteq Q$. For this reason, an approximate solution of GM is also an approximate solution of the correspondence problem.

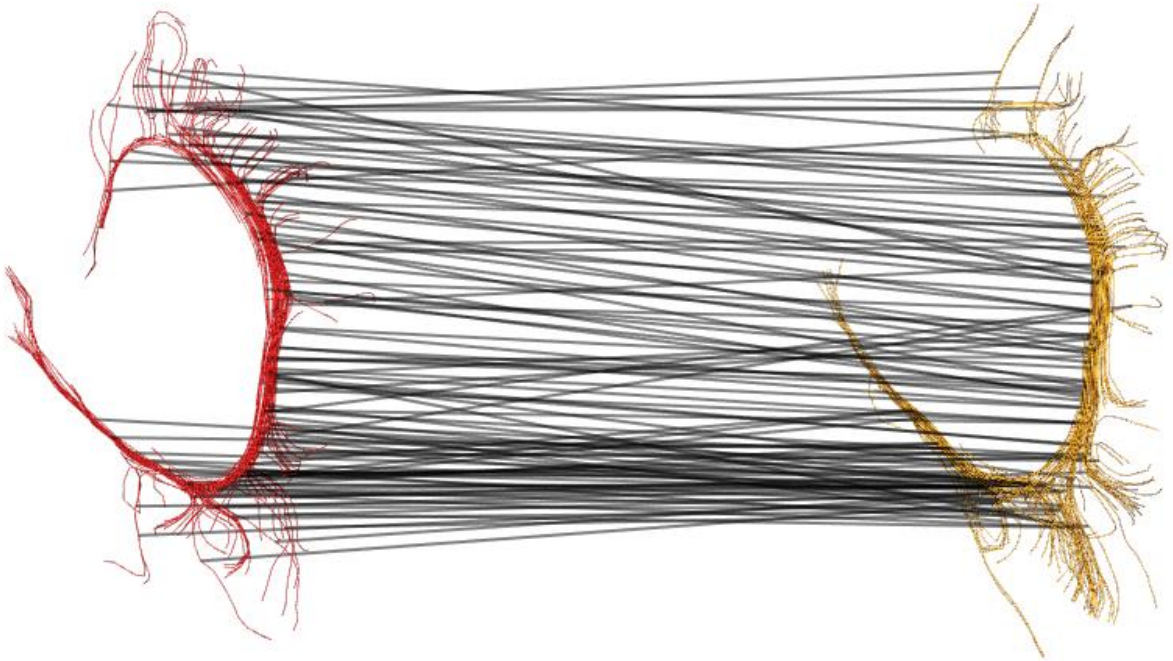

Figure 4.3: Graph matching example with cingulum (CG) tracts from two different tractograms: two tracts are in red and golden and the streamlines from two tracts matched by the GM. Matches are shown with black arrow lines.

In Figure 4.3, we have shown an example of the GM, with two cingulum bundle (CG) tracts from two different tractograms. Each of the tracts contains 113 and 116 streamlines, respectively. The tracts are displaced with the arbitrary displacement and black straight lines show the correctly identified corresponding streamlines through the GM.

[3]Historically, the GM problem refers to finding the vertices of G_B that match those of G_A, and not the contrary, which is the natural way to formulate the alignment problem.

4.1.3 Graph Matching Solutions

The graph matching problem is an NP-hard combinatorial problem. Due to the combinatorial nature, the exact optimal solution can only be found for small graphs (graph with 20 nodes). In case of large graphs, approximate solutions have been proposed in literature. A comprehensive review of GM solutions can be found in [33], [51]. Although approximate algorithms provide a near-optimal solution, it is reasonably easy to scale the algorithms for large graphs. Hence here we present an overview of the approximate graph matching solutions.

In general, approximate solutions can be divided into three different categories: tree search-based algorithms, spectral methods and continuous optimization. The first category is based on the approximate tree search algorithms [18, 145]. The basic idea of the tree based algorithms is the partial node matching, which obtains by assigning nodes from two graphs to each other. The algorithms iteratively find match based on the partial matching cost and the estimated matching cost of the remaining nodes of the graph. The second category is the spectral methods which deal with the spectral decomposition of graph adjacency matrices and based on the following assumption: the eigenvalues and the eigenvectors of the adjacency matrix are not vary with the permutation of the node of the graph [148, 37, 81].

The third category is based on the relaxation of the optimization problem, e.g. continuous relaxation. The main objective of the continuous relaxation is to relax a discrete optimization problem into a continuous problem, and solve the continuous problem by continuous optimization techniques. Various algorithms have been proposed for this particular approach [4, 58, 124]. Following we will discuss the efficiency of the algorithms in this category based on their computational complexity.

There have been many algorithms proposed in the domain of continuous relaxation technique over the years. It is not our intention to discuss the details of the algorithms. However, we feel that a comparative study among some of the algorithms could be useful. Therefore, we report a comparison of different algorithms, i.e. Linear programming (LP) [4], Relaxation labeling (RL) [50], Graduated Assignment (GA) [58], Reweighted Random Walks Matching (RRWM) [26], Integer Projected Fixed Point (IPFP) [82], Spectral matching (SM) [80], PATH following algorithm [163], fast Graduated Assignment (fastGA) [58], Projected Gradient (PG) [21], and Doubly Stochastic Projected Fixed-Point (DSPFP) algorithm [84]. Table 4.1 reports the comparison, in terms of, time complexity, space complexity, capability of the handling different size of the graph and convergence rate. Please note that complexities reported here are evaluated on graphs with equal size. The size of the graph is represented by n.

Algorithm	Time Complexity	Space Complexity	Handle the graph of different size	Convergence Guarantee	Convergence Rate
LP	$O(n^6)$	$O(n^4)$	NO	N/A	N/A
RL	$O(n^4)/iteration$	$O(n^2)$	YES	YES	Unknown
GA	$O(n^4)/iteration$	$O(n^4)$	YES	YES	Unknown
PRWM	$O(n^4)/iteration$	$O(n^4)$	YES	NO	N/A
IPFP	$O(n^4)/iteration$	$O(n^4)$	YES	YES	Unknown
SM	$O(n^4)$	$O(n^4)$	NO	N/A	N/A
PATH	$O(n^3)/iteration$	$O(n^2)$	YES	YES	Unknown
FastGA	$O(n^3)/iteration$	$O(n^2)$	YES	YES	Unknown
PG	$O(n^3)/iteration$	$O(n^2)$	YES	YES	Unknown
DSPFP	$O(n^3)/iteration$	$O(n^2)$	YES	YES	Linear

Table 4.1: Properties of the continuous relaxation based graph matching algorithms (adapted from the [83])

To the best of our knowledge and also from table 4.1, we observe that the computational time and the space

complexity of the most efficient algorithms [4] for GM are respectively $O(n^3)$/iteration and $O(n^2)$, reached only by the following algorithms (see [163, 84]): PG, fastGA, PATH and DSPFP. With such computational complexity, approximate solutions can be found for graphs with several thousands of vertices. To scale-up to larger graphs, it is necessary to derive methods with lower complexity per iteration or to introduce assumptions on the structure of the data. According to [84] and to our tests, the DSPFP algorithm outperforms others algorithms in terms of actual time and memory requirements, moreover with higher quality of the approximated solution. For this reason, we adapted DSPFP algorithm for the solution of the tractogram correspondence problem.

4.1.4 Graph Matching: further approximations

Addressing the tractogram correspondence with the graph matching is not straightforward. The computational and storage resources necessary to handle the matching of graphs generated from an entire tractogram, i.e. $n = 10^6$ nodes and 10^{10} edges, are beyond the capability of modern computers. We propose a three step process, in this regard:

1. Two tractograms are clustered into a fixed number of clusters, and a representative streamline is selected for each cluster.
2. Approximate GM is applied to find the matches between the representatives, i.e. to find the corresponding clusters.
3. For each pair of corresponding clusters, approximate GM is carried out in order to find corresponding streamlines.

For more details of each step, we refer to the Section 6.1.2 of Chapter 6.

4.1.5 The Doubly Stochastic Projected Fixed-Point (DSPFP) Algorithm

The DSPFP algorithm provides an approximate solution to the GM and sub-GM problems. In its original formulation (see [84]), the algorithm accounts for the similarity between both the weights of corresponding edges and the attributes of corresponding vertices. For sake of simplicity, here we omit the part pertaining vertex attributes, since it does not play a role in the proposed application of tractogram alignment[5]. In the following we report the main steps to describe DSPFP.

The minimization problem of Equation 4.1 can be recast as the maximization problem

$$P^* = \underset{X}{\operatorname{argmax}} \frac{1}{2} tr(X^\top A X^\top B) \tag{4.2}$$
$$\text{s.t.} \quad X\mathbf{1} = \mathbf{1}, X^\top \mathbf{1} = \mathbf{1}, x_{ij} \in \{0,1\}$$

see for example [84], Appendix A, for the complete derivation of Equation 4.2. By relaxing the constraint that $x_{ij} \in \{0,1\}$ into $x_{ij} \geq 0$, the original discrete space of the partial permutation matrices becomes the continuous one of doubly stochastic matrices. The quadratic maximization problem on this continuous space can be addressed by means of the projected fixed-point method, which is iterative:

$$X^{t+1} = (1-\alpha)X^t + \alpha\Pi(\nabla f(X^t)) \tag{4.3}$$

[4] All these algorithms are iterative, with some sort of convergence criteria.
[5] Technically, this means simply to set to zero the matrix K in all equations in [84].

where α is the step size, $\Pi(\cdot)$ is the doubly stochastic projection, $f(X)$ is the target function to be maximized, i.e. $f(X) = \frac{1}{2}tr(X^\top AX^\top B)$, so $\nabla f(X) = AXB$. The projection method adopted in DSPFP is based on a recent closed-form solution of doubly stochastic projection, proposed in [164], which is solved by iterating two successive projections until convergence: $\Pi(X) = \ldots \Pi_2\Pi_1\Pi_2\Pi_1(X)$, where[6]:

$$\Pi_1(X) = X + \left(\frac{1}{N_A}I + \frac{\mathbf{1}^\top X\mathbf{1}}{N_A^2} - \frac{1}{N_A}X\right)\mathbf{1}\mathbf{1}^\top - \frac{1}{N_A}\mathbf{1}\mathbf{1}^\top X \tag{4.4}$$

and

$$\Pi_2(X) = \frac{X + |X|}{2}. \tag{4.5}$$

The resulting procedure is reported in Algorithm 1, where Y is a $N_A \times N_A$ matrix, assuming $N_A \geq N_B$. The initialization of X and Y recommended in [84] is such that $x_{ij} = 1/(N_A N_B)$ and $y_{ij} = 0, \forall i, j$.

Data: A, B, α
Result: P
Initialize X and Y;
repeat
  $Y_{1:N_A,1:N_B} = AXB$;
  repeat
    $Y = Y + \left(\frac{1}{N_A}I + \frac{\mathbf{1}^\top Y\mathbf{1}}{N_A^2} - \frac{1}{N_A}Y\right)\mathbf{1}\mathbf{1}^\top - \frac{1}{N_A}\mathbf{1}\mathbf{1}^\top Y$;
    $Y = \frac{Y+|Y|}{2}$;
  until Y *converges*;
  $X = (1-\alpha)X + \alpha Y_{1:N_A,1:N_B}$;
  $X = X/max(X)$;
until X *converges*;
Discretize X to obtain P.

Algorithm 1: Doubly Stochastic Projected Fixed-Point (DSPFP), from [84].

The *discretization* of X, required in the last step of Algorithm 1, is a linear assignment problem, which can be implemented with the Hungarian method or approximated with a faster greedy algorithm for the linear assignment method, such as the one used in [80]. This greedy approach comprises the steps described in Algorithm 2.

Data: X
Result: P
Initialize P as $N_A \times N_B$ zero matrix and L as its set of indices $\{(i,j)\}_{i,j}$;
repeat
  $(i^*, j^*) = \text{argmax}_{(i,j)\in L} x_{ij}$;
  $p_{i^*,j^*} = 1$;
  remove from L all pairs (i,j) s.t. $i = i^*$ or $j = j^*$;
until L *is empty*;

Algorithm 2: Greedy algorithm for the linear assignment problem.

The implementation of DSPFP is available under a Free/OpenSource license at: `https://github.com/emanuele/DSPFP`.

[6] $\mathbf{1}$ indicates the vector with all elements equal to one.

4.2 Tract Segmentation

In the previous section, we showed that streamline correspondence has an impact on tractogram alignment. We have taken a further step on the application of the streamline correspondence to the tract segmentation task. We present a novel supervised tract segmentation approach based on streamline correspondence across subjects. In contrast to the previous work, we formulate the streamline correspondence problem as a linear assignment problem (LAP). Due to the high computational complexity of the GM algorithms and their inability to find the match between two graphs with such a large difference (by considering tract and tractogram as two graphs), we opted for the LAP problem, which is one of the fundamental combinatorial optimization problems.

In this thesis, we propose a novel supervised tract segmentation approach that segments tract by exploiting a set of examples from different subjects. Our supervised segmentation approach is based on the idea of streamline correspondence (see Section 3.3.2). As a common practice, streamline correspondence can be addressed by the NN strategy. In contrast with the NN strategy, we cast the streamline correspondence as the linear assignment problem (LAP). In this section, we first introduce the basic definitions and terminology of LAP and then we present the formalization of the tract segmentation problem as a linear assignment problem (LAP). A brief review of the solutions of the LAP, followed by an elaborate description of the adapted Jonker-Volgenant algorithm for Linear Assignment Problem (LAPJV) algorithm will be presented. We conclude this section with a detail description of the proposed tract segmentation approach.

4.2.1 Notation and Terminology

Linear Assignment Problem The LAP is a fundamental combinatorial optimization problem. Given two sets of objects $A = \{a_1, \ldots, a_M\}$ and $B = \{b_1, \ldots, b_M\}$ and the cost matrix $C = [c_{ij}]_{ij} \in \mathbb{R}^{M \times M}$ that provides the cost c_{ij} of assigning/matching a_i to b_j, the LAP aims to find the *one-to-one* correspondence between the two sets that has the minimum total cost. In our context, we use the LAP to find the correspondence between two sets of streamlines, as in [127]. In our case, the cost to minimize is the distance between the streamlines, i.e. $c_{i,j} = d(s_i^A, s_j^B)$. A one-to-one assignment can be represented with a binary matrix $P = [p_{ij}]_{ij}$, where $p_{ij} = 1$ if a_i corresponds to b_j and zero otherwise. The one-to-one constraint makes P a *permutation matrix*, i.e. only one element in each row and column is 1. Then, the LAP is defined as

$$P^* = \underset{P \in \mathcal{P}}{\operatorname{argmin}} \sum_{i,j=1}^{M} C_{ij} p_{ij}. \tag{4.6}$$

where P^* is the optimal assignment. When the size of the two sets differs, i.e. $|A| \neq |B|$, the problem is called *rectangular* linear assignment problem (RLAP) [12], a generalization of the LAP.

4.2.2 Tract Segmentation as (Rectangular) Linear Assignment Problem

Given the tract/bundle $t_A = \{s_1^A, \ldots, s_k^A\}$ of subject A and the tractogram $T_B = \{s_1^B, \ldots, s_M^B\}$ of subject B, where $k \lll M$, and a distance function $d()$ between streamlines, we denote as $C = [c_{ij}]_{i=1\ldots k, j=1\ldots M}$, the distance matrix between each streamline of t_A to each of T_B, i.e. $c_{ij} = d(s_i^A, s_j^B)$. Then, we define the corresponding streamlines of t_A in T_B as those found by the solution of the corresponding rectangular linear assignment problem (RLAP):

$$P^* = \underset{P \in \mathcal{P}}{\operatorname{argmin}} \sum_{i=1}^{k} \sum_{j=1}^{M} c_{ij} p_{ij} \tag{4.7}$$

where $[p_{ij}]_{ij} = P \in \mathcal{P}$ is a *partial* permutation matrix, i.e. $P = [p_{ij}]_{ij} \in \{0,1\}^{k \times M}$ and $\sum_{j=1}^{k} p_{ij} = 1$ but $\sum_{i=1}^{M} p_{ij} \leq 1$. P^* is the optimal assignment, i.e. the one with lowest overall cost. Once P^* is obtained, the segmented tract in T_B is defined as the set of streamlines in T_B corresponding to t_A according to P^*.

4.2.3 Solutions of Linear Assignment problem

Here we present the review of the existing solutions of the LAP.

Various algorithms for solving the LAP has been proposed in the literature. The proposed solutions of the LAP can be categorized into three groups, i.e. primal algorithm, dual algorithm and primal-dual algorithm [20]. Primal algorithms are the specialised version of the simplex method, i.e. a popular algorithm for solving the linear programming. Dual algorithms involve the shortest path algorithm to reach the solution of the LAP. Consequently, primal-dual algorithms solve the original LAP along with the dual formulation of it. However, primal algorithms have limited use due to their relatively complex implementation. Hence primal-dual algorithm and dual algorithms are widely used. A comprehensive review of all the proposed algorithms can be found in [20, 19, 2].

An extensive computational comparison among eight well known algorithms is presented in [39]. The algorithms are: Hungarian, signature, auction, pseudoflow, interior point method, Jonker-Volgenant for linear assignment problem (LAPJV). According to the survey, the Hungarian [76] algorithm and LAPJV [75] are the most efficient ones [126]. Note that we listed only six algorithms among the eight as other two are the variant of the auction algorithm. However, Hungarian algorithm is a well-known and notable algorithm in the class of the primal-dual algorithms [76]. Being proposed in 1955, Hungarian algorithm is the first algorithm that solves LAP in polynomial time, with the complexity $O(m^4)$ and later improved to $O(m^3)$ [97]. LAPJV [75] is in the group of the dual algorithms, and has received attention in the literature for its capability to solve the practical applications. Although both LAPJV and Hungarian have the same complexity, LAPJV appears to be faster than the Hungarian algorithm.

In many practical applications the two sets of the assignment problem have different sizes, i.e. the cost matrix is rectangular. A common solution of the rectangular cost matrix is adding $m-n$ (where m and n are the row and column of the cost matrix, respectively) dummy entries, so that the problem becomes a LAP with $(m-n)!$ optimal solutions. The time complexity of this solution becomes $O(m^3)$. A more efficient algorithm for solving the rectangular assignment problem can be found in [13], which is a rectangular extension of the Munkres algorithm. The complexity of this algorithm is $O(n^2 m)$. The rectangular version of LAPJV was proposed in [12], with a more efficient and robust solution than the original one in [75]. It is one of the most efficient algorithms for the rectangular cost matrix among the other proposed solutions in the literature. In this work, we adopted the rectangular version of LAPJV due to its efficiency.

4.2.4 Jonker-Volgenant Algorithm for Linear Assignment Problem (LAPJV)

We report the main steps of LAPJV in pseudocode in Algorithm 3. Note that we are not intended to give the technical details of the algorithm, instead we will provide here an overview of the steps of the algorithm. We refer the interested reader to [12, 75] for a comprehensive description of the LAPJV algorithm.

LAPJV consists of two main phases: *the initialization phase* and *the augmenting phase*. The initialization phase consists of three parts, i.e. *column reduction*, *reduction transfer* and *augmenting row reduction*.

The main purpose of the *column reduction* is to modify the cost matrix in such a way to have zero on each column. Initially, the minimum value of all columns over the rows is computed and subtracted the minimum value of each column from the value of the respective column. In such way, each column contains one zero and then,

assign those columns (with zero) to their corresponding row, see the steps 4 to 9 of Algorithm 3. *Reduction transfer* mainly helps to handle the unassigned row from the previous step (column reduction). For handling the unassigned row, it enables the row reduction, i.e. subtracting the minimum value of the row from each element each row, see steps 10 and 13 from Algorithm 3. After the reduction transfer, a set of paths are computed which starts from an unassigned row to an unassigned column. This step referred as *augmenting row reduction*. Initially, it starts from an unassigned row, find the 2nd smallest (minimum) value and subtract the value from the row. The unassigned row is assigned to the column that contain the 2nd smallest value and if the column is already assigned to any row, it makes the assigned row unassigned. This procedure is repeated for the unassigned row from the previous step until the unassigned column is found, see steps 15 to 22.

The *augmenting phase* computes the shortest path between the unassigned row and column with the modified Dijkstra's algorithm. Starting from an unassigned row, it finds the shortest path for it using the Dijkstra's algorithm and is assigned the unassigned row to the column found by the Dijkstra's algorithm. If the column is already assigned to any row, it marks the assigned row unassigned. The procedure is repeated for the unassigned row from the previous step until the unassigned column found, see step 25 to 30 of Algorithm 3). Finally, row and column solution matrices are updated with the minimum value for each row and its corresponding column.

The source code in Pascal can be found at `http://www.assignmentproblems.com/LAPJV.htm` and the Python implementation is adapted from `http://pymatgen.org/`.

4.2.5 Proposed Tract Segmentation Framework

In this thesis, we propose an example-based supervised tract segmentation approach. Given an anatomical tract of interest, e.g. the corticospinal tract (CST), and a set of examples of that tract, segmented from multiple subjects, our aim is to exploit the information from those examples in order to automatically segment the tract of interest in a new subject.

The overall framework of the proposed tract segmentation approach is illustrated in Figure 4.4. The inputs to the framework (blue dotted line) are the tract of interest from the different subjects (termed *example tract*) and the whole brain tractogram. The desired output (blue dotted line) of the framework is the segmented tract from the whole brain tractogram. Two different processes are involved in the proposed framework: *correspondence* and *refinement*.

The tract segmentation method that we propose consists of two main steps (see Figure 4.4. In the first step, each example tract uses the correspondence process to obtain a candidate segmentation in the new tractogram, see Figure 4.5. In the second step, the candidates generated from each example are merged together and then filtered through the refinement process, in order to obtain the final segmentation of the desired tract, taking into account the variability of the examples across subjects.

Tract Correspondence from a Single Example

Given one example of the tract of interest, $t_A = \{s_1^A, \ldots, s_k^A\}$, e.g. the segmented CST from subject A, the first step of the proposed method is able to extract the set of streamlines of subject B corresponding to t_A: $t_{A \to B} \subset T_B$. The extracted tract, $t_{A \mapsto B}$, is an approximation of the actual tract/bundle of interest in subject B, i.e. t_B. The procedure is based on the concept of streamline correspondence, i.e. on finding which streamline in the new tractogram corresponds to a given streamline in the example tract.

Input: Cost matrix, $C = \{c_{ij}\}_{i=1...k, j=1...M}$
Output: The assignment for each row of the cost matrix
Column Reduction
for j=n:1
find the minimum value over rows for column, j
if the row with lowest value at unassigned column **then**
assign the column with the lowest row index
end **if**
end **for**
Reduction Transfer
for each unassigned row:
transfer the unassigned to assigned row
end **for**
Augmenting Row Reduction
repeat
finding augmenting paths starting in an unassigned row, i
if j is unassigned **then**
augmentation solution is from the alternating path
else
reassigning column j to row i, reduction is transferred
end **if**
until no reduction transfer or augmentation.
Augmentation
repeat
Augment solution for each free rows
Construct the auxiliary network and determine from an unassigned row i to an unassigned column j
find an alternating path by the modified Dijkstra's shortest path method, which is used to augment the solution
Adjust the cost matrix.
update column values, and reset row and column assignments along the alternating path
until no unassigned rows
Final Assignment
Update all the assignment with the assigned row and column values to ensure minimum values for each row of the cost matrix.

Algorithm 3: LAPJV algorithm [from [115]]

Correspondence as (Rectangular) Linear Assignment Problem The segmentation method that we propose in this work is based on the (rectangular) linear assignment problem (LAP).

Given the tract/bundle $t_A = \{s_1^A, \ldots, s_k^A\}$ of subject A and the tractogram $T_B = \{s_1^B, \ldots, s_M^B\}$ of subject B, where $k \lll M$, and a distance function $d()$ between streamlines, we denote as $C = [c_{ij}]_{i=1...k, j=1...M}$, the distance matrix between each streamline of t_A to each of T_B, i.e. $c_{ij} = d(s_i^A, s_j^B)$. Then, we define the corresponding streamlines of t_A in T_B as those found by the solution of the corresponding rectangular linear assignment problem (RLAP):

$$P^* = \underset{P \in \mathcal{P}}{\operatorname{argmin}} \sum_{i=1}^{k} \sum_{j=1}^{M} c_{ij} p_{ij} \tag{4.8}$$

where $[p_{ij}]_{ij} = P \in \mathcal{P}$ is a *partial* permutation matrix, i.e. $P = [p_{ij}]_{ij} \in \{0,1\}^{k \times M}$ and $\sum_{j=1}^{k} p_{ij} = 1$ but $\sum_{i=1}^{M} p_{ij} \leq 1$. P^* is the optimal assignment, i.e. the one with lowest overall cost. Once P^* is obtained, the segmented tract in T_B is defined as the set streamlines in T_B corresponding to t_A according to P^*.

Finding the optimal solution of the LAP or RLAP is usually computationally very expensive. We refer Sec-

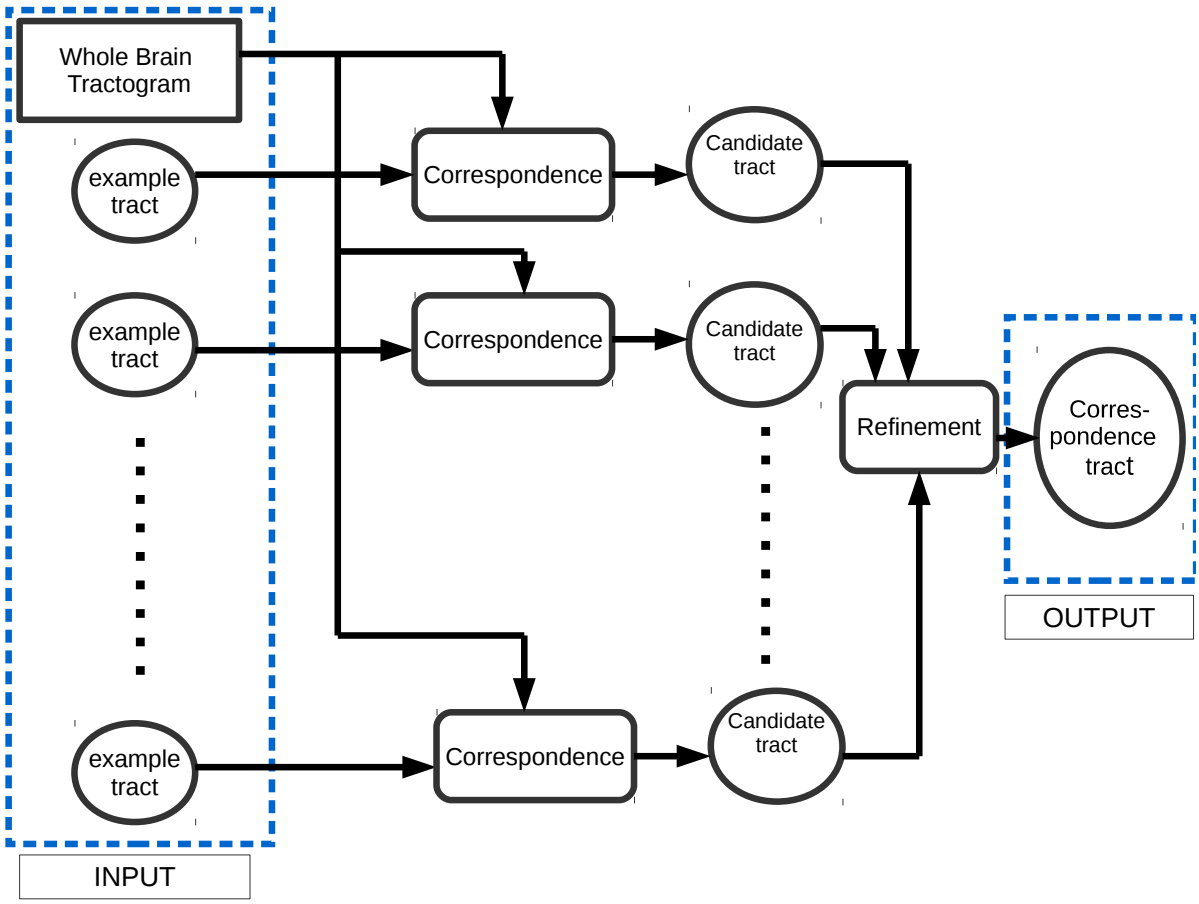

Figure 4.4: Proposed tract segmentation framework

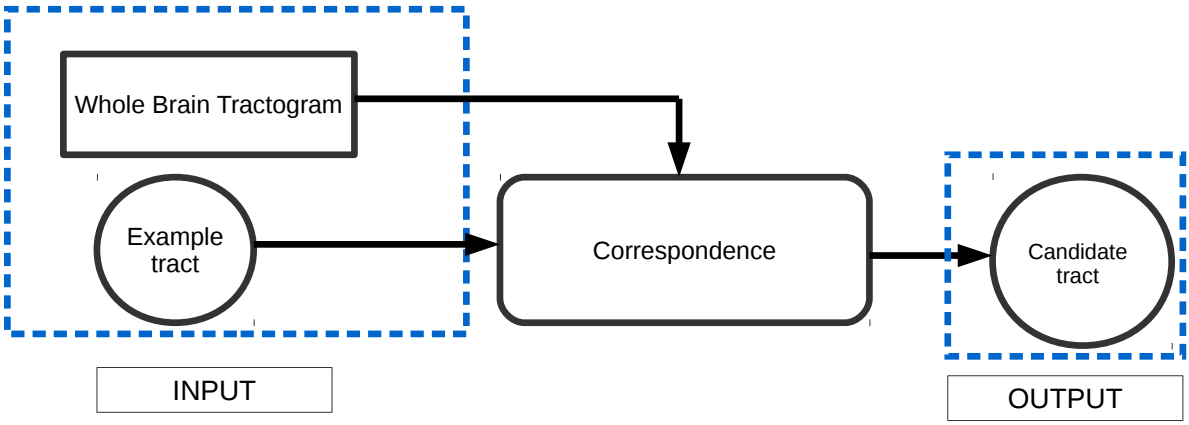

Figure 4.5: Tract correspondence from a single example

tion 4.2.4 for the description of the adopted LAPJV algorithm. Due to the computational cost of the algorithm, LAPJV cannot be directly applied to the full cost matrix, i.e. between the streamlines of the example tract and the whole set of streamlines of the target tractogram. Anyway, a key element of the scalability of our solution is

a further step that we introduce before starting the RLAP: the *sparsification* of the cost matrix C. In our experiments, we noticed that only a small part of the whole C is actually used in LAPJV. Specifically, for each streamline in t_A only the distance from the neighboring streamlines in T_B plays a role in the computation. For this reason, by leveraging the dissimilarity representation and k-d tree (see Section 4.3), we efficiently computed just a small subset of C instead of the whole matrix, saving a substantial amount of time and memory both in building C and in executing LAPJV. The small subset of streamlines of the target tractogram T_B is computed by the union of 500 nearest neighbors (NN) of the streamlines in the example tract t_A, $i \in \{1,\dots,N\}$. We refer to Section 4.3.3 for the detail procedure of the NN computation and Section 6.2.2, for the implementation of the steps.

Tract Correspondence from Multiple Examples

The quality the segmented tract/bundle obtained from a single example tract, is limited by inherent differences in the white matter anatomy between subject A and B. In order to reduce the bias of segmenting from a single specific example, here we describe a procedure to segment the desired tract/bundle from multiple examples, each from a different subject. In this way we try to exploit the anatomical variability in the sample of subject as if we had a model of the tract. The proposed procedure is based on first computing the correspondence between each example and the new tractogram and then on ranking all the corresponding streamlines according to how frequently they have been selected by the segmentation induced by each example. In the following we describe the details of the proposed procedure.

Refinement Through Ranking Given a tract/bundle of interest, e.g. the CST, the set of N examples segmentations of that tract from N different subjects is denoted as $\{t_{A_1},\dots,t_{A_N}\}$. For each example tract t_{A_i}, a corresponding tract $t_{A_i\to B} \subset T_B$ can be obtained following the RLAP procedure explained in Section 4.2.5, or other strategies like nearest neighbor. The resulting set of segmentations for t_B is denoted as $\{t_{A_1\to B},\dots,t_{A_N\to B}\}$. Our aim is to find an improved approximation of t_B, that we call $\hat{t}_B$, leveraging all N/ The proposed procedure to obtain $\hat{t}_B$ is the following:

1. Compute the union of the obtained segmentations: $t_{(A_1,\dots,A_N)\to B} = \bigcup_{i=1}^{N} t_{A_i\to B}$. This is a meaningful superset of t_B.

2. Score each streamline in $t_{(A_1,\dots,A_N)\to B} \subset T_B$ by counting how many time the streamline appears in $\{t_{A_1},\dots,t_{A_N}\}$. In this way, selected multiple times as potential streamline of t_B is considered evidence of being a reliable streamline. We further introduce other criterion in order to break ties in the ranking between streamlines selected the same number of times. Our proposed second criterion comes from the selection cost of the streamlines, i.e. the distance of the streamline during the time of selection. Lower cost means a more reliable matching. Once all scores are obtained, we ranked the streamlines according to their score.

3. We define the number of streamlines of $\hat{t}_B$ as the median number of streamlines of the example tracts: $\hat{k} = |\hat{t}_B| = median(t_{A_1\to B},\dots,t_{A_N\to B})$.

4. $\hat{t}_B$ is the set of $\hat{k}$ top ranked streamlines.

According to the ranking schema, we computed the score of each of the streamlines from the superset of t_B based on two criteria, i.e. i) the number of selection time of the streamlines and ii) the cost or the distance value during the selection. To justify these two criteria, we will elaborately discuss with an example here. For example, a streamline can be appeared in the superset five times or just once. Indeed the streamline with five times selection

will have the higher score compare to the streamline appeared just once. The second criterion comes into play when two streamlines have the same number of scores due to the same number of selections. To differentiate between these two streamlines, we further include other criteria, i.e. the cost or distance value of the streamlines during the time of selection as a correspondence streamline by the examples. Lower cost means a more reliable matching. As an example, if the two streamlines, s_1 and s_2 selected 5 times and their cost is 0.40 and 0.34, respectively, the highest rank will be given to the streamline s_2, due to the minimum cost compared to s_1. We believe that combining these two criteria is worthwhile to rank the streamlines as we are considering two different and important pieces of information.

Validation Approach After segmentation, we validated the segmented tract with two different evaluation metrics. Firstly, we followed the common practice, i.e. we computed the overlap between the segmented tract (extracted by the proposed method) and the ground truth tract. In order to generate the ground truth tract, we relied on the well-known parcellation-based segmentation approach, i.e. white matter query language (WMQL). The overlap is computed among the voxels of the two tracts. We computed the degree of overlap using the dice similarity coefficient (DSC) [43]. Secondly, we used the receiver operating characteristic (ROC) [15] curve analysis. ROC curve plots the true positive rates (TPR) against false positive rate (FPR) by moving the threshold in the ranking of streamlines. A higher TPR with respect to a given FPR indicates a better segmentation.

4.3 Scalable Nearest Neighbour (NN) for the Tractogram

In this thesis, we propose an efficient way to compute the nearest neighbors of a given set of streamlines. This is needed to obtain for an efficient implementation of graph matching and LAP solutions. Our proposed procedure to compute the NN greatly simplify the computation both in terms of time and number of logical steps. Our procedure includes a vectorial representation of the streamlines of the tractogram, based on the dissimilarity representation (DR) [106], and the construction of k-d (k-dimensional) tree [11] from the obtained vectors. Finally, by applying the efficient nearest neighbor query of the k-d tree, we can quickly retrieve the closest streamlines.

4.3.1 Notation and Terminology

K-d (k-dimensional) Tree A k-dimensional tree (k-d tree, see [11]) is a space partitioning data structure to efficiently store and retrieve vectorial data in k-dimensional space. The k-d tree provides fast nearest neighbor queries on large dataset. In this work, we use the k-d tree on the vectorial representation of streamlines, in order to quickly find the neighboring streamlines of a given streamline s. The computational complexity of building a k-d tree is $OM\log M$ and the nearest neighbor query is $O\log M$, where M is the number of streamlines of the tractogram. For example, a modern desktop computer can retrieve the 10 neighbors of a streamline in a tractogram in a few milliseconds[7].

4.3.2 Dissimilarity Representation and Prototype Selection

A vectorial representation of data is not an absolute requirement for machine learning and data mining. It facilitates the development of efficient algorithms, as it allows performing fast queries, as well as algorithms based on simple linear algebra operations. Given that the size and complex representation of the brain tractogram data is in contrast

[7] We measured the timing using the k-d tree implementation `sklearn.neighbors.KDTree` provided by the Python package Scikit-learn, see `http://scikit-learn.org`,

with the scalability requirement for the implementation of GM and LAP solutions, we apply a previously proposed vectorial representation for streamlines [106].

The DR [111] approach was mainly introduced for classification purposes. However, it has also been used in the context of unsupervised learning [111], [107]. In this approach, new features are defined for the objects, such that they are represented by their (dis)similarities to a set of objects that are representative of the problem at hand, i.e. the prototypes. In such way, every object is then represented by a vector of dissimilarities, instead of the attributes from the original feature space.

So, let us define the DR approach based on the tractogram application. Given $\mathcal{X}$ our space of objects, i.e.the streamlines, and the brain tractogram $T \subseteq \mathcal{X}$, let $\Pi = \{\hat{s}_1, \hat{s}_2, \ldots, \hat{s}_p\}$, $\Pi \subset \mathcal{X}$ be a set of prototypes of size p, and let $d : \mathcal{X} \times \mathcal{X} \to \mathbb{R}^+$ be a dissimilarity measure between streamlines. A mapping $\phi(\cdot, \Pi) : T \to \mathbb{R}^p$ is done, such that every object is associated with its dissimilarities to all prototypes in Π, $\phi(s_i, \Pi) = [d(s_i, \hat{s}_1), d(s_i, \hat{s}_2), \ldots, d(s_i, \hat{s}_p)]$. A way of handling the DR is to interpret the dissimilarity vectors as features. The obtained mapping to $\mathbb{R}^p$ is equipped with the traditional inner product and Euclidean metric, and we have the so-called dissimilarity space (DS). In this way, the dissimilarity matrix $\Phi(T, \Pi)$ is used as input for the classification or clustering algorithms [111], [46].

The prototypes, are usually selected as the most representative objects of the data set, i.e. $\Pi \subseteq T$, or Π might be even the equal to T. However, in our case, due to the large number of streamlines, computing the whole dissimilarity matrix would be computationally infeasible. Hence, we need to find a set of prototypes, such that the computational cost is reduced. Moreover, note that this Euclidean embedding is a lossy one, in the sense that in general it is not possible to reconstruct s_i from $\phi(s_i, \Pi)$. The quality of the representation is strongly dependent on the choice of d and the selection of the prototypes. Therefore, it is important that we use a suitable distance and an efficient method to select effective prototypes for our application.

Prototype Selection Method

Due to the size of tractogram data sets, the computation of the whole dissimilarity matrix, i.e. $\Pi = T$, for the DR approach has two main disadvantages: excessively large storage requirements and very high computational complexity. Therefore, it is required to compute a small set of prototypes, in order to tackle these problems. Nevertheless, we cannot use just any prototype selection method. In this case, we need an efficient procedure that can scale well on large data sets.

Random Selection for example, is a very common algorithm and with the lowest computational complexity $O(1)$. In this case, given our set of streamlines or tractogram T, a subset Π of p number of streamlines is randomly selected. This algorithm has shown to work reasonably well for the DR approach [114], [111].

In [106], the authors proposed the use of the Subset Farthest First (SFF) [147] algorithm for selecting effective prototypes from tractogram data. This procedure is a stochastic scalable approximation of the well known Farthest First Traversal (FFT) algorithm, which has a computational complexity of $O(p|T|)$. It is also claimed that it reduces the chances to select outliers [147]. The SFF first samples $m = [cp \log p]$ streamlines from T uniformly at random, where $c = 3$. Afterwards, FFT is applied on this subsample i.e. one streamline is randomly selected as prototype $\hat{s}_1$ and a new prototype is iteratively added such that it is the streamline maximising the distance to the already selected prototypes. It was proved that under the assumption of p clusters in T, the probability of not having a representative of some clusters in the sample is at most $pe^{\frac{-m}{p}}$ [147], i.e. a sample of size m is a meaningful summary of T. The computational complexity of SFF is $O(p^2 \log p)$. For large data sets and small p, this prototype selection policy has a much lower computational cost that FFT.

Even though the SFF policy has shown to be a suitable option for prototype selection in tractogram data sets, it is still based on an initial random selection of streamlines. Therefore, the final representation set will depend on

whether the random selection is a poor subsample of the tractogram or not.

We propose a new algorithm of prototype selection for tractogram data sets, named Spatial SFF (S+SFF). It is basically the SFF algorithm with a new heuristic, which is based on background knowledge information about the application. When looking at a full brain tractogram, it can be noticed that there are many short streamlines. It is very likely that these are just noise artifacts that have, of course, no anatomical meaning. Therefore, the first step of our algorithm is to exclude these streamlines for our selection. Thus, given z_{min}, a minimum allowed size for a streamline, we will just use the set of streamlines $T_{min} = \{s_1, s_2, \ldots, s_l\}$, such that $z_s > z_{min}$. Moreover, longer streamlines are believed to have greater potential to be useful landmarks, as they are more likely to be present in most subjects [54]. Hence, before proceeding with the selection, streamlines will be organized in descendant order according to their size. The goal of the selection step is to obtain a subsample of spatially distributed streamlines, such that streamlines from all brain areas are considered. The procedure is as follows: the longest streamline is selected and the next longest streamline is iteratively added, if it is not intersecting with any of the previously selected streamlines. Afterwards, the FFT is applied on the obtained subsample, as for the SFF algorithm. The computational cost of S+SFF is $O(|T| + l \log l + pl)$. This is more computationally expensive than SFF, but in practice $l << |T|$, therefore it is still feasible.

For more details of the prototype selections of the dissimilarity representation, we refer to Appendix B.

4.3.3 Procedure for Scalable Nearest Neighbor

In principle, the task of retrieving neighboring streamlines to a given one has a high computational cost. The straightforward solution entails computing the distance from the given streamline to all other streamlines in the new/target tractogram and then getting the minimum one.

In this thesis, we propose an efficient scalable nearest neighbor solution in order to simplify the computational cost, both in terms of logical steps and time. Given a tract t_A and tractogram T_A, we propose the following procedure to compute the nearest neighbor.

1. Compute a vectorial representation, e.g. the DR, of the streamlines of T_B and of t_A[8]
2. Build a k-d tree from the vectors of T_B.
3. For each streamline in t_A, in its vectorial form, perform a nearest neighbor query on the k-d tree.

[8]The DR of t_A is obtained using the prototypes of T_B.

Chapter 5

Materials

Overview

In the previous chapter, we presented the proposed methodologies to address the tractogram alignment and the tract segmentation problem. To validate the proposed methodologies, a large number of experiments will be conducted. We use the Human Connectome Project (HCP) dMRI dataset for conducting all the experiments. In this chapter, we briefly describe the HCP dMRI dataset. However, a key element for evaluating the proposed tractogram correspondence and tract segmentation is the ground truth tracts. In order to generate the ground truth tracts, we rely on the well-known parcellation-based segmentation approach, i.e. white matter query language (WMQL). In this chapter, we present a comprehensive details on how to apply the WMQL. We also briefly describe the anatomical definition of the extracted tracts with WMQL.

Organization of the Chapter

The chapter is structured as follows. We will describe the details of the HCP dMRI datasets in Section 5.1. The anatomical definition of the extracted tracts with the WMQL and detail procedures to apply the WMQL are described in Section 5.2.

5.1 HCP dataset

The HCP dataset is a publicly available dataset, acquired by the Washington University-University of Minnesota Human Connectome Project Consortium (WU-Minn HCP) [150, 56]. The HCP project aims to acquire accurately a large number of normal adult brain data, and also to make the data publicly available in a user-friendly manner. To accomplish the goals, they acquired 1200 healthy subjects dataset with different neuroimaging modalities, e.g. structural, functional and diffusion, including the $T1$-weighted ($T1W$) and T2-weighted ($T2W$) structural scans, resting-state [132]. The age of the healthy adults is in the range of 22 to 35 including the twins and their non-twin siblings [150]. A comprehensive detail of the HCP dataset can be found in [150, 56].

Data Acquisition

The structural images are being acquired by the $3T$ Siemens Skyra scanner using a 32-channel head coil. Both $T1W$ and $T2W$ images are obtained in high resolution with 0.7 mm isotropic. In case of $T1W$ images, the field of view was 224×224 mm^2 and matrix size = 320, 256 sagittal slices in a single slab. The voxel resolution was $1.25 \times 1.25 \times 1.25$ mm^3 with a repetition time (TR) $3200ms$ and echo time (TE) $565ms$. The measurements were performed in 3×90 gradient directions at $b-values$ = $1000, 2000$ and 3000 s/mm^2 [132] and 18 non-diffusion weighted images ($b = 0$). Total acquisition time includes a set of 20 *mins* structural scan and one diffusion imaging session of 1 *hour*.

Diffusion Preprocessing

Due to the large diffusion gradient, diffusion images can have the distortion caused by the eddy currents, which can lead to the artifacts in the brain imaging. Consequently, due to the inhomogeneities in the applied magnetic field, Echo-planar imaging (EPI) distortion can happen. However, the eddy and EPI distortion corrections [5] are done with the top-up tool from the FSL5 [1]. The Gaussian Process predictor is used to feed all the images with the estimated distortion, in order to compute the eddy-current induced field and the head motion for each image volume. Distortions are corrected with the eddy tool from the FSL5. For the more details of the preprocessing, we refer the work in [132].

In order to register the diffusion images, the transformation matrix is computed between the native diffusion space and the native structural space. Afterwards, the gradient non-linearity corrected mean $b0$ image is register with the $T1W$ structural image, using the $FSL/FLIRT$ in the $FMRIB$ software library. In the case of nonlinear registration, the deformation field is also computed and is available with the dataset. The Freesurfer [49] is used to generate the parcellation-based atlas.

Tractogram Generation

Generating the tractogram includes two steps: i) reconstruction and ii) tracking. For each subject, dMRI data are extracted with b-value 1000 s/mm^2 and the b-value threshold for the single-shell extraction is $b0 = 10$. The fiber orientation distribution in each voxel was reconstructed using the constrained spherical deconvolution model (CSD, see [142]). In CSD, the estimation of the fiber response function per voxel is an important preprocessing step. We use the *auto_response* function from the Dipy in module *dipy.reconst.csdeconv* to estimate the response using the FA image. Once the response function is estimated, it is used to generate the CSD model by the *ConstrainedSphericalDeconvModel* function from the *dipy.reconst.csdeconv* module. Then the *CSD* model is fitted with the function *peaks_from_model* with the values 0.5 and 25, for the parameters *relative_peak_threshold* and *min_separation_angle* respectively.

To generate the tractogram, we use the EuDX streamline tracking algorithm [53], with 10^6 seeds. The *FA* threshold for the auto response function is set to 0.7 and the angular threshold is 30°. The EuDX is used from the module in the DiPy [2] library, *dipy.tracking.eudx*. The resulting tractograms consist of approximately $100-140$ thousands streamlines.

[1] `https://fsl.fmrib.ox.ac.uk/fsl`
[2] `http://nipy.org/dipy`

5.2 White Matter Query Language (WMQL)

The TractQuerier, based on the WMQL [157], is a parcellation-based open source tool[3], to segment the whole brain tractogram. Using the parcellation from FreeSurfer and a database of ROIs, defined by the anatomical information of the tract, the WMQL extracts the anatomically meaningful tracts with a rule-based approach. It uses a query language based on a near-to-English texture syntax. Using the queries, three different kinds of operations are performed: anatomical, relative position and logical operations. If a streamline ends or traverses in certain anatomical regions of the brain, it referred as anatomical terms. If streamline lies on lateral or frontal of a certain anatomical structure, it referred as relative position terms. The logical operations include the conjunctions, disjunctions or exclusion of the anatomical and relative position terms.

WMQL Usage

For applying the WMQL queries on the tractogram, an atlas of the brain structures need to overlay on the top of the tractogram [157]. Although the WMQL is not depending on any particular atlas, the cortical and parcellation based white matter atlas are the commonly used one. To run the WMQL, the following procedure is followed:

- INPUT: Full brain tractogram with (.trk) or the (.vtk) file formate, and the parcellation as the Neuroimaging Informatics Technology Initiative (nifti) file formate. Parcellation is generated from the Freesurfer `https://surfer.nmr.mgh.harvard.edu/` with the same space as the tractogram.

- OUTPUT: List of tracts; each tract, as a set of streamlines in (.trk) or (.vtk) file formate.

Segmented Tracts with the Tract-Querier

In WM, three different kinds of tracts are found, based on the connection of the different parts of the brain. They are: association, projection and commissural tracts [60]. A sketch of the commonly found tracts is shown in Figure 5.1. WMQL currently contains the descriptions of 10 association, 8 projection, and 7 commissural tracts (see Figure 5.2). All those tracts can be segmented with the WMQL from the whole brain tractogram. Following a brief description of the segmented tracts are given:

Association Tracts The association tracts link the regions within the same hemisphere [52]. Associate tracts can be divided into two groups, based on the size of the tracts: long association tracts and short association tracts. The long association tracts are located in the deep white matter (DWM) which contains common anatomical feature across individuals. The short association tracts, also known as U-fibers, are located in the superficial white matter (SWM) which is the space between the DWM and the cortex. The common association tracts, extracted from the WMQL are the Cingulum Bundle (CB), Superior Longitudinal Fascicle (SLF), Arcuate Fascicle (AF), Inferior Longitudinal Fascicle (ILF), Inferior Occipito-Frontal Fascicle (IOFF), Middle Longitudinal Fascicle (MdLF), Uncinate Fascicle (UF) and the Extreme Capsule (EmC). Note that, the SLF tract segmented by WMQL has three parts: Superior Longitudinal Fascicle I (SLF I), Superior Longitudinal Fascicle II (SLF II) and Superior Longitudinal Fascicle III (SLF III).

[3] `http://tract-querier.readthedocs.io/en/latest/`

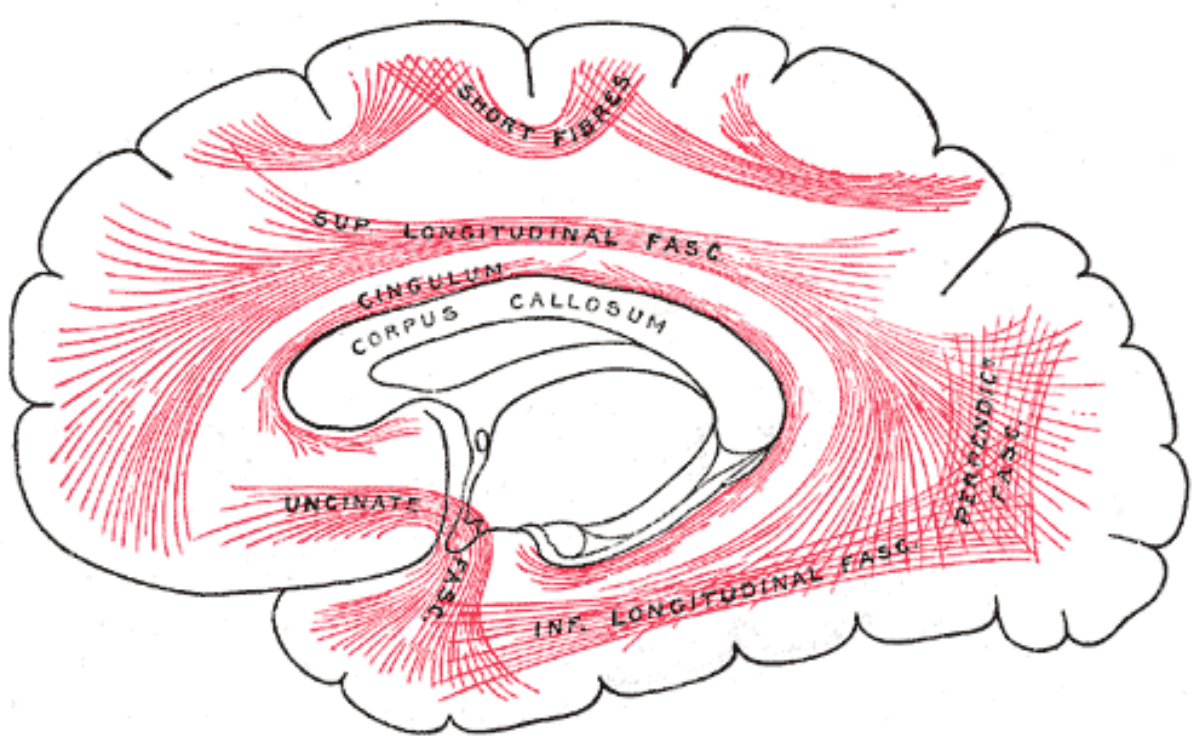

Figure 5.1: Diagram of association fibers in the cerebrum which shows that associate fibers connect fibers from the same hemisphere [from [60]]

Projection Tracts Projected tracts [60] link between the area of the cerebral cortex to a subcortical structure, e.g. the thalamus and spinal cord. The most well known projected tracts are the corticospinal tract (CST) and the thalamic radiations. The three segmented tracts with WMQL in this group is Cortico-Spinal Tract (CST), Cortico-thalamical Tracts, Cortico-striatal Tracts.

Commissural Tracts Commissural tracts [60] link the regions of the two cerebral hemispheres. The Corpus Callosum (CC) is the largest tracts of the human brain. Extracted CC with the WMQL has the seven sections as suggested by [160] .

Segmented Tracts Information with WMQL

All the subjects are aligned with the voxel based linear registration tool FLIRT/FSL[4] on the $b0$ images. After alignment, the WMQL is applied over thirty subjects to segment the whole brain tractogram.

In Table 5.1, we report the average and standard deviation of the number of streamlines and of voxels over 30 subjects for sixteen tracts. We observe that for four tracts, such as cst.left, cst.right, ilf.left, ilf.right, the variance in the number of streamlines is larger than the mean. This can happen due to two facts: i) the number of artifacts in the segmented tract, ii) inability to segmented those specific tracts for some subjects. To support our claim, in Table 5.2 and 5.3, we report the number of streamlines of all the 30 subjects from the HCP datasets.

It is worth noting that not all the tracts of the 30 subjects were used for the experiments in this thesis; rather

[4] `http://fsl.fmrib.ox.ac.uk/`.

Tract Name	# Streamline			# Voxels		
cst.left	39	±	39	957	±	625
cst.right	23	±	34	644	±	544
cg.left	1141	±	168	9039	±	1172
cg.right	982	±	159	8200	±	1087
ifof.left	173	±	94	3713	±	1295
ifof.right	123	±	76	2796	±	1212
ilf.left	96	±	71	1771	±	610
ilf.right	54	±	59	2035	±	566
uf.left	143	±	76	1794	±	844
uf.right	185	±	66	1140	±	819
af.left	248	±	138	3271	±	1342
af.right	102	±	156	1581	±	1784
mdlf.left	123	±	96	2254	±	1186
mdlf.right	98	±	77	1655	±	841
cc_2	433	±	120	4103	±	697
cc_7	408	±	116	5694	±	1115

Table 5.1: Data description. For each tract, the table reports the average and standard deviation of the number of streamlines and of voxels over 30 subjects.

we choose nine tracts from ten subjects which are consistent across subjects in terms of the number of streamlines for performing the tractogram alignment experiments. The set of tracts are: cg.left, cg.right, ifof.left, ifof.right, uf.left, uf.right, af.left, cc_3 and cc_7. In the case of tract segmentation experiments, we selected ten tracts based on two criteria: i) important in clinical studies and ii) consistent across subjects. The tracts are as follows: cst.left, cst.right, cg.left, cg.right, uf.left, uf.right, ifof.left, ifof.right, ilf.left, ilf.right.

	Tract Name							
Subject ID	cst.left	cst.right	cg.left	cg.right	ifof.left	ifof.right	ilf.left	ilf.right
100307	5	34	1181	969	169	152	26	29
124422	12	22	905	1002	183	69	56	1
161731	49	20	1235	974	66	20	31	163
199655	57	0	1326	1036	142	284	160	21
201111	45	5	1361	1247	92	131	45	0
239944	65	2	1185	1178	202	176	188	258
245333	0	3	1230	1050	54	40	85	42
366446	32	24	1126	904	290	311	6	34
528446	12	29	1396	1235	161	22	32	0
856766	4	1	1150	861	68	109	140	68
111716	28	17	1093	808	204	69	96	1
135932	31	0	1178	765	145	276	83	74
103414	116	10	979	671	85	64	139	47
110411	73	21	1237	1038	234	60	9	0
115320	44	45	965	734	403	172	98	70
126325	27	95	1146	1008	83	150	294	8
128632	26	21	1257	931	80	151	69	37
151526	64	10	1232	1026	332	93	50	108
127933	162	4	1431	1078	283	241	10	0
190031	68	7	703	901	186	36	95	41
756055	31	9	964	795	167	100	104	52
792564	18	86	1249	1160	299	134	250	84
984472	8	23	898	837	181	170	101	35
192540	12	159	1058	966	264	141	170	39
100408	18	1	1323	1377	293	232	44	19
105115	123	19	1125	1059	148	15	65	74
106016	3	17	1115	1002	175	97	206	194
111312	0	0	1048	821	68	71	42	50
117122	0	16	885	987	2	2	75	30
136833	46	0	1256	1050	138	106	116	54

Table 5.2: Tract/Bundle sizes, in terms of number of streamlines across the 30 subjects from the HCP dataset. The Tracts were segmented with WMQL, see [157].

	Tract Name							
Subject ID	uf.left	uf.right	af.left	af.right	mdlf.left	mdlf.right	cc_2	cc_7
100307	138	250	92	35	55	256	661	546
124422	193	158	333	190	116	40	283	431
161731	179	195	273	172	137	146	300	337
199655	166	244	176	1	69	27	302	442
201111	281	211	550	508	16	113	670	413
239944	60	73	124	2	11	244	407	247
245333	144	145	352	137	299	13	314	441
366446	296	182	200	8	239	128	638	577
528446	102	156	234	77	227	16	464	520
856766	66	41	172	0	22	27	628	319
111716	130	124	155	0	196	70	438	331
135932	296	265	240	49	286	86	449	454
103414	42	143	71	2	170	209	502	302
110411	76	96	128	81	65	37	349	591
115320	88	137	173	0	17	29	575	209
126325	25	91	330	0	176	86	478	597
128632	63	229	148	1	177	83	358	516
151526	168	278	351	638	146	45	368	520
127933	66	237	265	2	54	123	287	529
190031	160	240	9	1	371	170	514	393
756055	229	245	155	4	214	243	324	303
792564	168	150	195	28	48	66	413	513
984472	67	152	255	342	30	59	567	333
192540	159	236	328	197	27	18	391	388
100408	231	235	679	5	131	53	533	466
105115	226	341	277	192	23	81	263	275
106016	194	178	234	103	107	150	375	183
111312	143	217	192	40	112	109	409	286
117122	58	165	336	241	20	0	334	321
136833	93	160	433	22	143	242	422	467

Table 5.3: Tract/Bundle sizes, in terms of number of streamlines across the 30 subjects from the HCP dataset. The Tracts were segmented with WMQL, see [157].

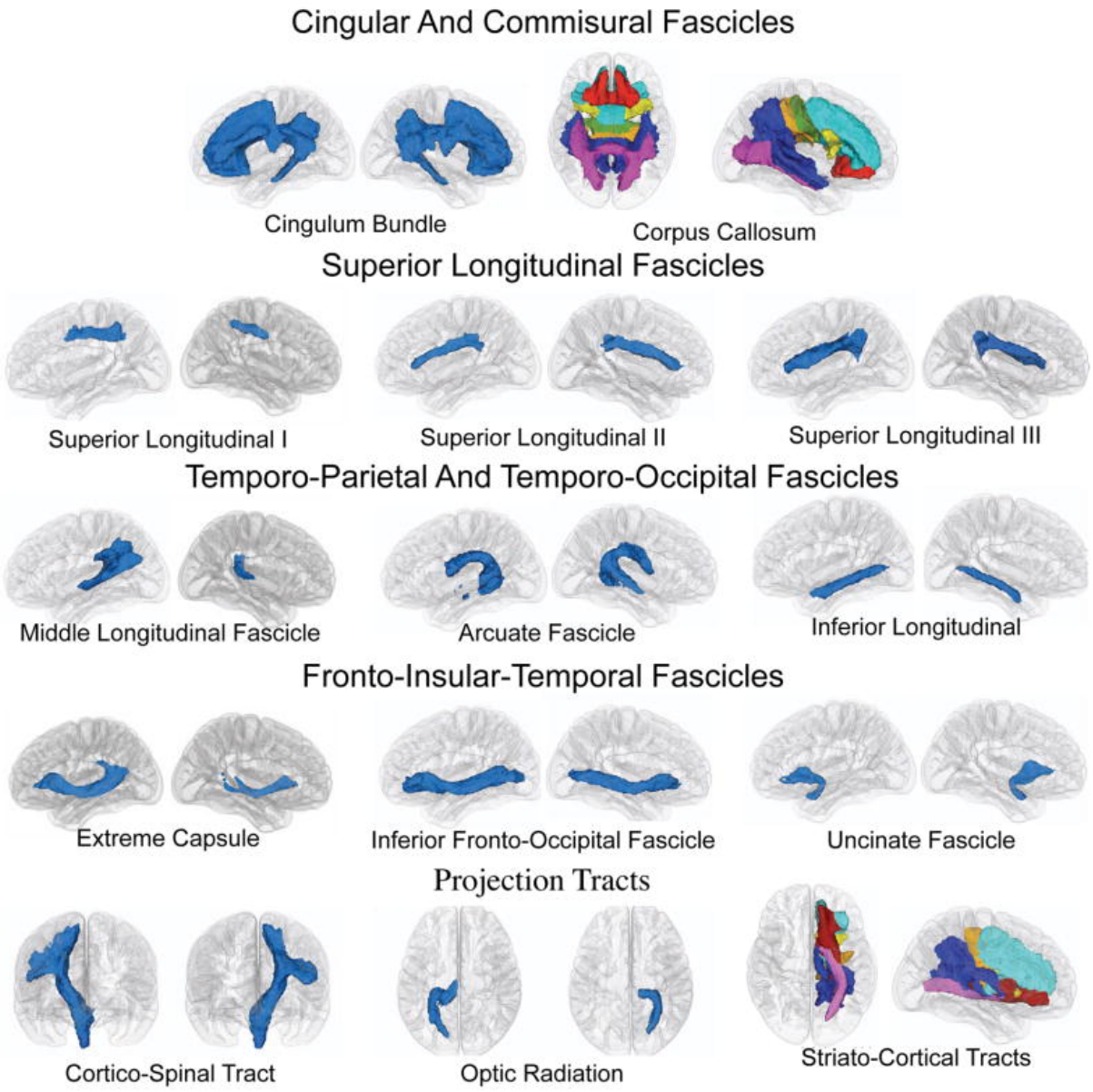

Figure 5.2: Segmented tracts with WMQL: ten association tracts and two projection tracts with the iso-surfaces [images are taken from [158]]

Chapter 6

Results

Overview

In the previous chapter, we describe the HCP dMRI dataset that has been used to conduct all the experiments. In this chapter, we present all the components for the quantitative validation of our proposed methods, i.e. tractogram correspondence and a novel approach for supervised tract segmentation. In this regard, we describe the evaluation metrics, details setup of the experiments and the experimental results for both methods. Moreover, for both of the proposed methods, we have performed the quantitative comparison of our methods with other existing methods and we report the comparison results in this chapter. We conclude this chapter by reporting the running time of our proposed scalable solution for the nearest streamline computation.

Note that we present the partial results of our experiments in this chapter; detail results can be found in Chapter 8 and Chapter 9. In this chapter, we report a meaningful subset of the experiments.

Organization of the Chapter

The chapter is structured as follows. In Section 6.1 and Section 6.2, we report the experimental results of the tractogram correspondence and tract segmentation, respectively. In Section 6.3 we demonstrate the running time for our proposed scalable nearest neighbor solution.

6.1 Tractogram Alignment

In this section, we describe the experiments to support the claims about the advantages of tractogram correspondence over registration methods for tractogram alignment. The experiment was conducted on ten subjects from the Human Connectome Project (HCP) dMRI dataset. In order to quantify the quality of tractogram alignment produced by the methods in the literature and by the proposed one, we relied on measuring the degree of overlap of corresponding anatomical bundles/tracts after whole tractogram alignment (see [55, 59]). Since the bundle/tract information is never used to compute alignments, we can safely assume that the better such overlap, the better the alignment of tractograms. In the following, we provide the details of the compared alignment methods and evaluation metrics in the comparison. Finally, we report the results of all experiments.

6.1.1 Evaluation Metrics

In order for quantitative evaluation, we followed the common practice, also described in [55] and [59], i.e. we computed the overlap in voxels of a set of corresponding anatomical tracts after the whole brain alignment is done. The fraction of overlapping voxels between the tract (t_A^{al}) of the aligned tractogram and the one (t_B) in the target tractogram, usually called Jaccard index J, is then:

$$J = \frac{|v(t_A^{al}) \cap v(t_B)|}{|v(t_B)|} \tag{6.1}$$

where $v(t)$ indicates the set of voxels crossed by the streamlines of tract t, while $|\cdot|$ is the set size.

6.1.2 Experiment Setup

We aligned all pairs of tractograms obtained from the 10 subjects, i.e. 45 pairs. We compared the following alignment methods: standard affine registration of voxels, affine registration of streamlines, nonlinear registration of voxels and the proposed method based on graph matching (GM). Voxel-level affine registration was computed with FSL/FLIRT on the b0 images. Streamline affine registration was computed with two different algorithms: the entropy-based group-wise registration (ENT) algorithm[1] from [102] and with the streamline linear registration (SLR) algorithm[2] from [55]. In all cases, affine registration was applied to streamline coordinates using the function `dipy.tracking.streamline.apply_affine()`, from DiPy. Nonlinear voxel-level registration was computed with FSL/FNIRT, using the deformation fields directly provided within the HCP dataset[3].

In order to compare quantitatively the 5 different whole-tractogram alignment methods, we followed the common practice, also described in [55] and [59], i.e. we computed the overlap in voxels of a set of corresponding anatomical tracts after the whole brain alignment is done. Before alignment, we segmented a set of tracts in each tractogram with the white matter query language (WMQL, see [157])[4] and then used the streamline IDs to obtain the tracts on the tractogram after alignment. The set of tracts comprised of Cingulum Bundle (left and right), Inferior Occipito Frontal Fascicle (left and right), Uncinate Fascicle (left and right), Arcuate Fascicle (left) and Corpus Callosum (part 2 and 7). We selected these specific 9 tracts because their segmentation, obtained through WMQL, was more consistent across subjects, in terms of number of streamlines.

Graph Matching: further approximation

In order to obtain the correspondence between tractograms, we introduced a further approximation with a simple 3-steps procedure, similar to the one proposed for the SLR algorithm in [55]:

1. We clustered each tractogram into a given number of clusters ($k = 1000$) and defined the median (centroid) streamline as *representative* for each cluster. We adopted the fast mini-batch k-means algorithm described in [104] and [113].

2. We computed graph matching between the two graphs made only with the k representatives, in order to obtain corresponding clusters.

[1] We adopted the software implementation provided by the authors of ENT, available at: `https://github.com/ljod/whitematteranalysis`.

[2] As implemented in DiPy, `http://dipy.org`.

[3] The estimation of the deformation fields of the HCP dataset is described in [56] in the following way: "After bias field correction of the T1w and T2w images, the T1w image is registered to MNI space with a FLIRT 12 DOF affine and then a FNIRT nonlinear registration, producing the final nonlinear volume transformation from the subject's native volume space to MNI space."

[4] According to the white matter parcellation provided by the HCP initiative.

3. For each pair of corresponding clusters, we computed the graph matching between their streamlines, in order to find streamline correspondence.

Notice that, in all cases, approximate graph matching was computed with the DSPFP algorithm (see Section 4.1.5), with random initialization, i.e. $x_{ij} \sim U[0,1]$. This is different from the initialization recommended in [84], i.e. $x_{ij} = 1/(N_A N_B)$, but we observed failure of convergence in a few cases with such constant value, while random initialization always converged. We also tried the initialization resulting from an initial affine registration (based on SLR) and we obtained very similar results. For generality of the proposed method, we prefer to recommend random initialization.

6.1.3 Results for Tractogram Correspondence

Performing the 3-steps procedure required approximately 30 minuets of computation for each pair of tractograms on a standard desktop computer. Linear registration required a few minutes of computation for FLIRT and SLR, and approximately 30 minutes for ENT. FNIRT deformation fields were already available within the HCP dataset, anyway they usually require a few minutes of computation.

Table 6.1 shows the summary of the results of all 45 pairs across the 5 different alignment methods, averaged over 9 tracts. The first column report the HCP subject identifiers of one tractogram with which the rest 9 of the tractograms are aligned. The remaining five columns report the degree of overlap between the aligned tractograms (J, higher is better), averaged over the 9 tracts considered, for the five methods considered in the comparison: FLIRT, ENT, SLR, FNIRT and GM. For each subject, the highest degree of overlap is indicated in bold face. In order to avoid unreasonable outliers, we filtered out the cases for which the difference in number of streamlines for the same tract was extreme, i.e. greater than 60%, denoting problems in the WMQL segmentation. See Appendix A for an analysis of this issue.

	Method				
Subject	FLIRT	ENT	SLR	FNIRT	GM
100307	0.22±0.05	0.22 ±0.06	0.25 ±0.05	0.44±0.04	**0.59±0.05**
124422	0.23±0.04	0.22±0.04	0.25±0.03	0.44±0.03	**0.55±0.04**
161731	0.22±0.06	0.23±0.06	0.26±0.05	0.45±0.05	**0.55±0.06**
199655	0.23±0.04	0.22±0.06	0.26±0.03	0.42±0.03	**0.58±0.06**
201111	0.24±0.06	0.23±0.07	0.25±0.05	0.41±0.02	**0.56±0.05**
239944	0.22±0.04	0.22±0.04	0.24±0.02	0.45±0.02	**0.55±0.05**
245333	0.21±0.04	0.23±0.05	0.26±0.02	0.43±0.02	**0.57±0.03**
366446	0.23±0.07	0.23±0.07	0.26±0.05	0.44±0.03	**0.57±0.06**
528446	0.21±0.05	0.21±0.07	0.27±0.03	0.43±0.03	**0.56±0.04**
856766	0.24±0.03	0.23±0.03	0.27±0.01	0.44±0.03	**0.59±0.03**

Table 6.1: Summary of the results: average voxel overlap between corresponding tracts after whole brain alignment for the FLIRT, ENT, SLR, FNIRT, and the proposed GM. The table reports the overlap for each subject averaged over all the 9 tracts and the remaining 9 subjects.

In Figure 6.1, we show one paradigmatic example where there is a systematic displacement between the corresponding tracts (Corpus Callosum, section 7, as defined by the WMQL) of two subjects (HCP ID1: 100307,

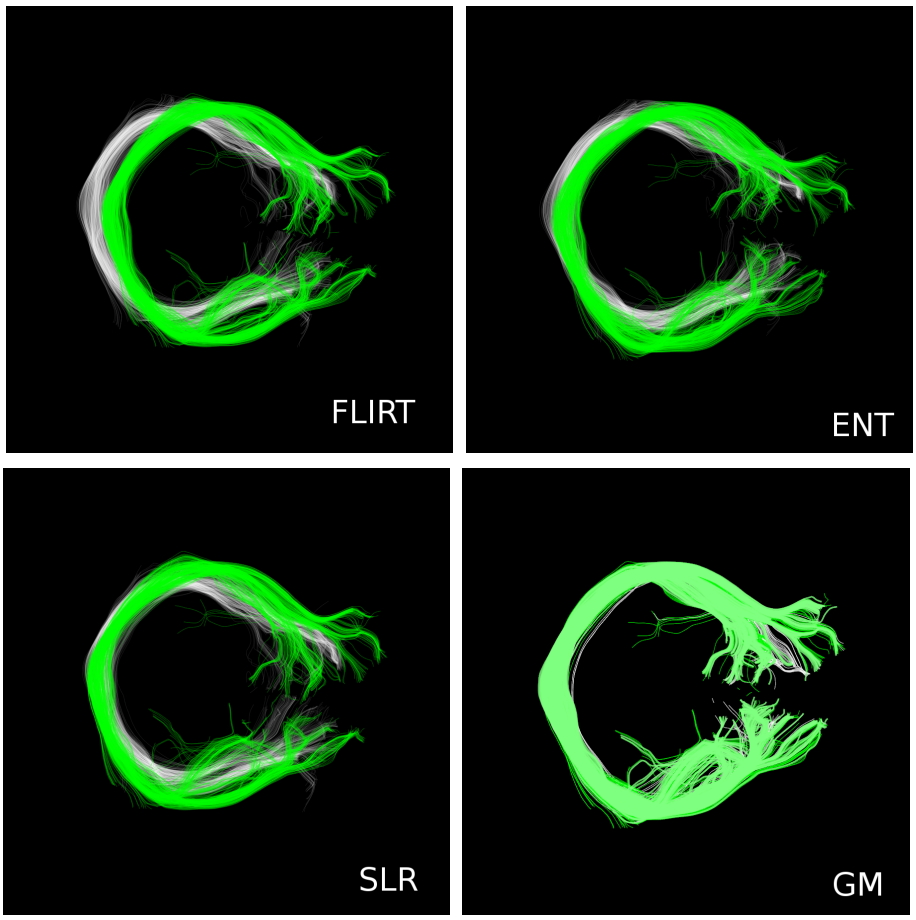

Figure 6.1: A paradigmatic example where there is a systematic displacement between the corresponding tract (CC, section 7) of two subjects after whole-brain affine registration, with FSL/FLIRT, ENT and SLR. Conversely, GM is able to provide much better alignment.

ID2: 199655) after whole-brain affine registration. White and green represent the two tracts after the registration computed with FSL/FLIRT, ENT and SLR[5]. In the same figure, we also report the alignment computed with GM, which shows a much superior match because GM acts also at the local level. For this specific example, the fractions of overlapping voxels for that tract are: $J_{FLIRT} = 0.18$, $J_{ENT} = 0.26$, $J_{SLR} = 0.24$, $J_{FNIRT} = 0.52$ and $J_{GM} = 0.81$.

6.2 Tract Segmentation

In this section, we present all the components for the quantitative validation for our proposed *LAP-based supervised tract segmentation method* . Experiments were performed on the Human Connectome Project (HCP) dMRI dataset. In order to quantify the quality of the segmentation results, we used the common approach by measuring the voxel overlap. Furthermore, we performed the receiver operating characteristic (ROC) curve analysis to validate our proposed segmentation approach.

[5]FSL/FNIRT is missing from this visual example because we did not apply the resulting deformation field to the streamlines: such procedure is not sufficiently analyzed in the literature. Nevertheless, we report the quantitative results at voxel-level.

6.2.1 Evaluation Metrics

To quantitatively evaluate the proposed LAP-based supervised segmentation framework, we adopted two different evaluation metrics, i.e. i) the dice similarity coefficient (DSC) [43] and ii) Receiver Operating Characteristic (ROC) curve [15] analysis. In the following, we will discuss the metrics in details.

Dice Similarity Coefficient (DSC): The common practice to validate the tract segmentation approaches is to compute the voxel overlap between the segmented tract and the ground truth tract. The degree of voxels overlap is measured through the DSC. In order to compute the DSC, we converted the each tract (both the segmented and the ground truth tract) to a binary mask where 1 indicates that a voxel is crossed by a streamline of the tract and 0 otherwise.

Given the segmented tract, $\hat{t}$, and the ground truth tract, t_g, the DSC is defined as follows:

$$DSC = \frac{2 \times (|v(\hat{t}) \cap v(t_g)|)}{|v(\hat{t})| + |v(t_g)|} \tag{6.2}$$

where $v(t)$ is the set of voxels crossed by the set of streamlines of the tract, t and $|v(t)|$ is the number of voxels in $v(t)$. The DSC varies between 0 to 1 and the higher value indicates better overlap.

Receiver Operating Characteristic (ROC) Curve: The analysis of the ROC curve is a standard measure for performance in the field of the medical image segmentation techniques [133]. It considers all possible degrees of sensitivity/specificity of the system to evaluate. We adopted such analysis to compare more in detail the performance of our proposed LAP-based segmentation method with respect to the nearest neighbor method.

The ROC curve plots the sensitivity, i.e. the *true positive rate* (TPR), against the specificity, i.e. the *false positive rate* (FPR) of the segmentation method at different thresholds. Here, the threshold refers to the ranking of the streamlines that we obtain in the refinement step, where we combine the segmentations obtained from each single example in a single ranking, see Section 4.2.5. In the proposed LAP-based method, we set such threshold as the median number of streamlines across the example tracts. In order to compute the ROC curve, here we span through all possible thresholds in the ranking to compute the curve. The TPR and FPR are computed by comparing the streamlines in the ranking above threshold (*positives*) and below threshold (*negatives*) with the ground truth, combining four numbers: the true positives (TP), i.e. the number of voxels of positives that are also in the ground truth tract, the false positives (FP), i.e. the number of voxels of the positives not in the ground truth, the true negatives (TN), i.e. the number of voxels of negatives not in the ground truth and the false negatives (FN), i.e. the number of voxels of negatives also in the ground truth. Hence the TPR and FPR are formulated as follows:

$$TPR = \frac{TP}{TP+FN}$$

$$FPR = \frac{FP}{FP+TN}$$

High values of TPR and (1-FPR) means good segmentation. Additionally, the ROC curve can be summarized in a single scalar value: the *area under ROC curve* (AUC) score, where higher AUC indicates better segmentation.

We adopted the python implementation of the ROC curve from scikit-learn [6], which requires to specify two important parameters, i.e. the true binary labels and the target scores. True binary labels are computed from the ground truth tract: given a voxel from the ground truth tract, if the voxel belongs to the segmented tract, the binary label of the voxel will be 1, otherwise 0. However, the target scores are accessed from the rank of each streamline which computed through the ranking scheme (described in 4.2.5). To compute the target score

[6] `https://http://scikit-learn.org/`.

at the voxel-level, we first convert the streamlines into voxels and then ranked the voxels accordingly with their corresponding streamlines. For example, if a streamline has the rank 1, all the voxels belong to that streamline will be ranked as 1.

6.2.2 Experiment Setup

Experiments were performed on thirty subjects from the Human Connectome Project (HCP) dMRI dataset. All the subjects were aligned with the voxel-based linear registration tool FLIRT/FSL[7]. After alignment, the WMQL was applied over thirty subjects to segment the whole brain tractogram. We divided the set of subjects into two groups, i.e. the *example group* and the *test group*, each of fifteen subjects. The tracts from the example group are used as prior information to guide the segmentation in the tractogram of new subjects. The tracts from the test group are used to quantify the quality of the obtained segmentation. A total amount of 300 tracts, will be considered as ground truth as well as examples for the experiments.

We compare our proposed LAP-based supervised tract segmentation method with the following methods: i) automatic ROI-based segmentation [167], two supervised segmentation based on the NN strategies, i.e. ii) an example-based multi-atlas approach with nearest neighbour strategy (hereafter denoted as MULTI_ATLAS) [162], iii) the proposed efficient nearest neighbor solution (see Section 4.2.5) with the minimum average distance measure (denoted as *DR_MAM*). In order to qualitative comparison among other segmentation approaches, we measure the degree of the voxel overlap through the DSC. Further, the ROC curve analysis performed to compare between the *DR_MAM* and proposed tract segmentation method with LAP (denoted as LAP). The reason behind this choice of methods for ROC analysis is due to the fact that for ROC analysis the probability or the score of each streamline of the segmented tract need to measure (referred as target scores). In the case of LAP and *DR_MAM*, the target scores of each segmented streamlines are measured through the proposed ranking schema. on the contrary, it is not possible to measure the rank between ROI-based segmentation and $MULTI\_ATLAS$, due to their methodology.

Tract Segmentation with LAP

As mentioned in Section 4.2.5, our proposed LAP-based supervised tract segmentation method consists of two parts: (i) Tract correspondence from a single example, through LAPJV and (ii) combination of the correspondences from multiple examples through ranking. Here we discuss the choice of the parameters in each part.

As described in Section 4.2.5, tract correspondence from a single example was obtained by solving the LAP between the streamline of the example and those of the target tractogram, with the rectangular LAPJV. Due to the computational cost of the algorithm, we could not directly apply it to the full cost matrix, computed between the streamlines of the example tract and the whole set of streamlines of the target tractogram. For this reason, the LAPJV algorithm was applied to a sparse cost matrix. The sparse cost matrix was computed by considering only a subset of the streamlines of the target tractogram T_B, specifically the union of all 500 nearest neighbors of the streamlines in the example tract t_A, $i \in \{1,\dots,N\}$, that we expect to be a superset of the ground truth tract t_B. In this way, instead of computing a cost matrix of size (approximately) $10^2 \times 10^5$ and solve the corresponding LAP, we reduced the problem to a cost matrix of size approximately $10^2 \times 10^3$. In order to compute such superset, we used the dissimilarity representation (DR) and a k-d tree. According to [106], 40 prototypes were selected from the whole brain tractogram, T_B, using the SFF heuristic and the MAM distance function. With them, we computed the DR, i.e. a 40-dimensional vectorial representation, of each streamlines in T_B. Afterwards, we put such vectors in a

[7] `http://fsl.fmrib.ox.ac.uk/`.

k-d tree, using the implementation provided by scikit-learn[8]. In the same way, all streamlines in the example tract (t_A) were represented as vectors using the previous prototypes. For each of those vectors, we computed 500 nearest neighbors from the k-d tree of T_B and defined the (expected) superset of the ground truth (t_B) as their union. Then, in order to compute the reduced/sparse cost matrix, the MAM distance between the each streamline in the example tract t_A those in the the union set, were computed. Finally, the LAPJV algorithm was applied on the constructed sparse cost matrix, in order to obtain the corresponding streamline from a single example (t_A).

Proceed with the second step with multiple examples, we consider the same segmented tracts of fifteen different subjects. We repeated the same procedure for fifteen examples and fifteen resulting correspondence tracts were extracted. By combining the fifteen extracted tracts, superset tract was obtained and refined by following the steps described in Section 4.2.5. In such a way, approximate tract of t_B, that we call $\hat{t}_B$, was segmented.

Note that, two extensive experiments were also performed to investigate the two important properties of the proposed segmentation method: i) to analysis the number of the nearest neighbor considered for each streamline in order to construct the sparse cost matrix, and ii) to select the appropriate number of examples in the case of multiple examples. We refer to the Chapter 8, for the details of the experiment.

Validation of LAP over Nearest Neighbor

We conducted the experiments to show the benefit of tract correspondence computed by the LAP over the NN. For this purpose, the tracts were extracted by using the nearest neighbor scenarios. We implement an efficient nearest neighbor solutions (DR_MAM), see the steps described in 4.2.5. We kept the same experiment setup, e.g. same embedding space, distance function, and refinement step, for the LAP and the DR_MAM to have an unbiased comparison. Hence we use the DR representation and kd-tree along with the MAM distance function. The procedure to compute the NN as follows: first, we transformed each streamline in T_B a 40-dimensional vectorial representation, using DR and we put such vector in a kd-tree. Second, each streamlines in the example tract represented as vectors using again the DR and compute its one nearest neighbor in T_B through the k-d tree query.

We plotted the average ROC curve (see Section 6.2.1) for ten well-known tracts of fifteen subjects and reported in Figure 6.3.

Comparison with the multi-atlas based approach in [162]

We compared our method with a multi-atlas example based tract segmentation technique, proposed in [162]. The main motivation of this comparison was to validate our method with the nearest neighbour solution provided by their work. As a further step, we implemented a faster version of their proposed algorithms by adopting the simplified nearest neighbor solution with the dissimilarity representation (DR) and kd-tree approach described in Section 4.2.5.

Proposed segmentation method in [162] consists of two parts : i) example data construction ii) automatic tract classification. For *example data construction*, multiple subjects are clustered and tracts are labeled by the expert. The extracted tracts further consider as a prior knowledge for the automatic segmentation. In the case of *automatic tract classification*, every streamline of the new subject is labeled by the following procedure: Firstly, for every streamline of the new subject, the nearest neighbor is extracted from the example data. Secondly, with the proposed voting scheme, every example subjects votes the streamlines based on two thresholds, i.e. *distance threshold* and *vote threshold*. Based on the majority of the votes, every streamline is labeled.

[8] `http://scikit-learn.org`.

The proposed method in [162] has the limitation of the time complexity and implemented on the GPU. In the case of nearest neighbor computation, every streamline from the new subject needs to compare with every streamline from each cluster of each subject from the example data, which increases the computational complexity of the proposed method. Therefore, we propose to use a simplified version of the nearest neighbor computation as described in 4.2.5. By adapting this, in contrary with the GPU implementation of the proposed method, tracts are extracted within two minutes with computer CPU core.

In this experiment, for the example dataset construction, we used 15 subjects from the example subject group, each segmented by the WMQL. All the parameters, e.g. streamline re-sampling, distance threshold, voting threshold, were set as suggested in [162]. Therefore, we used 32 points to re-sample the streamlines, 200 as distance thresholds and 7 as the voting threshold. Experiments were performed on a desktop computer with an intel Xeon(R) processor with 16*G* of RAM.

Comparison with ROI-based segmentation

We compared our method against well-known automatic ROI-based segmentation method proposed in [167]. To validate, we extracted ten tracts from fifteen test subjects with ROI-based segmentation.

Ten tracts were extracted based on the ROIs and atlas, which are available at `http://lbam.med.jhmi.edu/cmrm/Data_Yajing/fiberMenu.htm`. We registered the 15 subjects from the test group with the atlas, which is in MNI (Montreal Neurological Institute) space. The available ROIs has two way-points and streamlines go through the both way-points of the ROIs are extracted as *segmented tract*. Hence by placing the ROIs on the registered test subjects, we extracted the following ten tracts: left-right corticospinal tract (CST), left-right cingulum (CG), left-right inferior fronto-occipital fasciculus (IFOF), left-right Uncinate Fascicle (UF) and left-right inferior longitudinal fasciculus (ILF).

6.2.3 Results for Tract Segmentation

	Method			
Tract	ROI-based	DR_MAM	MULTI_ATLAS	LAP
cg.left	0.37 ± 0.05	0.66 ± 0.02	0.61 ± 0.02	$\mathbf{0.74 \pm 0.02}$
cg.right	0.38 ± 0.02	0.67 ± 0.02	0.60 ± 0.02	$\mathbf{0.72 \pm 0.02}$
ifof.left	0.41 ± 0.02	0.68 ± 0.02	0.57 ± 0.03	$\mathbf{0.71 \pm 0.02}$
ifof.right	0.36 ± 0.02	0.57 ± 0.04	0.55 ± 0.02	$\mathbf{0.60 \pm 0.04}$
uf.left	0.35 ± 0.03	0.61 ± 0.05	0.61 ± 0.03	$\mathbf{0.69 \pm 0.05}$
uf.right	0.39 ± 0.03	0.65 ± 0.05	0.65 ± 0.02	$\mathbf{0.69 \pm 0.05}$
cst.left	0.18 ± 0.02	0.43 ± 0.04	0.38 ± 0.02	$\mathbf{0.51 \pm 0.04}$
cst.right	0.19 ± 0.02	0.38 ± 0.02	0.29 ± 0.02	$\mathbf{0.44 \pm 0.04}$
ilf.left	0.20 ± 0.03	0.56 ± 0.04	0.60 ± 0.02	$\mathbf{0.65 \pm 0.04}$
ilf.right	0.13 ± 0.02	0.56 ± 0.02	0.38 ± 0.05	$\mathbf{0.60 \pm 0.03}$

Table 6.2: Summary of the results: average voxel overlap between the segmented tracts and ground truth tracts for the ROI-based, DR_MAM, MULTI_ATLAS, and the proposed LAP-based segmentation. The table reports the degree of voxel overlap, in terms of Dice similarity coefficient (DSC), for each tract averaged over fifteen subjects.

Table 6.2 reports the degree of overlap, as mean DSC, of ten different tracts for four different segmentation approaches. The means are computed for each segmented tract over fifteen test subjects. The first column reports the name of the tract and the remaining four columns report the average DSC (higher is better) for each tract, along with the standard deviation of the average DSC. For each tract, the highest degree of overlap among four different methods is indicated in bold face.

Figure 6.3 illustrates the average ROC curves of ten tracts with two different segmentation approaches, i.e. i) DR_MAM and ii) LAP. The average ROC is computed over fifteen subjects for ten segmented tracts. Each sub-figure demonstrates the average ROC curves for each tract with the DR_MAM and LAP, decoded with two different colors. The corresponding AUC scores are reported in left below of each sub-figure.

We further visually validated our proposed segmentation technique. Figure 6.2 illustrated the segmented tracts by our proposed segmentation method along with the ground truth tracts by WMQL. Instead of the voxel, we consider the streamlines information for visualization in order to demonstrate clearly the comparison between the segmented tract and ground truth tract. We measured the true positive (TP), the false positive (FP) and the false negative (FN) in units of streamlines, by comparing the segmented result of our proposed segmentation method to the ground truth tracts from WMQL method. The TP, FP, and FN are depicted with *Salmon*, *Dark_Sea*$_G$*reen* and *Gold*, respectively. This figure visually validates our method as every tract is visually similar with the ground truth tract in terms of the shape of the tract.

6.3 Scalable Nearest Neighbor (NN) for the Tractogram

We proposed a simple procedure to efficiently compute the approximate nearest neighbor of a streamline, that reduces the speed of computations and the time, from hours to minutes.

6.3.1 Experiment Setup

The purpose of this experiment is to collect the evidence that the computational cost can be reduced by using the nearest neighbor strategy by leveraging the dissimilarity representation (*DR*) and the k-d tree.

We conceived the following scenario to observe the computational time: given a tract (t_a) of tractogram (T_A) , the nearest streamlines for each streamline in t_a were extracted from a whole brain tractogram (T_B). In order to extract the nearest streamlines, we follow the steps of the proposed scalable NN solutions, as described in Subsection 4.3.3. Further we compare with the standard approach to find the nearest neighbor of the streamlines that follows two steps: i) streamline-streamline distance computed between each streamline from the tract t_a t_a to all the streamline from tractogram (T_B), ii) find the closest streamline, based on the distance measure from the previous step (see, Equation 3.22).

For the evaluating this experiment, we report the time for computing the nearest streamline for the both approaches. For our proposed scalable nearest neighbor solution, we measured the time by dividing the process into three parts, i.e. i) dissimilarity representation which includes the prototype sections and dissimilarity matrix computation, ii) To build the k-d tree, iii) Query of the nearest streamlines for the given k-d tree. For the standard algorithm, we measure the time for the distance matrix construction and for finding the nearest neighbor. For unbiased comparison, in both cases, we consider the MAM distance in order to compute the dissimilarity matrix and distance matrix, respectively. The experiment was performed on a desktop computer with an intel Xeon(R) processor with 16*GB* of RAM.

6.3.2 Computational Time

In Table 6.3, we report the time to compute the 1-nearest neighbor (1*NN*) for a given tract to a whole brain tractogram. For all the streamlines (1181 streamlines) of a given Cingulum Bundle-left tract from the subject, HCP ID:100408, the 1NN is computed from all of the streamlines (117354 streamlines) from the subject, HCP ID:100307. The second and third column of the table report the time with our proposed solution (denoted as DR_KDTREE) and the standard way to compute the nearest neighbor (denoted MAM_ARGMIN). The result shows a substantial amount of time which can be reduced by adopting the solution with the scalable nearest neighbor computation. More precisely, it shows the 100% improvement in terms of the time with our proposed method.

	Method	
	DR_KDTREE	MAM_ARGMIN
Time	15.19s [a]	2179.2s [b]

[a] 14.81s for DR, 0.30s for *k*-d tree, 0.08 for Query

[b] 2179.07s for the distance matrix computation, 0.13s for Query

Table 6.3: Computational time: finding the 1NN streamline for all the streamlines of a Cingulum Bundle-left tract (1181 streamlines) from one tractogram with approximately 1*M* streamlines with two different nearest neighbor scenario.

We generate a runtime profile (based on the result presented in Table 6.3) of our proposed scalable nearest neighbour solution in order to observe the computational time require at each step (three steps mention in the 6.3.1). Figure 6.4 shows the computational time by breaking down the time into three parts. We observe that 98% time was devoted to the computation of the dissimilarity representation (including the prototype selection and the dissimilarity matrix construction), whereas 1.5% from the total amount of time was required for the *k*-d tree construction, and a very little amount of the time was required for the 1*NN* query based on the *k*-d tree.

Furthermore, we extend the experiments to explicitly observe the effect of the execution time for a different number of prototypes selection from the full tractogram. We report the time in Figure 6.5. We observe 25% increase of the time with the increase of the number of the prototype from 10 to 60.

In Figure 6.6, we also illustrate the time required to compute the different number of *k*d-tree query for all the streamlines of the Cingulum Bundle-left tract. From the figure, it clearly shows that the computational time increases with the number of the nearest neighbors. However, the total amount of time for computing the 1000 nearest streamlines from the full tractogram (approximately 1*M* streamlines) for all the streamlines (1181 streamline), it requires a very small amount of time, i.e. 1.5 seconds.

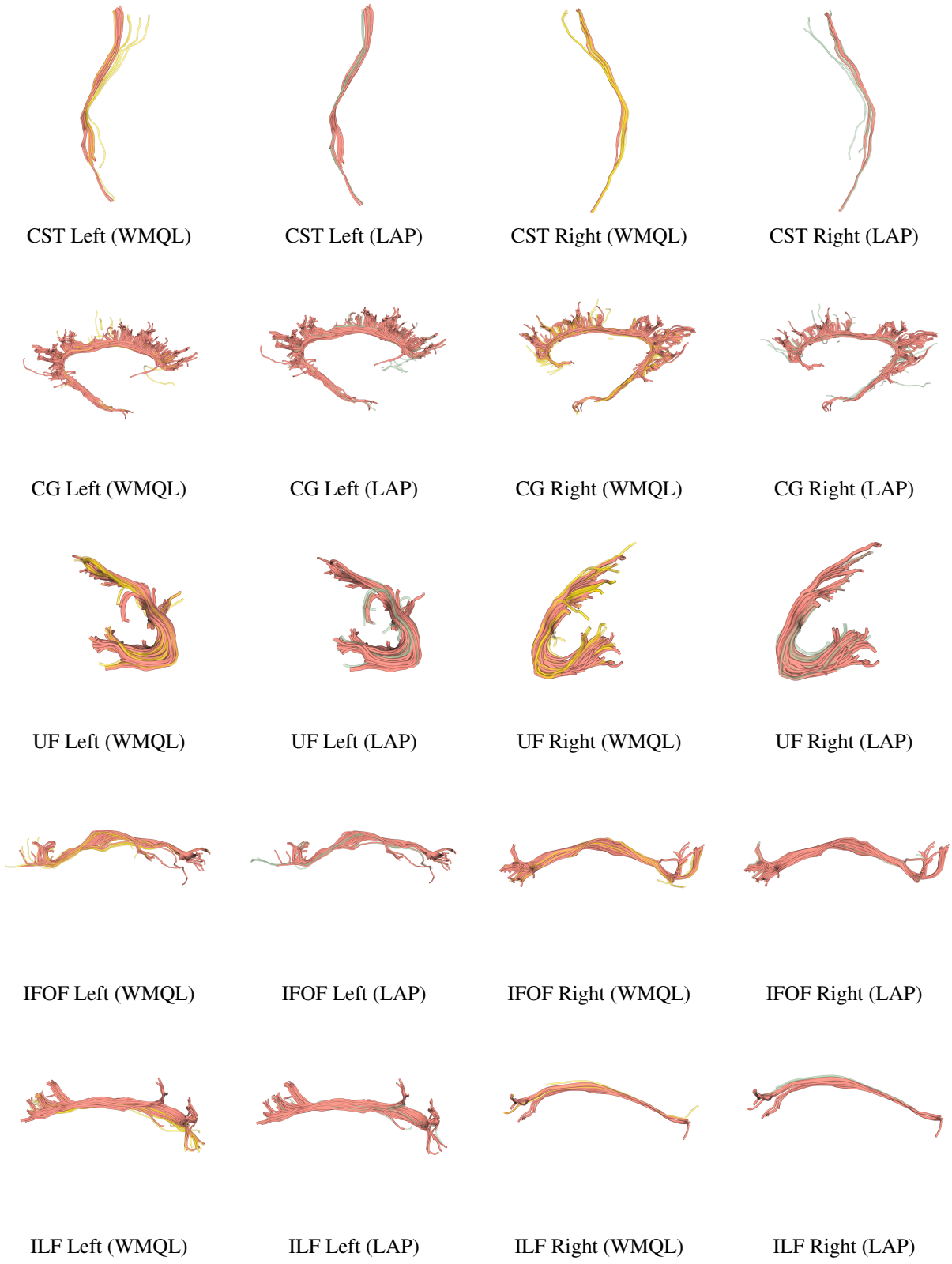

Figure 6.2: Comparison of ground truth tracts segmented with WMQL and the automatically obtained tracts with our proposed LAP-based method. The tracts in the first and third columns represent the ground truth tracts, those in the second and fourth column represents tracts using our proposed method. Each tract entitled with two color. With the *Salmon*, *Dark_Sea_Green* and *Gold* colors the true positive (TP) and false positive (FP) and false negative (FN) streamlines represented, respectively.

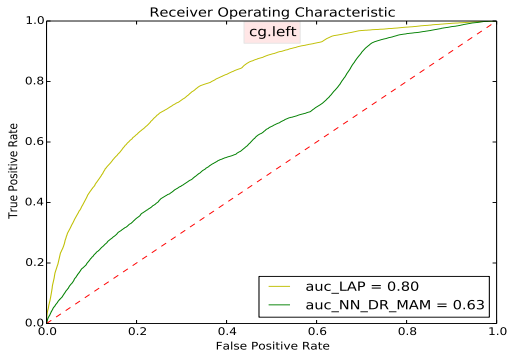
Receiver Operating Characteristic
cg.left
auc_LAP = 0.80
auc_NN_DR_MAM = 0.63
True Positive Rate
False Positive Rate

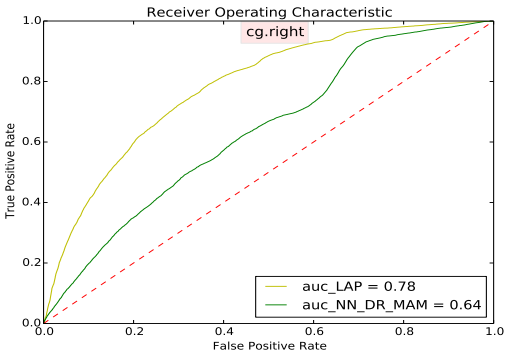
Receiver Operating Characteristic
cg.right
auc_LAP = 0.78
auc_NN_DR_MAM = 0.64
True Positive Rate
False Positive Rate

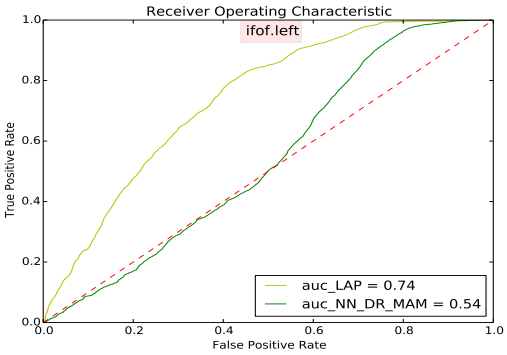
Receiver Operating Characteristic
ifof.left
auc_LAP = 0.74
auc_NN_DR_MAM = 0.54
True Positive Rate
False Positive Rate

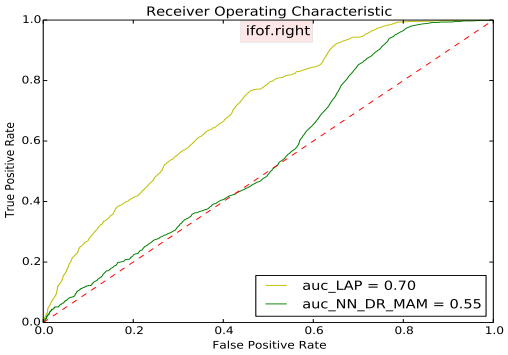
Receiver Operating Characteristic
ifof.right
auc_LAP = 0.70
auc_NN_DR_MAM = 0.55
True Positive Rate
False Positive Rate

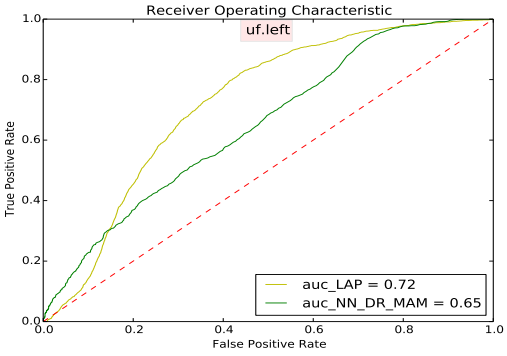
Receiver Operating Characteristic
uf.left
auc_LAP = 0.72
auc_NN_DR_MAM = 0.65
True Positive Rate
False Positive Rate

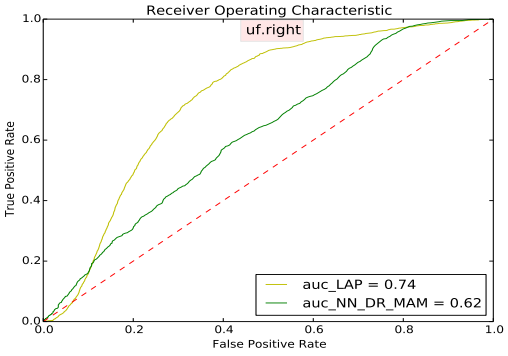
Receiver Operating Characteristic
uf.right
auc_LAP = 0.74
auc_NN_DR_MAM = 0.62
True Positive Rate
False Positive Rate

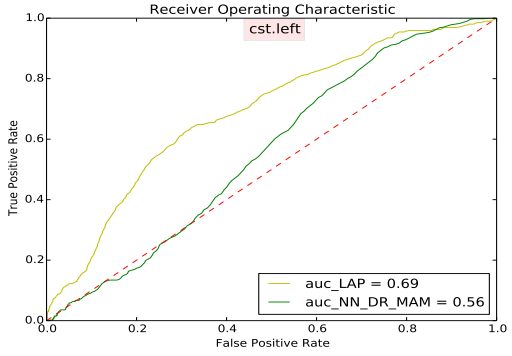
Receiver Operating Characteristic
cst.left
auc_LAP = 0.69
auc_NN_DR_MAM = 0.56
True Positive Rate
False Positive Rate

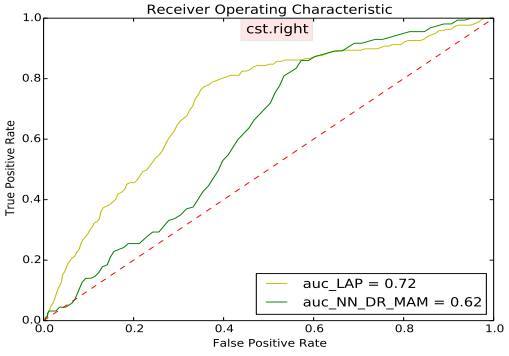
Receiver Operating Characteristic
cst.right
auc_LAP = 0.72
auc_NN_DR_MAM = 0.62
True Positive Rate
False Positive Rate

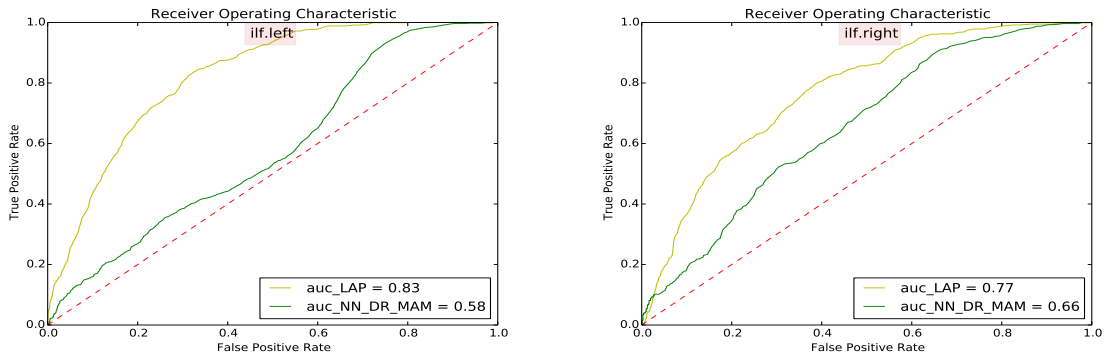

Figure 6.3: Receiver operating characteristic (ROC) analysis between segmented tracts and ground truth tracts for the DR_MAM and the proposed LAP-based segmentation. Each Subfigure shows the average ROC curve for each tract averaged over fifteen subjects.

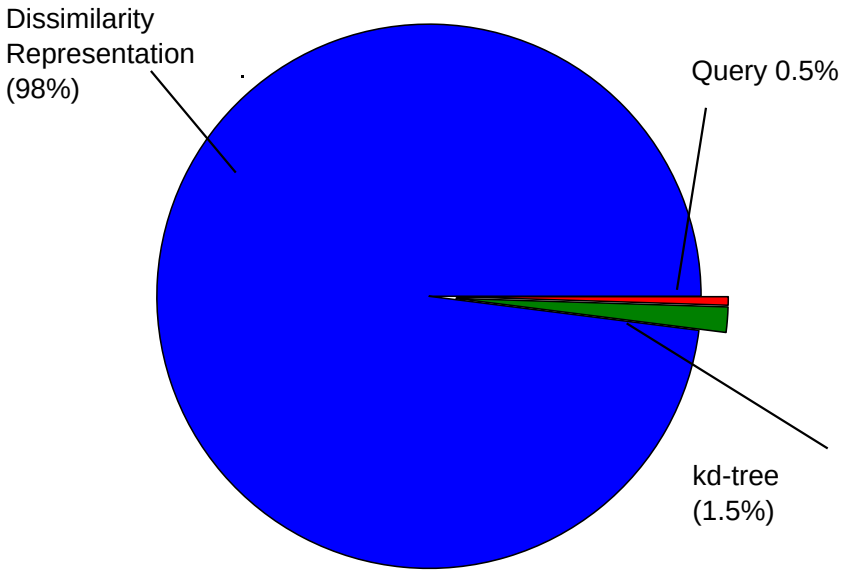

Figure 6.4: A runtime profile for computing the one nearest neighbor for all the streamlines, for a given Cingulum Bundle-left tract from one subject (HCP ID:100408), from the whole tractogram (HCP ID:100307).

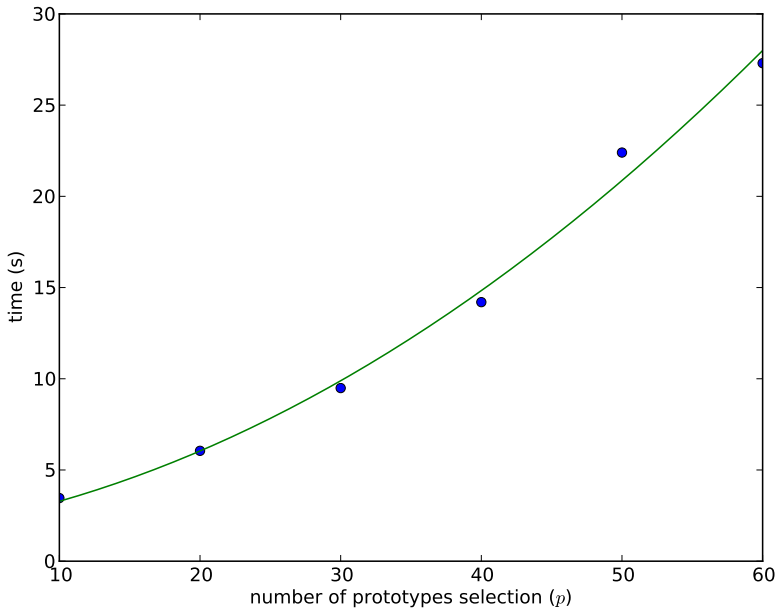

Figure 6.5: Time in second, required for different number of prototypes selection from the whole tractogram for the dissimilarity representation

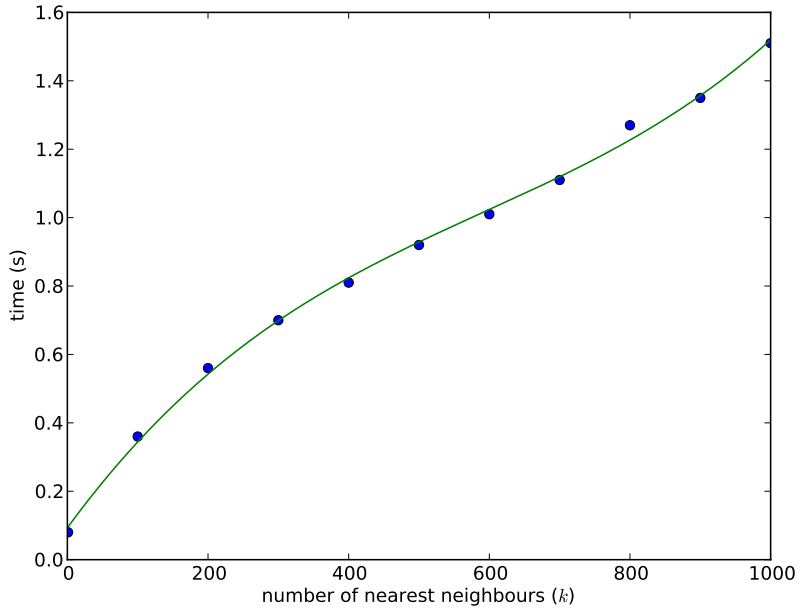

Figure 6.6: Time in second, required for different number of nearest neighbor query on the k-d tree based on the dissimilarity matrix of the whole tractogram

Chapter 7

Discussion and Conclusions

Overview

In this final chapter of Part I, we first present the discussion of the results of our proposed methods, which are reported in the previous chapter. Technical perspectives and the limitations of our proposed methods are discussed in Section 7.1. We conclude our work by reviewing our contributions in Section 7.2, and future directions and a potential perspective of the proposed methodology is presented in Section 7.3.

7.1 Discussion

In this thesis, we exploit the idea of streamline correspondence, that is, finding which streamlines correspond across tractograms, to optimize some quality of interest. We have shown that with such correspondence, it is possible to obtain the accurate alignment. Consequently, alignment based on streamline correspondence provides intermediate means to address practical tasks such as tract segmentation. We have also proposed a novel tract segmentation approach based on streamline correspondence across tractograms.

7.1.1 Tractogram Correspondence as Graph Matching

We addressed the whole brain tractogram alignment based on computing streamline correspondence across subjects as a graph matching problem. This work is the first to present the quantitative comparison across streamline-based alignment methods for tractograms. The comparison results are reported in Table 6.1. Results clearly show that tractogram correspondence, implemented as graph matching (GM), is able to align tractograms much better than what global affine registration can do, both voxel-based and streamline-based. The overlap of voxels of the aligned tracts, with respect to the target tracts, is two times better with the proposed method than with affine methods. This occurs uniformly across all subjects and all tracts. We also notice that, as expected, all affine-based registration methods exhibit comparable results within the reported standard deviations, meaning that there is an inherent limitation in affine transformations, irrespective of the loss function they optimize.

Such a positive result for GM against affine methods is not surprising because it is expected that one global linear transformation cannot reconcile local systematic differences between white matter bundles across subjects. Differently, GM is designed to optimize the match both at the global and local level. This aspect is clearly exemplified in Figure 6.1 where some notable displacement between the tracts remains after global affine alignment,

but not in the case of GM. The locality of GM and, more generally, of the correspondence-based alignment, act as if each streamline in one tractogram is deformed to exactly match the corresponding streamline in the other tractogram. This corresponds to a different deformation for each streamline. The global aspect is also preserved because GM is a joint optimization problem across all vertices/streamlines.

The results in Table 6.1 show the quality of alignment obtained through nonlinear registration of volumes by means of FSL/FNIRT (5th column). Since nonlinear registration is able to operate local changes, the quality of such alignment is, as expected, much better than that of linear methods. By comparing the results of GM and FNIRT, we observe that the quality of GM is still superior, i.e. $J_{FNIRT} = 0.43 \pm 0.02$ vs. $J_{GM} = 0.57 \pm 0.05$, although not by a large margin. Our interpretation of this result is that FNIRT optimized the match of the T1 images, which contain white matter boundaries but not the detailed structure, while our GM-based alignment procedure optimized the match of streamlines. Hence the main difference between the two methods is as follows: the proposed method operates on streamlines, which is the focus of this work, while the nonlinear volume-based algorithms, such as FNIRT, operate on voxel-level information. However, although the evaluation is based on volume-level information on the corresponding anatomical white matter tracts, the GM has shown the better result.

One of the properties of the proposed method is to use the relational information of each streamline, that is, its distance from the other streamlines in the subject space. This kind of distance has proved the effectiveness of the clustering algorithms to group the streamlines into clusters. Nevertheless, tractogram registration techniques have yet to explore it. In this thesis, we have shown that the streamline distance in subject space impacts the tractogram alignment. However, the current literature of the streamline-based tractogram registration used the across-subject streamline distance, that is, a streamline from one tractogram to a streamline in another tractogram. For computing such distances, two tractograms are required to be in the same space, which is obtained by the voxel-based registration method. Voxel-based registration has its own limitation of approximation of the alignment that may affect the accuracy of the streamline-based registration.

As mentioned in Chapter 4, the computational time and space complexity of the most efficient algorithms for GM are $O(n^3)$/iteration and $O(n^2)$ respectively. With such complexity, an approximate graph matching solution is limited when the number of nodes exceeds a few thousand. The computational and storage resources required to handle the matching of graphs generated from an entire tractogram, that is $n = 10^5$ nodes and 10^{10} edges, are beyond the capability of modern computers. For this reason, to obtain the correspondence between tractograms, we introduced a further approximation with a simple three-step procedure which includes the k-means clustering and the graph matching (see Section 4.1.4). The total amount of time required by the proposed method is a function of the number of clusters (k) chosen during the clustering-based approximation. Performing the three-step procedure with $k = 1000$ required approximately 30 minutes of computation for each pair of tractograms on a standard desktop computer. In Chapter 9, we refer to the details of the computational time to perform the graph matching on sets of streamlines.

Despite clearly positive results, the solution proposed in this work suffers various limitations that provide ground for interesting future work. At a general level, the idea of putting in correspondence streamlines across tractograms may be limited by the quality of the tractography algorithms, a topic on which there is still major debate. For example, if a tractogram contains a large number of artifactual streamlines, it is challenging to find the correspondence for the artifacts as these should not have the corresponding streamline. To handle this issue of artifactual streamlines, two possible directions are i) to implement the corresponding algorithm in such a way that it can avoid the artifactual streamlines, and ii) to apply the tractogram cleaning algorithms, such as SIFT, COMMIT, LIFE (see Section 2.3.2), in order to filter out the artifactual streamlines.

At the implementation level, GM has the sub-optimal constraint of one-to-one correspondence, which is driven

to simplify the mathematical formulation of the GM problem. It is worth noting that this constraint is not completely appropriate for the neuroanatomical perspective, that is, there is no anatomical basis for which streamline of one tractogram there has to exist the corresponding streamline in the other tractogram. Nevertheless, our experiments shows that, in practice, the benefit of the constraint is much greater than its downsides. Inspired by this streamline correspondence, in future work we address the correspondence at the level of a set of streamlines, to find the correspondence between groups of streamlines across tractograms. In principle, the group of streamlines can be the anatomical meaningful tract. In that case, such correspondence is completely anatomically meaningful as it is expected that homologous anatomical structures are present across all subjects.

At the application level, aligning tractograms for transferring anatomical knowledge to a new subject, for example, for segmentation of tracts, is the straightforward application of the proposed method. Despite the usefulness of correspondence for the segmentation task, it is still unclear how to address other common tasks, such as alignment at the group-level and atlas construction, on which we are focusing our future work. From this point of view, the idea of exploiting the correspondence between streamlines opens up new directions of research and new opportunities for improvement of neuroscientific and clinical applications.

7.1.2 Tract Segmentation as Linear Assignment Problem

We present a novel supervised tract segmentation approach based on streamline correspondence across subjects. We formulate the streamline correspondence problem as a linear assignment problem (LAP). Our proposed LAP-based segmentation method is able to segment a given tract of interest in the tractogram of a new subject using a set of examples as prior information.

We performed a comparative study across three alternative methods: i) an automatic ROI-based segmentation [167]; and two supervised segmentation based on the nearest neighbor (NN) strategies: ii) an example-based multi-atlas approach with NN strategy (denoted as MULTI_ATLAS) [162], iii) the proposed efficient NN solution (see Section 4.2.5) with the minimum average distance measure (denoted as *DR_MAM*). Table 6.2 clearly shows that tract segmentation formulated as LAP is able to segment tracts much better than the automatic ROI-based segmentation and supervised segmentation based on the NN approach. Tract segmentation with LAP outperformed across all ten tracts over 15 subjects the highest dice similarity coefficient (DSC) value. We also noticed that all NN approaches, that is, *DR_MAM* and the example-based multi-atlas approaches (MULTI_ATLAS), give comparable results to each other.

For all tracts our method showed better results in terms of DSC than the ROI-based segmentation approach. The result from the ROI-based segmentation approach is quite low. This could be due to a registration error which occurs during the registration of the test subject to the atlas, in a way of obtaining the segmented tracts through the ROIs.

To validate our proposed segmentation method with the NN techniques, we further performed a quantitative comparison based on ROC curve analysis between the LAP and DR_MAM. Figure 6.3 shows that for each tract, our method shows better performance than the DR_MAM, in terms of ROC curve analysis and the AUC score. A significant difference between the ROC curves of LAP and DR_MAM is also observed.

The results of Table 6.2 and Figure 6.3 also show the quality of the segmentation of the NN approach. According to the results based on the two evaluation metrics, that is, the degree of voxel overlap in the DSC and the ROC curve analysis, we found the quality of the segmentation is poor compared to our proposed segmentation approach. Since the NN strategy aims to minimize the distance of each streamline locally without taking into account the distances of other streamlines, the solution is a greedy one. By always greedily selecting the closest streamlines, it ends up exhibiting the same streamlines in the target tractogram for the multiple streamlines in the

example. For this reason, the number of streamlines of the estimated correspondence streamlines from the target tractogram is low, leading to a systematic and unrealistic thinning of the segmented tract. This is one of the reasons for such results with the NN strategy.

Table 6.2 and Figure 6.3 clearly show that our proposed streamline correspondence based segmentation method is able to segment the tracts much better than the ROI-based and NN-based segmentation techniques. Although our proposed method showed a very positive result in terms of the voxel overlap, the accurate segmentation with 100% voxel overlap is quite difficult to achieve due to the variability of the tracts across subjects. Although we incorporate the multiple examples to address the issue of variability, the quality of the examples (segmented tracts used as the prior knowledge) have a major impact on the segmentation results. Nevertheless, segmentation results can be improved by migrating to expert-based segmentation as examples.

From Table 6.2 we also observed high variance of the DSC for a few tracts, for example, cst.left, cst.right, ilf.left and ilf.right. This is due to the fact that the WMQL were not accurately segmented these two tracts (see Table 5.2 and Table 5.3). Nevertheless, we consider these two tracts as a part of the segmentation result as these tracts are important in clinical applications.

Although our proposed LAP-based supervised tract segmentation method shows very positive experiment results, it has some limitations which can be addressed in future. The proposed segmentation method is biased on the streamlines generated with the various tracking algorithms, for example, deterministic and probabilistic tracking algorithms. The tracking algorithms have their own criteria about the number of streamlines, that is, probabilistic tracking algorithms generate a larger number of streamlines compared to deterministic. If both the example and test tractogram are reconstructed by the same tracking algorithm, then the segmentation method is the beneficiary. This is due to the fact that the distribution of the streamline in both cases is the same, which helps to find the streamline correspondence in an appropriate way. In contrast, the proposed segmentation method may suffer by the streamlines generated from different tracking algorithms. As an example, given that the example tract and the test tractogram are generated by the deterministic and probabilistic tracking algorithm respectively, the correspondence streamline is difficult to find as the density, in terms of the number the streamlines, in the two cases is totally different.

Another crucial point for our proposed segmentation method is the size of the tracts, that is, the number of streamlines of the example tract and the segmented tract. If the number is very different, this may affect the result of the proposed segmentation method. This may happen due to imposing the one-to-one constraint with the LAP formulation. With this formulation, for one streamline from the example tract, only one correspondence streamline from the test subject can be extracted. This constraint also limits our method when the example tract contains less streamlines compared to the segmented tract from the test subject with the proposed method. In such cases the segmented tract contains the same number of streamlines as the example. In future, our idea is to refine and relax the constraint of one-to-one.

7.1.3 Scalable Nearest Neighbor (NN) for the Tractogram

In order to efficiently adapt the implementation of the GM and LAP, we have addressed the issue of computational cost due to the large number of streamlines in the full brain tractogram. To reduce the amount of computations, in both cases we represent the streamlines as vectors through dissimilarity representation, known as the Euclidean embedding technique. We then obtained fast NN queries through the use of *k*d-tree queries. In this way, with a scalable solution of NN for the tractogram, we address the computational issue.

In the case of GM, in order to accelerate the convergence of the DSPFP algorithms, instead of the random initialization, we initialize the permutation matrix with the one nearest neighbor (1NN) streamline, that is, to

compute the 1NN of the test tractogram A from the reference tractogram B. To compute the 1NN, we used our proposed scalable solution for extraction of the nearest streamline. With the standard approach (see Section 4.3), to compute the 1NN streamlines for the tractogram of approximately $1M$ streamlines takes three days with a standard computer. In contrast, with our proposed solution it only takes a few minutes to compute the 1NN from the whole brain tractogram.

In the case of adapting the rectangular extension of the LAPJV, due to the computational cost, the algorithm can be directly applied on the full cost matrix computed between one tract and the whole tractogram. For this reason, instead of the full cost matrix, we computed sparse instance of the cost matrix. The sparse cost matrix is computed by considering a subset of streamlines of the target tractogram. Regarding the subset, we consider the NNs of the tract from the target tractogram. For this purpose, we adapted the scalable solution of the NN, which reduces a large amount of the computational time; the extraction of 1000 nearest streamlines from the full tractogram for a given example takes less than one minute. On the other hand, the common procedure based on the distance measure (see Section 6.3.1) requires approximately 40 minutes. An explicit computational time regarding this issue is reported in Section 6.3.1.

7.2 Conclusions

In this thesis, we have proposed new methods for aligning the tractograms and segmenting the tract based on the concept of streamline correspondence. The major original contributions of this thesis can be identified as novel and efficient methods for both problems. We also made some minor contributions throughout the process of adapting the solutions in an efficient way. In the following, we present a summary of our contributions and an overview of the contents of the thesis.

In this thesis, we have addressed the problem of aligning the tractograms by taking into consideration the across-subjects correspondence between streamlines that we call *tractogram correspondence*. In principle, tractogram correspondence is based on the idea of streamline correspondence, to find which streamlines correspond across tractograms. We have proposed an operational procedure to find the optimal correspondence through the graph matching problem. We have represented tractograms as graphs and have adopted the actual algorithm for graph matching solutions from the literature to approximate the solution of the tractogram correspondence problem. We have reported the empirical evidence of tractogram correspondence as graph matching provides much better alignment than the linear registration and comparable nonlinear registration.

We have proposed a novel supervised method for automatic tract segmentation from the massive tractogram dataset. Our proposed method segments the tract of interest, for example the arcuate fasciculus, by exploiting a set of example tracts from different subjects. In an analogy to tractogram alignment, our proposed supervised segmentation approach is based on the concept of streamline correspondence, that is, on finding which streamlines correspond across tractograms. We have framed the streamline correspondence problem by means of the tract segmentation problem as a linear assignment problem (LAP), a cornerstone of combinatorial optimization. We adopted one of the efficient algorithms for solving the optimal correspondence of the streamlines. Furthermore, we have added a strategy for merging correspondences coming from different examples, that is, from different subjects, in order to account for the anatomical variability across the population.

In order to reduce the computational cost of adapting the solutions of GM and LAP, we have proposed to represent streamlines as vectors through a Euclidean embedding technique called dissimilarity representation. In the case of dissimilarity representation, prototype selection is crucial. We have proposed a heuristic approach to select the prototypes. However, with such representation of the dissimilarity representation, we have obtained fast

NN queries through the use of *k*d-trees. By using the proposed technique, we have observed a dramatic reduction of computational time.

These above contributions required the background knowledge of the dMRI, tractogram and the existing literature of the tractogram alignment and tract segmentation. We also made an effort to mathematically formulate the alignment and segmentation problem. Additionally, from a methodological point of view, this thesis required explicit knowledge about the two fundamental problems of the combinatorial optimization problem, that is, GM and LAP. To find efficient solutions for GM and LAP, an extensive literature review was required. Among the many solutions available in literature, finding one fit for our particular problem was a real challenge.

A large number of experiments were conducted to validate our proposed solutions. We have performed the experimental assessment on real data from the Human Connectome Project dataset. The experimental results presented here, for both the tractogram correspondence and tract segmentation, not only validate our claim, but also show the potential of our method.

To solve the tractogram alignment and tract segmentation problems, we exploit the idea of correspondence between streamlines. We show that streamline correspondence is a powerful principle to transfer the anatomical information from one subject to another one. We have provided a thorough experimental analysis for validating our proposed concepts based on the correspondence. We believe that the idea of exploiting the correspondence between streamlines opens up new directions of research and opportunities for improvement in neuroscientific and clinical applications.

7.3 Future works

In this section, we present potential extensions and future directions for our proposed methodologies.

- **Many-to-many correspondence** The proposed formulation of the streamline correspondence problem (both GM and LAP) has the assumption of the one-to-one constraint. In principle, the correspondence problem is a many-to-many or many-to-one problem, that is, different streamlines of one tractogram may correspond to the same streamline in another tractogram. Our aim is to address the many-to-many correspondence among the streamlines in future. One of our activities regarding the GM will be solving the many-to-many constraint with a continuous relaxation approach. In the case of LAP, the problem of many-to-many constraints can be addressed with the generalized assignment problem. Our idea is to address the issue with the suboptimal solution of the generalized assignment problem.

- **Efficient way to address the whole brain alignment** We addressed the whole brain tractogram alignment by applying the clustering algorithm to group the tractograms into groups and then find the matches between each cluster. In future, we aim to handle the whole brain in an efficient way, such as by using the sparse graph representation.

- **Clinical application** We quantify our proposed correspondence-based tract segmentation method with the healthy dataset from the HCP dataset. In the future, we will extend the experiments with the patient dataset. It would be interesting to see the correspondence effect in the patient dataset.

- **Correspondence with different tracking algorithm** All experiments were performed on tractograms generated by the EudX deterministic tracking algorithm (see Chapter 5). In future, we will investigate the impact of tracking algorithms on the correspondence problem by generating the tractograms with the different tracking algorithm.

- **Software for the tract segmented framework** Developing a user friendly software framework for our proposed tract segmentation approach is one of the activities that will take place in the near future.

Part II

Published and Submitted Work

Overview

Part II presents the published works and the manuscript (under review), with the results presented in this thesis. This part consists of three different chapters.

Chapter 8: The work described in this chapter is based on our contributions on tract segmentation. In this work, we proposed a novel supervised tract segmentation method and this chapter is comprised manuscript of the segmentation method. This manuscript is in under review phase. The details of the publication are as follows: **Nusrat Sharmin**, Emanuele Olivetti, and Paolo Avesani. *White Matter Tract Segmentation as Multiple Linear Assignment Problems*.

Chapter 9: The work described in this chapter is based on our contributions to the tractogram alignment problem. The work is published in Frontiers in Neuroscience, 2016. The details of the publication are as follows: Emanuele Olivetti, **Nusrat Sharmin**, and Paolo Avesani. *Alignment of Tractograms As Graph Matching*. Frontiers in Neuroscience, 2016. *DOI* : $10.3389/fnins.2016.00554$.

Chapter 10: The work described in this chapter is published in the Computational Diffusion MRI (CDMRI), MICCAI Workshop. This work is based on the tract segmentation with the concept of the corresponding streamlines. This work showed a powerful principle to transfer the anatomical information from one brain to another through the streamlines correspondence. As well as this work support our claim that the alignment can provide more useful information when enriched with the correspondence of streamlines across tractograms. Following the details of the publication: "**Nusrat Sharmin**, Emanuele Olivetti, and Paolo Avesani. *Alignment of Tractograms as Linear Assignment Problem*. Computational Diffusion MRI (CDMRI), Mathematics and Visualization, pages 109-120. Springer International Publishing, 2016." *DOI* : $10.1007/978-3-319-28588-7\_10$.

Chapter 8

White Matter Tract Segmentation as Multiple Linear Assignment Problem

White Matter Tract Segmentation as Multiple Linear Assignment Problems

Nusrat Sharmin [1,2,*], **Emanuele Olivetti** [1,2] **and Paolo Avesani** [1,2]

[1] *NeuroInformatics Laboratory (NILab), Bruno Kessler Foundation, Trento, Italy*
[2] *Center for Mind and Brain Sciences (CIMeC), University of Trento, Italy*

Correspondence*:
Nusrat Sharmin
sharmin@fbk.eu

ABSTRACT

Diffusion magnetic resonance imaging (dMRI) allows to reconstruct the main pathways of axons within the white matter of the brain as a set of polylines, called streamlines. The set of streamlines of the whole brain is called the tractogram. Organizing tractograms into anatomically meaningful structures, called tracts, is known as the tract segmentation problem, with important applications to neurosurgical planning and tractometry. Automatic tract segmentation techniques can be unsupervised or supervised. A common criticism of unsupervised methods, like clustering, is that there is no guarantee to obtain anatomically meaningful tracts. In this work, we focus on supervised tract segmentation, which is driven by prior knowledge from anatomical atlases or from examples, i.e. segmented tracts from different subjects. We present a supervised tract segmentation method that segments a given tract of interest in the tractogram of a new subject using multiple examples as prior information. Our proposed tract segmentation method is based on the idea of streamline correspondence i.e. on finding corresponding streamlines across different tractograms. In the literature, streamline correspondence has been addressed with the nearest neighbor (NN) strategy. Differently, here we formulate the problem of streamline correspondence as a linear assignment problem (LAP), which is a cornerstone of combinatorial optimization. With respect to the NN, the LAP introduces a constraint of one-to-one correspondence between streamlines, that forces the correspondences to follow the local anatomical differences between the example and the target tract, neglected by the NN. In the proposed solution, we combined the Jonker-Volgenant algorithm (LAPJV) for solving the LAP together with an efficient way of computing the nearest neighbors of a streamline, which massively reduces the total amount of computations needed to segment a tract. Moreover, we propose a ranking strategy to merge correspondences coming from different examples. We validate the proposed method on tractograms generated from the human connectome project (HCP) dataset and compare the segmentations with the NN method and the ROI-based method. The results show that LAP-based segmentation is vastly more accurate than ROI-based segmentation and substantially more accurate than the NN strategy. We provide a Free / OpenSource implementation of the proposed method.

Keywords: Diffusion magnetic resonance imaging (dMRI), Bundle/Tract, Tract Segmentation, Tractogram, Nearest Neighbor (NN), Combinatorial Optimization Problem, Linear Assignment Problem (LAP)

1 INTRODUCTION

The white matter of the brain mainly contains neuronal axons which are responsible for transferring signal between the regions of the grey matter Douglas Fields (2008). Diffusion magnetic resonance imaging

(dMRI) Basser et al. (1994) is the brain imaging technique for identifying the main pathways of large assemblies of axons and, in some cases, pathologies of the white matter Douglas Fields (2008). DMRI data quantify the local orientation of the axons of the white matter in vivo, at the voxel-level. From these local orientations, approximate $3D$ pathways can be reconstructed, using tractography algorithms. The resulting $3D$ polylines are called *streamlines* and the set of whole streamlines is called the *tractogram*, which usually contains a number of streamlines in the order of $10^5 - 10^6$.

In neurological studies and neurosurgical planning, it is often important to identify the group of streamlines belonging to the same anatomical region, called *tract* or *bundle*, e.g. the corticospinal tract. The problem of grouping or organising streamlines of the whole tractogram into anatomically meaningful tracts is known as the *tractogram segmentation problem* O'Donnell and Westin (2007). Moreover, extracting a specific tract of interest from the whole brain is known as the *tract segmentation problem* Clayden et al. (2007). Once the segmentation is done, the statistical analysis over the tract(s) is used in multiple applications, for example, to study gender differences Ingalhalikar et al. (2014), to observe the changes in age Salat et al. (2005) and to correlate it with diseases Bozzali et al. (2002); Park et al. (2004). This kind of studies require the analysis of groups of subjects. Therefore, automatic tract segmentation, conducted in a comparative manner over groups of subjects, is crucial in order to accomplish this goal. One main step of such task is to study how much *corresponding* are homologous anatomical structures across the subjects.

Several manual and automatic tract segmentation methods have been developed over the years. The manual approach, also known as *virtual dissection* Catani et al. (2002); Mori et al. (2005); Wakana et al. (2007), extracts the desired tract using cortical regions of interest (ROIs) defined by neuroanatomical knowledge, by an expert. Such method is time consuming and it is limited to manual selection of ROIs. A different approach is the one of automatic tract segmentation, which can be divided into three different groups: *ROI-based*, also known as *parcellation-based*, *unsupervised* and *supervised*.

Automatic ROI-based tract segmentation is based on cortical parcellation. It requires that linear or non-linear registration is performed in advance, with respect to an anatomical atlas Aarnink et al. (2014); Zhang et al. (2010). It has to be noted that the registration to the atlas can cause loss of information present in the diffusion images Tunç et al. (2014). However, automatic ROI-based methods are known to provide remarkable results Zhang et al. (2010) so, sometimes, they are used as ground truth to extensively validate the result of other segmentation methods. Among the parcellation-based automatic segmentation methods Siless et al. (2016), the Tract Querier, based on the white matter query language (WMQL) Wassermann et al. (2013, 2016), is one of the most adopted.

The unsupervised approach, usually called *fiber clustering*, is one of the most widely used tractogram segmentation technique in the literature Shimony et al. (2002); Garyfallidis et al. (2012); Tunç et al. (2014); Reichenbach et al. (2015). The purpose of clustering is to group the streamlines according to their mutual geometrical similarity (or distance). Clustering methods mostly address single tractograms and not the joint analysis of multiple subjects O'Donnell et al. (2013). A common criticism of clustering methods is that there is no guarantee to obtain anatomically meaningful tracts Toga (2015). For this reason, some authors propose to incorporate prior knowledge in the process, e.g. anatomical information from atlases or expert labelling on previous data.

Supervised segmentation is an approach based on prior knowledge. Prior knowledge can come from expert labelling of an anatomical atlas, see Maddah et al. (2005), or from labelling clusters of streamlines from multiple subjects, in a process of atlas creation, see O'Donnell and Westin (2007); Vercruysse et al. (2014); Guevara et al. (2012, 2017); Yoo et al. (2015); Labra et al. (2016), or labelling clusters of

streamlines from single subject in order to obtain segmented tract of interest Garyfallidis et al. (2017). In the former category, also known as *example-based tract segmentation*, once the atlas is available, the segmentation of the tract of interest in a new subject can be carried out. Existing example-based methods have some limitations, the main ones being the high computational cost O'Donnell and Westin (2007); Vercruysse et al. (2014), the dependency of the number of subjects to construct the atlas in case of multiple atlas Guevara et al. (2012) and the dependency on the definition of threshold values Yoo et al. (2015); Labra et al. (2016).

In supervised segmentation, besides atlases, other kinds of prior information can be used as prior knowledge, such as models or features of tracts/bundles. In this case, we call the task *model-based* supervised tract segmentation. Various parametric models of tracts have been proposed in the literature, e.g. the beta mixture model of similarity cosines Clayden et al. (2007), the gamma mixture model of the distance Maddah et al. (2008), the Gaussian process of tract probability map Wassermann et al. (2010), the hierarchical Dirichlet process mixture model Wang et al. (2011). Notice that models are built to describe tracts/bundles and not the whole tractogram.

In this work we propose an example-based tract segmentation, which segment a single specific tract from the whole tractogram of a new subject, using the prior information of the previous segmentations of the same tract/bundle from the tractogram of other subjects. The proposed method comprises two main steps: in the first step, for each streamline of an example tract, we find the corresponding streamline in the new tractogram. This step is related to our recent work in Sharmin et al. (2016), where we showed that streamline correspondence can be a powerful principle to transfer the anatomical information of a given bundle from one subject to another one. In the second step, we combine the correspondences found from all examples, i.e. from all other subjects, into one desired segmented tract within the new tractogram, using a ranking scheme. This second step accounts for the variability across the examples/subjects and the anatomical bias of the specificity of each subject. In the literature, given a set of streamlines of one subject, the problem of finding the corresponding streamlines in the tractogram of another subject has been addressed with a nearest neighbour strategy Yoo et al. (2015); Labra et al. (2016); Garyfallidis et al. (2017). There, after co-registering the two tractograms, for each streamline of the example subject, the corresponding streamline in the new tractogram has been proposed to be the geometrically nearest one. In this work, we compare the nearest neighbour strategy to that of finding corresponding streamlines as a Linear Assignment Problem (LAP, see Burkard et al. (2009)), that we introduced in Sharmin et al. (2016). The LAP is a combinatorial optimization problem that finds corresponding objects between two sets imposing a one-to-one constraint, while minimizing the sum of the distances.

Finding corresponding streamlines through a LAP is different from using the nearest neighbor strategy. The main reason is that the nearest neighbour algorithm is greedy, i.e. it optimizes the selection of the correspondence individually for each streamline. Differently, the LAP jointly optimizes the correspondence of all streamlines, because of the one-to-one constraint. Intuitively, the benefit of this joint optimization can be seen in Figure 1, discussed below. In practical cases, it is common to observe some systematic displacement between homologous anatomical structures across subjects, even after an initial registration, because of the inherent variability of the local white matter anatomy across the population. In such cases, the nearest neighbor strategy is expected to provide poor correspondences: each streamline will be put in correspondence with its closest one in the other tractogram, without considering such systematic displacements. Differently, the one-to-one constraint of LAP will force the correspondence to follow such systematic displacements. We show a paradigmatic toy example of this difference in Figure 1. There, two sets of five simulated streamlines are depicted in blue and red before the initial alignment, see subfigure (a).

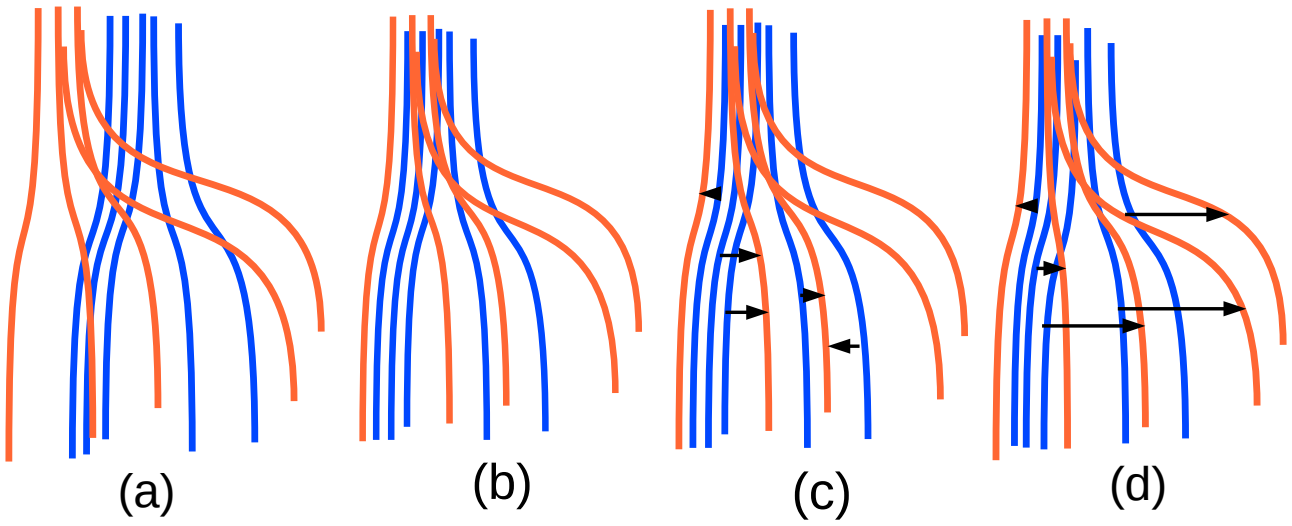

Figure 1. Simplified sketch of streamline correspondence showing the difference between nearest neighbour vs. the proposed linear assignment problem (LAP). In blue and red we show two sets of 5 homologous streamlines each, before registration (a), after initial registration (b), with arrows showing the correspondence from the blue streamlines to red ones with nearest neighbour (NN) (c) and with streamline correspondence with LAP (d). NN (c) misses the two streamlines on the right side, while LAP (d) does not.

Subfigure (b) illustrates the two sets of streamlines after linear registration. In subfigure, (c) and (d) we show the streamline correspondence between blue streamlines and red streamlines, through the nearest neighbour and the LAP strategies, respectively. There black arrows show the corresponding streamlines across the two sets. In (c), the nearest neighbour misses the two red streamlines on the right side. Differently, in (d), LAP correctly matches all the streamlines of the blue an red sets.

In this work, in addition to the main contribution of extending the correspondence-based segmentation of Sharmin et al. (2016) to the case of multiple tracts/bundles used as examples, we provide a substantial improvement in the speed of the computations, reducing the time required to segment, from hours to minutes. The newly adopted Jonker-Volgenant algorithm for LAP (LAPJV), see Bijsterbosch and Volgenant (2010), for the rectangular LAP (RLAP), together with the use of an efficient way to compute the nearest neighbours of given streamlines, result in a 50x speed up of the computations with respect to what we presented in Sharmin et al. (2016). This improvement makes it possible to apply the proposed method in practical cases. Moreover, the efficient nearest neighbours computation can be used to vastly improve the speed of the method proposed in Yoo et al. (2015), similarly to Labra et al. (2016).

Together with the comparison against the nearest neighbours strategy, in this work, we compare the proposed method against the automatic ROI-based segmentation Zhang et al. (2010), because it is the most adopted one. We conducted experiments on the dMRI data of multiple subjects from the Human Connectome Project (HCP, see Van Essen et al. (2013); Sotiropoulos et al. (2013); Glasser et al. (2013)) dataset. We observed that the proposed LAP strategy, together with the proposed ranking scheme, are able to segment the bundles much more accurately than the ROI-based segmentation Zhang et al. (2010) and the nearest neighbors strategy of Yoo et al. (2015). In the remaining part of the article, we first review the literature related to the different scientific areas touched by this work, see Section 2. Then we introduce the necessary methodological ingredients, together with the detailed description of the proposed method,

in Section 3. The experiments are reported in Section 5, followed by their discussion in Section 6. We conclude this work by mentioning multiple future activities that arise from what we present.

2 RELATED WORKS

2.1 Supervised Tract Segmentation

Here we review the literature on supervised tractogram segmentation and on the linear assignment problem. In order to organize the body of work in this field, we articulate the discussion on supervised tract segmentation along these five topics: alignment, embedding space, similarity/distance, correspondence techniques, and refinement step.

2.1.1 Alignment

In supervised tract segmentation, tractograms are initially aligned to an atlas. Both voxel-based and streamline-based atlases have been used in literature, e.g. white matter ROI-based anatomical atlas Maddah et al. (2005), high dimensional atlas O'Donnell and Westin (2007); Vercruysse et al. (2014), example-based single atlas Guevara et al. (2012); Labra et al. (2016), example-based multi-atlas Yoo et al. (2015). To the best of our knowledge, the specific step of alignment has been conducted with standard methods: in most of the cases with voxel-based linear registration O'Donnell and Westin (2007); Guevara et al. (2012); Yoo et al. (2015) and in the others with nonlinear voxel-based registration Vercruysse et al. (2014).

2.1.2 Embedding space

Streamlines are complex geometrical objects with a different number of points one from another. They are unfit to be directly given as input to many efficient data analysis algorithms which, instead, require vectors all with the same number of dimensions. Tractograms are large collections of streamlines, from hundreds of thousands to millions of streamlines, and their analysis is often limited by the required computational cost. A common preprocessing step before using algorithms like clustering, or nearest neighbor, is to transform streamlines into vectors, a process called *Euclidean embedding*. Different authors opted for different embedding approaches, like the spectral embedding O'Donnell and Westin (2007), the re-sampling of all streamlines to the same number of points Yoo et al. (2015); Guevara et al. (2012); Labra et al. (2016), the use of B-splines with re-sampling Maddah et al. (2005) and the dissimilarity representation Olivetti and Avesani (2011). Re-sampling all streamlines to a fixed number of points is the most common approach to obtain the embedding. In principle, up-sampling/down-sampling to a particular number of points may cause the loss of information. On the other hand, spectral embedding has high computation cost. The dissimilarity representation has shown remarkable results in terms of machine learning applications Olivetti et al. (2013) and exploration of tractograms Porro-Muñoz et al. (2015), at a moderate computational cost.

2.1.3 Streamline Distance

In order to find corresponding streamlines from one tractogram to another one, the definition of the streamline distance plays a crucial role. Most commonly, the corresponding streamline in the new tractogram is defined as the closest one, for the given streamline distance function. Similarly, when doing clustering for tract segmentation, the streamline distance function is a fundamental building block. Different streamline distance functions have been used in the supervised tract segmentation literature, e.g. minimum closest point (MCP) O'Donnell and Westin (2007), symmetric minimum average distance (MAM) Olivetti and Avesani (2011), minimum average flip distance (MDF) Yoo et al. (2015); Garyfallidis

et al. (2017), Hausdorff distance Maddah et al. (2005), normalized Euclidean distances Labra et al. (2016), Mahalanobis distance Yoo et al. (2015).

2.1.4 Correspondence technique

One crucial aspect of supervised tract segmentation is the mechanism to find the corresponding streamline between the tractograms of different subjects, in order to transfer anatomical knowledge. A common approach for addressing such problem is to use the nearest neighbor strategy, i.e. finding the nearest streamline or centroid in the atlas and labelling the streamlines of the new subject based on that. In O'Donnell and Westin (2007); O'Donnell et al. (2017), a high dimensional atlas was reconstructed from multiple tractograms. Then the new subject was aligned with the atlas and the closest cluster centroids from atlas were computed to assign the anatomical label. In Guevara et al. (2012), nearest centroids of the new subject were computed from a single atlas from multiple subjects, with the normalized Euclidean distance. Recently, a faster implementation has been proposed in Labra et al. (2016). There, they proposed to label each single streamline instead of cluster centroids and to accelerate the computation time by filtering the streamlines in advance, using properties of the normalized Euclidean distance. A limitation is that an appropriate threshold has to be defined for each tract to be segmented. Similarly, in Yoo et al. (2015), the nearest neighbor strategy is used to find corresponding streamlines between those of the tractogram of a new subject, with those of multiple example-subjects (12, in their experiments). Again, two thresholds, i.e. a distance threshold and a voting threshold, are required to be set in order to obtain the segmentation. The proposed implementation requires a GPU.

A different approach based on graph matching, instead of the nearest neighbor, was proposed by us for tractogram alignment, see Olivetti et al. (2016). Such idea could be extended to the tract segmentation problem.

2.1.5 Refinement

After segmentation, in order to improve the accuracy of the segmented tract, some authors propose a refinement step, for example, to identify and remove outliers. In Mayer et al. (2011), a tree-based refinement step was introduced. Initially, they padded the segmented tract with the nearest neighbors and then used a probabilistic boosting tree classifier to identify the outliers. Another approach to increase the accuracy of the segmented tract is majority voting Rohlfing et al. (2004); Yoo et al. (2015); Vercruysse et al. (2014); Jin et al. (2012). The main concept of the majority voting is to reach the agreement on the segmented streamlines (or voxel) coming from different examples, usually removing the infrequent ones.

2.2 Linear Assignment Problem Solutions

The linear assignment problem (LAP) computes the optimal one-to-one assignment between the N elements of two sets of objects minimizing the total cost. The LAP takes as input the cost matrix that describes the cost of assigning each object of the first set to each object of the second set. Various algorithms for solving the LAP in polynomial time has been proposed in literature. A comprehensive review of all the proposed algorithms can be found in Burkard et al. (2009) Burkard and Cela (1999). An extensive computational comparison among eight well known algorithms is in Dell'Amico and Toth (2000). The algorithms are: Hungarian, signature, auction, pseudoflow, interior point method, Jonker-Volgenant (LAPJV). According to the survey, the Hungarian Kuhn (1955) algorithm and Jonker-Volgenant algorithm (LAPJV, Jonker and Volgenant (1987)) are the most efficient ones Serratosa (2015), with complexity $\mathcal{O}(N^3)$. According to Dell'Amico and Toth (2000); Burkard et al. (2009), LAPJV is faster than other algorithms in multiple applications, see also Bijsterbosch and Volgenant (2010). Moreover, in many

practical applications, the two sets of objects[1] on which to compute the LAP have different sizes, i.e. the related cost matrix is rectangular. In Bijsterbosch and Volgenant (2010), the rectangular version of LAPJV was proposed with a more efficient and robust solution than the original one in Jonker and Volgenant (1987). In this work, we adopted the rectangular version of LAPJV because of its efficiency and because we need to compute the correspondence between an example tract and the target tractogram which, clearly, have different number of streamlines.

3 METHODS

In this section, we first introduce basic definitions and terminology and then the details of the proposed tract segmentation method. The proposed method provides automatic segmentation of a tract/bundle of interest from a set of examples from different subjects. The proposed method comprises two main steps: in the first, a preliminary segmentation of the tract is obtained from each example. This step is accomplished by casting the segmentation problem as a rectangular linear assignment problem (LAP), which we implement with the rectangular version of Jonker-Volgenant algorithm (LAPJV). The second step merges the segmentations coming from different examples, with a ranking scheme. In this way, it is possible to obtain the final segmentation of the tract of interest that comprises the anatomical information coming from the different examples/subjects.

3.1 Basic Definitions

A *streamline* s is a polyline in $3D$ space, i.e. $s = \{\mathbf{x}_1, \mathbf{x}_2, \dots \mathbf{x}_{n_s}\}$, where $\mathbf{x}_i \in \mathbb{R}^3$. Let $T = \{s_1, s_2, \dots, s_M\}$ be the whole brain *tractogram*, represented as a set of M streamlines[2]. A *tract*, also called *bundle*, is denoted as $t \subset T$. Note that, in this work, *tract* will be referred as a set of streamlines with particular anatomical meaning, e.g. the cortico-spinal tract (CST).

3.1.1 Streamline Distance

In the literature, multiple inter-streamline distance functions have been proposed Garyfallidis et al. (2012). In this work, we adopt the most common one, i.e. the symmetric minimum average mean distance (MAM) Garyfallidis et al. (2012). Given two streamlines s_a and s_b:

$$d_{MAM}(s_a, s_b) = \frac{1}{2}(D(s_a, s_b) + D(s_b, s_a)) \tag{1}$$

where $D(s_a, s_b) = \frac{1}{|s_a|}\sum_{i=1}^{|s_a|} d(\mathbf{x}_i^a, s_b)$ and $d(\mathbf{x}_i^a, s_b) = \min_{j=1,\dots,|s_b|} ||\mathbf{x_i^a} - \mathbf{x}'_j||_2$.

3.1.2 Dissimilarity Representation

The *dissimilarity representation* (DR) is a Euclidean embedding technique to represent generic objects in a vector space Pekalska and Duin (2005) when a distance between the objects is available. In this work, we use the DR to represent the streamlines in vector space[3], as proposed in Olivetti et al. (2012). The DR is defined by the distance function between streamlines and by defining a (usually small) subset of the tractogram, called the *prototypes*. Given the distance and the prototypes, each streamline is then represented as the vector of the distances from the prototypes. Given a tractogram T and the set of

[1] Two sets of streamlines, in our case.

[2] Usually, $M \approx 10^5 - 10^6$.

[3] Notice that a streamline is not a vector but a sequence of points in 3D space and that different streamlines are sequences of different length, in general.

prototypes $\Pi = \{s_1^*, s_2^* \ldots, s_p^*\}$, the dissimilarity representation of $s \in T$ is the p-dimensional vector:

$$x_\Pi(s) = [d(s, s_1^*), d(s, s_2^*), \ldots, d(s, s_p^*)]. \tag{2}$$

As shown in Olivetti et al. (2012); Porro-Muñoz et al. (2015), the DR of streamlines is very accurate with a few tens of prototypes selected by means of the Subset Farthest First (SFF) algorithm, which requires just a few seconds of computation.

3.1.3 K-d (k-dimensional) Tree

A k-dimensional tree (k-d tree, see Bentley (1975)) is a space partitioning data structure to efficiently store and retrieve vectorial data in k-dimensional space. The k-d tree provides fast nearest neighbor queries on large datasets. In this work, we use the k-d tree on the vectorial representation of streamlines, in order to quickly find the neighboring streamlines of a given streamline s. The computational time complexity of building a k-d tree is $\mathrm{O}\big(M \log M\big)$ and the nearest neighbor query has time complexity $\mathrm{O}\big(\log M\big)$, where M is the number of streamlines of the tractogram. For example, a modern desktop computer can retrieve the 10 neighboring streamlines of a given streamline from a whole tractogram in just a few milliseconds[4].

3.1.4 Linear Assignment Problem

The Linear Assignment Problem (LAP) is a fundamental combinatorial optimization problem. Given two sets of objects $A = \{a_1, \ldots, a_M\}$ and $B = \{b_1, \ldots, b_M\}$ and the cost matrix $C = \{c_{ij}\}_{ij} \in \mathbb{R}^{M \times M}$ that provides the cost c_{ij} of assigning/matching a_i to b_j, the LAP aims to find the *one-to-one* correspondence between the two sets that has the minimum total cost. In our context, we use the LAP to find the correspondence between two sets of streamlines, as we recently proposed in Sharmin et al. (2016). In our case, the cost to minimize is the distance between the streamlines, i.e. $c_{i,j} = d(s_i^A, s_j^B)$. A one-to-one assignment can be represented with a binary matrix $P = \{p_{ij}\}_{ij}$, where $p_{ij} = 1$ if a_i corresponds to b_j and zero otherwise. The one-to-one constraint makes P a *permutation matrix*, i.e. only one element in each row and column is 1. Then, the LAP is defined as

$$P^* = \underset{P \in \mathcal{P}}{\operatorname{argmin}} \sum_{i,j=1}^{M} C_{ij} p_{ij}. \tag{3}$$

where P^* is the optimal assignment and $\mathcal{P}$ is the space of all possible assignments. When the size of the two sets differs, i.e. $|A| \neq |B|$, the problem is called *rectangular* linear assignment problem (RLAP) Bijsterbosch and Volgenant (2010), a generalization of the LAP. Further information is provided below, in Section 3.2.1.

3.2 Proposed Tract Segmentation Framework

In this work, we propose an example-based supervised tract segmentation approach. Given an anatomical tract of interest, e.g. the corticospinal tract (CST), and a set of examples of that tract, segmented from multiple subjects, our aim is to exploit the information from those examples in order to automatically segment the tract of interest in a new subject. The tract segmentation method that we propose consists of two main steps, illustrated in Figure 2. In the first step, each example tract is used to obtain a candidate segmentation in the new tractogram, see Figure 3. In the second step, the candidates generated from each

[4] We measured the timing using the k-d tree implementation `sklearn.neighbors.KDTree` provided by the Python package Scikit-learn, see `http://scikit-learn.org`, and the tractograms in our experiments represented as vectors through the DR.

example are merged together and then filtered, in order to obtain the final segmentation of the desired tract, taking into account the variability of the examples across subjects. In the following, we describe the details of the two main steps.

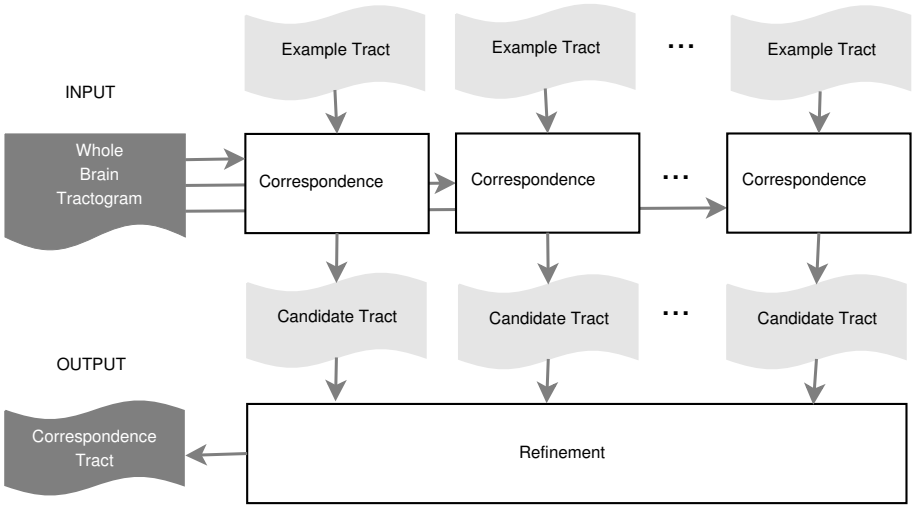

Figure 2. Proposed Tract Segmentation Framework

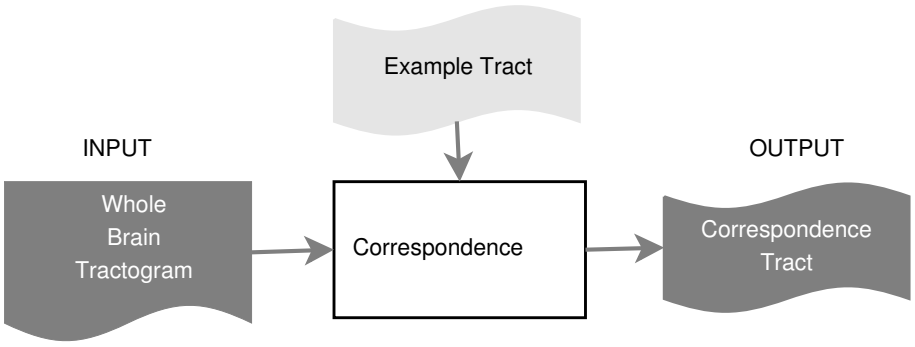

Figure 3. Tract Segmentation from a Single Example

3.2.1 Tract Segmentation from a Single Example

Given one example of the tract of interest, $t_A = \{s_1^A, \ldots, s_k^A\}$, e.g. the segmented CST from subject A, the first step of the proposed method is able to extract the set of streamlines of subject B corresponding to t_A, that we call $t_{A \to B} \subset T_B$. The extracted tract, $t_{A \mapsto B}$, is an approximation of the actual tract/bundle of interest in subject B, i.e. t_B. The procedure is based on the concept of streamline correspondence, i.e. on finding which streamline in the new tractogram corresponds to a given streamline in the example tract.

As explained in Section 2, the literature reports that the most common strategy to obtain corresponding streamlines across two subjects is based on the idea of Nearest Neighbor (NN). Assuming that the set of streamlines of two subjects are registered in a common space, usually by means of an affine transformation, the streamline of the subject B corresponding to a given s_i^A of subject A, is defined as the closest (nearest) one

$$s_{A,i}^B = \underset{s^B \in T_B}{\operatorname{argmin}}\, d(s^B, s_i^A) \tag{4}$$

In principle, the task of retrieving neighboring streamlines has high computational cost. The straightforward solution entails computing the distance from the given streamline to all other streamlines in the new/target tractogram and then getting the one with minimum distance. The approaches currently adopted in the literature are more efficient and based on several pre-processing steps, that may involve clustering, the definition of thresholds and the use of fast graphics processing units (GPUs), see Yoo et al. (2015); Labra et al. (2016). In this work, we claim that segmentation based on nearest neighbor is fairly sub-optimal and can be improved with the idea of linear assignment (see below). Nevertheless, in this work we also propose the following procedure to greatly simplify such computation of nearest neighbors, both in terms of logical steps and time:

1. Compute a vectorial representation, e.g. the dissimilarity representation (DR), of the streamlines of T_B and of t_A[5]
2. Build a k-d tree from the vectors of T_B.
3. For each streamline in t_A, in vector form, perform a nearest neighbor query on the k-d tree and obtain the closest streamline.

Correspondence as (Rectangular) Linear Assignment Problem

The segmentation method that we propose in this work is based on the (rectangular) linear assignment problem (LAP). We observed that finding corresponding streamlines with the nearest neighbor strategy is suboptimal. A typical problem with the nearest neighbor is that homologous anatomical structures of two different subjects may have a systematic displacement even after the initial affine registration. In those cases, the nearest neighbor strategy would be too greedy and would fail to retrieve the correct corresponding streamlines because of the systematic displacement, selecting instead the closest ones, see Figure 1. For this reason, we claim that introducing the further constraint of *one-to-one* correspondence between streamlines forces the correspondence to follow the local displacements that may occur.

Given the tract/bundle $t_A = \{s_1^A, \ldots, s_k^A\}$ of subject A and the tractogram $T_B = \{s_1^B, \ldots, s_M^B\}$ of subject B, where $k \lll M$, and a distance function $d()$ between streamlines, we denote as $C = [c_{ij}]_{i=1\ldots k, j=1\ldots M}$, the $k \times M$ distance matrix between each streamline of t_A and each of T_B, i.e. $c_{ij} = d(s_i^A, s_j^B)$. Then, we define the corresponding streamlines of t_A in T_B as those found by the solution of the corresponding rectangular linear assignment problem (RLAP):

$$P^* = \underset{P \in \mathcal{P}}{\operatorname{argmin}} \sum_{i=1}^{k} \sum_{j=1}^{M} c_{ij} p_{ij} \tag{5}$$

where $[p_{ij}]_{ij} = P \in \mathcal{P}$ is a *partial* permutation matrix, i.e. $P = [p_{ij}]_{ij} \in \{0,1\}^{k \times M}$ and $\sum_{j=1}^{k} p_{ij} = 1$ but $\sum_{i=1}^{M} p_{ij} \leq 1$, because the tract has less streamlines then the tractogram. P^* is the optimal assignment, i.e. the one with lowest overall cost. Once P^* is obtained, the segmented tract in T_B is defined as the set streamlines in T_B corresponding to t_A according to P^*.

Finding the optimal solution of the LAP or RLAP is usually computationally very expensive. As mentioned before, we adopted the rectangular LAPJV that we do not describe here because its description is fairly technical. We refer the interested reader to Bijsterbosch and Volgenant (2010); Jonker and Volgenant (1987) for a comprehensive description, as to Section 2 for a concise analysis of the literature on this topic. Anyway, a key element of the scalability of our solution, is a further step that we introduce before starting

[5] The DR of t_A is obtained using the prototypes of T_B.

the RLAP: the *sparsification* of the cost matrix C. In our experiments, we noticed that only a small part of the whole C is actually used in LAPJV. Specifically, for each streamline in t_A only the distance from the neighboring streamlines in T_B play a role in the computation. For this reason, by leveraging the DR and the k-d tree introduced above, we efficiently computed just a small subset of C instead of the whole matrix, saving a substantial amount of time and memory both in building C and in executing LAPJV. In Section 5, we show the details of this step and the gain obtained.

3.2.2 Tract Correspondence from Multiple Examples

The quality of the segmented tract/bundle obtained from a single example, as described in Section 3.2.1, is limited by inherent differences in the white matter anatomy between subject A and B. In order to reduce the bias of segmenting from a single specific example, here we describe a procedure to segment the desired tract/bundle from multiple examples, each from a different subject. In this way we try to exploit the anatomical variability in the sample of subject as if we had a model of the tract. The proposed procedure is based on first computing the correspondence between each example and the new tractogram, as detailed in Section 3.2.1, and then on ranking all the corresponding streamlines based on how frequently they were selected by the segmentation induced by each example. In the following, we describe the details of the proposed procedure.

Refinement through Ranking

Given a tract/bundle of interest t, e.g. the CST, the set of N examples segmentations of that tract from N different subjects is denoted as $\{t_{A_1}, \ldots, t_{A_N}\}$. For each example tract t_{A_i}, a corresponding tract $t_{A_i \to B} \subset T_B$ can be obtained following the RLAP procedure explained in Section 3.2.1, or other strategies like the nearest neighbor. The resulting (approximate) segmentations for t_B are then $\{t_{A_1 \to B}, \ldots, t_{A_N \to B}\}$. Our aim is to find an improved approximation of t_B, that we call $\hat{t}_B$, leveraging all of them. The proposed procedure to obtain $\hat{t}_B$ is the following:

1. Compute the union of the obtained segmentations: $t_{(A_1,\ldots,A_N)\to B} = \bigcup_{i=1}^{N} t_{A_i \to B}$, which we expect to be a superset of t_B.
2. Score each streamline in $t_{(A_1,\ldots,A_N)\to B} \subset T_B$ by counting how many time the streamline appears in $\{t_{A_1}, \ldots, t_{A_N}\}$. In this way, being selected multiple times as potential streamline of t_B is considered evidence of being a reliable streamline. We further introduce other criteria in order to break ties in the ranking between streamlines selected the same number of times. Our proposed second criterion comes from the selection cost of the streamlines, i.e. the distance of the streamline during the time of selection. Lower cost means a more reliable matching. Once all scores are obtained, we ranked the streamlines according to their score.
3. We define the number of streamlines of $\hat{t}_B$ as the median number of streamlines of the example tracts: $\hat{k} = |\hat{t}_B| = median(t_{A_1 \to B}, \ldots, t_{A_N \to B})$.
4. $\hat{t}_B$ is the set of $\hat{k}$ top scoring streamlines.

4 MATERIALS

In this section, we describe the datasets used to conduct the experiments, as well as the procedure to obtain to ground truth of the segmentations, i.e. through the white matter query language (WMQL). A total amount of 300 segmented tracts will be considered in our experiments.

4.1 Datasets

Thirty healthy subjects from the Human Connectome Project (HCP) Sotiropoulos et al. (2013) public datasets were selected at random and their MRI data retrieved. The diffusion MRI dataset from HCP consists of 3×90 gradient directions at b-values of 1000, 2000 and 3000 s/mm^2, with 18 non-diffusion weighted images, with voxel size of $1.25mm$. The fiber orientation distribution (FOD) function at each voxel was computed using the constrained spherical deconvolution algorithm (CSD) Tournier et al. (2007) with a single shell (b=1000). The tractograms were obtained with the Euler Delta Crossing (EuDX) algorithm, see Garyfallidis et al. (2014), implemented in DiPy [6], with 10^6 seeds. The number of streamlines of the resulting tractograms is approximately $100 - 140$ thousands.

4.2 Tractogram Segmentation with WMQL

The TractQuerier, based on the White Matter Query Language (WMQL) Wassermann et al. (2013, 2016), is a parcellation-based Open Source tool [7] to segment the whole brain tractogram. Using the parcellation from FreeSurfer and a database of ROIs, defined by the anatomical information of the tract, the WMQL extracts the anatomically meaningful tracts with a rule-based approach. Here, WMQL is applied over thirty subjects from the HCP dataset to produce a set of tracts, specifically: corticospinal tract (CST), cingulum (CG), arcuate fasciculus (AF), inferior longitudinal fasciculus (ILF), Uncinate Fascicle(UF), inferior fronto-occipital fasciculus (IFOF), 1, 2, and 3 left-right superior longitudinal fasciculus (SLF1,2,3), and finally, corpus callosum (CC) with seven parts (CC1-7). Among all the tracts, we selected those showing more consistency across subjects, resulting in a set of ten different tracts: left and right corticospinal tract (CST), left and right cingulum (CG), left and right inferior fronto-occipital fasciculus (IFOF), left and right Uncinate Fascicle (UF) and left and right inferior longitudinal fasciculus (ILF). These tracts will be used as *exampled tracts*, as well as for the quantitative comparison of the tract segmentation methods. Note that no further manual filtering is performed on the segmented tracts. In Table 1, we report the mean and standard deviation of the number of streamlines and of voxels over 30 subjects for the ten selected tracts.

Tract Name	# Streamline			# Voxels		
CST.Left	39	±	39	957	±	625
CST.Right	23	±	34	644	±	544
CG.Left	1141	±	168	9039	±	1172
CG.Right	982	±	159	8200	±	1087
IFOF.Left	173	±	94	3713	±	1295
IFOF.Right	123	±	76	2796	±	1212
ILF.Left	96	±	71	1771	±	610
ILF.Right	54	±	59	2035	±	566
UF.Left	143	±	76	1794	±	844
UF.Right	185	±	66	1140	±	819

Table 1. Data description. For each tract, the table reports the mean and standard deviation of the number of streamlines and of voxels over 30 subjects.

[6] `http://www.dipy.org`

[7] `https://github.com/demianw/tract_querier`.

5 EXPERIMENTS

In this section, we present all the components for the quantitative validation of our proposed supervised tract segmentation method based on LAP. Experiments were performed on 30 subjects from the Human Connectome Project (HCP) dMRI dataset, as described in Section 4. The tractograms of all subjects were aligned to the MNI152 template with the voxel-based linear registration tool FLIRT/FSL[8]. After alignment, the WMQL was applied over thirty subjects to segment the whole brain tractogram and obtain 10 different tracts: left-right corticospinal tract (CST), left-right cingulum (CG), left-right inferior fronto-occipital fasciculus (IFOF), left-right Uncinate Fascicle (UF) and left-right inferior longitudinal fasciculus (ILF). We divided the set of subjects into two groups, i.e. the *example group* and the *test group*, each of 15 subjects. The tracts from the example group were used as prior information to guide the segmentation in the tractogram of new subjects. The tracts from the test group were used to quantify the quality of the obtained segmentation.

We compared our proposed LAP-based supervised tract segmentation method against the automatic ROI-based segmentation, see Zhang et al. (2010), and the example-based multi-atlas approach with nearest neighbor strategy (hereafter denoted as NN_MULTI_ATLAS) of Yoo et al. (2015). The experiments are divided in two parts. In the first part, we segmented tracts with the three methods, i.e. ROI-based, NN_MULTI_ATLAS, LAP-based and measured the degree of voxel overlap with the ground truth, see Figure 4. In the second part, we performed a more in-depth analysis between the nearest neighbor strategy and the proposed LAP-based segmentation, ruling out confounds such as the different refinement strategy, the different embedding and different streamline distance function. In order to do that, we first show that the NN_MULTI_ATLAS method and our efficient nearest neighbor implementation (hereafter denoted as NN_DR_MAM, see Section 3.2.1) provide very similar results, see Figure 7, despite the differences in the refinement step, embedding and streamline distance function. Then, we show the results of a ROC/AUC analysis comparing NN_DR_MAM and the proposed LAP-based segmentation, illustrating the advantage of LAP over nearest neighbor, see Table 2 and Figure 8. Moreover, we provide additional results that enrich our work, such as visual examples of segmented tracts by the different methods, see Figure 5 and 6, or the role of the number of examples for the quality of segmentation, see Figure 9. In the following, we provide all the necessary details and descriptions of the results and how we obtained them.

5.1 Performance Analysis

To quantitatively evaluate the proposed LAP-based supervised segmentation, we adopted two different evaluation metrics: (i) the dice similarity coefficient (DSC) Dice (1945) and (ii) the Receiver Operating Characteristic (ROC) curve Brown and Davis (2006) analysis. In the following, we will discuss these metrics in details.

5.1.1 Dice Similarity Coefficient (DSC)

The common practice to evaluate tract segmentation methods is to compute the overlap, in terms of voxels, between the segmented tract and the ground truth tract Jin et al. (2014). The degree of voxel overlap can be measured through the common dice similarity coefficient (DSC). In order to compute the DSC, we converted the segmented tract and the ground truth tract into the binary mask where 1 indicates that a voxel is crossed by a streamline of the tract and 0 otherwise. Given the segmented tract, $\hat{t}$, and the ground truth

[8] http://fsl.fmrib.ox.ac.uk/.

tract t

$$DSC = \frac{2 \times (|v(\hat{t}) \cap v(t)|)}{|v(\hat{t})| + |v(t)|} \tag{6}$$

where $v(t)$ is the set of voxels crossed by the streamlines of t and $|v(t)|$ is the number of voxels of $v(t)$. The DSC varies between 0 to 1 and higher values indicate better overlap.

5.1.2 Receiver Operating Characteristic (ROC) Curve

The analysis of the ROC curve is a standard measure for performance in the field of the medical image segmentation techniques Southall et al. (2000). It considers all possible degrees of sensitivity/specificity of the segmentation method under evaluation. We adopted such analysis to compare the performance of our proposed LAP-based segmentation method with respect to the nearest neighbor method.

The ROC curve plots the sensitivity, i.e. the *true positive rate* (TPR), against the specificity, i.e. *false positive rate* (FPR) of the segmentation method at different thresholds. Here, the threshold refers to the number of streamlines to consider as segmented tract after ranking the streamlines that we obtain in the refinement step, where we combine the segmentations obtained from each single example in a single ranking, see Section 3.2.2. In the proposed LAP-based method, we set such threshold as the median number of streamlines across the example tracts. In order to compute the ROC curve, here we span through all possible thresholds in the ranking. The TPR and FPR are computed by comparing the streamlines above threshold (*positives*) and below threshold (*negatives*) with the ground truth, combining four numbers: the true positives (TP), i.e. the number of voxels of positives that are also in the ground truth tract, the false positives (FP), i.e. the number of voxels of the positives not in the ground truth, the true negatives (TN), i.e. the number of voxels of negatives not in the ground truth and the false negatives (FN), i.e. the number of voxels of negatives also in the ground truth. Hence, the TPR and FPR are formulated as follows:

$$TPR = \frac{TP}{TP + FN} \tag{7}$$

$$FPR = \frac{FP}{FP + TN} \tag{8}$$

High values of TPR and (1-FPR) means good segmentation. Additionally, the ROC curve can be summarized in a single scalar value: the *Area under ROC curve* (AUC) score, where higher AUC indicates better segmentation.

5.2 ROI-based Tract Segmentation

For each test subject, the 10 tracts of interest were segmented based on their related pair of cortical ROIs, obtained from the atlas in MNI space available at `http://lbam.med.jhmi.edu/cmrm/Data_Yajing/fiberMenu.htm`, see Zhang et al. (2010). For each subject and tract, given their two ROIs, the segmented/estimated tract was obtained by keeping the streamlines of the tractogram that intersected them. The quality of the segmented tract, with respect to the ground truth, is reported in Figure 4, as DSC, see the red bars. The segmentation of a single tract took, approximately, a few seconds of computation on a modern desktop computer.

5.3 Tract Segmentation with Nearest Neighbor (NN_MULTI_ATLAS method)

Following the NN_MULTI_ATLAS method of Yoo et al. (2015), we segmented each of the 10 tracts of interest for each subject of the test set using the example tracts from the 15 example subjects. First, all

streamlines of all tractograms, from the example set and test set, were re-sampled to 32 points. Then, given an example tract of interest from the example set and the tractogram of a test subject, we computed the nearest streamlines of that example in the test tractogram, using the Mahalanobis distance. As in Yoo et al. (2015), the nearest neighbor computation was carried out with the trivial algorithm, i.e. by first computing all possible pairwise distances between the streamlines of the example tract and the test tractogram and then by keeping the one at minimum distance. We repeated such procedure for all 15 examples of the example set and pooled all the obtained segmented streamlines. Following Yoo et al. (2015), we excluded all streamlines distant more than 200 units (in Mahalanobis distance) from their corresponding example streamline and then ranked the remaining ones according to the number of times they were selected by different examples. As in Yoo et al. (2015), we defined the resulting segmented tract as the set of streamlines that were selected by at least half of the examples. The quality of the segmented tract, with respect to the ground truth, is reported in Figure 4, as DSC, see the blue bars.

The segmentation of a single tract took, approximately, from half an hour to more than two hours, depending on the size of the tracts. The segmentations were conducted on a modern desktop computer, specifically with an Intel Xeon processor, 16Gb of RAM, 8 cores. The segmentations were computed in parallel, one example per core. Our implementation was in Python code, using the Free / OpenSource libraries NumPy, SciPy and DiPy [9]. The core part of the computation, i.e. the computation of all pairwise Mahalanobis distances, was implemented in C language, using `scipy.spatial.cdist()`. We could not use the GPU implementation of NN_MULTI_ATLAS mentioned in Yoo et al. (2015), because not provided by the authors.

5.4 Tract Segmentation with LAP

As mentioned in Section 3, our proposed LAP-based supervised tract segmentation method consists of two parts: (i) Tract correspondence from a single example, through LAPJV and (ii) merging of the correspondences from multiple examples through ranking. Here we discuss the choice of the parameters in each part.

As described in Section 3.2.1, tract correspondence from a single example was obtained by solving the LAP between the streamline of the example and those of the target tractogram, with the rectangular LAPJV. Due to the computational cost of the algorithm, we could not directly apply it to the full cost matrix, computed between the streamlines of the example tract and the whole set of streamlines of the target tractogram. For this reason, the LAPJV algorithm was applied to a reduced cost matrix. The reduced cost matrix was computed by considering only a subset of the streamlines of the target tractogram T_B, specifically the union of all 500 nearest neighbors of the streamlines in the example tract t_A, $i \in \{1, \ldots, N\}$. We expect such union set to be a superset of the ground truth tract t_B and we motivate the choice of 500 neighbors below, see Section 3.2.1 and Figure 10. In this way, instead of computing a cost matrix of size (approximately) $10^2 \times 10^5$ and solve the corresponding LAP, we reduced the problem to a cost matrix of size approximately $10^2 \times 10^3$. In order to compute such superset, we used the dissimilarity representation (DR) and a kd-tree. According to Olivetti et al. (2012), 40 prototypes were selected from the whole brain tractogram, T_B, using the SFF heuristic and the MAM distance function. With them, we computed the DR, i.e. a 40-dimensional vectorial representation, of each streamline in T_B. Afterwards, we put such vectors in a kd-tree, using the implementation provided by scikit-learn[10]. In the same way, all streamlines in the example tract t_A were represented as vectors using the previous prototypes. For each of those vectors, we

[9] `http://nipy.org/dipy`

[10] `http://scikit-learn.org`.

computed 500 nearest neighbors from the kd-tree of T_B and defined the superset of the ground truth t_B as their union. Then, in order to compute the reduced cost matrix, the MAM distance between the each streamline in the example tract t_A and those in the union set, were computed. Finally, the LAPJV algorithm was applied to the constructed cost matrix, in order to obtain the corresponding streamline from a single example (t_A).

Afterwards, we proceeded to the second step, considering multiple examples, i.e. the same anatomical tract from the 15 example subjects. We repeated the segmentation procedure as above for each of the 15 examples, obtaining 15 segmented tracts. After computing the union of those 15 sets of streamlines, we ranked the streamlines according to the frequency in which they appeared in the segmentations, as described in Section 3.2.2. The resulting segmentation of tract of ground truth tract t_B, that we referred to as $\hat{t}_B$, was obtained by taking the first m streamlines in the ranking, where m is the median number of streamlines among the example tracts [11].

We qualitatively evaluated our proposed segmentation method first with the DSC and then with the ROC curve analysis (see later). We measured the degree of overlap between the tract segmented by the LAP, $\hat{t}_B$ and the ground truth tract, t_g, through the DSC, at the voxel-level. We computed the average and standard deviation of the mean DSC values for each ten tracts from the fifteen subjects of the test group. The results are reported in Figure 4.

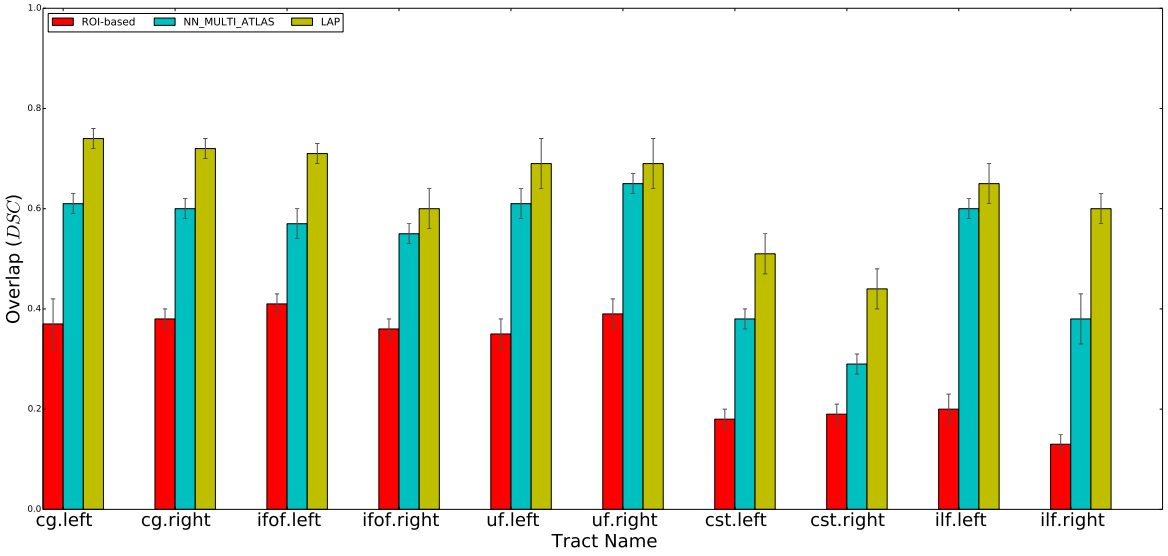

Figure 4. Summary of the results: average voxel overlap between segmented tracts and ground truth tracts for the ROI-based, NN_MULTI_ATLAS, and the proposed LAP. The bar graph shows the degree of overlap, in terms of dice similarity coefficient (DSC), for each tract averaged over fifteen subjects.

We implemented the proposed LAP-based approach with a combination of Python and Cython[12] code, leveraging Numpy, SciPy, scikit-learn (for k-d tree) and Pymatgen (for LAPJV). We developed a parallel version of the proposed method in order to compute the segmentation of multiple subjects at the same time,

[11] In case of ROC/AUC computation, such number varied, in order to explore sensitivity and specificity of the method.

[12] http://cython.org/

across the available cores of the CPU. On average, on a modern desktop computer [13], for each subject, the DR took approximately 30 seconds of computation time, whereas the k-d tree construction needed 20 seconds, for the whole brain tractogram. The correspondence with LAPJV required 10-30 seconds per tract, depending on the number of streamlines of the tract. In total, the segmentation of one tract from 15 examples required less than two minutes of computation. The software implementation of the proposed method is available under a Free / OpenSource license from here: `https://github.com/FBK-NILab/LAP_tract_segmentation`.

We further validated our proposed segmentation technique in a visual way. Figure 5 and 6 presents tracts as segmented by our proposed segmentation method (LAP) and the corresponding ground truth (GT). For all the tracts considered in this experiments, we report the segmentations with highest DSC (first column) and lowest DSC (third column), together with the respective ground truths (second and fourth column). In the figure, for LAP, we indicate the correctly segmented streamlines (TP) in salmon color and the incorrect ones (FP) in green. For GT, we indicate again the TP of LAP in salmon color and the missed streamlines (FN) in yellow color.

5.5 LAP vs. NN: ROC/AUC Analsysis

We further investigated the differences between the proposed method, based on the LAP, and the one of Yoo et al. (2015) based on the nearest neighbor (NN) strategy. Here, our main aim is to make the most direct comparison between the two different principles used to find corresponding streamlines: LAP using a *joint* minimization of distances over all streamlines (imposed by the one-to-one constraint) and NN using instead a *greedy* distance minimization of each streamline, individually.

We noticed that the NN_MULTI_ATLAS method of Yoo et al. (2015) differs from the proposed one on multiple aspects: the embedding procedure (re-sampling to 32 points vs. dissimilarity representation), the streamline distance function (Mahalanobis vs. MAM), the refinement step (majority-vote ranking with two thresholds vs. nesting of two rankings and median threshold, see Section 3.2.2) and the minimization function (NN vs. LAP). Since we are interested only in the last one of such differences, we wanted to avoid the effects of the other differences which could be confounds affecting the result. For this reason, we created a different NN implementation, based on the DR, k-d tree, MAM distance and the proposed refinement step, that we called NN_DR_MAM, and used instead of NN_MULTI_ATLAS. In Section 3, we have already shown that with these new elements we can retrieve the nearest neighbor streamlines in a very short time (milliseconds), making this alternative implementation of NN very convenient from the computational point of view with respect to the one of Yoo et al. (2015). Despite all the differences introduced in our implementation of NN, we verified that the quality of segmentation of NN_DR_MAM did not substantially differ from NN_MULTI_ATLAS. In Figure 7, we report the DSC values obtained with the two implementations over all 150 segmented tracts. The interpolating line, obtained with a robust linear regression algorithm[14], has a slope of 0.89, showing that NN_DR_MAM is equal or marginally superior to NN_MULTI_ATLAS.

In Table 2 we report the summary of the results of the ROC/AUC analysis of NN_DR_MAM vs. LAP, where the threshold changed during the sensitivity/specificity analysis was the number of streamline considered starting from the top of the ranking. In Figure 8, we report the detailed ROC curves for each tract, macro-averaged over the 15 test subjects.

[13] 8 cores CPU, Intel Xeon 3.50GHz, 16Gb RAM.

[14] The Huber regression algorithm.

	Method	
Tract	NN_DR_MAM	LAP
CG.Left	0.81	**0.90**
CG.Right	0.81	**0.88**
IFOF.Left	0.70	**0.86**
IFOF.Right	0.68	**0.80**
UF.Left	0.69	**0.84**
UF.Right	0.70	**0.83**
CST.Left	0.63	**0.79**
CST.Right	0.66	**0.75**
ILF.Left	0.71	**0.88**
ILF.Right	0.67	**0.84**

Table 2. Summary of the results: The average area under the Receiver operating characteristic (ROC) analysis between segmented tracts and ground truth tracts for the NN_DR_MAM and the proposed LAP. The table reports the area under curve (AUC) scores for each tract averaged over fifteen subjects. For each tract the **voxel** information has considered for the ROC curve analysis and For each subject **same** threshold has chosen.

5.6 LAP Segmentation: Number of Examples and of Neighbors

In this last part of the experiments, we investigated the effect of two important parameters on the proposed LAP segmentation: (i) the number of example tracts, i.e. 15 examples, and (ii) the number of nearest neighbors when building the superset for massively reducing the computational cost of LAP.

In Figure 9, we plotted the quality of the segmentation in terms of ROC/AUC score for each tract, averaged over all test subjects, when the number of example tracts varied from 1 to 15. Due to the variability of anatomy across subjects, having a larger set of examples is desirable for segmenting. Expectedly, all graphs show an increase in the score when the number of examples increases. The increase between 10 and 15 is modest, indicating that 15 examples are a meaningful example set size for segmenting.

In Figure 10, we show the effect of using different numbers of nearest neighbors of example tract when computing the superset on which the LAP is carried out. The graphs show the ROC/AUC score for each tract of interest, averaged over the test subjects when the number of neighbors span from a few tens to 1000. A small number of neighbors for each example streamline result in a small superset. It is expected that, if such superset is too small, then it might not contain all the streamlines of the actual target tract, i.e. the ground truth, preventing the proposed LAP method to get good quality of segmentation. In other words, a too small superset acts as an artificial upper bound on the score of LAP. Nevertheless, all the graphs show that, when the number of neighbors is above a 200, such issue completely disappears, for all tracts. Notice that, in the experiments, we always used 500 neighbors, a value which safely larger and, thus, justified.

6 DISCUSSION

In this section, we discuss the results obtained in Section 5 and show their impact on our claims.

We performed a set of experiments where the proposed LAP-based segmentation method is compared against two alternative methods: i) the commonly used automatic ROI-based segmentation Zhang et al. (2010) and ii) a recent example-based multi-atlas method based on the idea of correspondence implemented with the nearest neighbor algorithm (NN_MULTI_ATLAS) Yoo et al. (2015). The quality of segmentations

of 10 tracts for 15 test subjects, obtained by each of the 3 methods, was scored according to their voxel-overlap (as DSC) with the ground truth, obtained through WMQL Wassermann et al. (2013). Figure 4 reports the result of average DSC for ten tracts, averaged over fifteen test subjects. For each tract, three bar plots are reported, one for each segmentation method, along with the standard deviation of mean. The bar-plots show that proposed LAP-based method is able to segment tracts much better than the automatic ROI-based segmentation and remarkably better than example-based segmentation with the NN strategy. Additionally, notice that our results independently reproduce the result reported in Yoo et al. (2015), on a different dataset, where the multi-atlas NN method outperformed the ROI-based segmentation.

Across all tracts, our method showed strongly improved results, in terms of voxel overlap, with respect to ROI-based segmentation, usually doubling (or more) its score, i.e. from 0.15-0.40 vs. 0.45-0.75. The result from the ROI-based segmentation approach is indeed quite modest with respect to the other methods, as already seen in Yoo et al. (2015). This could be due to the limitations of registration, occurring when aligning the test subject to the cortical atlas.

Figure 4 showed that LAP-based segmentation is a substantial improvement over the NN-based method of Yoo et al. (2015). Nevertheless, we conducted a further analysis to make a detailed and more general comparison between the greedy optimization of the NN strategy, which defines the corresponding streamlines as those with minimum distance, and the proposed solution based on the LAP, which *jointly* minimizes the distances among all example streamlines and the target tractogram, introducing a one-to-one constraint. Our claim is that the segmentation with the NN strategy may fail in some cases, like when there is still a local systematic displacement between homologous anatomical structures, after the tractograms of the example and target subjects are registered. In such cases, the tract segmented with NN will be under estimated, see Figure 1. Differently, the one-to-one constraint of LAP should force the correspondence to correctly follow such displacement.

In order to conduct a careful analysis without confounds, we implemented an alternative version of the multi-example NN segmentation algorithm of Yoo et al. (2015), in order to match all the aspects of the proposed LAP-based segmentation method, see Section 5.5. We supported such argument by showing that our implementation, called NN_DR_MAM, provides equivalent results to that of Yoo et al. (2015), called NN_MULTI_ATLAS, see Figure 4. Then, we conducted a ROC/AUC analysis between NN_DR_MAM and our LAP-based segmentation. In Figure 8 we presented the ROC curves for each tract of interest, averaged over the 15 test subjects. Those curves are summarized in Table 2, where the ROC/AUC scores are reported. The LAP-based segmentation always obtains high ROC/AUC scores, i.e. 0.75-0.90, always remarkably higher than the ones of NN, i.e. 0.63-0.81, proving our claim. Notice that this result is even more insightful than that of Figure 4, because the ROC/AUC analysis is independent from the arbitrary choice of the number of streamlines for the target tract that we defined as the median value of the size of the example tracts. In other words, this result is independent from the choice of the threshold that we introduced with the proposed method.

Another important aspect of the proposed method is its computational cost. In the experiments, we have shown that the time required to segment one tract from 15 examples may be even more than two hours of computation, when using the NN method of Yoo et al. (2015). Instead, the proposed LAP-based segmentation requires only a couple of minutes of computation, obtaining also a higher quality of the results. Nevertheless, with the efficient computational tools of the dissimilarity representation and k-d tree adopted for the proposed method, we also implemented an alternative version of the multi-example NN segmentation method, called NN_DR_MAM. We have shown that it requires even less time than the LAP-based segmentation and obtains comparable results to those of Yoo et al. (2015). Our fast implementation

of NN-based segmentation from multiple examples is comparable to that of Labra et al. (2016) in terms of speed-up.

Despite all the positive results, there is notable variability in the quality of segmentations of all methods, including the proposed LAP-based one. In Figure 5 and Figure 6 we show 20 examples of segmented tracts obtained with the proposed LAP-based method, together with the respective ground truth (GT) obtained with WMQL. There, we show 2 examples of segmentations for each of the tracts of interest. These two examples are the one where the LAP-based method obtained the highest DSC score (column A) and the one with lowest DSC score (column B). The salmon-colored streamlines are the correctly segmented ones (TP). The green streamlines are the incorrectly segmented ones (FP) and the yellow streamlines are the missed ones (FN). In column A (highest DSC), for all the 10 tracts considered in this study, the large majority of streamlines are correctly segmented. Differently, in column B (lowest DSC), many tracts are poorly segmented. This fact occurs for two reasons: first, despite remarkable progress with respect to previous automatic segmentation methods, the proposed LAP-based segmentation cannot be considered as a final answer. The problem of automatic tract segmentation, even with the support of multiple examples, still have substantial room for future improvement. Secondly, the quality of the ground truth, both for examples and test tracts, should be improved. As it is clearly visible in Figure 5 and Figure 6, column B, some of the ground truth tracts are questionable, e.g. CST Right and ILF left, and could be easily challenged by an expert neuroanatomist. If the ground truth is poor, we cannot expect example-based segmentation methods to succeed. The common use of WMQL for defining the ground truth is appealing because of its low cost: like in our case, obtaining 300 high-quality segmentations from expert neuroanatomists would be vastly beyond reach from a single research group. At the same time, the limited quality of some of the tracts limits the generalization ability of example-based methods. This limitation is also a call to our community to collaboratively share segmented tracts by experts, in order to reach sufficient numbers to enable creation and assessment of higher-quality automatic methods.

One important question is about the size of the example set, that we set to 15 examples in our study. Given the variability of white matter anatomy in the healthy population, it is important to understand what is the trade-off between the cost of acquiring more examples and the gain in quality of segmentation. We analyzed this aspect and reported the results in Figure 9, where we observed the expected increase in ROC/AUC score when increasing the number of examples used by the proposed LAP-based segmentation method. This increase confirms what already has been observed in Yoo et al. (2015) (see Figure 11 there) for the case of NN-based segmentation and, in comparison to that study, in Garyfallidis et al. (2017) (see Table 1 and 2 there, in particular the Jaccard index[15]), where a variation of the NN from a single example is presented. For our LAP-based segmentation, we also observed moderate improvement of the quality of segmentation when using more than 10 examples, justifying the choice of 15 presented in this paper. Of course, such result may be limited by the quality of the ground truth tracts. With more homogeneous ground truth tracts, we might expect a steeper curve than the one in Figure 9, which would shift the desirable size of the set of examples to a higher value.

Although our proposed LAP-based tract segmentation method showed very positive experimental results, there is a critical parameter: the threshold that defines the number of streamlines for the segmented tract. In this work, we defined such threshold as the median value among the sizes of the example tracts. The median is a simple sensible choice because it is the number that deviates less from what has been observed in the example set. Moreover, it is more robust to outliers than the sample mean value. Nevertheless,

[15] Given the much larger size of the segmented tract with respect to the ground truth, the main value to consider against other segmentation methods is the Jaccard index.

such threshold is based only on example data and ignores the specificity of the test subject. This current limitation reveals an implicit assumption of our method, as well as the ones based on NN, i.e. that the number of streamlines of the tract of interest across all subjects should not change much. Besides the unavoidable subject variability in the white matter anatomy, the main implication of this assumption is that example and target tractograms should have a similar number of streamlines. Frequently, this is the case only when all tractograms are generated with the same tracking algorithm and same parameters. Different tracking algorithms, or even different parameter values, usually result in significant differences in a number of streamlines of the tractogram. As a consequence, both NN and LAP algorithms should not be used on non homogeneous (or inhomogeneous) sets of tractograms, at the current state.

The one-to-one constraint introduced by the LAP-based segmentation gives a clear advantage over NN-based segmentation but, sometimes, it can be seen as a limitation. Even in the case of homogeneous tractograms, the number of streamlines of a given tract of interest may substantially vary across subjects. In such case, each LAP will find the exact same number of streamlines between example and target tractogram, which may be sub-optimal. In future, we plan to refine and partly relax this constraint to find a more convenient compromise between the who extremes of NN and LAP.

7 CONCLUSIONS AND FUTURE WORK

In this work, we present a novel method for supervised tract segmentation based on the idea of streamlines correspondence across subjects as a set of linear assignment problems (LAPs). Our proposed segmentation method is able to segment a given tract of interest in the tractogram of a new subject using a set of example tracts from other subjects, as prior information. The results of multiple experiments show that the proposed method provides a very large improvement over ROI-based segmentation and a remarkable improvement over nearest-neighbor (NN) segmentation. The time required to segment a tract of interest is just a few minutes and we provide a Free / OpenSource implementation of the proposed method.

The proposed method has some limitations, on which we plan to work in near future. First, We plan to improve the reliablity of the results presented in this work by adding higher-quality tracts segmented by expert neuroanatomists, thus extending the current large dataset of 300 tracts used in our experiments. Secondly, we plan to address the limitation of defining the size of the target tract just from the examples, i.e. with the median value, that currently does not adapt to the target tractogram. To conclude, we plan to address automatic segmentation between tractograms generated from different tracking algorithms and with different parameters values. This last challenge should have an important impact on the adoption of supervised automatic segmentation systems, because we cannot expect to always have segmented tracts from homogeneous tractograms during deployment. In such cases, practitioners should provide homogeneous segmented examples before being able to use the supervised segmentation systems at their best.

ACKNOWLEDGMENTS

The research was funded by the Autonomous Province of Trento, Call “Grandi Progetti 2012”, project “Characterizing and improving brain mechanisms of attention - ATTEND”.

Data were provided [in part] by the Human Connectome Project, WU-Minn Consortium (Principal Investigators: David Van Essen and Kamil Ugurbil; 1U54MH091657) funded by the 16 NIH Institutes and Centers that support the NIH Blueprint for Neuroscience Research; and by the McDonnell Center for Systems Neuroscience at Washington University.

REFERENCES

Aarnink, S. H., Vos, S. B., Leemans, A., Jernigan, T. L., Madsen, K. S., and Baaré, W. F. C. (2014). Automated longitudinal intra-subject analysis (ALISA) for diffusion MRI tractography. *NeuroImage* 86, 404–416

Basser, P. J., Mattiello, J., and LeBihan, D. (1994). MR diffusion tensor spectroscopy and imaging. *Biophysical journal* 66, 259–267. doi:10.1016/s0006-3495(94)80775-1

Bentley, J. L. (1975). Multidimensional binary search trees used for associative searching. *Communications of the ACM* 18, 509–517

Bijsterbosch, J. and Volgenant, A. (2010). Solving the Rectangular assignment problem and applications. *Annals of Operations Research* doi:10.1007/s10479-010-0757-3

Bozzali, M., Falini, A., Franceschi, M., Cercignani, M., Zuffi, M., Scotti, G., et al. (2002). White matter damage in Alzheimer's disease assessed in vivo using diffusion tensor magnetic resonance imaging. *Journal of Neurology, Neurosurgery & Psychiatry* 72, 742–746. doi:10.1136/jnnp.72.6.742

Brown, C. D. and Davis, H. T. (2006). Receiver operating characteristics curves and related decision measures: A tutorial. *Chemometrics and Intelligent Laboratory Systems* 80, 24–38

Burkard, R. E. and Cela, E. (1999). *Linear assignment problems and extensions* (Springer)

Burkard, R. E., Dell'Amico, M., and Martello, S. (2009). *Assignment Problems, Revised Reprint* (Siam)

Catani, M., Howard, R. J., Pajevic, S., and Jones, D. K. (2002). Virtual in vivo interactive dissection of white matter fasciculi in the human brain. *NeuroImage* 17, 77–94

Clayden, J. D., Storkey, A. J., and Bastin, M. E. (2007). A probabilistic model-based approach to consistent white matter tract segmentation. *Medical Imaging, IEEE Transactions on* 26, 1555–1561

Dell'Amico, M. and Toth, P. (2000). Algorithms and codes for dense assignment problems: the state of the art. *Discrete Applied Mathematics* 100, 17–48

Dice, L. R. (1945). Measures of the amount of ecologic association between species. *Ecology* 26, 297–302

Douglas Fields, R. (2008). White Matter Matters. *Sci Am* 298, 54–61. doi:10.1038/scientificamerican0308-54

Garyfallidis, E., Brett, M., Amirbekian, B., Rokem, A., van der Walt, S., Descoteaux, M., et al. (2014). Dipy, a library for the analysis of diffusion MRI data. *Frontiers in Neuroinformatics* 8, 1+

Garyfallidis, E., Brett, M., Correia, M. M., Williams, G. B., and Nimmo-Smith, I. (2012). QuickBundles, a Method for Tractography Simplification. *Frontiers in neuroscience* 6. doi:10.3389/fnins.2012.00175

Garyfallidis, E., Côté, M.-A., Rheault, F., Sidhu, J., Hau, J., Petit, L., et al. (2017). Recognition of white matter bundles using local and global streamline-based registration and clustering. *NeuroImage* doi:10.1016/j.neuroimage.2017.07.015

Glasser, M. F., Sotiropoulos, S. N., Wilson, J. A., Coalson, T. S., Fischl, B., Andersson, J. L., et al. (2013). The minimal preprocessing pipelines for the Human Connectome Project. *NeuroImage* 80, 105–124. doi:10.1016/j.neuroimage.2013.04.127

Guevara, M., Román, C., Houenou, J., Duclap, D., Poupon, C., Mangin, J. F., et al. (2017). Reproducibility of superficial white matter tracts using diffusion-weighted imaging tractography. *NeuroImage* 147, 703–725

Guevara, P., Duclap, D., Poupon, C., Marrakchi-Kacem, L., Fillard, P., Le Bihan, D., et al. (2012). Automatic fiber bundle segmentation in massive tractography datasets using a multi-subject bundle atlas. *Neuroimage* 61, 1083–1099

Ingalhalikar, M., Smith, A., Parker, D., Satterthwaite, T. D., Elliott, M. A., Ruparel, K., et al. (2014). Sex differences in the structural connectome of the human brain. *Proceedings of the National Academy of Sciences* 111, 823–828

Jin, Y., Shi, Y., Zhan, L., Gutman, B. A., de Zubicaray, G. I., McMahon, K. L., et al. (2014). Automatic clustering of white matter fibers in brain diffusion MRI with an application to genetics. *Neuroimage* 100, 75–90

Jin, Y., Shi, Y., Zhan, L., Li, J., de Zubicaray, G. I., McMahon, K. L., et al. (2012). Automatic population HARDI white matter tract clustering by label fusion of multiple tract atlases. In *International Workshop on Multimodal Brain Image Analysis* (Springer), 147–156

Jonker, R. and Volgenant, A. (1987). A shortest augmenting path algorithm for dense and sparse linear assignment problems. *Computing* 38, 325–340. doi:10.1007/bf02278710

Kuhn, H. W. (1955). The Hungarian method for the assignment problem. *Naval Research Logistics* 2, 83–97. doi:10.1002/nav.3800020109

Labra, N., Guevara, P., Duclap, D., Houenou, J., Poupon, C., Mangin, J.-F., et al. (2016). Fast Automatic Segmentation of White Matter Streamlines Based on a Multi-Subject Bundle Atlas. *Neuroinformatics* , 1–16doi:10.1007/s12021-016-9316-7

Maddah, M., Mewes, A. U. J., Haker, S., Grimson, and Warfield, S. K. (2005). Automated atlas-based clustering of white matter fiber tracts from DTMRI. In *Medical image computing and computer-assisted intervention–MICCAI 2005* (Springer). 188–195

Maddah, M., Zollei, L., Grimson, Westin, C. F., and Wells, W. M. (2008). A mathematical framework for incorporating anatomical knowledge in DT-MRI analysis. In *Biomedical Imaging: From Nano to Macro, 2008. ISBI 2008. 5th IEEE International Symposium on* (IEEE), 105–108

Mayer, A., Zimmerman-Moreno, G., Shadmi, R., Batikoff, A., and Greenspan, H. (2011). A supervised framework for the registration and segmentation of white matter fiber tracts. *IEEE transactions on medical imaging* 30, 131–145

Mori, S., Wakana, S., Van Zijl, P. C. M., and Nagae-Poetscher, L. M. (2005). *MRI atlas of human white matter*, vol. 16 (Am Soc Neuroradiology)

O'Donnell, L. J., Golby, A. J., and Westin, C.-F. (2013). Fiber clustering versus the parcellation-based connectome. *NeuroImage* 80, 283–289

O'Donnell, L. J., Suter, Y., Rigolo, L., Kahali, P., Zhang, F., Norton, I., et al. (2017). Automated white matter fiber tract identification in patients with brain tumors. *NeuroImage: Clinical* 13, 138–153

O'Donnell, L. J. and Westin, C.-F. F. (2007). Automatic tractography segmentation using a high-dimensional white matter atlas. *IEEE transactions on medical imaging* 26, 1562–1575. doi:10.1109/tmi.2007.906785

Olivetti, E. and Avesani, P. (2011). Supervised segmentation of fiber tracts. In *Proceedings of the First international conference on Similarity-based pattern recognition* (Berlin, Heidelberg: Springer-Verlag), SIMBAD'11, 261–274. doi:10.1007/978-3-642-24471-1_19

Olivetti, E., Nguyen, T. B., and Garyfallidis, E. (2012). The Approximation of the Dissimilarity Projection. *IEEE Intl Workshop on Pattern Recognition in NeuroImaging* 0, 85–88. doi:10.1109/prni.2012.13

Olivetti, E., Nguyen, T. B., Garyfallidis, E., Agarwal, N., and Avesani, P. (2013). Fast Clustering for Interactive Tractography Segmentation. In *Pattern Recognition in Neuroimaging (PRNI), 2013 International Workshop on* (IEEE), 42–45. doi:10.1109/prni.2013.20

Olivetti, E., Sharmin, N., and Avesani, P. (2016). Alignment of Tractograms As Graph Matching. *Frontiers in Neuroscience* 10

Park, H.-J., Westin, C.-F., Kubicki, M., Maier, S. E., Niznikiewicz, M., Baer, A., et al. (2004). White matter hemisphere asymmetries in healthy subjects and in schizophrenia: a diffusion tensor MRI study. *Neuroimage* 23, 213–223

Pekalska, E. and Duin, R. P. W. (2005). *The Dissimilarity Representation for Pattern Recognition: Foundations And Applications (Machine Perception and Artificial Intelligence)* (World Scientific Publishing Company)

Porro-Muñoz, D., Olivetti, E., Sharmin, N., Nguyen, T., Garyfallidis, E., and Avesani, P. (2015). Tractome: a visual data mining tool for brain connectivity analysis. *Data Mining and Knowledge Discovery* 29, 1258–1279. doi:10.1007/s10618-015-0408-z

Reichenbach, A., Goldau, M., Heine, C., and Hlawitschka, M. (2015). V–Bundles: Clustering Fiber Trajectories from Diffusion MRI in Linear Time. In *Medical Image Computing and Computer-Assisted Intervention–MICCAI 2015* (Springer). 191–198

Rohlfing, T., Brandt, R., Menzel, R., and Maurer, C. R. (2004). Evaluation of atlas selection strategies for atlas-based image segmentation with application to confocal microscopy images of bee brains. *NeuroImage* 21, 1428–1442

Salat, D. H., Tuch, D. S., Greve, D. N., Van Der Kouwe, A. J. W., Hevelone, N. D., Zaleta, A. K., et al. (2005). Age-related alterations in white matter microstructure measured by diffusion tensor imaging. *Neurobiology of aging* 26, 1215–1227

Serratosa, F. (2015). Speeding up fast bipartite graph matching through a new cost matrix. *International Journal of Pattern Recognition and Artificial Intelligence* 29, 1550010

Sharmin, N., Olivetti, E., and Avesani, P. (2016). Alignment of Tractograms as Linear Assignment Problem. In *Computational Diffusion MRI* (Springer). 109–120

Shimony, J. S., Snyder, A. Z., Lori, N., and Conturo, T. E. (2002). Automated fuzzy clustering of neuronal pathways in diffusion tensor tracking. In *Proc. Intl. Soc. Mag. Reson. Med*. vol. 10, 1

Siless, V., Chang, K., Fischl, B., and Yendiki, A. (2016). Hierarchical Clustering of Tractography Streamlines Based on Anatomical Similarity. In *International Conference on Medical Image Computing and Computer-Assisted Intervention* (Springer), 184–191

Sotiropoulos, S. N., Jbabdi, S., Xu, J., Andersson, J. L., Moeller, S., Auerbach, E. J., et al. (2013). Advances in diffusion MRI acquisition and processing in the Human Connectome Project. *NeuroImage* 80, 125–143

Southall, B., Buxton, B. F., Marchant, J. A., and Hague, T. (2000). On the performance characterisation of image segmentation algorithms: a case study. In *European Conference on Computer Vision* (Springer), 351–365

Toga, A. W. (2015). *Brain mapping: An encyclopedic reference* (Academic Press)

Tournier, J.-D., Calamante, F., and Connelly, A. (2007). Robust determination of the fibre orientation distribution in diffusion MRI: Non-negativity constrained super-resolved spherical deconvolution. *NeuroImage* 35, 1459–1472. doi:10.1016/j.neuroimage.2007.02.016

Tunç, B., Parker, W. A., Ingalhalikar, M., and Verma, R. (2014). Automated tract extraction via atlas based adaptive clustering. *Neuroimage* 102, 596–607

Van Essen, D. C., Smith, S. M., Barch, D. M., Behrens, T. E. J., Yacoub, E., and Ugurbil, K. (2013). The WU-Minn Human Connectome Project: An overview. *NeuroImage* 80, 62–79. doi:10.1016/j.neuroimage.2013.05.041

Vercruysse, D., Christiaens, D., Maes, F., Sunaert, S., and Suetens, P. (2014). Fiber Bundle Segmentation Using Spectral Embedding and Supervised Learning. In *Computational Diffusion MRI* (Springer). 103–114

Wakana, S., Caprihan, A., Panzenboeck, M. M., Fallon, J. H., Perry, M., Gollub, R. L., et al. (2007). Reproducibility of quantitative tractography methods applied to cerebral white matter. *Neuroimage* 36, 630–644

Wang, X., Grimson, W. E., and Westin, C.-F. F. (2011). Tractography segmentation using a hierarchical Dirichlet processes mixture model. *NeuroImage* 54, 290–302. doi:10.1016/j.neuroimage.2010.07.050

Wassermann, D., Bloy, L., Kanterakis, E., Verma, R., and Deriche, R. (2010). Unsupervised white matter fiber clustering and tract probability map generation: applications of a Gaussian process framework for white matter fibers. *NeuroImage* 51, 228–241. doi:10.1016/j.neuroimage.2010.01.004

Wassermann, D., Makris, N., Rathi, Y., Shenton, M., Kikinis, R., Kubicki, M., et al. (2013). On describing human white matter anatomy: the white matter query language. *Medical image computing and computer-assisted intervention : MICCAI ... International Conference on Medical Image Computing and Computer-Assisted Intervention* 16, 647–654

Wassermann, D., Makris, N., Rathi, Y., Shenton, M., Kikinis, R., Kubicki, M., et al. (2016). The white matter query language: a novel approach for describing human white matter anatomy. *Brain structure & function*

Yoo, S. W., Guevara, P., Jeong, Y., Yoo, K., Shin, J. S., Mangin, J.-F., et al. (2015). An Example-Based Multi-Atlas Approach to Automatic Labeling of White Matter Tracts. *PloS one* 10. doi:10.1371/journal.pone.0133337

Zhang, Y., Zhang, J., Oishi, K., Faria, A. V., Jiang, H., Li, X., et al. (2010). Atlas-guided tract reconstruction for automated and comprehensive examination of the white matter anatomy. *Neuroimage* 52, 1289–1301

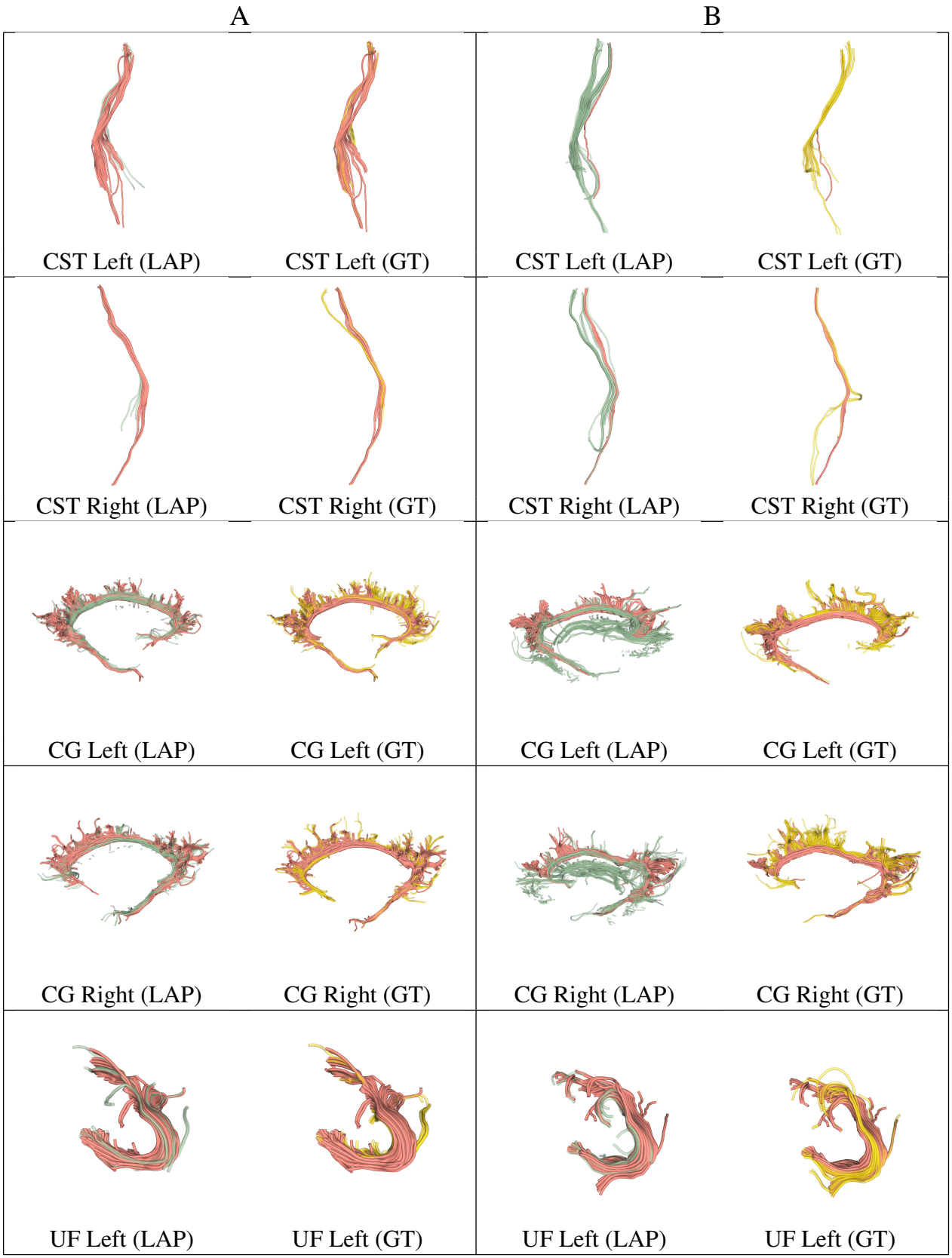

Figure 5. In each row, in column A, we show the tract obtained with LAP-based segmentation (LAP) with highest DSC score among all test subjects, together with the related ground truth (GT). In column B, we show the one with lowest DSC score, together with the ground truth. The streamline of salmon color are TP, the ones in green are FP and the ones in yellow are FN. The tracts are: CST (left, right), CG (left, right) and UF (left).

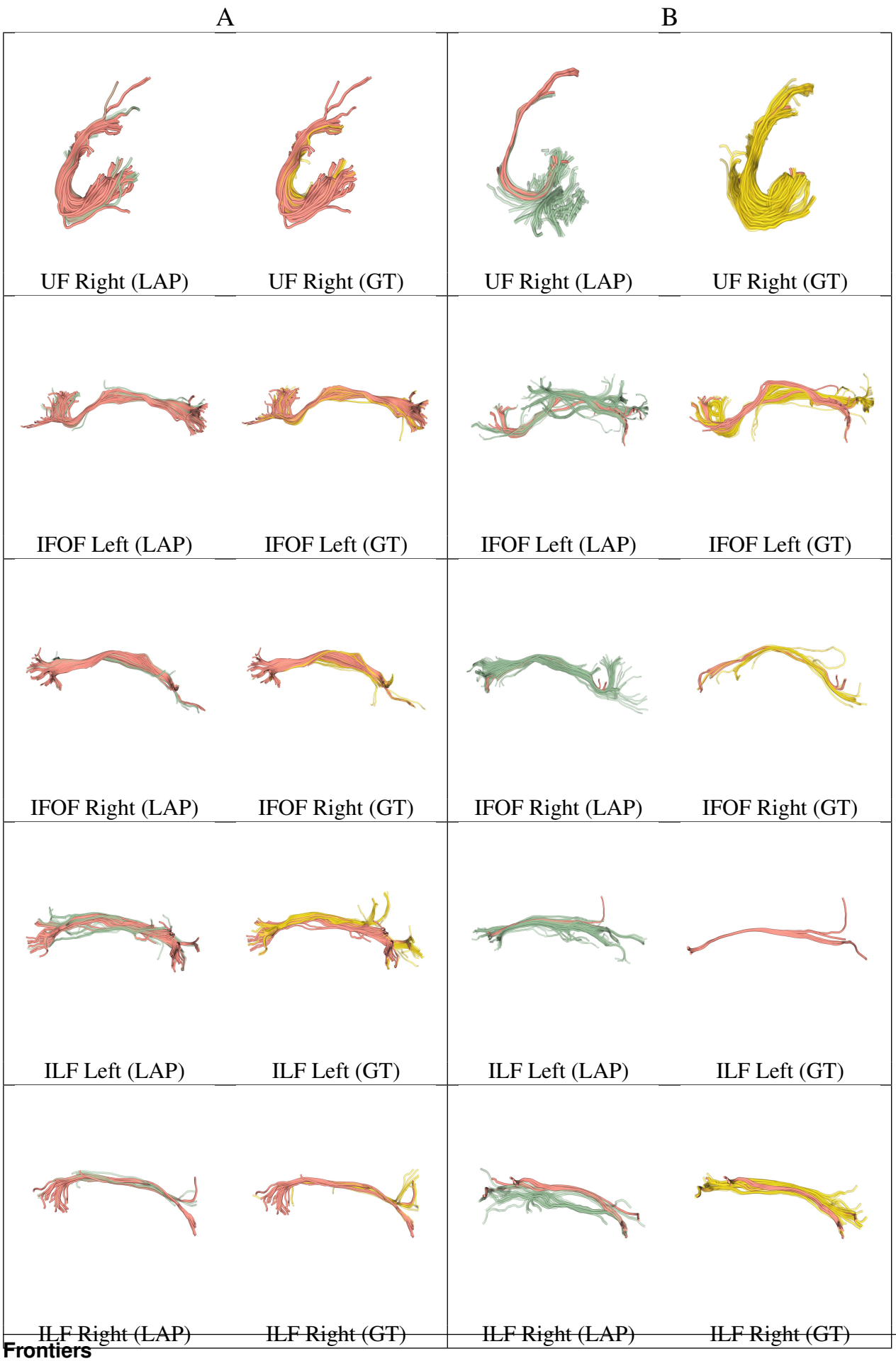

Figure 6. In each row, in column A, we show the tract obtained with LAP-based segmentation (LAP) with highest DSC score among all test subjects, together with the related ground truth (GT). In column B, we show the one with lowest DSC score, together with the ground truth. The streamline of salmon color are TP, the ones in green are FP and the ones in yellow are FN. The tracts are: and UF (right), IFOF (left, right)

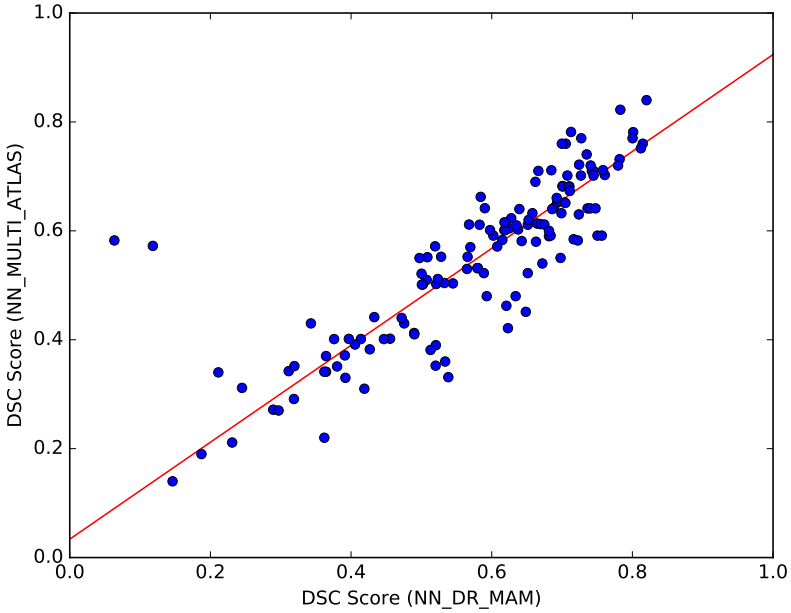

Figure 7. Comparison of the results between NN_DR_MAM and NN_MULTI_ATLAS. For each of the 10 tracts of the 15 test subjects (10 X 15) = 150 points in total), the graph reports DSC computed with NN_DR_MAM (x-axis) and the NN_MULTI_ATLAS method (y-axis).

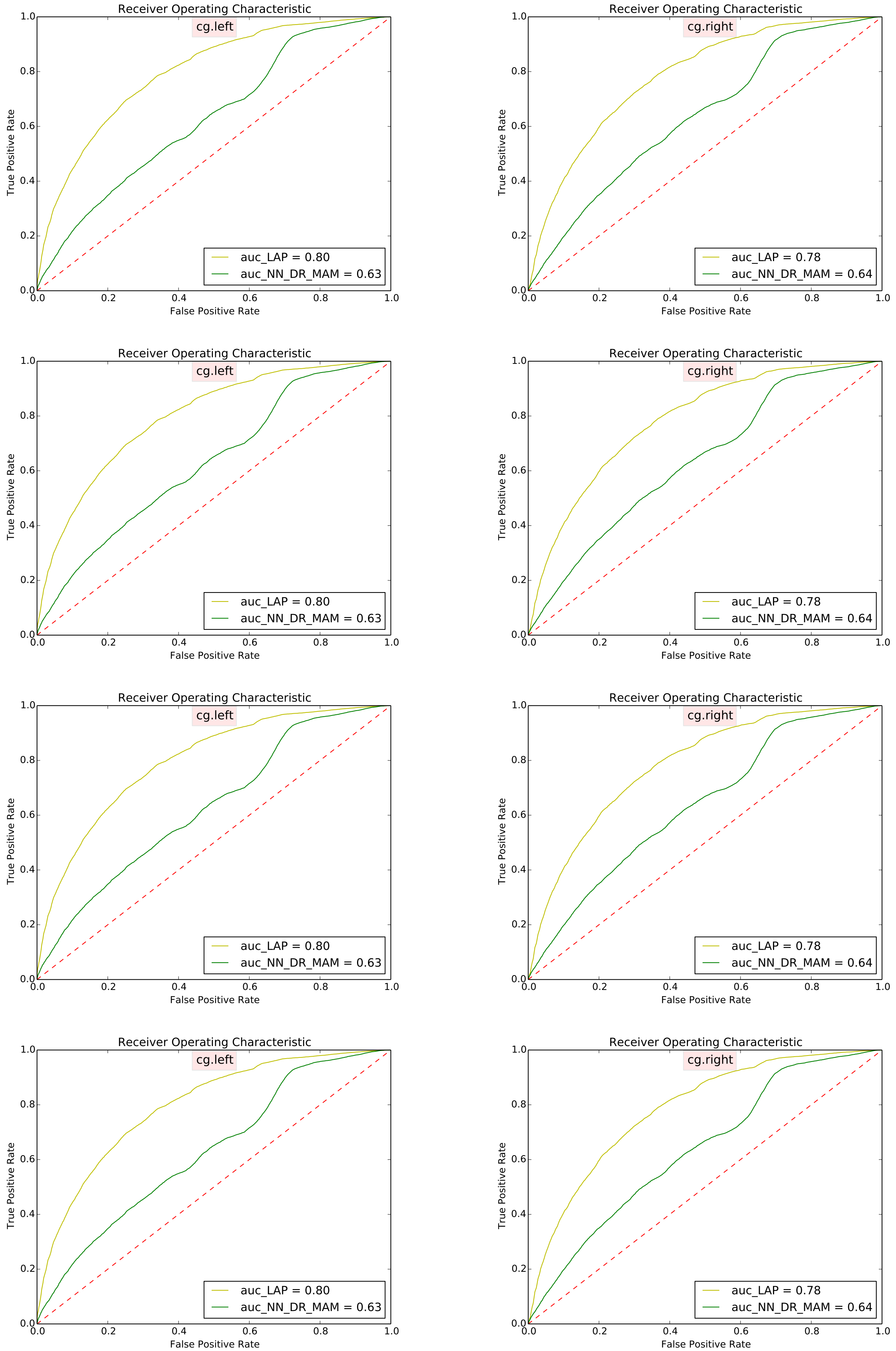
Receiver Operating Characteristic
cg.left
True Positive Rate
False Positive Rate
auc_LAP = 0.80
auc_NN_DR_MAM = 0.63
Receiver Operating Characteristic
cg.right
True Positive Rate
False Positive Rate
auc_LAP = 0.78
auc_NN_DR_MAM = 0.64

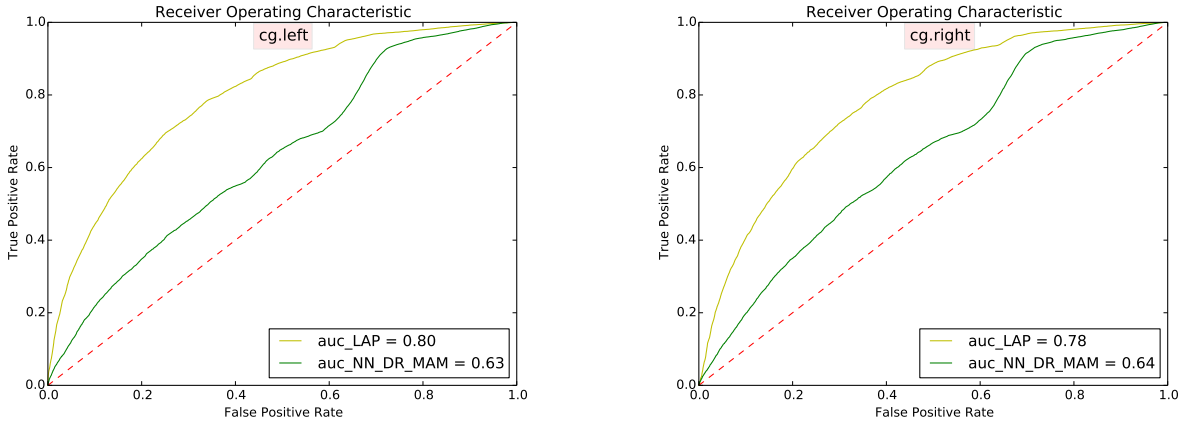

Figure 8. Receiver operating characteristic (ROC) analysis between segmented tracts and ground truth tracts for the NN_DR_MAM and the proposed LAP. Each subfigure shows the average ROC curve for each tract averaged over fifteen subjects. For each tract the **voxel** information has consider for the ROC curve analysis and For each subject **different** thresholds has chosen

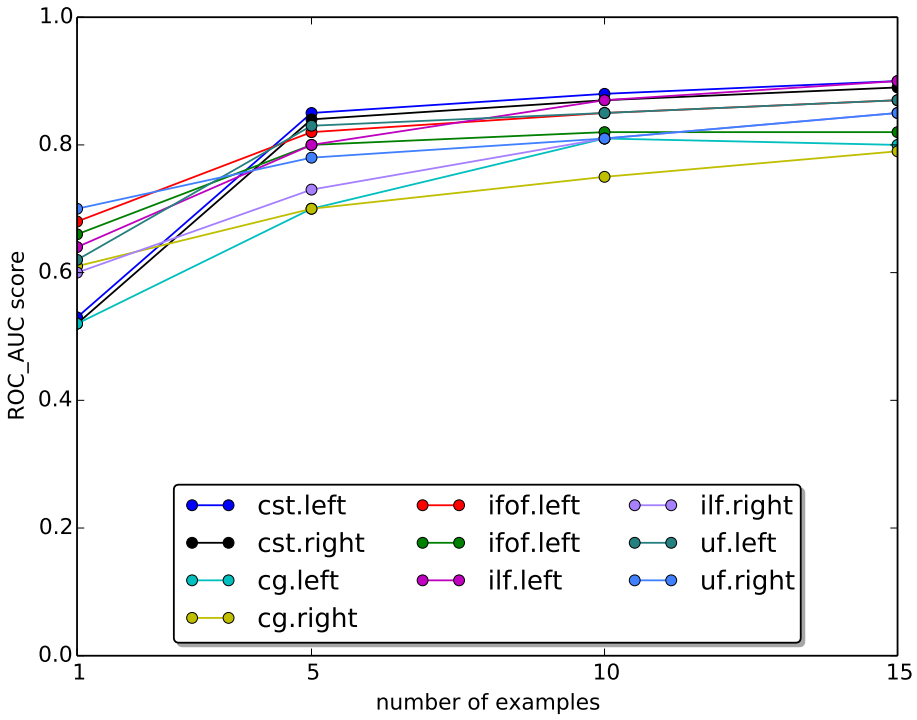

Figure 9. Change in the AUC score with the number of examples tracts. The plot reports the average Area Under Curve (AUC) scores for ten tracts over fifteen subjects. Expectedly, the AUC score increases as the number of examples increase.

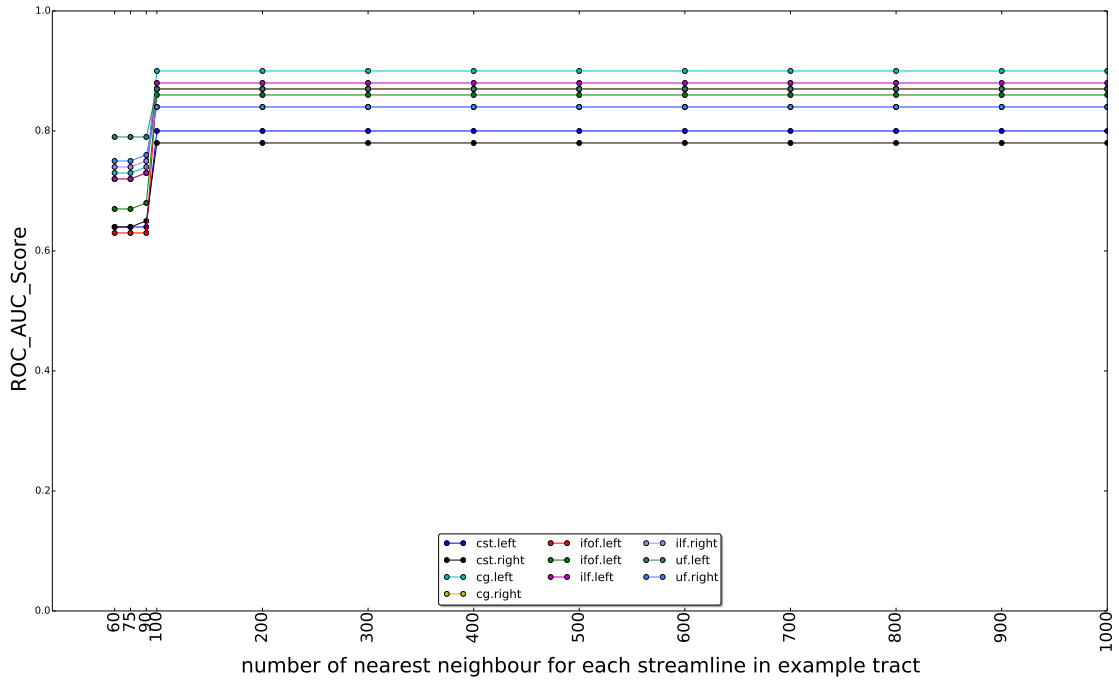

Figure 10. Change on the AUC score with the number of the nearest neighbors for each streamline in example tract used to compute the superset of each example, in order to sparsify the cost matrix of the LAP. The plot reports the AUC scores for ten tracts over fifteen subjects as the number of nearest neighbors increases from 60 to 1000. After 100 neighbors the results are stable, i.e. the target tract is always included in the superset.

Chapter 9

Alignment of Tractograms as Graph Matching

frontiers in Neuroscience

METHODS
published: 05 December 2016
doi: 10.3389/fnins.2016.00554

Alignment of Tractograms As Graph Matching

Emanuele Olivetti[1,2]*, *Nusrat Sharmin*[1,2] *and Paolo Avesani*[1,2]

[1] NeuroInformatics Laboratory, Bruno Kessler Foundation, Trento, Italy, [2] Center for Mind and Brain Sciences, University of Trento, Trento, Italy

The white matter pathways of the brain can be reconstructed as 3D polylines, called streamlines, through the analysis of diffusion magnetic resonance imaging (dMRI) data. The whole set of streamlines is called tractogram and represents the structural connectome of the brain. In multiple applications, like group-analysis, segmentation, or atlasing, tractograms of different subjects need to be aligned. Typically, this is done with registration methods, that transform the tractograms in order to increase their similarity. In contrast with transformation-based registration methods, in this work we propose the concept of tractogram correspondence, whose aim is to find which streamline of one tractogram corresponds to which streamline in another tractogram, i.e., a map from one tractogram to another. As a further contribution, we propose to use the relational information of each streamline, i.e., its distances from the other streamlines in its own tractogram, as the building block to define the optimal correspondence. We provide an operational procedure to find the optimal correspondence through a combinatorial optimization problem and we discuss its similarity to the graph matching problem. In this work, we propose to represent tractograms as graphs and we adopt a recent inexact sub-graph matching algorithm to approximate the solution of the tractogram correspondence problem. On tractograms generated from the Human Connectome Project dataset, we report experimental evidence that tractogram correspondence, implemented as graph matching, provides much better alignment than affine registration and comparable if not better results than non-linear registration of volumes.

Keywords: diffusion MRI, tractography, alignment, combinatorial optimization, graph matching

OPEN ACCESS

Edited by:
Maxime Descoteaux, Université de Sherbrooke, Canada

Reviewed by:
Demian Wassermann, INRIA Sophia Antipolis, France
Lauren Jean O'Donnell, Harvard Medical School, USA
Stanley Durrleman, INRIA, France

***Correspondence:**
Emanuele Olivetti
olivetti@fbk.eu

Specialty section:
This article was submitted to Brain Imaging Methods, a section of the journal Frontiers in Neuroscience

Received: *08 August 2016*
Accepted: *17 November 2016*
Published: *05 December 2016*

Citation:
Olivetti E, Sharmin N and Avesani P (2016) Alignment of Tractograms As Graph Matching. Front. Neurosci. 10:554. doi: 10.3389/fnins.2016.00554

1. INTRODUCTION

Diffusion magnetic resonance imaging (dMRI) data (Basser et al., 1994), provide quantitative information about the white matter of the brain, in terms of local main direction(s) of the neuronal axons. Such information allows to approximate the main paths of large sets of axons with polylines, called streamlines. The whole set of streamlines is called tractogram and represents the structural connectome of the brain (Sporns et al., 2005).

In multiple applications, like group-analysis, segmentation, or atlasing, tractograms of different subjects need to be aligned (O'Donnell et al., 2012), i.e., it is necessary to find corresponding anatomical structures across tractograms. Typically, two tractograms can be aligned by first estimating a transformation between the corresponding volumetric images, like T1, fractional anisotropy (FA, see Basser et al., 1994), or orientation distribution functions (ODFs, see Raffelt et al., 2011; Christiaens et al., 2012, and then by applying such transformation to the streamlines

of the tractograms[1]. In the literature, both linear and non-linear methods have been proposed to register volumetric data, see Christiaens et al. (2014). In case of linear methods, an affine transformation is estimated, e.g., with FSL/FLIRT, see Jenkinson et al. (2002), and then applied to the coordinates of the streamlines. In case of non-linear volumetric transformations, the tractogram is usually re-generated after transforming the dMRI data accordingly. The literature on non-linear transformations directly on streamlines is focused on fiber bundle alignment. In Ziyan et al. (2007), corresponding bundles are aligned across subjects by warping their spatial probability maps computed from the coordinates of the streamlines. In Ziyan et al. (2009), consistency clustering is used to label streamlines in an iterative process with polyaffine transformations. In Wassermann et al. (2011) a diffeomorphic registration algorithm is used on the Gaussian process representation of streamline density maps. In Durrleman et al. (2011), the use of the framework of *currents* is proposed to warp the streamlines of bundles, for registration, atlasing, and variability analysis. This literature addresses non-linear bundle alignment but not whole tractogram alignment, also for the high computational cost of the algorithms. Another approach to non-linear registration of streamlines is to use deformation fields, computed from non-linear volume registration, directly on streamlines. This approach is mentioned in Christiaens et al. (2012), but without a quantitative evaluation of its effect.

Recently, new linear methods have been proposed to directly register whole tractograms, see O'Donnell et al. (2012) and Garyfallidis et al. (2015), without the intermediate indirect step of registering volumetric images. These methods find an affine transformation that minimizes a given loss function computed only from streamlines. In O'Donnell et al. (2012), the loss function is based on the entropy of a random subset of the coordinates of the streamlines. In Garyfallidis et al. (2015), the loss function is based on a streamline-streamline distance of a subset of all streamlines.

It is common experience that a single affine transformation can reconcile only part of the differences between the tractograms of two subjects. Many differences remain at the local level, e.g., systematic displacement of entire tracts, thinner/thicker, or longer/shorter tracts. We show a simple toy example of these issues in **Figure 1**, where two tracts (see **Figure 1A**), one U-shaped and the other one elongated, and the corresponding two tracts after some local changes (see **Figure 1B**), are presented. This second set of streamlines, (B), is artificially constructed from the first set (A) by adding a small displacement between the two tracts and a moderate magnification of the U-shaped one. By construction it is not possible to find a global affine transformation that reconciles the difference between A and B, because the difference is *local* and not global. In **Figure 1C** we show the overlap between (A) and (B) with the best affine transform obtained with the streamline linear registration (SLR, see Garyfallidis et al., 2015) algorithm. It is clearly visible that the overlap between the green (A) and white (B) sets is poor.

As in O'Donnell et al. (2012) and in Garyfallidis et al. (2015), in this work we are eminently interested in methods for tractogram alignment that directly operates on streamlines, without resorting to volume-based registration. This is due to two main reasons: first, in many practical cases, tractogram alignment is based on registration of images that either do not contain diffusion MRI information at all, i.e., T1 images, or contain just a portion of it, e.g., FA images, which is clearly suboptimal. In case full ODFs are considered (see for example Raffelt et al., 2011), the effects of re-orientation may create problems when re-generating the tractogram, see Christiaens et al. (2012). The second reason is that the cost of re-generating tractograms, after registering volumes, may be high, in terms of computation time and required knowledge to operate the full pipelines of, preprocessing, reconstruction, tracking, and filtering, see Pestilli et al. (2014).

In this work, we propose to avoid transformations and to directly find the correspondence between streamlines of two different tractograms, i.e., to find which streamline of one tractogram corresponds to which streamline in the other tractogram. This idea is inspired by our recent work on bundle segmentation (Sharmin et al., 2016). The concept of corresponding streamlines has been used before, for example in the context of streamline clustering. There, the aim is to find corresponding clusters across subjects or to label them from an atlas. The cluster correspondence is achieved by finding the correspondence between the representative streamlines, one per cluster. See for example Maddah et al. (2005), O'Donnell and Westin (2007), Guevara et al. (2012), and Yoo et al. (2015). In this work, we take one step further and target streamline correspondence for all streamlines in the tractogram. This can be thought as the limit case of cluster correspondence, when the size of the cluster decreases till one single streamline. It is true that, given two tractograms, we cannot assume that *every* streamline in one tractogram has a corresponding streamline in the other tractogram. This occurs because, for example, some streamlines could be artifactual and have no anatomical counterpart. Nevertheless, in Section 3, show that, in practice, such cases do not disrupt the quality of the resulting alignment and that, for this reason, the number of problematic streamlines is quite small.

The alignment based on streamline correspondence, in a sense, acts as a non-linear alignment of the first set of streamlines onto the second one. It can be seen as a transformation, where each streamline of one tractogram is moved and deformed to become of the exact shape and position of the corresponding streamline in the other tractogram. From this point of view, the proposed method can be thought as an extremely local registration method. In **Figure 1D**, we show the result of computing such correspondence. There, the two sets of streamlines are displayed with arbitrary displacement and yellow straight lines, found by the proposed algorithm, correctly connect the midpoints of the corresponding streamlines across the two sets. After alignment, the resulting aligned set of white streamlines will be identical to the set of green streamlines.

[1]In the whole paper we use *alignment* as the generic term to indicate the task of putting in correspondence two anatomical structures. We use the term *registration* to specifically indicate the transformation-based methods to obtain alignment.

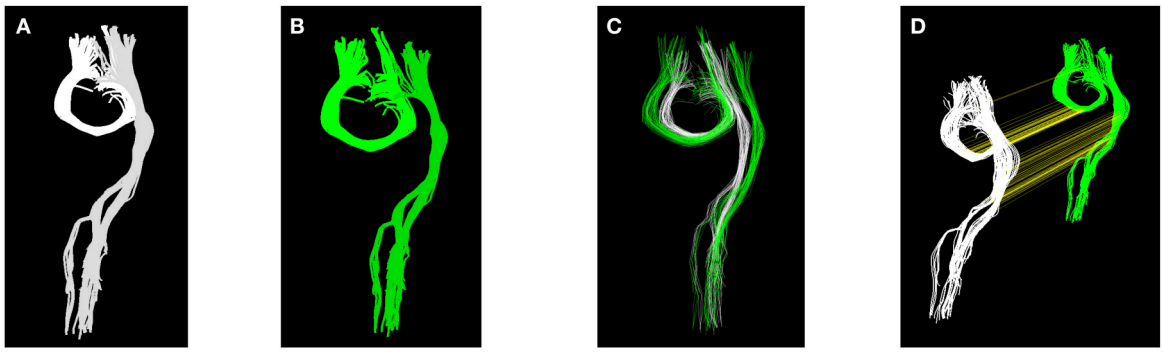

FIGURE 1 | Panels **(A,B)** show two equivalent sets of streamlines, with local differences. Panel **(C)** shows the effect and limits of linear registration of panels **(A,B)**. Panel **(D)** shows the result of the proposed tractogram correspondence, where streamlines of panel **(A)** are connected with a yellow straight line to the corresponding ones of **(B)**.

Alignment based on streamline correspondence provides immediate means to address practical tasks such as bundle segmentation and streamline labeling. Once the label of a streamline is known in one subject, then such label can be directly assigned to the corresponding streamline in the tractogram of the other subject. In such applications, the interest is in transferring anatomical information to a specific target subject, for example in the context of pre-surgical planning. Notice that this aim is different from, for example, that of constructing atlases, see Durrleman et al. (2011). In that scenario the interest is to find a common model from multiple subjects and, for this reason, none of them can be considered as ground truth.

The algorithmic problem of finding the correspondence between streamlines of different tractograms can be framed as a combinatorial optimization problem. Given a loss function that measures how good such correspondence is, the task is to explore the combinatorial space of all possible correspondences in order to find the one that minimizes such loss. To define the loss function, in this work, we propose to encode each tractogram as a large fully-connected weighted graph, where each node/vertex corresponds to a streamline and the weights of the graph's edges are the distances between streamlines within the same set. Given two tractograms, i.e., two graphs, the original problem of finding the correspondence between two sets of streamlines, can be recast as the problem of finding corresponding nodes/vertices between the two graphs, a famous combinatorial optimization problem called *graph matching*, see Conte et al. (2004). In this work, we provide an operational procedure to compute tractogram alignment based on a recent approximate graph matching algorithm, i.e., the doubly stochastic fixed-point (DSPFP) algorithm.

In the following sections of this paper, we formally present the tractogram correspondence problem and explore its similarity to the graph matching problem (see Section 2), from whose literature we draw the actual algorithm adopted in our experiments. In Section 3, on dMRI data from the Human Connectome Project (HCP) dataset, see Sotiropoulos et al. (2013), we show the efficacy of tractogram correspondence, where it achieves much better alignment across subjects than standard affine-based global registration and comparable, if not better, results to non-linear voxel-based methods. We conclude this work by discussing the merits and limitations of the proposed method and by mentioning future work.

2. METHODS

In this section, we first introduce the basic terminology and notation. Then we describe the details of tractogram correspondence in general and its implementation based on relational information. We proceed to describe the strong similarity with the problem of graph matching in order to adopt an efficient approximate solution from its literature, i.e., the DSPFP algorithm.

Let $s = [\mathbf{x}_1, \ldots, \mathbf{x}_{n_s}]$, $\mathbf{x}_i \in \mathbb{R}^3$, be a *streamline* (or track, or fiber), i.e., a polyline made of a sequence of n_s points in 3D space. Let $T = \{s_1, \ldots, s_N\}$ be a *tractogram* (or track set) of the whole brain and $t \subset T$ a *tract* (or bundle). Let $d : T \times T \mapsto \mathbb{R}^+$ be a distance function between streamlines. Several anatomically meaningful distances have been proposed in the literature, based on the idea that streamlines with similar path and shape belong to the same anatomical structure, see Gerig et al. (2004), Corouge et al. (2004), Zhang et al. (2008), and Jiao et al. (2010). In this work we use the commonly adopted mean average minimum (MAM) distance, a modified Hausdorff distance sometimes called also mean closest point distance (see Corouge et al., 2004):

$$d_{MAM}(s, s') = \frac{1}{2}(D(s, s') + D(s', s)) \tag{1}$$

where $D(s, s') = \frac{1}{n_s}\sum_{i=1}^{n_s} d(\mathbf{x}_i, s')$, and $d(\mathbf{x}, s') = \min_{j=1,\ldots,n_{s'}} ||\mathbf{x} - \mathbf{x}'_j||_2$. Other distances can be used without changes to the procedure we propose here.

Let $G = (V, E, f)$ be a fully-connected undirected edge-weighted graph, made of a finite set of vertices V, the corresponding set of edges E, and a weighting function $f : E \mapsto \mathbb{R}$. We represent the tractogram T with the graph G: each vertex of

G correspond[2] to one streamline of T and the weight of each edge is the distance between the related streamlines, i.e., $G = (id(T), E, d)$, where $id(s_i) = i$, $id(T) = \{id(s_1), \ldots, id(s_N)\}$, $E \subseteq id(T) \times id(T)$ and $f((i,j)) = d(s_i, s_j)$. Two different tractograms T_A and T_B are then represented by two different graphs, G_A and G_B. We denote as $A \in \mathbb{R}^{N_A \times N_A}$ and $B \in \mathbb{R}^{N_B \times N_B}$ the adjacency matrices of the weighted graphs G_A and G_B, respectively. Given a matrix A, we call a_{ij} the corresponding element at row i and column j.

2.1. Tractogram Alignment As Tractograms Correspondence

We cast the problem of aligning two tractograms, T_A and T_B, as the problem of finding the corresponding streamlines between them. Once such correspondence has been established, T_A will be aligned to T_B by transforming each streamline $s^A \in T_A$ into the corresponding streamline $s^B \in T_B$, as if to perfectly match it. Notice that such transformation is not explicit, i.e., no deformation field is computed. Knowing s^B, i.e., knowing its coordinates, is enough obtain the aligned s^A.

In order to solve the correspondence problem, we define the binary matrix $Q = [q_{ik}]_{ik} \in \{0,1\}^{N_B \times N_A}$, that we call *correspondence matrix*, such that q_{ik} is 1 when streamline i of T_A corresponds to streamline k of T_B and 0 otherwise. We require that $\sum_k q_{ik} = 1$, i.e., each streamline in T_A must have a corresponding one in T_B, while the contrary is not necessarily true. This last case, for example, occurs when $N_A \neq N_B$, i.e., when the one-to-one correspondence cannot be made. In particular, when $N_A > N_B$ multiple streamlines of T_A may correspond to the same streamline of T_B.

In the meanwhile, we notice that the discrete space on which the loss function needs to be minimized is extremely large, i.e., there are $N_B^{N_A}$ different possible correspondences. Given the typical size of tractograms, in the order of 10^5 streamlines, it is apparent that the combinatorial optimization problem is extremely hard to solve and that approximations should be introduced (see Section 2.4).

2.2. Correspondence Based on Relational Information

Finding the best correspondence between two tractograms requires two ingredients: the definition of a loss function, i.e., a function that scores the correspondence, and the exploration of the combinatorial space in order to actually find the best correspondence. Notice that the definition of a loss function for tractogram correspondence should not be based on the direct distance between streamlines across different tractograms, because such distance becomes anatomical meaningful only *after* the alignment is done. For this reason, as the building block of the loss function, we propose that two streamlines of different tractograms should correspond when their respective set of distances, with other streamlines in their own tractograms, are similar. This idea is motivated by our results in Olivetti et al. (2012), where it was shown that representing a streamline as the set of distances from the other streamlines in its own tractogram is indeed an accurate Euclidean embedding, i.e., the geometrical information of the streamlines is preserved.

Formally, if Q is a correspondence matrix of T_A to T_B, then the matrix $QAQ^\top \in \mathbb{R}^{N_B \times N_B}$ represents A after applying such correspondence. To better understand this step, consider that, in the special case where $N_A = N_B$ and Q is a one-to-one correspondence, then Q is a permutation matrix and $QAQ^\top$ is a matrix where rows and columns are obtained just by permuting those of A according to Q. As a consequence, a meaningful definition of distance, i.e., loss L, between T_A and T_B is the matrix distance (Frobenius norm, $||\cdot||_F$) between the mapped A and B: $L = ||B - QAQ^\top||_F^2$. Then, the problem of finding the best possible correspondence Q^* between T_A and T_B becomes the combinatorial optimization problem

$$Q^* = \underset{Q \in \mathcal{Q}}{\operatorname{argmin}} ||B - QAQ^\top||_F^2 \tag{2}$$

where $\mathcal{Q}$ is the space of all possible correspondences. As noted before, $\mathcal{Q}$ is extremely large and, clearly, this problem is extremely hard to solve. In the following, we describe its similarity with another combinatorial optimization problem, i.e., graph matching, in order to draw approximate solutions from its literature.

2.3. Graph Matching

A combinatorial optimization problem, that is strongly related to the tractogram correspondence problem, is *graph matching* (GM) (see Conte et al., 2004; Zaslavskiy et al., 2009). The GM problem aims at finding the corresponding vertices in two graphs, G_A and G_B, of equal size, with adjacency matrices A and B. Differently from the correspondence of streamlines described in Section 2.2, the correspondence of GM is a one-to-one (bijection). Formally, the GM problem is formulated as

$$P^* = \underset{P \in \mathcal{P}}{\operatorname{argmin}} ||A - PBP^\top||_F^2 \tag{3}$$

which is very similar[3] to the correspondence problem of Equation (2). Specifically, when the correspondence between streamlines is a permutation of indices, then the matrix Q is a permutation matrix and the correspondence problem of Equation (2) becomes identical to the graph matching problem of Equation (3): $||A - PBP^\top||_F^2 = ||B - QAQ^\top||_F^2$ when $P = Q$, so $Q^* = P^*$.

When the two graphs have different sizes, the GM problem is called *sub-graph matching* (sub-GM) problem and the goal is to find the corresponding vertices from the small graph to the large graph. The GM and sub-GM problems are known to be NP-hard (Conte et al., 2004), in general, and only approximate solutions can be obtained in most of the practical cases, i.e., when the number of vertices is more than twenty. Notice that a matching P can also be considered a correspondence, i.e., $P \in \mathcal{P} \subseteq \mathcal{Q}$. For this reason, an approximate solution of GM is also an approximate solution of the correspondence problem.

[2]Technically, each vertex is an object whose property is the identifier of the streamline to which it is associated.

[3]Historically, the GM problem refers to finding the vertices of G_B that match those of G_A, and not the contrary, which is the natural way to formulate the alignment problem.

2.4. Graph Matching: Approximate Solutions

Finding good approximate solutions to the GM and sub-GM problems is a difficult task with extensive literature. The main solutions available are divided in two groups (Zaslavskiy et al., 2009): the first group operates on spectral representations of the adjacency matrices (see for example Umeyama, 1988). The second group is based on relaxation methods (see for example Zaslavskiy et al., 2009), i.e., on solving the optimization problem on a continuous superset of $\mathcal{P}$, where more efficient continuous optimization techniques can be used, and then by projecting the result back to $\mathcal{P}$. To the best of our knowledge, the computational time and space complexity of the most efficient algorithms[4] for sub-GM are, respectively, $\mathcal{O}(n^3)$/iteration and $\mathcal{O}(n^2)$, reached only by the following algorithms (see Zaslavskiy et al., 2009; Lu et al., 2016): projected gradient, graduated assignment, PATH, and DSPFP. With such computational complexity, approximate solutions can be found for graphs with several thousands of vertices. To scale-up to larger graphs, it is necessary to derive methods with lower complexity per iteration or to introduce assumptions on the structure of the data.

According to Lu et al. (2016) and to our tests, the DSPFP algorithm outperforms others algorithms in terms of actual time and memory requirements, moreover with higher quality of the approximated solution. For this reason we adopted that algorithm for the experiments of Section 3. In the following we briefly review DSPFP. For a comprehensive description see Lu et al. (2016).

2.5. The Doubly Stochastic Projected Fixed-Point (DSPFP) Algorithm

The DSPFP algorithm provides an approximate solution to the GM and sub-GM problems. In its original formulation (see Lu et al., 2016), the algorithm accounts for the similarity between both the weights of corresponding edges and the attributes of corresponding vertices. For sake of simplicity, here we omit the part pertaining vertex attributes, since it does not play a role in the proposed application of tractogram alignment[5]. In the following we report the main steps to describe DSPFP.

The minimization problem of Equation (3) can be recast as the maximization problem

$$P^* = \underset{X}{\operatorname{argmax}} \frac{1}{2} tr(X^\top A X^\top B) \qquad (4)$$
$$\text{s.t.} \quad X\mathbf{1} = \mathbf{1}, X^\top \mathbf{1} = \mathbf{1}, x_{ij} \in \{0,1\}$$

see for example Lu et al. (2016), Appendix A, for the complete derivation of Equation (4). By relaxing the constraint that $x_{ij} \in \{0,1\}$ into $x_{ij} \geq 0$, the original discrete space of the partial permutation matrices becomes the continuous one of doubly stochastic matrices. The quadratic maximization problem on this continuous space can be addressed by means of the projected fixed-point method, which is iterative:

$$X^{t+1} = (1-\alpha)X^t + \alpha \Pi(\nabla f(X^t)) \qquad (5)$$

where α is the step size, $\Pi(\cdot)$ is the doubly stochastic projection, $f(X)$ is the target function to be maximized, i.e., $f(X) = \frac{1}{2} tr(X^\top A X^\top B)$, so $\nabla f(X) = AXB$. The projection method adopted in DSPFP is based on a recent closed-form solution of doubly stochastic projection, proposed in Zass and Shashua (2006), which is solved by iterating two successive projections until convergence: $\Pi(X) = \ldots \Pi_2 \Pi_1 \Pi_2 \Pi_1 (X)$, where[6]:

$$\Pi_1(X) = X + \left(\frac{1}{N_A} I + \frac{\mathbf{1}^\top X \mathbf{1}}{N_A^2} - \frac{1}{N_A} X \right) \mathbf{1}\mathbf{1}^\top - \frac{1}{N_A} \mathbf{1}\mathbf{1}^\top X \qquad (6)$$

and

$$\Pi_2(X) = \frac{X + |X|}{2}. \qquad (7)$$

The resulting procedure is reported in Algorithm 1, where Y is a $N_A \times N_A$ matrix, assuming $N_A \geq N_B$. The initialization of X and Y recommended in Lu et al. (2016) is such that $x_{ij} = 1/(N_A N_B)$ and $y_{ij} = 0, \forall i, j$.

Data: A, B, α
Result: P
Initialize X and Y;
repeat
  $Y_{1:N_A,1:N_B} = AXB$;
  repeat
    $Y = Y + \left(\frac{1}{N_A} I + \frac{\mathbf{1}^\top Y \mathbf{1}}{N_A^2} - \frac{1}{N_A} Y \right) \mathbf{1}\mathbf{1}^\top - \frac{1}{N_A} \mathbf{1}\mathbf{1}^\top Y$;
    $Y = \frac{Y + |Y|}{2}$;
  until Y *converges*;
  $X = (1-\alpha)X + \alpha Y_{1:N_A,1:N_B}$;
  $X = X/max(X)$;
until X *converges*;
Discretize X to obtain P.

Algorithm 1: Doubly Stochastic Projected Fixed-Point (DSPFP), from Lu et al. (2016).

The *discretization* of X, required in the last step of Algorithm 1, is a linear assignment problem, which can be implemented with the Hungarian method or approximated with a faster greedy algorithm for the linear assignment method, such as the one used in Leordeanu and Hebert (2005). This greedy approach comprises the steps described in Algorithm 2.

3. EXPERIMENTS

In this section, we describe the experiments to support the claims about the advantages of tractogram correspondence over registration methods for tractogram alignment. The experiment was conducted on the Human Connectome Project (HCP) dMRI

[4] All these algorithms are iterative, with some sort of convergence criteria.
[5] Technically, this means simply to set to zero the matrix K in all equations in Lu et al. (2016).
[6] $\mathbf{1}$ indicates the vector with all elements equal to one.

Data: X
Result: P
Initialize P as $N_A \times N_B$ zero matrix and L as its set of indices $\{(i,j)\}_{i,j}$;
repeat
  $(i^*, j^*) = \text{argmax}_{(i,j)\in L}\, x_{ij}$;
  $p_{i^*,j^*} = 1$;
  remove from L all pairs (i,j) s.t. $i = i^*$ or $j = j^*$;
until L *is empty*;

Algorithm 2: Greedy algorithm for the linear assignment problem.

dataset, see Van Essen et al. (2013), Sotiropoulos et al. (2013), and Glasser et al. (2013). From that, we extracted data of 10 random subjects, single shell (b = 1000), with the original voxel size (isotropic, 1.25 mm) and 90 gradients. Reconstruction was computed using the constrained spherical deconvolution algorithm (CSD, see Tournier et al., 2007) and tracking was based on the Euler Delta Crossing method (EuDX, see Garyfallidis et al., 2014), with 10^6 seeds. The resulting tractograms consist of approximately 100–140 thousands streamlines, as reported in **Table 1**, third and fourth columns.

In order to quantify the quality of tractogram alignment produced by the methods in the literature and by the proposed one, we relied on measuring the degree of overlap of corresponding anatomical bundles/tracts after whole tractogram alignment (see Golding et al., 2011; Garyfallidis et al., 2015). Since the bundle/tract information is never used to compute alignments, we can safely assume that, the better such overlap, the better the alignment of tractograms. In the following, we provide details of the set of alignment methods used in the comparison and of the procedure to obtain the bundles/tracts. Then we report the results of all experiments.

3.1. Alignment of Tractograms

We aligned all pairs of tractograms obtained from the 10 subjects, i.e., 45 pairs. We compared the following alignment methods: standard affine registration of voxels, affine registration of streamlines, non-linear registration of voxels and the proposed method based on graph matching (GM). Voxel-level affine registration was computed with FSL/FLIRT on the B0 images. Streamline affine registration was computed with two different algorithms: the entropy-based group-wise registration (ENT) algorithm[7] from O'Donnell et al. (2012) and with the streamline linear registration (SLR) algorithm[8] from Garyfallidis et al. (2015). In all cases, affine registration was applied to streamline coordinates using the function `dipy.tracking.streamline.apply_affine()`, from DiPy. Non-linear voxel-level registration was computed with FSL/FNIRT, using the deformation fields directly provided within the HCP dataset[9]. GM-based alignment was computed using the DSPFP algorithm described in Section 2.5 and implemented by us in Python language. Our implementation is available under a Free/OpenSource license at: https://github.com/emanuele/DSPFP.

In order to quantitatively compare the five different whole-tractogram alignment methods we followed the common practice, also described in Garyfallidis et al. (2015) and Golding et al. (2011), i.e., we computed the overlap in voxels of a set of corresponding anatomical tracts after the whole brain alignment is done. Before alignment, we segmented a set of tracts in each tractogram with the white matter query language (WMQL, see Wassermann et al., 2013)[10] and then used the streamline IDs to obtain the tracts on the tractogram after alignment. The set of tracts comprised: Cingulum Bundle (left and right), Inferior Occipito Frontal Fascicle (left and right), Uncinate Fascicle (left and right), Arcuate Fascicle (left), and Corpus Callosum (part 2 and 7). We selected these specific nine tracts because their segmentation, obtained through WMQL, was more consistent across subjects, in terms of number of streamlines, see Supplementary Material for additional details. In Supplementary Material, we extend also this analysis to include further bundles/tracts, which are known to have high variability across subjects. The fraction of overlapping voxels between the tract (t_A^{al}) of the aligned tractogram and the one (t_B) in the target tractogram, usually called Jaccard index J, is then:

$$J = \frac{|v(t_A^{al}) \cap v(t_B)|}{|v(t_B)|} \tag{8}$$

where $v(t)$ indicates the set of voxels crossed by the streamlines of tract t, while $|\cdot|$ is the set size.

3.2. Graph Matching: Further Approximation

As mentioned in Section 2.4, one limitation of the algorithms for approximate graph matching is the high computational cost when the number of nodes exceeds a few thousands. Specifically, for the adopted DSPFP, see **Figure 2** for the exact timing to perform graph matching on sets of streamlines till size 3000. The computational and storage resources necessary to handle the matching of graphs generated from an entire tractogram, i.e., $n = 10^5$ nodes and 10^{10} edges, are beyond the capability of modern computers. For this reason, in order to obtain the correspondence between tractograms, we introduced a further approximation with a simple three-steps procedure, similar to the one proposed for the SLR algorithm in Garyfallidis et al. (2015):

1. We clustered each tractogram into a given number of clusters ($k = 1000$) and defined the median (centroid) streamline as the *representative* for each cluster. We adopted the fast mini-batch k-means algorithm described in Olivetti et al. (2013) and Porro-Muñoz et al. (2015).
2. We computed graph matching between the two graphs made only with the k representatives, in order to obtain corresponding clusters.

[7] We adopted the software implementation provided by the authors of ENT, available at: https://github.com/ljod/whitematteranalysis.

[8] As implemented in DiPy, http://nipy.org/dipy.

[9] The estimation of the deformation fields of the HCP dataset is described in Glasser et al. (2013) in the following way: "After bias field correction of the T1w and T2w images, the T1w image is registered to MNI space with a FLIRT 12 DOF affine and then a FNIRT non-linear registration, producing the final non-linear volume transformation from the subject's native volume space to MNI space."

[10] According to the white matter parcellation provided by the HCP initiative.

TABLE 1 | All results of tractograms alignment with FLIRT, ENT, SLR, FNIRT, and the proposed GM across all pairs of subjects.

ID subj.A	ID subj.B	$\|T_A\|$	$\|T_B\|$	J_{FLIRT}	J_{ENT}	J_{SLR}	J_{FNIRT}	J_{GM}
100307	124422	117354	107891	0.26	0.27	0.26	0.43	**0.59**
	161731	117354	105490	0.33	0.32	0.36	0.44	**0.64**
	199655	117354	134759	0.21	0.24	0.25	0.44	**0.62**
	201111	117354	145364	0.18	0.19	0.18	0.45	**0.51**
	239944	117354	116598	0.22	0.23	0.23	0.47	**0.63**
	245333	117354	106215	0.22	0.20	0.24	0.45	**0.62**
	366446	117354	138380	0.19	0.21	0.20	0.47	**0.61**
	528446	117354	123856	0.16	0.10	0.25	0.44	**0.53**
	856766	117354	116532	0.25	0.26	0.27	0.45	**0.59**
124422	161731	107891	105490	0.28	0.27	0.28	0.42	**0.56**
	199655	107891	134759	0.19	0.20	0.21	0.41	**0.46**
	201111	107891	145364	0.21	0.20	0.21	0.44	**0.54**
	239944	107891	116598	0.26	0.19	0.26	0.45	**0.56**
	245333	107891	106215	0.26	0.28	0.29	0.44	**0.54**
	366446	107891	138380	0.19	0.17	0.24	0.44	**0.59**
	528446	107891	123856	0.19	0.17	0.27	0.44	**0.55**
	856766	107891	116532	0.24	0.23	0.25	0.42	**0.60**
161731	199655	105490	134759	0.17	0.21	0.24	0.41	**0.53**
	201111	105490	145364	0.14	0.17	0.19	0.43	**0.48**
	239944	105490	116598	0.23	0.24	0.24	0.42	**0.58**
	245333	105490	106215	0.28	0.27	0.29	0.45	**0.57**
	366446	105490	138380	0.16	0.11	0.20	**0.45**	0.43
	528446	105490	123856	0.18	0.24	0.27	0.44	**0.54**
	856766	105490	116532	0.23	0.22	0.27	0.44	**0.58**
199655	201111	134759	145364	0.25	0.25	0.23	0.43	**0.57**
	239944	134759	116598	0.23	0.17	0.30	0.42	**0.65**
	245333	134759	106215	0.18	0.10	0.26	0.44	**0.58**
	366446	134759	138380	0.30	0.28	0.30	0.43	**0.62**
	528446	134759	123856	0.26	0.30	0.30	0.43	**0.58**
	856766	134759	116532	0.25	0.22	0.27	0.40	**0.63**
201111	239944	145364	116598	0.25	0.29	0.27	0.41	**0.58**
	245333	145364	106215	0.20	0.25	0.27	0.44	**0.57**
	366446	145364	138380	0.33	0.35	0.33	0.44	**0.64**
	528446	145364	123856	0.29	0.10	0.31	0.43	**0.58**
	856766	145364	116532	0.27	0.28	0.28	0.42	**0.54**
239944	245333	116598	106215	0.24	0.23	0.24	0.42	**0.53**
	366446	116598	138380	0.21	0.22	0.25	0.40	**0.57**
	528446	116598	123856	0.17	0.22	0.24	0.39	**0.47**
	856766	116598	116532	0.20	0.17	0.24	0.41	**0.58**
245333	366446	106215	138380	0.14	0.23	0.22	0.41	**0.54**
	528446	106215	123856	0.17	0.25	0.24	0.44	**0.60**
	856766	106215	116532	0.20	0.25	0.26	0.41	**0.55**
366446	528446	138380	123856	0.29	0.28	0.32	0.45	**0.54**
	856766	138380	116532	0.27	0.23	0.28	0.44	**0.62**
528446	856766	123856	116532	0.22	0.19	0.27	0.45	**0.61**
average over all 45 pairs				0.23	0.22	0.26	0.43	**0.57**
standard dev. over all 45 pairs				±0.05	±0.06	±0.03	±0.02	±0.05

In each row are indicated the pairs of subjects IDs, the size of the two tractograms and the five degrees of overlap after alignment,in terms of Jaccard index (J), averaged over nine tracts. The averages and standard deviations over all 45 pairs are reported in the last row.

This table reports the results of the comparison of five different methods across multiple pairs of subjects. In each row, the score of each of the five methods is reported: J_{FLIRT}, J_{ENT}, J_{SLR}, J_{FNIRT}, J_{GM}. In each row, the higher the value, the better. The number in bold face is the highest value among the five values in the same row, i.e., it indicates the best method for each pair of subjects [highest overlap score (J) for each pair of subjects].

3. For each pair of corresponding clusters, we computed the graph matching between their streamlines, in order to find streamline correspondence.

Notice that, in all cases, approximate graph matching was computed with the DSPFP algorithm (see Section 2.5), with random initialization, i.e., $x_{ij} \sim U[0, 1]$. This is different from the initialization recommended in Lu et al. (2016), i.e., $x_{ij} = 1/(N_A N_B)$, but we observed failure of convergence in a few cases with such constant value, while random initialization always converged. We also tried the initialization resulting from an initial affine registration (based on SLR) and we obtained very similar results. For generality of the proposed method, we prefer to recommend random initialization.

The steps introduced above aim at simplifying the original tractograms, in order to reduce the computational problem of graph matching. Other choices can be made, for example using different clustering algorithms, see for example Garyfallidis et al. (2012), or recent specific methods for tractogram simplification, like Gori et al. (2016). The motivation of our choice, for adopting the algorithm described in Olivetti et al. (2013), is eminently computational. The time required to carry out the simplification, which is in the order of a couple of minutes, see **Figure 2**, is substantially inferior to that of other algorithms in the literature.

3.3. Results

Performing the three-steps procedure required approximately 30 min of computation for each pair of tractograms on a standard desktop computer. In **Figure 2**, we report the time to compute mini-batch k-means for streamlines on a full tractogram[11] Linear registration required a few minutes of computation for FLIRT and SLR and approximately 30 min for ENT. FNIRT deformation fields were already available within the HCP dataset, anyway they usually require a few minutes of computation.

Table 1 shows the results of all 45 pairs across the five different alignment methods, averaged over nine tracts. The

[11] reproducing the results in Olivetti et al. (2013). and the time for DSPFP, for various k.

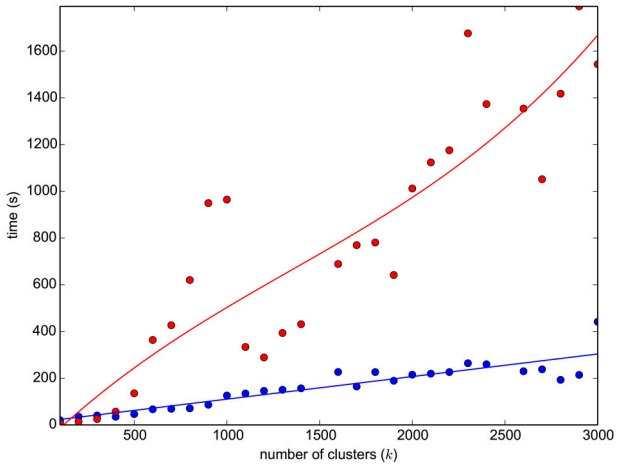

FIGURE 2 | The graph reports the time required to simplify a 110K-streamlines tractogram (HCP subject ID:100307) with the mini-batch *k*-means (blue dots, plus linear interpolation), as a function of the number of clusters. It reports also the time required to run graph matching (DSPFP, red dots, plus cubic interpolation) between two simplified graphs, each of *k* streamlines/vertices, of two subjects (HCP ID1:100307, ID2:124422).

first two columns report the HCP subject identifiers of the two tractograms considered in the alignment. The third and fourth columns report the size of the tractograms of the two subjects in terms of number of streamlines. The remaining five columns report the degree of overlap between the aligned tractograms (J, higher is better), averaged over the NINE tracts considered, for the five methods considered in the comparison: FLIRT, ENT, SLR, FNIRT, and GM. For each pair of subjects, the highest degree of overlap is indicated in bold face. In order to avoid unreasonable outliers, we filtered out the cases for which the difference in number of streamlines for the same tract was extreme, i.e., $>$ 60%, denoting problems in the WMQL segmentation. See Supplementary Material for an analysis of this issue.

Figure 3 reports a visual aggregated summary of the results of the experiments. In the upper graph, for each subject, five barplots are reported. Each barplot indicates the overlap of tractograms after alignment (J, higher is better) averaged over the nine pairs that include that subject and all nine tracts. The graph in the lower part of **Figure 3** shows the results for each tract, where the overlap for each of the five methods in the comparison is averaged over the 45 pairs of subjects.

In order to show the performance of the proposed method, with respect to the difference between the same bundle in two different subjects, in **Figure 4** we report the quality of alignment (J_{GM}) as a function of the difference between $|t_A|$ and $|t_B|$, where $|t|$ is the number of streamlines of tract/bundle t. Such difference is quantified as: $\Delta_{AB} = \frac{||t_A|-|t_B||}{max(|t_A|,|t_B|)}$, which is 0 for bundles with the same number of streamlines and increases up to one according to how much the two sizes differ. Each point represents one tract for one pair of subjects, e.g., Cingulum left for the pair HCP ID:100307 and HCP ID:124422. Thus, there are $45 \times 9 = 405$ points in total. In Supplementary Material we report the equivalent graphs for the other alignment methods in the comparison.

In **Figure 5** we show one paradigmatic example where there is a systematic displacement between the corresponding tracts (Corpus Callosum, Section 7, as defined by the WMQL) of two subjects (HCP ID1: 100307, ID2: 199655) after whole-brain affine registration. In white and green we show the two tracts after the registration computed with FSL/FLIRT, ENT, and SLR[12]. In the same figure, we also report the alignment computed with GM, which shows a much superior match because GM acts also at the local level. For this specific example, the fractions of overlapping voxels for that tract are: $J_{FLIRT} = 0.18$, $J_{ENT} = 0.26$, $J_{SLR} = 0.24$, $J_{FNIRT} = 0.52$, and $J_{GM} = 0.81$.

3.4. A Technical Comment About ENT

As reported in the last row of **Table 1**, we noticed that the ENT algorithm, from O'Donnell et al. (2012), exhibited substantially higher variance in the results with respect to other algorithms and in particular with respect to the SLR algorithm, which is the most similar one. We explored this issue and, from preliminary experiments, we believe that such increased variance is mainly due to the way in which the tractograms are simplified, in order to reduce the amount of computation. In ENT, a random subsample of streamlines for each tractogram is used, while in SLR the subsample is the set of representatives of the clusters. The random subsample of ENT is of 20000 streamlines[13] and then it is repeatedly reduced within that algorithm. Conversely, SLR registration is based on 2000–3000 representatives, see Garyfallidis et al. (2015). Additionally, ENT is optimized for the joint alignment of multiple subjects. All these facts contributes to the explanation of the observed increased variance[14].

4. DISCUSSION AND CONCLUSIONS

In this work, we present whole brain tractogram alignment based on computing streamline correspondence across subjects as a graph matching problem. This work is the first one that presents a quantitative comparison across streamline-based alignment methods for tractograms. **Table 1** and **Figure 3** clearly show that tractogram correspondence, implemented as graph matching (GM), is able to align tractograms much better than what global affine registration can do, both voxel-based and streamline-based. The overlap, in terms of voxels, of the aligned tracts with respect to the target tracts is two times better with the proposed method than with affine methods. This occurs uniformly across all subjects and all tracts. We also notice that, as expected, all the affine-based registration methods exhibit comparable results between each other, within the reported standard deviations, meaning that there is an inherent limitation

[12]FSL/FNIRT is missing from this visual example because we did not apply the resulting deformation field to the streamlines: such procedure is not sufficiently analyzed in the literature. Nevertheless, we report the quantitative results at voxel-level.

[13]According to the guidelines in https://github.com/ljod/whitematteranalysis.

[14]We thank Reviewer 2 for insightful comments on this part.

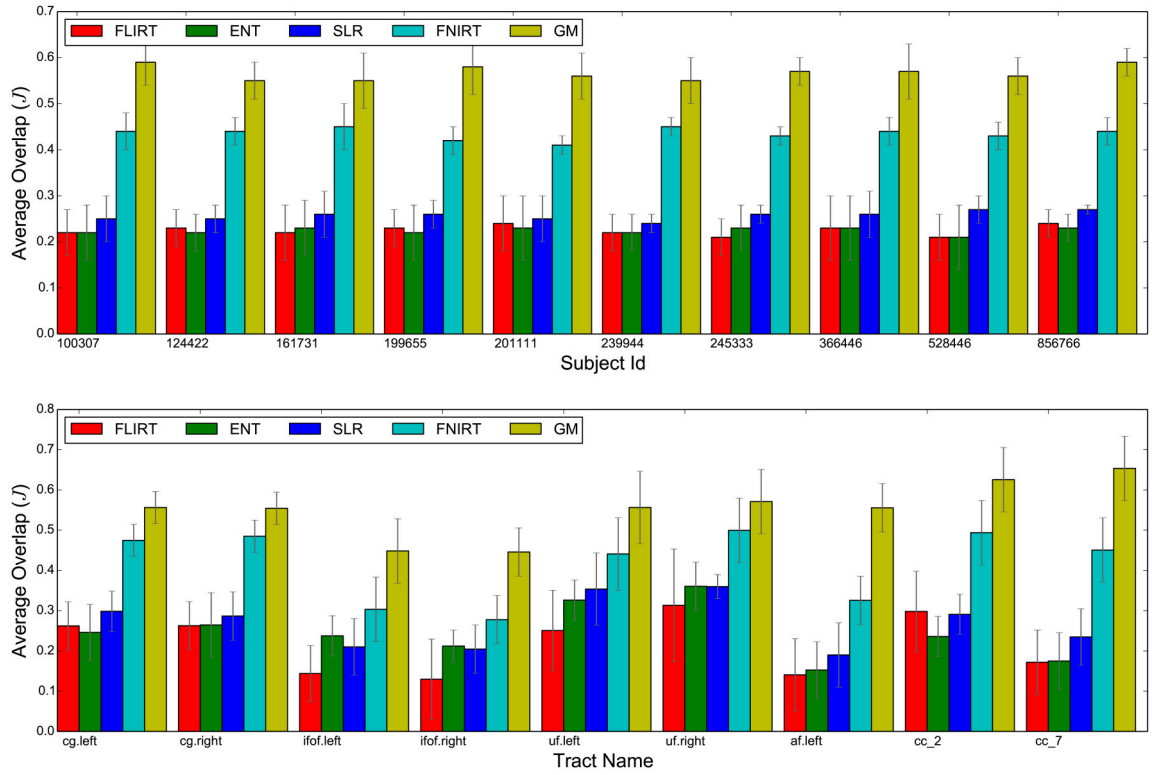

FIGURE 3 | Summary of the results: average overlap between corresponding tracts after whole brain alignment for the FLIRT, ENT, SLR, FNIRT, and the proposed GM. The upper bar-graph shows the overlap for each subject averaged over all nine tracts and the remaining nine subjects. The lower bar graph shows the overlap for each tract averaged over all pairs of subjects.

in affine transformations, irrespective of the loss function they optimize.

Such a positive result for GM against affine methods is not surprising, because it is expected that one global linear transformation cannot reconcile local systematic differences between white matter bundles across subjects. Differently, GM is designed to optimize the match both at the global and local level. This aspect is clearly exemplified in **Figure 5**, where some notable displacement between the tracts remains after global affine alignment, but not in the case of GM. The locality of GM and, more in general, of the correspondence-based alignment, act as if each streamline in one tractogram is deformed to exactly match the corresponding streamline in the other tractogram. This corresponds to a different deformation for each streamline. The global aspect is also preserved because GM is a joint optimization problem across all vertices/streamlines.

The results in **Table 1** show also the quality of alignment obtained through non-linear registration of volumes, by means of FSL/FNIRT (eighth column). Since non-linear registration is able to operate local changes, the quality of such alignment is much better than that of linear methods, as expected. By comparing the results of GM and FNIRT, we observe that the quality of GM is still superior, i.e., $J_{FNIRT} = 0.43 \pm 0.02$ vs. $J_{GM} = 0.57 \pm 0.05$, even though not by a large margin. Our interpretation of this result is that FNIRT optimized the match of the T1 images, which contain white matter boundaries but not the detailed structure, while our GM-based alignment procedure optimized the match of streamlines. Since the evaluation is based on corresponding anatomical white matter tracts, our proposed method has an advantage, that may explain part of difference in the results. It is true that non-linear volumes-based alignment can target other kinds of volumes that incorporates dMRI information, like FA (fractional anisotropy) or B0. For this reason, further experiments are needed in order explore this comparison. Nevertheless, a main difference remain: the proposed method operates on streamlines, which is the focus of this paper, while the non-linear volume-based algorithms, like FNIRT, operate on voxel-level information.

The quality of whole brain alignment provided by GM is expected to decrease when the difference in number of streamlines between corresponding bundles is large. In **Figure 4**, the trend line shows this expected decay, at the level of individual pairs of bundles. Nevertheless we can also expect that, given one bundle, large differences do not occur between all pairs of subjects. This is confirmed in **Figure 3** (lower part), where standard deviations are moderate. This is further confirmed in Supplementary Materials, where the result is extended to SLF II (right) and MDLF (right and left), which are known to be highly variable across subjects. Nevertheless, we have also to take into account the limitations of the ground

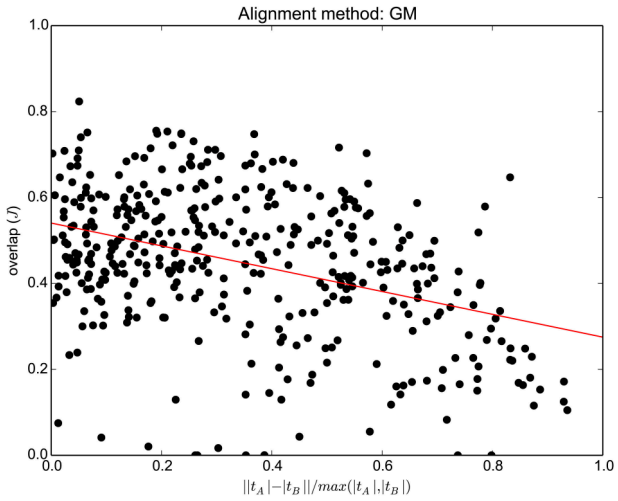

FIGURE 4 | For each of the 45 pairs of subjects and 9 tracts/bundles (45 × 9 = 405 points in total), the graph shows the tract overlap after whole tractogram alignment performed with GM, as a function of the difference between that tract across the two subjects. The difference, in number of streamlines, is quantified as $\Delta_{AB} = \frac{||t_A|-|t_B||}{max(|t_A|,|t_B|)}$.

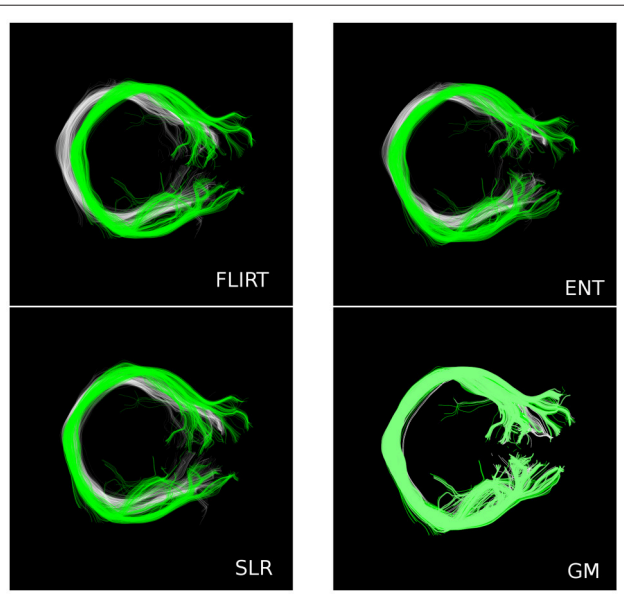

FIGURE 5 | A paradigmatic example where there is systematic displacement between the corresponding tract (CC, Section 7) of two subjects after whole-brain affine registration, with FSL/FLIRT, ENT and SLR. Conversely, GM is able to provide much better alignment.

truth used in this study, which is based on automatic bundle segmentation, see Wassermann et al. (2013). The limitations of such segmentation are explored in Supplementary Materials and may contribute to the variability of the results observed in **Figure 4**. The use of expert-based segmentation might partly mitigate this problem.

The proposed GM algorithm, despite multiple approximations, can recover a substantial portion of what other methods miss. It has to be noted that this improvement comes at the cost of a substantial increase in the time of computation, at least with respect to FLIRT, SLR, and FNIRT. The time required by the proposed implementation of the GM-based algorithm is ten times more than that required by these algorithms. The total amount of time required by the proposed method is a function of the number of clusters (k) chosen during the clustering-based approximation, as illustrated in **Figure 2**. Specifically, it is composed by the time to obtain the clustering, the time to compute the graph matching between cluster representatives and the time for graph matching between the streamlines of corresponding clusters. Notice that the proposed clustering-based approximation could be used for addressing the scalability issues of other algorithms, such as the one of Durrleman et al. (2011). Future work has to be done in this direction.

Despite clearly positive results, the solution proposed in this work suffers various limitations, that provide ground for interesting future work. At a general level, the idea of putting in correspondence streamlines across tractograms may be limited by the quality of the tractography algorithms, topic on which there is still major debate. Moreover, finding the correspondence for *all* streamlines across tractograms may be challenged because, for example, artifactual streamlines should not have a corresponding one. A filtering mechanism to avoid such cases is currently not available. In the same way, at the implementation level, the sub-optimal constraint of one-to-one correspondence of GM may be excessive in some cases. Future work should address the relaxation of such constraint. At the application level, aligning tractograms for transferring anatomical knowledge to a new subject, e.g., for segmentation of bundles, is the straightforward application of the proposed method. Despite the usefulness of such task, it is still not clear how to address other common tasks, like alignment at the group-level and atlas construction, on which we are focusing our future work. From this point of view, the idea of exploiting the correspondence between streamlines opens up new directions of research and opportunities for improvement in neuroscientific and clinical applications.

AUTHOR CONTRIBUTIONS

EO conceived the ideas, designed the experiments, conducted the experiments, and wrote the manuscript. NS contributed to the design of the experiments, conducted the experiments, and contributed to the manuscript. PA contributed to the ideas and to the manuscript.

ACKNOWLEDGMENTS

The research was funded by the Autonomous Province of Trento, Call "Grandi Progetti 2012," project "Characterizing and improving brain mechanisms of attention - ATTEND." Data was provided (in part) by the Human Connectome Project, WU-Minn Consortium (Principal Investigators:

David Van Essen and Kamil Ugurbil; 1U54MH091657) funded by the 16 NIH Institutes and Centers that support the NIH Blueprint for Neuroscience Research; and by the McDonnell Center for Systems Neuroscience at Washington University.

SUPPLEMENTARY MATERIAL

The Supplementary Material for this article can be found online at: http://journal.frontiersin.org/article/10.3389/fnins.2016.00554/full#supplementary-material

REFERENCES

Basser, P. J., Mattiello, J., and LeBihan, D. (1994). MR diffusion tensor spectroscopy and imaging. *Biophys. J.* 66, 259–267. doi: 10.1016/S0006-3495(94)80775-1

Christiaens, D., Dhollander, T., Maes, F., Sunaert, S., and Suetens, P. (2012). "The effect of reorientation of the fibre orientation distribution on fibre tracking," in *MICCAI 2012 Workshop on Computational Diffusion MRI* (Nice).

Christiaens, D., Dhollander, T., Maes, F., Sunaert, S., and Suetens, P. (2014). "Groupwise deformable registration of fiber track sets using track orientation distributions," in *Computational Diffusion MRI and Brain Connectivity, Mathematics and Visualization*, eds T. Schultz, G. Nedjati-Gilani, A. Venkataraman, L. O'Donnell, and E. Panagiotaki (Nagoya: Springer International Publishing), 151–161.

Conte, D., Foggia, P., Sansone, C., and Vento, M. (2004). Thirty years of graph matching in pattern recognition. *Int. J. Patt. Recogn. Artif. Intell.* 18, 265–298. doi: 10.1142/S0218001404003228

Corouge, I., Gouttard, S., and Gerig, G. (2004). "Towards a shape model of white matter fiber bundles using diffusion tensor MRI," in *IEEE International Symposium on Biomedical Imaging: Nano to Macro, 2004*, Vol. 1 (Arlington, VA: IEEE), 344–347. doi: 10.1109/isbi.2004.1398545

Durrleman, S., Fillard, P., Pennec, X., Trouvé, A., and Ayache, N. (2011). Registration, atlas estimation and variability analysis of white matter fiber bundles modeled as currents. *Neuroimage* 55, 1073–1090. doi: 10.1016/j.neuroimage.2010.11.056

Garyfallidis, E., Brett, M., Amirbekian, B., Rokem, A., van der Walt, S., Descoteaux, M., et al. (2014). Dipy, a library for the analysis of diffusion MRI data. *Front. Neuroinform.* 8:8. doi: 10.3389/fninf.2014.00008

Garyfallidis, E., Brett, M., Correia, M. M., Williams, G. B., and Nimmo-Smith, I. (2012). QuickBundles, a method for tractography simplification. *Front. Neurosci.* 6:175. doi: 10.3389/fnins.2012.00175

Garyfallidis, E., Ocegueda, O., Wassermann, D., and Descoteaux, M. (2015). Robust and efficient linear registration of white-matter fascicles in the space of streamlines. *Neuroimage* 117, 124–140. doi: 10.1016/j.neuroimage.2015.05.016

Gerig, G., Gouttard, S., and Corouge, I. (2004). "Analysis of brain white matter via fiber tract modeling," in *The 26th Annual International Conference of the IEEE Engineering in Medicine and Biology Society*, Vol. 2 (IEEE), 4421–4424. doi: 10.1109/IEMBS.2004.1404229

Glasser, M. F., Sotiropoulos, S. N., Wilson, J. A., Coalson, T. S., Fischl, B., Andersson, J. L., et al. (2013). The minimal preprocessing pipelines for the human connectome project. *Neuroimage* 80, 105–124. doi: 10.1016/j.neuroimage.2013.04.127

Golding, D., Tittgemeyer, M., Anwander, A., and Douglas, T. (2011). "A comparison of methods for the registration of tractographic fibre images," in *Proceedings of the Twenty-Second Annual Symposium of the Pattern Recognition Association of South Africa*, eds P. Robinson and A. Nel (Vanderbijlpark), 55–59.

Gori, P., Colliot, O., Marrakchi-Kacem, L., Worbe, Y., De Vico Fallani, F., Chavez, M., et al. (2016). Parsimonious approximation of streamline trajectories in white matter fiber bundles. *IEEE Trans. Med. Imaging.* doi: 10.1109/tmi.2016.2591080. [Epub ahead of print].

Guevara, P., Duclap, D., Poupon, C., Marrakchi-Kacem, L., Fillard, P., Le Bihan, D., et al. (2012). Automatic fiber bundle segmentation in massive tractography datasets using a multi-subject bundle atlas. *Neuroimage* 61, 1083–1099. doi: 10.1016/j.neuroimage.2012.02.071

Jenkinson, M., Bannister, P., Brady, M., and Smith, S. (2002). Improved optimization for the Robust and accurate linear registration and motion correction of brain images. *Neuroimage* 17, 825–841. doi: 10.1006/nimg.2002.1132

Jiao, F., Phillips, J., Stinstra, J., Krger, J., Varma, R., Hsu, E., et al. (2010). "Metrics for uncertainty analysis and visualization of diffusion tensor images," in *Medical Imaging and Augmented Reality, Vol. 6326, Lecture Notes in Computer Science*, eds H. Liao, Edwards, X. Pan, Y. Fan, and G.-Z. Yang (Berlin; Heidelberg: Springer), 179–190. doi: 10.1007/978-3-642-15699-1_19

Leordeanu, M., and Hebert, M. (2005). "A spectral technique for correspondence problems using pairwise constraints," in *International Conference on Computer Vision* (Beijing: IEEE). doi: 10.1109/iccv.2005.20

Lu, Y., Huang, K., and Liu, C.-L. (2016). A fast projected fixed-point algorithm for large graph matching. *Pattern Recognit*. 60, 971–982. doi: 10.1016/j.patcog.2016.07.015

Maddah, M., Mewes, A. U. J., Haker, S., Grimson, and Warfield, S. K. (2005). "Automated atlas-based clustering of white matter fiber tracts from DTMRI," in *Medical Image Computing and Computer-Assisted Intervention MICCAI 2005*, Vol. 3749 *Lecture Notes in Computer Science*, Chapter 24, eds J. S. Duncan and G. Gerig (Berlin; Heidelberg; Palm Springs, CA: Springer), 188–195.

O'Donnell, L. J., Wells, W. M. III., Golby, A. J., and Westin, C.-F. F. (2012). Unbiased groupwise registration of white matter tractography. *Med. Image Comput. Comput. Assist. Interv.* 15(Pt 3), 123–130. doi: 10.1007/978-3-642-33454-2

O'Donnell, L. J., and Westin, C.-F. F. (2007). Automatic tractography segmentation using a high-dimensional white matter atlas. *IEEE Trans. Med. Imaging* 26, 1562–1575. doi: 10.1109/TMI.2007.906785

Olivetti, E., Nguyen, T. B., and Garyfallidis, E. (2012). "The approximation of the dissimilarity projection," in *IEEE Intl. Workshop on Pattern Recognition in NeuroImaging* (London), 85–88. doi: 10.1109/prni.2012.13

Olivetti, E., Nguyen, T. B., Garyfallidis, E., Agarwal, N., and Avesani, P. (2013). "Fast clustering for interactive tractography segmentation," in *International Workshop on Pattern Recognition in Neuroimaging (PRNI), 2013* (Philadelphia, PA: IEEE), 42–45. doi: 10.1109/PRNI.2013.20

Pestilli, F., Yeatman, J. D., Rokem, A., Kay, K. N., and Wandell, B. A. (2014). Evaluation and statistical inference for human connectomes. *Nat. Meth.* 11, 1058–1063. doi: 10.1038/nmeth.3098

Porro-Muñoz, D., Olivetti, E., Sharmin, N., Nguyen, T., Garyfallidis, E., and Avesani, P. (2015). Tractome: a visual data mining tool for brain connectivity analysis. 29, 1258–1279. doi: 10.1007/s10618-015-0408-z

Raffelt, D., Tournier J. D., Fripp, J., Crozier, S., Connelly, A., and Salvado, O. (2011). Symmetric diffeomorphic registration of fibre orientation distributions. *Neuroimage* 56, 1171–1180. doi: 10.1016/j.neuroimage.2011.02.014

Sharmin, N., Olivetti, E., and Avesani, P. (2016). "Alignment of tractograms as linear assignment problem," in *Computational Diffusion MRI, Mathematics and Visualization,* eds Fuster, A., Ghosh, A., Kaden, E., Rathi, Y., and M. Reisert (Munich: Springer International Publishing), 109–120.

Sotiropoulos, S. N., Jbabdi, S., Xu, J., Andersson, J. L., Moeller, S., Auerbach, E. J., et al. (2013). Advances in diffusion MRI acquisition and processing in the human connectome project. *Neuroimage* 80, 125–143. doi: 10.1016/j.neuroimage.2013.05.057

Sporns, O., Tononi, G., and Kötter, R. (2005). The human connectome: a structural description of the human brain. *PLoS Comput. Biol.* 1:e42. doi: 10.1371/journal.pcbi.0010042

Tournier, J.-D., Calamante, F., and Connelly, A. (2007). Robust determination of the fibre orientation distribution in diffusion MRI: non-negativity constrained super-resolved spherical deconvolution. *Neuroimage* 35, 1459–1472. doi: 10.1016/j.neuroimage.2007.02.016

Umeyama, S. (1988). An Eigen decomposition approach to weighted graph matching problems. *IEEE Trans. Pattern Anal. Mach. Intell.* 10, 695–703. doi: 10.1109/34.6778

Van Essen, D. C., Smith, S. M., Barch, D. M., Behrens, T. E. J., Yacoub, E., and Ugurbil, K. (2013). The WU-Minn human connectome project: an overview. *Neuroimage* 80, 62–79. doi: 10.1016/j.neuroimage.2013.05.041

Wassermann, D., Makris, N., Rathi, Y., Shenton, M., Kikinis, R., Kubicki, M., et al. (2013). On describing human white matter anatomy: the white matter query language. *Med. Image Comput. Comput. Assist. Interv.* 16(Pt 1), 647–654. doi: 10.1007/978-3-642-40811-3_81

Wassermann, D., Rathi, Y., Bouix, S., Kubicki, M., Kikinis, R., Shenton, M., et al. (2011). White matter bundle registration and population analysis based on Gaussian processes. *Inf. Process Med. Imaging* 22, 320–332. doi: 10.1007/978-3-642-22092-0_27

Yoo, S. W., Guevara, P., Jeong, Y., Yoo, K., Shin, J. S., Mangin, J.-F., et al. (2015). An example-based multi-atlas approach to automatic labeling of white matter tracts. *PLoS ONE* 10:e0133337. doi: 10.1371/journal.pone.0133337

Zaslavskiy, M., Bach, F., and Vert, J.-P. (2009). A path following algorithm for the graph matching problem. *IEEE Trans. Pattern Anal. Mach. Intell.* 31, 2227–2242. doi: 10.1109/TPAMI.2008.245

Zass, R., and Shashua, A. (2006). "Doubly Stochastic normalization for spectral clustering," in *Advances in Neural Information Processing Systems 19, Proceedings of the Twentieth Annual Conference on Neural Information Processing Systems* (Vancouver, BC), 1569–1576.

Zhang, S., Correia, S., and Laidlaw, D. H. (2008). Identifying white-matter fiber bundles in DTI data using an automated proximity-based fiber-clustering method. *IEEE Trans. Vis. Comput. Graph.* 14, 1044–1053. doi: 10.1109/TVCG.2008.52

Ziyan, U., Sabuncu, M. R., Grimson, W. E. and Westin, C.-F. (2009). Consistency clustering: a robust algorithm for group-wise registration, segmentation and automatic atlas construction inädiffusion MRI. *Int. J. Comput. Vis.* 85, 279–290. doi: 10.1007/s11263-009-0217-1

Ziyan, U., Sabuncu, M. R., O'Donnell, L. J., and Westin, C.-F. F. (2007). Nonlinear registration of diffusion MR images based on fiber bundles. *Med. Image Comput. Comput. Assist. Interv.* 10(Pt 1), 351–358. doi: 10.1007/978-3-540-75757-3_43

Conflict of Interest Statement: The authors declare that the research was conducted in the absence of any commercial or financial relationships that could be construed as a potential conflict of interest.

Chapter 10

Alignment of Tractograms as Linear Assignment Problem

Alignment of Tractograms as Linear Assignment Problem

Nusrat Sharmin, Emanuele Olivetti and Paolo Avesani

NeuroInformatics Laboratory (NILab), Bruno Kessler Foundation, Trento, Italy
Center for Mind and Brain Sciences (CIMeC), University of Trento, Italy
http://nilab.fbk.eu

Abstract. Diffusion magnetic resonance imaging (dMRI) offers a unique approach to study the structural connectivity of the brain. DMRI allows to reconstruct the 3D pathways of axons within the white matter as a set of polylines (*streamlines*), called the *tractogram*. Tractograms of different brains need to be aligned in a common representation space for various purposes, such as group-analysis, segmentation or atlas construction. Typically, such alignment is obtained with affine registration, through which tractograms are globally transformed, with the limit of not reconciling local differences. In this paper, we propose to improve registration-based alignment by what we call *mapping*. The goal of mapping is to find the correspondence between streamlines across brains, i.e. to find the map of which streamline in one tractogram correspond to which streamline in the other tractogram. We frame the mapping problem as a *rectangular linear assignment problem* (RLAP), a cornerstone of combinatorial optimization. We adopt a variant of the famous Hungarian method to get the optimal solution of the RLAP. We validate the proposed method with a tract alignment application, where we register two tractograms and, given one anatomical tract, we segment the corresponding one in the other tractogram. On dMRI data from the Human Connectome Project, we provide experimental evidence that mapping, implemented as a RLAP, can vastly improve both the true positive rate and false discovery rate of registration-based alignment, establishing a strong argument in favor of what we propose. We conclude by discussing the limitations of the current approach, which gives perspective for future work.

Keywords: Diffusion MRI, Tractogram Alignment, Registration, Linear Assignment Problem

1 Introduction

Diffusion magnetic resonance imaging (dMRI) [1] provides information about the local orientation of white matter axons in each voxel of a brain image. Reconstruction and tracking algorithms aim at connecting voxels, based on the orientation within each voxel, in order to reconstruct the approximate trajectories of fibers as 3D polylines, called *streamlines*. A streamline, is a vectorial

representation of thousands of neuronal axons following the same pathway. The whole set of streamlines is called *tractogram* and it represents the anatomical connectivity of the brain.

Tracts are sets of streamlines with specific neuroanatomical meaning. A manual procedure of virtual dissection allows the segmentation of streamlines for a given tract of interest. For example, shape and size of a tract can be helpful for a neurologist to assess the progress of a neurodegenerative disease [5]. Such analysis compares the tract from a tractogram of a patient to that healthy subjects, or atlas [13]. The common practice is based on the quantifying the number of voxels shared by the two tracts [7], which requires that the two tracts are first aligned in a common representation space.

The alignment of two tractograms is still an open problem. The best practice is based on the affine registration of the corresponding structural images, such as T1 or FA (Fractional Anisotropy) [1], and by applying the estimated transformation to the coordinates of streamlines. Improvements of these methods have been proposed by using more informative volumetric images, such as the orientation distribution functions (ODFs) [14]. More recently, a new approach has been investigated by computing the affine transformation directly in the space of the streamlines [6]. The intuitive idea is to find the affine transformation that minimizes a loss function based on the distance between streamlines. Computational issues prevent the use a whole tractogram, i.e. the registration is usually based on a small subset of the streamlines.

We claim that the alignment of tractograms based on registration methods has two main limitations. The first is concerned with the affine transformation, which is a global one. Local anatomical differences between two subjects/tractograms cannot be reconciled by a global linear transformation. Nonlinear/elastic registration methods may overcome this limitation, but it is not straightforward how to preserve the orientation information of dMRI images after the distortion of the volumetric space. Evidence of this problem is the absence of literature on this topic. The second limitation is related to the use of transformations for alignment, that indeed reduces the differences between tractograms, but it is still not able to provide the correspondence between anatomical structures at the local level. We claim that alignment can provide more useful information when enriched with correspondence of streamlines across tractograms.

In this work we propose to overcome these limitations by introducing the notion of *mapping*. We claim that, when the ultimate goal is alignment and comparison of tracts across subjects, the registration in a common space is not enough and the additional step of finding which streamline in a tractogram correspond to which streamline in another tractogram should be computed.

In principle, the correspondence between streamlines across tractograms can be one-to-one, one-to-many or many-to-many. Here we restrict to the one-to-one case, and defer the other more general cases to future work. Under this assumption, the problem of finding corresponding streamlines can be cast as an *assignment problem* [4]. The assignment problem is a fundamental combinatorial optimization problem. Given two sets of objects, A and B, and a cost function to

assign one element of A to one of B, the goal is to find the injective assignments of each element of A, to one of B, such that the total cost of the assignments is minimized. If the numbers of items are equal and the total cost is given by the sum of each assignment cost, the problem is called linear assignment problem (LAP). When $|A| \neq |B|$, the problem is called rectangular LAP (RLAP) [2], which is a generalization of the LAP.

Efficient and well known algorithms for solving the LAP are the Hungarian method [11] and Jonker-Volgenant algorithm (LAPJV) [9], both giving the optimal solution with complexity $\mathcal{O}(n^3)$, $n = |A|$. For the rectangular case, where $m = |B| > n$, efficient variants of the previous algorithms are available in the literature, such as [3] which has complexity $\mathcal{O}(n^2 m)$ and provide the optimal solution. In this work we adopt that algorithm.

We designed an experiment about segmenting a desired tract in a tractogram. On dMRI data from the Human Connectome Project [15], we show experimental evidence that mapping through the RLAP greatly improves the quality of segmentation, both in terms of true positive rate (TPR) and false discovery rate (FDR), with respect to that of affine registration. This result confirms that the concept of mapping should be considered as a new useful tool in the context of alignment of tractograms and that its implementation as an assignment problem is effective, despite some limitations.

The paper is structured as follows. In Section 2 we define the notation and formally introduce mapping and the RLAP, together with the algorithm adopted here. In Section 3 we describe the details of the experiment and its results. A brief discussion about the merits a limitations is reported in Section 4.

2 Methods

In this section we briefly introduce the notation, the concept of mapping and the formal description of the linear assignment problem (LAP), with details of its *rectangular* (RLAP) version and references to efficient solutions.

2.1 Notation and Streamline Distance

Let the polyline $s = \{\mathbf{x}_1, \mathbf{x}_2, \ldots\}$, where $\mathbf{x}_i \in \mathbb{R}^3$, be a *streamline*, reconstructed from dMRI data through reconstruction and tractography algorithms. Let the *tractogram*, $T = \{s_1, s_2, \ldots, s_M\}$ be defined as a set of M streamlines, where $M \approx 10^5$. Let $t = \{s_1, s_2, \ldots, s_k\} \subset T$, be a subset of the tractogram, called *tract*, usually with a specific anatomical meaning, e.g. the cortico-spinal tract (CST).

Multiple distance functions between streamlines have been proposed in the literature [18]. Here we adopt the most common one, i.e. the symmetric minimum average distance (MAM). Given two streamlines, s_a and s_b:

$$d_{MAM}(s_a, s_b) = \frac{1}{2}(D(s_a, s_b) + D(s_b, s_a)) \tag{1}$$

where

$$D(s_a, s_b) = \frac{1}{|s_a|} \sum_{i=1}^{|s_a|} d(\mathbf{x}_i^a, s_b) \tag{2}$$

and

$$d(\mathbf{x}, s_b) = \min_{j=1,\dots,|s_b|} ||\mathbf{x} - \mathbf{x}'_j||_2 \tag{3}$$

2.2 Mapping

The alignment of two tractograms, T_A and T_B, is usually implemented through registration algorithms, that transform the coordinates of the streamlines into a common space. Here we propose a different way of aligning tractograms, based on finding corresponding streamlines across two tractograms, without operating any transformation. The problem of finding which streamline $s_j^B \in T_B$ correspond to a given streamline $s_i^A \in T_A$ is a combinatorial one and its solution is a correspondence map between the two sets. For this reason, we call this kind of alignment as *mapping*. We denote the map as a binary matrix $P = [p_{ij}]_{ij} \in \{0,1\}^{|T_A| \times |T_B|}$, that we call *mapping* matrix, such that p_{ij} is 1 when streamline $s_i^A \in T_A$ corresponds to streamline $s_j^B \in T_B$, and 0 otherwise.

In practical cases, it is common to observe that different tractograms have different number of streamlines, i.e. $|T_A| \neq |T_B|$. Moreover, corresponding tracts across different subjects may have different size, meaning that different streamlines of one tractogram may correspond to the same streamline in the other one. For these reasons, in general, the correspondence between streamlines cannot be a bijective or an injective map but a many-to-one or many-to-many map. A very simple many-to-one greedy solution to the mapping problem is assigning the nearest streamline of the second tractogram to each streamline of the first tractogram, after affine registration in a common space. We refer to this baseline solution as *registration + nearest neighbor* (NN). The main limitation of this solution is that it strongly rely on the assumption that the affine registration reconciles most of the differences between the two tractograms, which is generally not true.

In order to propose an improvement over NN, in this work, we add the restrictive assumption that that different streamlines in T_A correspond to different streamlines in T_B, i.e. we assume the mapping to be injective[1]. In Section 3 and 4 we show that this restriction does not prevent the proposed approach to reach major improvements over NN. Under the assumption just mentioned, and in order to find the desired mapping between two tractograms, we cast the mapping problem into a well known optimization problem, called *assignment problem* [4]. In the following we formally introduce the linear assignment problem along with its rectangular version.

[1] Additionally we introduce the technical assumption that $|T_A| \leq |T_B|$.

2.3 The Linear Assignment Problem

Given two sets of objects of the *same size*, $T_A = \{s_1^A, \ldots, s_n^A\}$ and $T_B = \{s_1^B, \ldots, s_n^B\}$, the problem of finding the optimal bijective assignment of each s_i^A to one element in T_B, given the cost matrix $C = [c_{ij}]_{ij} \in \mathbb{R}^{n \times n}$, where c_{ij} is the cost of assigning s_i^A to s_j^B, is called *linear assignment problem* (LAP). In our case, the cost is the distance between streamlines. The bijective assignment between the streamlines of two tractograms can be represented by permutation matrix $P = [p_{ij}]_{ij} \in \{0,1\}^{n \times n}$, where $p_{ij} = 1$ if s_i^A is assigned to s_j^B, and 0 otherwise. Notice that, since P represents a bijective correspondence, then $\forall i \in \{1, \ldots, n\}$, $\sum_j p_{ij} = 1$ and $\forall j \in \{1, \ldots, n\}$, $\sum_i p_{ij} = 1$. The formal definition of the LAP is then:

$$P^* = \underset{P \in \mathcal{P}}{\operatorname{argmin}} \sum_{i,j=1}^{n} c_{ij} p_{ij} \tag{4}$$

where $\mathcal{P}$ is the set of all possible $n \times n$ permutation matrices and P^* is the optimal assignment with lowest overall cost.

Among the most efficient algorithm in the literature to find P^*, the Hungarian method is the most famous one. Its first formulation [10] had time complexity $\mathcal{O}(n^4)$, which was later improved to $\mathcal{O}(n^3)$ by Munkres [11]. Another prominent algorithm in this group is LAPJV [9] which has the same complexity, $\mathcal{O}(n^3)$.

2.4 Rectangular Assignment Problem

When $|A| \neq |B|$, LAP is called *rectangular assignment problem* [2] (RLAP). In that case, let $n = |A|$ and $m = |B|$ and $n \leq m$, the problem consists in finding the injective assignment of all $s_i^A \in A$ within B. Formally:

$$P^* = \underset{P \in \mathcal{P}}{\operatorname{argmin}} \sum_{i=1}^{n} \sum_{j=1}^{m} c_{ij} p_{ij} \tag{5}$$

where $[p_{ij}]_{ij} = P \in \mathcal{P}$ is a *partial* permutation matrix[2] and $C = [c_{ij}]_{ij}$ is the cost matrix.

The literature about algorithms to find the optimal solution to the RLAP is much smaller than then one on the LAP. See [2] for a brief review, with adaptations of the most effective LAP algorithms to the RLAP case.

A common solution for the RLAP is adding $m-n$ dummy entries, so that the RLAP becomes a LAP with $(m-n)!$ optimal solutions. The time complexity of this solution is then $\mathcal{O}(m^3)$. In this paper we adopt a more efficient algorithm [3], which is a rectangular extension of the Munkres algorithm. Its time complexity is $O(n^2 m)$, which is convenient in the setting of our experiments where $m \ggg n$ (see Section 3).

[2] A partial permutation matrix is a rectangular version of the permutation matrix, i.e. $P = [p_{ij}]_{ij} \in \{0,1\}^{n \times m}$ and $\sum_{j=1}^{n} p_{ij} = 1$ but $\sum_{i=1}^{m} p_{ij} \leq 1$.

3 Experiments

Experiments were performed on 10 randomly selected subjects from the Human Connectome Project (HCP) [15,16] dMRI datasets. We preprocessed the data with single shell ($b = 1000$) and isometric up-scaling ($2mm$). The tractography was reconstructed using a diffusion tensor model (DTI) and the tracking was computed with the Euler Delta Crossing (EuDX) algorithm, using the DiPy toolbox[3]. We used the white matter query language (WMQL)[17], a parcellation-based method, to virtually dissect several types of neuroanatomical tracts: arcuate fasciculus (AF), corticospinal tract (CST), cingulum (CG), uncinate fasciculus (UF) optical radiation (OR), medial longitudinal fasciculus (MDLF), inferior longitudinal fasciculus (ILF), inferior occipitofrontal fasciculus (IFOF). Considering both left and right hemispheres, we obtained 16 different tracts for all the 10 subjects. A summary of the information after the virtual dissection are reported in Table 1, specifically the average and standard deviation of the number of streamlines and the number of voxels of all tracts.

Table 1. Data description. For each tract, the table reports the average and standard deviation of the number of streamlines and of voxels over 10 subjects.

Tract Name	# Streaml.	# Voxels
CST_LEFT	50 ± 41	1478 ± 725
CST_RIGHT	23 ± 17	1075 ± 478
CG_LEFT	947 ± 135	12075 ± 1602
CG_RIGHT	833 ± 100	10920 ± 1507
AF_LEFT	290 ± 107	5437 ± 1617
AF_RIGHT	186 ± 144	4046 ± 1916
UF_LEFT	189 ± 71	2913 ± 932
UF_RIGHT	171 ± 87	2583 ± 1117
OR_LEFT	78 ± 68	1547 ± 2171
OR_RIGHT	83 ± 22	2246 ± 418
MDLF_LEFT	195 ± 116	4152 ± 2022
MDLF_RIGHT	180 ± 119	3339 ± 1482
ILF_LEFT	199 ± 82	2568 ± 1923
ILF_RIGHT	133 ± 115	2475 ± 1283
IFOF_LEFT	175 ± 58	4794 ± 1068
IFOF_RIGHT	145 ± 88	4681 ± 1636

The purpose of the experiment was to collect empirical evidence that exploiting the correspondence of streamlines across tractograms improves the alignment

[3] `http://dipy.org`

of tracts with respect to what affine registration can do. The experiment was conceived in the following way: after alignment, given a tract, its corresponding voxels were extracted, as well as those of the same tract in the second tractogram. The overlap over the two sets of voxels [7], in terms of of true positive rate (TPR) and false discovery rate (FDR), was computed. We considered three scenarios: (i) registration-only alignment, without additional mapping of streamlines; (ii) registration and mapping as nearest-neighbor (NN); (iii) registration and mapping as optimal solution of the RLAP.

In each scenario, the first step was the projection of the two tractograms in a common space. The registration was performed with respect to the standard MNI space using FSL FLIRT, that implements a voxel-based affine registration [8].

For scenarios (ii) and (iii), the second step was concerned with the computation of the correspondence among streamlines, from a source tract t_A to a target tractogram T_B. We call the *true* target tract, as obtained through WMQL segmentation, as t_B and its approximation, through mapping or registration, as $\widehat{t}_B$. For each tract in Table 1, we computed TPR and FDR for all possible pairs over the 10 subjects, i.e. 45 pairs. We excluded those pairs where the difference in the number of streamlines was $\geq 60\%$. We may reasonably assume that such extreme differences in the number of streamlines for the same tract were related to limitations in the virtual dissection with the WMQL.

Denoted as $v(t)$ the set of voxels corresponding to a tract t, the quantification of the overlap between $\widehat{t}_B$ and t_B was the following:

$$\text{TPR} = \frac{|v(\widehat{t}_B) \cap v(t_B)|}{|v(t_B)|} \tag{6}$$

$$\text{FDR} = \frac{|v(\widehat{t}_B) \setminus v(t_B)|}{|v(\widehat{t}_B)|} \tag{7}$$

In Table 2 are reported the results, in term of TPR and FDR for the three methods. The results clearly show that the computation of the correspondence of streamlines between tracts is beneficial for alignment. Even the simplest implementation of mapping, i.e. the NN heuristic explained in Section 2, introduces a consistent improvement over affine registration. Such improvement is much greater when adopting the optimal solution of the RLAP. The results of RLAP are consistently better for all tracts, except for the TPR of IFOF RIGHT. However, for IFOF RIGHT, the TPR of RLAP is similar to that of NN and the TDR is much lower. We noticed that the NN mapping, which computes a many-to-one correspondence, tends to underestimate the number of streamlines, i.e usually $|\widehat{t}_B| < |t_B|$. For this reason and for the strong assumption that the affine registration is able to reduce the local and global differences, the alignment based on NN achieves lower values of TPR with respect to the RLAP.

While RLAP looks effective for tract alignment, the same solution is not viable for full tractograms alignment, because of the computational cost. In Figure 1 it is reported the time required by the rectangular Munkres algorithm of [3], as implemented in Scikit-Learn[4], to compute the optimal solution for the

[4] `http://scikit-learn.org`

Table 2. Average, over multiple pairs of subjects, of true positive rate (TPR, higher is better) and false discovery rate (FDR, lower is better) for three methods: Registration, Registration+NN (nearest neighbor), Registration+RLAP. Each row corresponds to a different anatomical tract.

Tract Name	Registration		Registration +NN		Registration +Assignment	
	TPR	FDR	TPR	FDR	TPR	FDR
CST_LEFT	0.10	0.63	0.24	0.64	**0.38**	**0.11**
CST_RIGHT	0.06	0.76	0.21	0.70	**0.32**	**0.32**
CG_LEFT	0.24	0.38	0.33	0.62	**0.67**	**0.20**
CG_RIGHT	0.25	0.37	0.36	0.56	**0.69**	**0.14**
AF_LEFT	0.15	0.55	0.27	0.69	**0.69**	**0.18**
AF_RIGHT	0.11	0.57	0.31	0.67	**0.67**	**0.15**
UF_LEFT	0.24	0.45	0.37	0.57	**0.71**	**0.21**
UF_RIGHT	0.32	0.31	0.39	0.56	**0.80**	**0.18**
OR_LEFT	0.06	0.75	0.14	0.75	**0.23**	**0.26**
OR_RIGHT	0.07	0.64	0.13	0.77	**0.27**	**0.30**
MDLF_LEFT	0.13	0.68	0.24	0.66	**0.53**	**0.18**
MDLF_RIGHT	0.15	0.48	0.24	0.70	**0.57**	**0.16**
ILF_LEFT	0.18	0.61	0.29	0.64	**0.67**	**0.26**
ILF_RIGHT	0.07	0.66	0.18	0.75	**0.39**	**0.13**
IFOF_LEFT	0.16	0.59	0.29	0.65	**0.66**	**0.17**
IFOF_RIGHT	0.16	0.31	**0.60**	0.64	0.56	**0.28**

tracts for same of the cases in our experiments. For low values of n (< 50), the computation required less than a minute, while for large values of n (> 600) it required several hours.

In Figure 3 we report a visual snapshot of the alignment of the arcuate fasciculus (AF) between two subjects. The picture[5] shows the voxels correctly mapped both by NN and RLAP (blue), those correctly mapped by only the RLAP (red), and the ones missed by both (green). In this example, no correct voxel was found by NN and not by RLAP. The benefit of RLAP with respect to NN is illustrated as a meaningful increment of the number of voxels correctly aligned (red).

4 Conclusion and Future Work

In the present work we addressed the task of aligning sets of streamlines. We introduced the notion of correspondence between streamlines, that we call mapping, as additional step to improve the registration of tractograms based on

[5] For simplicity we limit the view to one slice only.

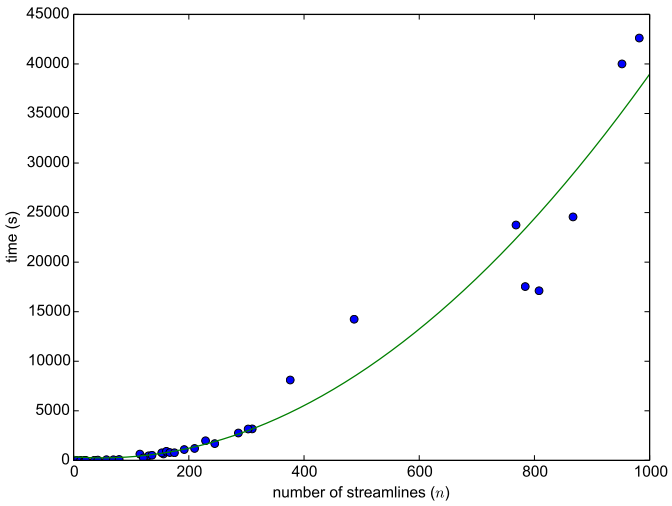

Fig. 1. Time, in seconds, required to solve the RLAP with the rectangular version of the Munkres aglorithm [3], for tracts with various sizes (n). The quadratic dependence of the time complexity term is shown in green. Notice that $m \approx 10^5$.

affine transformation. We proposed to recast the problem of computing the correspondence as a rectangular linear assignment problem (RLAP). We performed an experimental assessment on real data from the Human Connectome Project dataset and, in Section 3, we provided strong empirical evidence of the improvement for tract alignment.

Despite the very positive results presented in Section 3, many questions require further investigation. First of all, the RLAP approach presented here is based on the assumptions that the mapping is injective and that the distance function between streamlines across different tractograms is meaningful. The first assumption, even though quite restrictive in principle (see Section 2.2), provides clearly better results than the nearest neighbor (NN) solution, which is a many-to-one mapping. Nevertheless, investigating more refined many-to-one and many-to-many solutions seems be more anatomically meaningful. The second assumption requires that the affine registration is sufficient to make the streamline distance function meaningful across tractograms. Given that without initial registration such distance may be non-informative, this step requires further understanding on when and how registration becomes crucial. This issue provides motivation for completely avoiding the computation of streamline distances across tractograms, a direction that we recently proposed using a graph matching approach [12].

In the short term, the solution presented in this work can be improved on at least two levels: reducing the computational time and investigating the effect

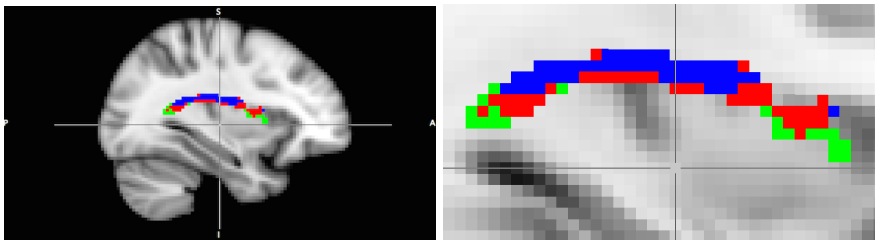

Fig. 2. Mapping of Arcuate Fasciculus (AF). The pictures (left: whole brain; right: zoomed detail) report one slice ($x = 61, y = 53, z = 37$) of the projection of the AF tract from a source subject (ID=124422) to a target subject (ID=239944) of the Human Connectome Project dataset. Voxels in blue are the ones correctly detected by NN and RLAP, in red by only RLAP and in green the missed ones. No correct voxel was found by NN and not by RLAP.

of different streamlines distance functions. We plan to investigate sub-optimal solutions to the RLAP, in order to reduce the computational complexity so to address the problem of mapping whole tractograms.

Acknowledgment

The research was funded by the Autonomous Province of Trento, Call "Grandi Progetti 2012", project "Characterizing and improving brain mechanisms of attention - ATTEND".

Data were provided [in part] by the Human Connectome Project, WU-Minn Consortium (Principal Investigators: David Van Essen and Kamil Ugurbil; 1U54MH091657) funded by the 16 NIH Institutes and Centers that support the NIH Blueprint for Neuroscience Research; and by the McDonnell Center for Systems Neuroscience at Washington University.

References

1. Basser, P.J., Mattiello, J., LeBihan, D.: MR diffusion tensor spectroscopy and imaging. Biophysical journal 66(1), 259–267 (Jan 1994), http://dx.doi.org/10.1016/s0006-3495(94)80775-1
2. Bijsterbosch, J., Volgenant, A.: Solving the Rectangular assignment problem and applications. Annals of Operations Research (Jun 2010), http://dx.doi.org/10.1007/s10479-010-0757-3
3. Bourgeois, F., Lassalle, J.C.: An extension of the Munkres algorithm for the assignment problem to rectangular matrices. Communications of the ACM 14(12), 802–804 (1971)
4. Burkard, R., Dell'Amico, M., Martello, S.: Assignment Problems. Society for Industrial and Applied Mathematics, 2 edn. (Sep 2012), http://dx.doi.org/10.1137/1.9781611972238

5. Catani, M., Allin, M.P.G., Husain, M., Pugliese, L., Mesulam, M.M., Murray, R.M., Jones, D.K.: Symmetries in human brain language pathways correlate with verbal recall. Proceedings of the National Academy of Sciences 104(43), 17163–17168 (2007)
6. Garyfallidis, E., Wassermann, D., Descoteaux, M.: Direct native-space fiber bundle alignment for group comparisons. In: International Society for Magnetic Resonance Imaging (ISMRM). Milan, Italy (2014), https://hal.inria.fr/hal-00991740
7. Golding, D., Tittgemeyer, M., Anwander, A., Douglas, T.: A comparison of methods for the registration of tractographic fibre images. In: Robinson, P., Nel, A. (eds.) Proceedings of the Twenty-Second Annual Symposium of the Pattern Recognition Association of South Africa. pp. 55–59 (2011)
8. Jenkinson, M., Smith, S.: A global optimisation method for robust affine registration of brain images. Medical image analysis 5(2), 143–156 (Jun 2001), http://view.ncbi.nlm.nih.gov/pubmed/11516708
9. Jonker, R., Volgenant, A.: A shortest augmenting path algorithm for dense and sparse linear assignment problems. Computing 38(4), 325–340 (Dec 1987), http://dx.doi.org/10.1007/bf02278710
10. Kuhn, H.W.: The Hungarian method for the assignment problem. Naval Research Logistics 2(1-2), 83–97 (1955), http://dx.doi.org/10.1002/nav.3800020109
11. Munkres, J.: Algorithms for the assignment and transportation problems. Journal of the Society for Industrial & Applied Mathematics 5(1), 32–38 (1957)
12. Nguyen, T.B., Olivetti, E., Avesani, P.: Mapping tractography across subjects (2014), the 4th NIPS workshop on Machine Learning and Interpretation in Neuroimaging (MLINI), accepted (forthcoming)
13. O'Donnell, L.J., Wells, W.M., Golby, A.J., Westin, C.F.F.: Unbiased groupwise registration of white matter tractography. Medical image computing and computer-assisted intervention : MICCAI - International Conference on Medical Image Computing and Computer-Assisted Intervention 15(Pt 3), 123–130 (2012), http://www.ncbi.nlm.nih.gov/pmc/articles/PMC3638882/
14. Raffelt, D., Tournier, Fripp, J., Crozier, S., Connelly, A., Salvado, O.: Symmetric Diffeomorphic Registration of Fibre Orientation Distributions. NeuroImage (Feb 2011), http://dx.doi.org/10.1016/j.neuroimage.2011.02.014
15. Sotiropoulos, S.N., Jbabdi, S., Xu, J., Andersson, J.L., Moeller, S., Auerbach, E.J., Glasser, M.F., Hernandez, M., Sapiro, G., Jenkinson, M., Feinberg, D.A., Yacoub, E., Lenglet, C., Van Essen, D.C., Ugurbil, K., Behrens, T.E., WU-Minn HCP Consortium: Advances in diffusion MRI acquisition and processing in the Human Connectome Project. NeuroImage 80, 125–143 (Oct 2013), http://view.ncbi.nlm.nih.gov/pubmed/23702418
16. Van Essen, D.C., Smith, S.M., Barch, D.M., Behrens, T.E., Yacoub, E., Ugurbil, K., Consortium, W.M.H., et al.: The wu-minn human connectome project: an overview. Neuroimage 80, 62–79 (2013)
17. Wassermann, D., Makris, N., Rathi, Y., Shenton, M., Kikinis, R., Kubicki, M., Westin, C.F.F.: On describing human white matter anatomy: the white matter query language. Medical image computing and computer-assisted intervention : MICCAI ... International Conference on Medical Image Computing and Computer-Assisted Intervention 16(Pt 1), 647–654 (2013), http://www.ncbi.nlm.nih.gov/pmc/articles/PMC4029160/
18. Zhang, S., Correia, S., Laidlaw, D.H.: Identifying White-Matter Fiber Bundles in DTI Data Using an Automated Proximity-Based Fiber-Clustering Method. IEEE Transactions on Visualization and Computer Graphics 14(5), 1044–1053 (Sep 2008), http://dx.doi.org/10.1109/tvcg.2008.52

Appendices

Appendix A

Supplementary Material

A.1 Tracts/Bundles with High Variability across Subjects

We investigated a larger set of tracts/bundles than that described in the paper. In Table A.1 we report the size, in number of streamlines, of 18 tracts for each of the 10 subjects considered in our study. Each tract was automatically segmented with the white matter query language (WMQL), see [157]. As it is clearly shown, the variability in number of streamlines across subjects changes dramatically from one tract to another. For example the Cingulum left (cg.left, 1st row), has a moderate variability across subjects, around 20%. Differently the Arcuate Fasciculus right (af.right, 10th row) shows extreme variability, e.g. 508 streamlines in subject 5 and ≤ 2 streamlines in subjects 4, 6 and 10. For this reason, we divided the tracts in two groups, of low and high variability. In the upper part of Table A.1 we report the tracts with low variability, that were included in the study. In the lower part of Table A.1, below the mid line, we report the tracts with very high variability, that were excluded from our study.

It is expected that part of the observed variability is due to anatomical differences across the population. Nevertheless, we believe that part of the reason for the extremes we observe in the lower part of Table A.1 is due to poor segmentation and, possibly, also due to limitations in tractography data and white matter parcellation. An expert-made segmentation instead of the automatic one, might reduce the issue. Given this problem, in this work we want to decouple the variability intrinsic to the methods from the variability in the ground truth, which here can be considered as unwanted noise. Such considerations led us not to consider the tracts in the lower part of Table A.1 from our study.

In order to enrich the results presented in the paper, here in Supplementary Material we extend the experiments with three more tracts that were previously excluded: SLF II, MDLF left and MDLF right. We chose these tracts because they exhibit less extreme variability among the excluded ones. For these tracts, in Figure A.2, we show the average overlap after whole tractogram alignment with FLIRT, ENT, SLR, FNIRT and the proposed GM. The height of each bar in the graph represents the average overlap, computed over the 45 pairs of subjects considered in the study. From those results, we observe that, in general, the overlap of linear methods was lower than the cases reported in the paper, i.e. $J \in [0.10, 0.15]$. FNIRT and GM showed much higher degree of overlap than linear methods and comparable results between each other, i.e. $J \in [0.45, 0.55]$. Nevertheless these results are among the lowest values obtained for other tracts in the paper.

With the three new bundles considered here, in Figure A.3, for the proposed GM, we extend Figure 4 of the paper by showing the degree of overlap (J_{GM}) vs. the difference between the corresponding bundles, at the level of individual pairs of subjects (45 pairs) and bundle (now 12 bundles): $45 \times 12 = 540$ points. In Figure A.4, we

bundle	subj1 100307	subj2 124422	subj3 161731	subj4 199655	subj5 201111	subj6 239944	subj7 245333	subj8 366446	subj9 528446	subj10 856766
cg.left	1181	905	1235	1326	1361	1185	1230	1126	1396	1150
cg.right	969	1002	974	1036	1247	1178	1050	904	1235	861
ifof.left	169	183	66	142	92	202	54	290	161	68
ifof.right	152	69	20	284	131	176	40	311	22	109
uf.left	138	193	179	166	281	60	144	296	102	66
uf.right	250	158	195	244	211	73	145	182	156	41
cc_7	546	431	337	442	413	247	441	577	520	319
cc_2	661	283	300	302	670	407	314	638	464	628
af.left	92	333	273	176	550	124	352	200	234	172
af.right	35	190	172	1	508	2	137	8	77	0
slf1.left	11	0	0	0	0	0	0	0	0	0
slf1.right	22	1	8	27	0	20	0	16	18	3
slf2.left	193	64	0	130	30	36	0	0	0	1
slf2.right	257	22	25	182	67	1	62	79	74	20
slf3.left	4	0	0	0	0	0	0	0	0	0
slf3.right	0	0	1	2	19	0	43	71	18	0
mdlf.left	55	116	137	69	16	11	299	239	227	22
mdlf.right	256	40	146	27	113	244	13	128	16	27

Figure A.1: Tract/Bundle sizes, in terms of number of streamlines across the 10 subjects considered in this study. The Tracts were segmented with WMQL, see [157].

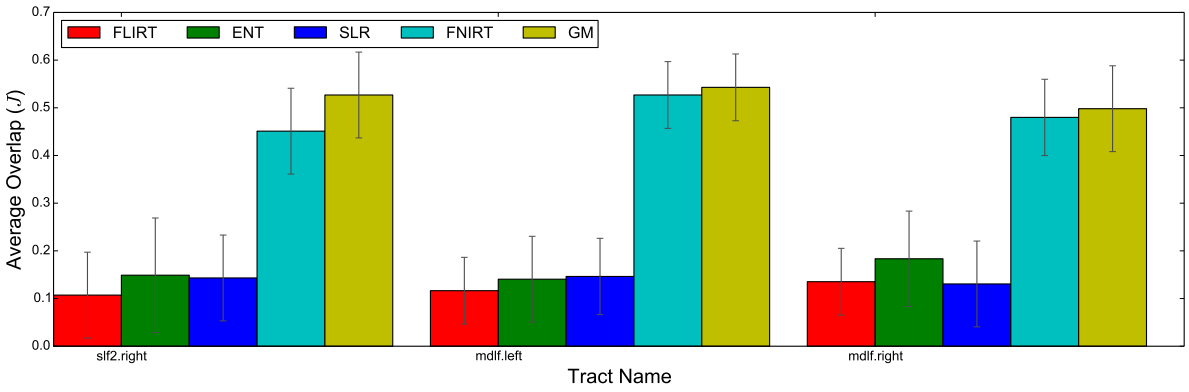

Figure A.2: additional tracts

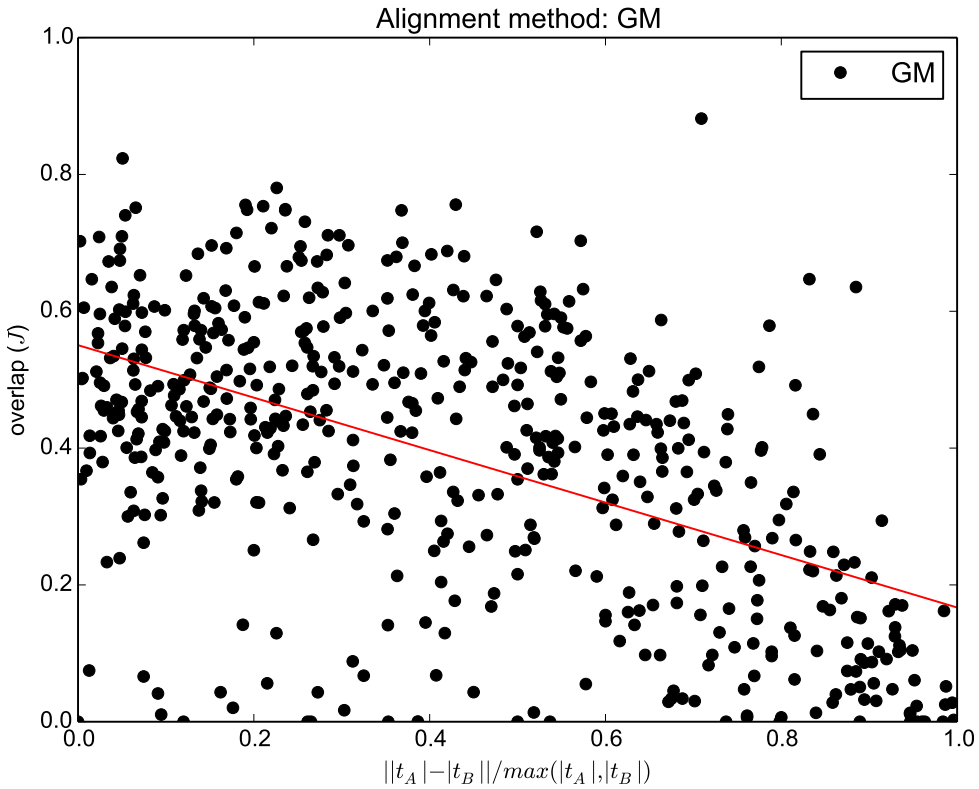

Figure A.3: For each of the 45 pairs of subjects and 12 tracts/bundles ($45 \times 12 = 540$ points in total), the graph shows the tract overlap after whole tractogram alignment performed with GM, as a function of the difference between that tract across the two subjects. The difference, in number of streamlines, is quantified as $\Delta_{AB} = \frac{||t_A|-|t_B||}{max(|t_A|,|t_B|)}$.

also report the equivalent graphs for FLIRT, ENT, SLR and FNIRT. As expected, in all cases the trend, as linear interpolation (red line), shows the decay of overlap when the corresponding bundle across two subjects greatly differ in number of streamlines. These graphs also show that GM and FNIRT align tractograms much better than FLIRT, ENT and SLR.

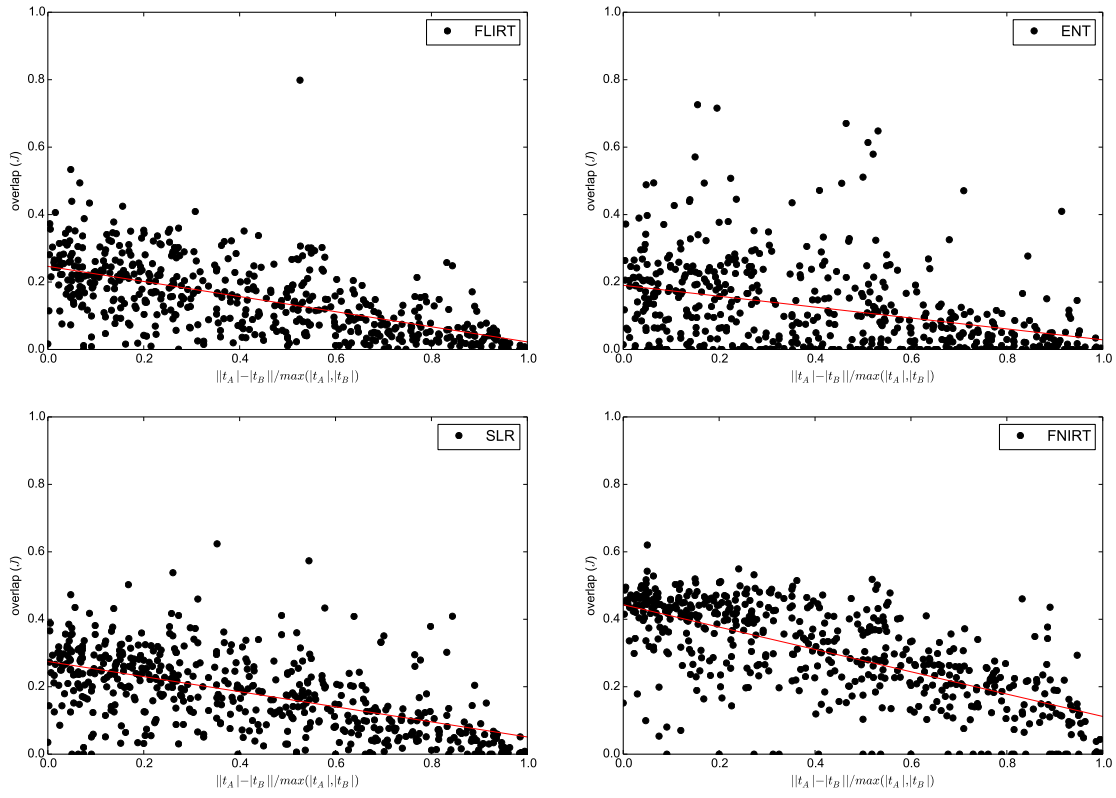

Figure A.4: For each of the 45 pairs of subjects and 12 tracts/bundles ($45 \times 12 = 540$ points in total), the graph shows the tract overlap after whole tractogram alignment performed with FLIRT, ENT, SLR and FNIRT, as a function of the difference between that tract across the two subjects. The difference, in number of streamlines, is quantified as $\Delta_{AB} = \frac{||t_A|-|t_B||}{max(|t_A|,|t_B|)}$.

Appendix B

Dissimilarity Representation

B.1 Prototype Selection for Dissimilarity Representation

For these experiments we used the dMRI recordings of 10 healthy subjects (100307, 124422, 161731, 245333, 528446, 556766, 201111, 199655, 239944 and 366446) from the Human Connectome Project [149], [132]. They were acquired on a Siemens Skyra 3T scanner (90 gradients; b-value= $1000 s/mm^2$; anatomical scan ($1.25 \times 1.25 \times 1.25 mm^3$)). From these data we reconstructed the streamlines using EuDX, a deterministic tracking algorithm [52] from the DiPy library [53]. The obtained tractography for each subject consists of approximately of 5×10^5 streamlines.

First step is to project the tractogram data into the dissimilarity space $\mathbb{R}^p$. With this purpose, a set of prototypes has to be selected in advance. Next, we present a study of the degree of approximation of the dissimilarity representation across different prototype selection policies i.e. Random, SFF and S+SFF, and different numbers of prototypes. The aim is to investigate the trade-off between accuracy and computational cost. For SFF we chose $c = 3$ in order to have high probability (> 0.95) of accurately representing T through the subset. For S+SFF, only streamlines with size $z > 10$ will be used. By using this value, the set of streamlines to be analysed is drastically reduced in the order of 10^5 times.

In order to evaluate how accurate our dissimilarity representation is, we investigate the relationship between the distribution of distance among objects in $\mathcal{X}$ through d and the corresponding distances in the dissimilarity space through Δ^d_Π, where $\Delta^d_\Pi : \phi(s) \times \phi(s') \to \mathbb{R}^+$ and $\Delta^d_\Pi = ||\phi(s) - \phi(s')||_2$. It was claimed in [106], that a good dissimilarity representation must be able to accurately preserve the partial order of the distances, i.e. if $d(s,s') \leq d(s,s'')$ then $\Delta^d_\Pi(s,s') \leq \Delta^d_\Pi(s,s'')$ for each s, s' , $s'' \in \mathcal{X}$ almost always. As a measure of the degree of approximation of the dissimilarity representation we define the Pearson correlation coefficient ρ between the two distances over all possible pairs of objects in $\mathcal{X}$:

$$\rho = \frac{\mathrm{Cov}(d(s,s'), \Delta^d_\Pi(s,s'))}{\sigma_{d(s,s')} \sigma_{\Delta^d_\Pi(s,s')}} \tag{B.1}$$

where given P_s a probability distribution over $\mathcal{X}$, $s, s' \sim P_s$. In practical cases P_s is unknown and only a finite sample F is available. We can approximate ρ as the *sample* correlation r where $s, s' \in F$. An accurate approximation of the relative distances between objects in $\mathcal{X}$ results in values of ρ far from zero and close to 1[1].

[1] Note that negative correlation is not considered as accurate approximation. Moreover it never occurred during experiments.

The correlation and standard deviation for each prototype selection strategy are shown in Figure B.1 [2]. The correlation ρ between distances in the original space and the corresponding distances in the projected space was estimated by computing 50 repetitions for each subject.

We can observe that, as an overall behaviour for all subjects, SFF significantly outperformed the random policy, in agreement to what was reported in [106]. Moreover, it can be seen that S+SFF, outperformed the other two policies. In particular, we conducted a one-tailed t-test comparing the correlation values of the 50 repetitions of S+SFF against those of SFF for each number of prototypes p (11 values) and for each of the 10 subjects. Of these $11 \times 10 = 110$ tests, when $p \geq 5$, the obtained p-values were always lower than 5.2×10^{-13}. Even considering an overly conservative Bonferroni correction, the p-values were sufficiently low to reject the null hypothesis of S+SFF equal to SFF for $p \geq 5$.

We observe that S+SFF reached the highest correlation of 0.95 on average (50 repetitions) with respect to the distances in the original space, using only $15-25$ prototypes, which is half of the amount used in the previous paper with the SFF policy [106].

It is also worth to notice that the standard deviation with this last approach, $\hat{\sigma}_{\text{S+SFF}}$, is smaller than that of SFF, $\hat{\sigma}_{\text{SFF}}$, thus implying that the proposed heuristic is more stable. To support this point, we conducted a one-tailed t-test of the standard deviations of correlation for the 10 subjects, comparing S+SFF vs. SFF for each number of prototypes p (11 values). In all these 11 tests, the p-values were always lower than 1.2×10^{-5}. Even considering a very restrictive Bonferroni correction, the p-values were sufficiently low to reject the null hypothesis of $\hat{\sigma}_{\text{S+SFF}} = \hat{\sigma}_{\text{SFF}}$.

From these results we can conclude that the dissimilarity representation works well for preserving the relative distances. Given the number of prototypes with which the maximum correlation was reached, it is proven that this approach can produce compact feature spaces for this kind of data. Moreover, we observed that the S+SFF policy can be easily computed on a standard computer even in the case of a large tractographies. Therefore, we use the S+SFF to obtain an efficient and effective selection of the prototypes in our tool.

In Table B.1 and Table B.2, reported in this document, we show the p-values for all the 121 tests that were performed for the two presented hypotheses.

[2] The figure is restricted to 6 of the 10 subjects for lack of space. The graphs of all subjects showed an equivalent behaviour.

Table B.1: p-values from the 110 one-tailed t-tests for null hypothesis: S+SFF policy performs the same as SFF. These 110 tests correspond to the 10 subjects and 11 values of prototypes.

Subjects	# of prototypes (p)										
	p=3	p=5	p=10	p=15	p=20	p=25	p=30	p=35	p=40	p=45	p=50
Subj1	2.4×10^{-7}	5.9×10^{-30}	4.5×10^{-27}	4.6×10^{-33}	2.4×10^{-26}	4.5×10^{-34}	8.1×10^{-35}	9.8×10^{-38}	1.5×10^{-38}	1.9×10^{-35}	1.1×10^{-41}
Subj2	9.3×10^{-04}	1.5×10^{-24}	3.1×10^{-23}	2.4×10^{-33}	8.7×10^{-33}	2.1×10^{-29}	4.5×10^{-31}	9.1×10^{-41}	4.7×10^{-37}	1.9×10^{-43}	1.2×10^{-41}
Subj3	4.4×10^{-05}	2.9×10^{-16}	1.8×10^{-20}	3.6×10^{-25}	6.8×10^{-32}	9.8×10^{-25}	1.9×10^{-33}	8.6×10^{-38}	1.8×10^{-38}	3.7×10^{-34}	5.5×10^{-44}
Subj4	1.1×10^{-04}	1.5×10^{-13}	4.4×10^{-27}	1.9×10^{-31}	4.2×10^{-30}	3.3×10^{-32}	1.9×10^{-39}	2.6×10^{-40}	6.1×10^{-46}	1.9×10^{-38}	1.8×10^{-44}
Subj5	1.7×10^{-05}	9.3×10^{-18}	2.9×10^{-24}	3.6×10^{-35}	2.5×10^{-38}	2.7×10^{-39}	3.7×10^{-41}	6.5×10^{-44}	4.6×10^{-43}	1.1×10^{-41}	6.4×10^{-41}
Subj6	1.9×10^{-04}	3.6×10^{-19}	1.3×10^{-17}	3.9×10^{-28}	6.1×10^{-28}	1.3×10^{-32}	9.7×10^{-32}	1.5×10^{-41}	3.8×10^{-35}	1.3×10^{-35}	3.9×10^{-41}
Subj7	5.1×10^{-07}	5.2×10^{-13}	8.1×10^{-21}	1.5×10^{-18}	1.8×10^{-23}	1.4×10^{-26}	7.8×10^{-30}	2.1×10^{-29}	6.8×10^{-22}	1.0×10^{-26}	3.4×10^{-30}
Subj8	2.3×10^{-05}	2.5×10^{-23}	5.7×10^{-24}	1.9×10^{-24}	1.9×10^{-31}	3.5×10^{-34}	3.4×10^{-34}	1.5×10^{-33}	4.2×10^{-33}	1.5×10^{-36}	1.4×10^{-40}
Subj9	1.1×10^{-04}	2.6×10^{-19}	3.8×10^{-25}	2.3×10^{-29}	3.7×10^{-29}	6.7×10^{-32}	2.2×10^{-33}	1.9×10^{-34}	8.9×10^{-35}	1.8×10^{-39}	1.3×10^{-36}
Subj10	2.0×10^{-05}	7.3×10^{-20}	9.1×10^{-27}	1.9×10^{-32}	1.4×10^{-33}	4.4×10^{-34}	7.3×10^{-33}	5.1×10^{-41}	2.3×10^{-42}	1.4×10^{-42}	1.8×10^{-47}

Table B.2: p-values from the 11 one-tailed t-tests for null hypothesis: $\hat{\sigma}_{\text{S+SFF}}$ is the same as $\hat{\sigma}_{\text{SFF}}$.

# of prototypes (p)										
p=3	p=5	p=10	p=15	p=20	p=25	p=30	p=35	p=40	p=45	p=50
1.4×10^{-08}	1.2×10^{-05}	9.7×10^{-07}	1.8×10^{-07}	$5.\times10^{-09}$	4.9×10^{-07}	8.4×10^{-10}	1.9×10^{-06}	3.3×10^{-07}	7.9×10^{-07}	7.1×10^{-07}

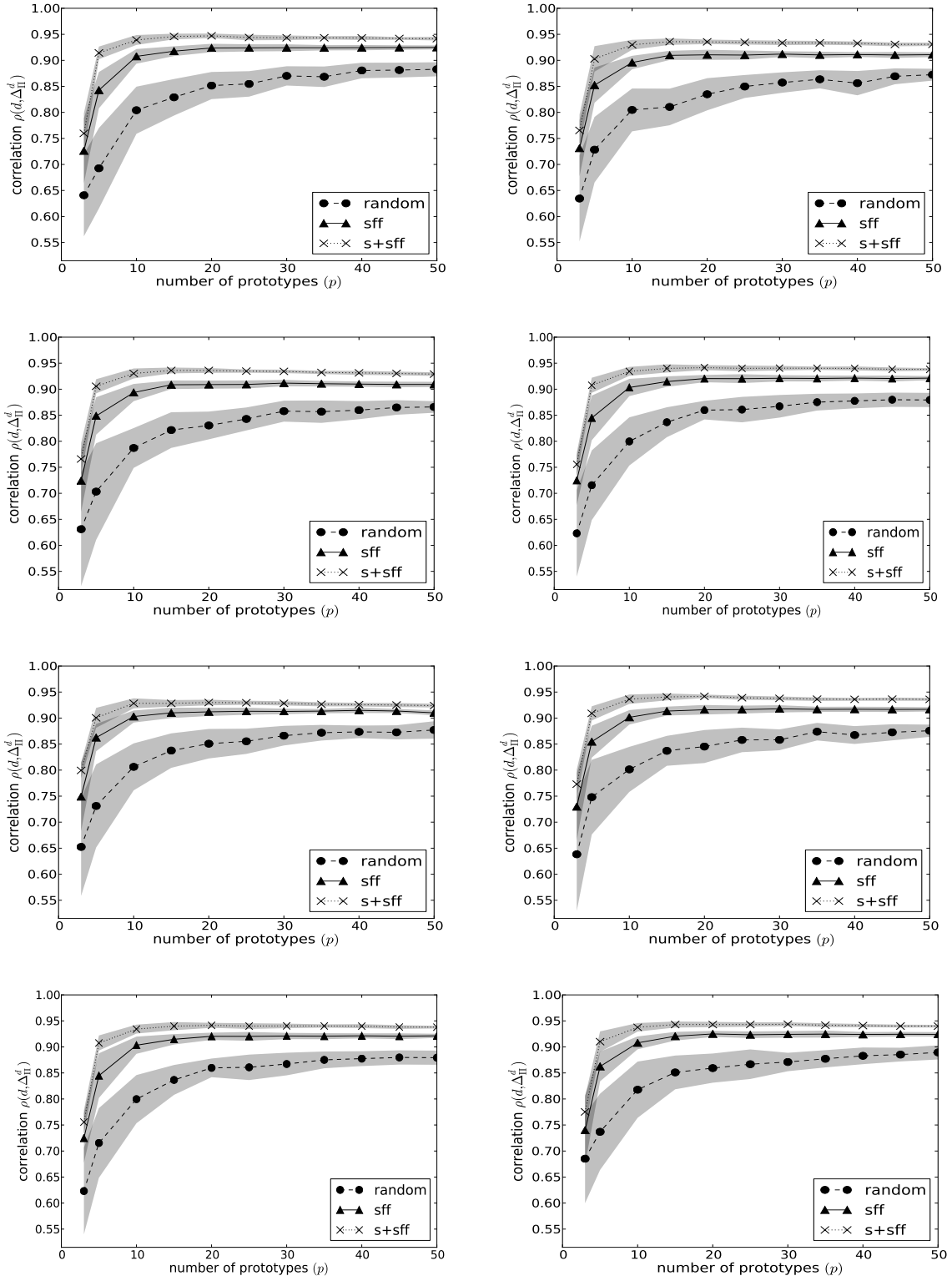

Figure B.1: Average correlation between d and Δ^d_Π across the different prototype selection policies and different numbers of prototypes. Each figure corresponds to a different subject.

Bibliography

[1] Saskia H. Aarnink, Sjoerd B. Vos, Alexander Leemans, Terry L. Jernigan, Kathrine S. Madsen, and William F. C. Baaré. Automated longitudinal intra-subject analysis (ALISA) for diffusion MRI tractography. *NeuroImage*, 86:404–416, 2014.

[2] Mustafa Akgül. The linear assignment problem. In *Combinatorial optimization*, pages 85–122. Springer, 1992.

[3] Daniel C. Alexander and James C. Gee. Elastic matching of diffusion tensor images. *Computer Vision and Image Understanding*, 77(2):233–250, 2000.

[4] H. A. Almohamad and Salih O. Duffuaa. A linear programming approach for the weighted graph matching problem. *IEEE Transactions on pattern analysis and machine intelligence*, 15(5):522–525, 1993.

[5] Jesper L. R. Andersson, Stefan Skare, and John Ashburner. How to correct susceptibility distortions in spin-echo echo-planar images: application to diffusion tensor imaging. *Neuroimage*, 20(2):870–888, 2003.

[6] Haz-Edine Assemlal, David Tschumperlé, Luc Brun, and Kaleem Siddiqi. Recent advances in diffusion MRI modeling: Angular and radial reconstruction. *Medical image analysis*, 15(4):369–396, 2011.

[7] Brian B. Avants, Charles L. Epstein, Murray Grossman, and James C. Gee. Symmetric diffeomorphic image registration with cross-correlation: evaluating automated labeling of elderly and neurodegenerative brain. *Medical image analysis*, 12(1):26–41, 2008.

[8] P. J. Basser, J. Mattiello, and D. LeBihan. MR diffusion tensor spectroscopy and imaging. *Biophysical journal*, 66(1):259–267, January 1994.

[9] Peter J. Basser, Sinisa Pajevic, Carlo Pierpaoli, Jeffrey Duda, and Akram Aldroubi. In vivo fiber tractography using DT-MRI data. *Magnetic resonance in medicine*, 44(4):625–632, 2000.

[10] T. E. J. Behrens, H. Johansen Berg, Saad Jbabdi, M. F. S. Rushworth, and M. W. Woolrich. Probabilistic diffusion tractography with multiple fibre orientations: What can we gain? *Neuroimage*, 34(1):144–155, 2007.

[11] Jon L. Bentley. Multidimensional binary search trees used for associative searching. *Communications of the ACM*, 18(9):509–517, 1975.

[12] J. Bijsterbosch and A. Volgenant. Solving the Rectangular assignment problem and applications. *Annals of Operations Research*, June 2010.

[13] Francois Bourgeois and Jean-Claude Lassalle. An extension of the Munkres algorithm for the assignment problem to rectangular matrices. *Communications of the ACM*, 14(12):802–804, 1971.

[14] M. Bozzali, A. Falini, M. Franceschi, M. Cercignani, M. Zuffi, G. Scotti, G. Comi, and M. Filippi. White matter damage in Alzheimer's disease assessed in vivo using diffusion tensor magnetic resonance imaging. *Journal of Neurology, Neurosurgery & Psychiatry*, 72(6):742–746, June 2002.

[15] Christopher D. Brown and Herbert T. Davis. Receiver operating characteristics curves and related decision measures: A tutorial. *Chemometrics and Intelligent Laboratory Systems*, 80(1):24–38, 2006.

[16] Anders Brun, Hans Knutsson, Hae-Jeong Park, Martha E. Shenton, and Carl-Fredrik Westin. Clustering fiber traces using normalized cuts. In *Medical Image Computing and Computer-Assisted Intervention–MICCAI 2004*, pages 368–375. Springer, 2004.

[17] Ed Bullmore and Olaf Sporns. Complex brain networks: graph theoretical analysis of structural and functional systems. *Nature reviews. Neuroscience*, 10(3):186–198, March 2009.

[18] Horst Bunke and Gudrun Allermann. Inexact graph matching for structural pattern recognition. *Pattern Recognition Letters*, 1(4):245–253, 1983.

[19] Rainer E. Burkard and Eranda Cela. *Linear assignment problems and extensions*. Springer, 1999.

[20] Rainer E. Burkard, Mauro Dell'Amico, and Silvano Martello. *Assignment Problems, Revised Reprint*. Siam, 2009.

[21] Paul H. Calamai and Jorge J. Moré. Projected gradient methods for linearly constrained problems. *Mathematical programming*, 39(1):93–116, 1987.

[22] Paul T. Callaghan. *Principles of nuclear magnetic resonance microscopy*. Oxford University Press on Demand, 1993.

[23] Jennifer S. W. Campbell, Peter Savadjiev, Kaleem Siddiqi, and G. Bruce Pike. Validation and regularization in diffusion mri tractography. In *Biomedical Imaging: Nano to Macro, 2006. 3rd IEEE International Symposium on*, pages 351–354. IEEE, 2006.

[24] Marco Catani, Matthew P. G. Allin, Masud Husain, Luca Pugliese, Marsel M. Mesulam, Robin M. Murray, and Derek K. Jones. Symmetries in human brain language pathways correlate with verbal recall. *Proceedings of the National Academy of Sciences*, 104(43):17163–17168, 2007.

[25] Yi-Ping Chao, Jyh-Horng Chen, Kuan-Hung Cho, Chun-Hung Yeh, Kun-Hsien Chou, and Ching-Po Lin. A multiple streamline approach to high angular resolution diffusion tractography. *Medical engineering & physics*, 30(8):989–996, 2008.

[26] Minsu Cho, Jungmin Lee, and Kyoung M. Lee. Reweighted random walks for graph matching. In *European conference on Computer vision*, pages 492–505. Springer, 2010.

[27] Gary E. Christensen and Hans J. Johnson. Consistent image registration. *IEEE transactions on medical imaging*, 20(7):568–582, 2001.

[28] Gary E. Christensen, Richard D. Rabbitt, and Michael I. Miller. Deformable templates using large deformation kinematics. *IEEE transactions on image processing*, 5(10):1435–1447, 1996.

[29] Daan Christiaens, Thijs Dhollander, Frederik Maes, Stefan Sunaert, and Paul Suetens. The effect of reorientation of the fibre orientation distribution on fibre tracking. In *MICCAI 2012 Workshop on Computational Diffusion MRI*, 2012.

[30] Daan Christiaens, Thijs Dhollander, Frederik Maes, Stefan Sunaert, and Paul Suetens. Groupwise Deformable Registration of Fiber Track Sets Using Track Orientation Distributions. In Thomas Schultz, Gemma Nedjati-Gilani, Archana Venkataraman, Lauren O'Donnell, and Eleftheria Panagiotaki, editors, *Computational Diffusion MRI and Brain Connectivity*, Mathematics and Visualization, pages 151–161. Springer International Publishing, 2014.

[31] Jonathan D. Clayden. Imaging connectivity: MRI and the structural networks of the brain. *Functional neurology*, 28(3):197–203, 2013.

[32] Jonathan D. Clayden, Amos J. Storkey, and Mark E. Bastin. A probabilistic model-based approach to consistent white matter tract segmentation. *Medical Imaging, IEEE Transactions on*, 26(11):1555–1561, 2007.

[33] D. Conte, P. Foggia, C. Sansone, and M. Vento. Thirty years of graph matching in pattern recognition. *Int. J. Patt. Recogn. Artif. Intell.*, 18(03):265–298, May 2004.

[34] Thomas E. Conturo, Nicolas F. Lori, Thomas S. Cull, Erbil Akbudak, Abraham Z. Snyder, Joshua S. Shimony, Robert C. McKinstry, Harold Burton, and Marcus E. Raichle. Tracking neuronal fiber pathways in the living human brain. *Proceedings of the National Academy of Sciences*, 96(18):10422–10427, 1999.

[35] I. Corouge, S. Gouttard, and G. Gerig. Towards a shape model of white matter fiber bundles using diffusion tensor MRI. In *Biomedical Imaging: Nano to Macro, 2004. IEEE International Symposium on*, pages 344–347 Vol. 1. IEEE, April 2004.

[36] Marc-Alexandre Côté, Gabriel Girard, Arnaud Boré, Eleftherios Garyfallidis, Jean-Christophe Houde, and Maxime Descoteaux. Tractometer: Towards validation of tractography pipelines. *Medical Image Analysis*, 17(7):844–857, October 2013.

[37] Timothee Cour, Praveen Srinivasan, and Jianbo Shi. Balanced graph matching. *Advances in Neural Information Processing Systems*, 19:313, 2007.

[38] Alessandro Daducci, Alessandro Dal Palù, Alia Lemkaddem, and Jean-Philippe Thiran. COMMIT: convex optimization modeling for microstructure informed tractography. *IEEE transactions on medical imaging*, 34(1):246–257, 2015.

[39] Mauro Dell'Amico and Paolo Toth. Algorithms and codes for dense assignment problems: the state of the art. *Discrete Applied Mathematics*, 100(1):17–48, 2000.

[40] M. Descoteaux, R. Deriche, T. R. Knosche, and A. Anwander. Deterministic and Probabilistic Tractography Based on Complex Fibre Orientation Distributions. *IEEE Transactions on Medical Imaging*, 28(2):269–286, February 2009.

[41] Maxime Descoteaux. *High angular resolution diffusion MRI: from local estimation to segmentation and tractography*. PhD thesis, INRIA Sophia Antipolis, France, 2010.

[42] Maxime Descoteaux. High angular resolution diffusion imaging (Hardi). *Wiley Encyclopedia of Electrical and Electronics Engineering*, 2015.

[43] Lee R. Dice. Measures of the amount of ecologic association between species. *Ecology*, 26(3):297–302, 1945.

[44] Zhaohua Ding, John C. Gore, and Adam W. Anderson. Classification and quantification of neuronal fiber pathways using diffusion tensor MRI. *Magnetic Resonance in Medicine*, 49(4):716–721, 2003.

[45] R. Douglas Fields. White Matter Matters. *Sci Am*, 298(3):54–61, March 2008.

[46] Robert P. W. Duin and Elżbieta PĂŹkalska. The dissimilarity space: Bridging structural and statistical pattern recognition. *Pattern Recognition Letters*, 33(7):826–832, May 2012.

[47] Stanley Durrleman, Pierre Fillard, Xavier Pennec, Alain Trouvé, and Nicholas Ayache. Registration, atlas estimation and variability analysis of white matter fiber bundles modeled as currents. *NeuroImage*, 55(3):1073–1090, April 2011.

[48] Adelino R. Ferreira da Silva. Computational representation of white matter fiber orientations. *Journal of Biomedical Imaging*, 2013:15, 2013.

[49] Bruce Fischl. FreeSurfer. *NeuroImage*, 62(2):774–781, August 2012.

[50] Martin A. Fischler and Robert A. Elschlager. The representation and matching of pictorial structures. *IEEE Transactions on computers*, 22(1):67–92, 1973.

[51] Pasquale Foggia, Gennaro Percannella, and Mario Vento. Graph matching and learning in pattern recognition in the last 10 years. *International Journal of Pattern Recognition and Artificial Intelligence*, 28(01):1450001, 2014.

[52] Eleftherios Garyfallidis. *Towards an accurate brain tractography*. PhD thesis, University of Cambridge, 2013.

[53] Eleftherios Garyfallidis, Matthew Brett, Bagrat Amirbekian, Ariel Rokem, Stefan van der Walt, Maxime Descoteaux, Ian Nimmo-Smith, and Dipy Contributors. Dipy, a library for the analysis of diffusion MRI data. *Frontiers in Neuroinformatics*, 8(8):1+, February 2014.

[54] Eleftherios Garyfallidis, Matthew Brett, Marta M. Correia, Guy B. Williams, and Ian Nimmo-Smith. QuickBundles, a Method for Tractography Simplification. *Frontiers in neuroscience*, 6, 2012.

[55] Eleftherios Garyfallidis, Omar Ocegueda, Demian Wassermann, and Maxime Descoteaux. Robust and efficient linear registration of white-matter fascicles in the space of streamlines. *NeuroImage*, 117:124–140, August 2015.

[56] Matthew F. Glasser, Stamatios N. Sotiropoulos, J. Anthony Wilson, Timothy S. Coalson, Bruce Fischl, Jesper L. Andersson, Junqian Xu, Saad Jbabdi, Matthew Webster, Jonathan R. Polimeni, David C. Van Essen, and Mark Jenkinson. The minimal preprocessing pipelines for the Human Connectome Project. *NeuroImage*, 80:105–124, October 2013.

[57] Alvina Goh and René Vidal. Algebraic Methods for Direct and Feature Based Registration of Diffusion Tensor Images. In Aleš Leonardis, Horst Bischof, and Axel Pinz, editors, *Computer Vision âĂŞ ECCV 2006*, volume 3953 of *Lecture Notes in Computer Science*, pages 514–525. Springer Berlin Heidelberg, 2006.

[58] Steven Gold and Anand Rangarajan. A Graduated Assignment Algorithm for Graph Matching. *IEEE Transactions on Pattern Analysis & Machine Intelligence*, 18(4):377–388, April 1996.

[59] Dan Golding, Marc Tittgemeyer, Alfred Anwander, and Tania Douglas. A comparison of methods for the registration of tractographic fibre images. In P. Robinson and A. Nel, editors, *Proceedings of the Twenty-Second Annual Symposium of the Pattern Recognition Association of South Africa*, pages 55–59, 2011.

[60] Henry Gray. Anatomy of the Human Body. Philadelphia: Lea & Febiger; Bartleby. com, 2000, 1918.

[61] P. Guevara, C. Poupon, D. Rivière, Y. Cointepas, M. Descoteaux, B. Thirion, and J-F F. Mangin. Robust clustering of massive tractography datasets. *NeuroImage*, 54(3):1975–1993, February 2011.

[62] Pamela Guevara, Delphine Duclap, Cyril Poupon, Linda Marrakchi-Kacem, Pierre Fillard, Denis Le Bihan, Marion Leboyer, Josselin Houenou, and J. F. Mangin. Automatic fiber bundle segmentation in massive tractography datasets using a multi-subject bundle atlas. *Neuroimage*, 61(4):1083–1099, 2012.

[63] Pamela B. Guevara Alvez. *Inference of a human brain fiber bundle atlas from high angular resolution diffusion imaging*. PhD thesis, Paris 11, 2011.

[64] Zhe Guo, Yi Wang, Tao Lei, Yangyu Fan, and Xiuwei Zhang. DTI Image Registration under Probabilistic Fiber Bundles Tractography Learning. *BioMed Research International*, 2016, 2016.

[65] Madhura Ingalhalikar, Alex Smith, Drew Parker, Theodore D. Satterthwaite, Mark A. Elliott, Kosha Ruparel, Hakon Hakonarson, Raquel E. Gur, Ruben C. Gur, and Ragini Verma. Sex differences in the structural connectome of the human brain. *Proceedings of the National Academy of Sciences*, 111(2):823–828, 2014.

[66] Madhura Ingalhalikar, Jinzhong Yang, Christos Davatzikos, and Ragini Verma. DTI-DROID: diffusion tensor imaging-deformable registration using orientation and intensity descriptors. *International Journal of Imaging Systems and Technology*, 20(2):99–107, 2010.

[67] Saad Jbabdi, M. W. Woolrich, J. L. R. Andersson, and T. E. J. Behrens. A Bayesian framework for global tractography. *Neuroimage*, 37(1):116–129, 2007.

[68] Mark Jenkinson, Peter Bannister, Michael Brady, and Stephen Smith. Improved Optimization for the Robust and Accurate Linear Registration and Motion Correction of Brain Images. *NeuroImage*, 17(2):825–841, October 2002.

[69] Mark Jenkinson, Christian F. Beckmann, Timothy E. J. Behrens, Mark W. Woolrich, and Stephen M. Smith. Fsl. *NeuroImage*, 62(2):782–790, 2012.

[70] Ben Jeurissen, Jacques-Donald Tournier, Thijs Dhollander, Alan Connelly, and Jan Sijbers. Multi-tissue constrained spherical deconvolution for improved analysis of multi-shell diffusion MRI data. *NeuroImage*, 103:411–426, 2014.

[71] Bing Jian, Baba C. Vemuri, Evren Özarslan, Paul R. Carney, and Thomas H. Mareci. A novel tensor distribution model for the diffusion-weighted MR signal. *NeuroImage*, 37(1):164–176, 2007.

[72] Yan Jin, Yonggang Shi, Liang Zhan, Junning Li, Greig I. de Zubicaray, Katie L. McMahon, Nicholas G. Martin, Margaret J. Wright, and Paul M. Thompson. Automatic population HARDI white matter tract clustering by label fusion of multiple tract atlases. In *International Workshop on Multimodal Brain Image Analysis*, pages 147–156. Springer, 2012.

[73] L. Jonasson, P. Hagmann, J. Thiran, and V. Wedeen. Fiber tracts of high angular resolution diffusion MRI are easily segmented with spectral clustering. In *Proceedings of 13th Annual Meeting ISMRM, Miami*, number EPFL-CONF-87232, page 1310. SPIE, 2005.

[74] D. K. Jones. Tractography gone wild: Probabilistic tracking using the wild bootstrap. In *Proc ISMRM*, page 435, 2006.

[75] R. Jonker and A. Volgenant. A shortest augmenting path algorithm for dense and sparse linear assignment problems. *Computing*, 38(4):325–340, December 1987.

[76] H. W. Kuhn. The Hungarian method for the assignment problem. *Naval Research Logistics*, 2(1-2):83–97, 1955.

[77] Nicole Labra, Pamela Guevara, Delphine Duclap, Josselin Houenou, Cyril Poupon, Jean-François Mangin, and Miguel Figueroa. Fast Automatic Segmentation of White Matter Streamlines Based on a Multi-Subject Bundle Atlas. *Neuroinformatics*, pages 1–16, 2016.

[78] E. W. Lang, A. M. Tomé, I. R. Keck, J. M. Górriz Sáez, and C. G. Puntonet. Brain Connectivity Analysis: A Short Survey. *Intell. Neuroscience*, 2012, January 2012.

[79] Alexander Leemans, Jan Sijbers, Steve De Backer, Everhard Vandervliet, and Paul M. Parizel. Affine coregistration of diffusion tensor magnetic resonance images using mutual information. In *International Conference on Advanced Concepts for Intelligent Vision Systems*, pages 523–530. Springer, 2005.

[80] M. Leordeanu and M. Hebert. A spectral technique for correspondence problems using pairwise constraints. In *International Conference on Computer Vision*. IEEE, October 2005.

[81] Marius Leordeanu, Martial Hebert, and Rahul Sukthankar. Beyond local appearance: Category recognition from pairwise interactions of simple features. In *2007 IEEE Conference on Computer Vision and Pattern Recognition*, pages 1–8. IEEE, 2007.

[82] Marius Leordeanu, Martial Hebert, and Rahul Sukthankar. An integer projected fixed point method for graph matching and map inference. In *Advances in neural information processing systems*, pages 1114–1122, 2009.

[83] Yao Lu, Kaizhu Huang, and Cheng-Lin Liu. A Fast Projected Fixed-Point Algorithm for Large Graph Matching, August 2012.

[84] Yao Lu, Kaizhu Huang, and Cheng-Lin Liu. Doubly Stochastic Projected Fixed-Point Algorithm for Large Graph Matching. *Pattern Recognition*, July 2016.

[85] João Maciel and João P. Costeira. A global solution to sparse correspondence problems. *IEEE Transactions on Pattern Analysis and Machine Intelligence*, 25(2):187–199, 2003.

[86] Mahnaz Maddah, Grimson, Simon K. Warfield, and William M. Wells. A unified framework for clustering and quantitative analysis of white matter fiber tracts. *Medical image analysis*, 12(2):191–202, 2008.

[87] Mahnaz Maddah, Andrea U. J. Mewes, Steven Haker, Grimson, and Simon K. Warfield. Automated Atlas-Based Clustering of White Matter Fiber Tracts from DTMRI. In James S. Duncan and Guido Gerig, editors, *Medical Image Computing and Computer-Assisted Intervention âĂŞ MICCAI 2005*, volume 3749 of *Lecture Notes in Computer Science*, chapter 24, pages 188–195. Springer Berlin / Heidelberg, Berlin, Heidelberg, 2005.

[88] Mahnaz Maddah, William M. Wells, Simon K. Warfield, Carl-Fredrik Westin, and Grimson. Probabilistic clustering and quantitative analysis of white matter fiber tracts. In *Biennial International Conference on Information Processing in Medical Imaging*, pages 372–383. Springer, 2007.

[89] Mahnaz Maddah, Lilla Zollei, Grimson, Carl F. Westin, and William M. Wells. A mathematical framework for incorporating anatomical knowledge in DT-MRI analysis. In *Biomedical Imaging: From Nano to Macro, 2008. ISBI 2008. 5th IEEE International Symposium on*, pages 105–108. IEEE, 2008.

[90] Arnaldo Mayer and Hayit Greenspan. Bundles of interest based registration of white matter tractographies. In *2008 5th IEEE International Symposium on Biomedical Imaging: From Nano to Macro*, pages 919–922. IEEE, 2008.

[91] Arnaldo Mayer, Gali Zimmerman-Moreno, Ran Shadmi, Amit Batikoff, and Hayit Greenspan. A supervised framework for the registration and segmentation of white matter fiber tracts. *IEEE transactions on medical imaging*, 30(1):131–145, January 2011.

[92] Tim McGraw, Baba C. Vemuri, Bob Yezierski, and Thomas Mareci. Von Mises-Fisher mixture model of the diffusion ODF. In *Biomedical Imaging: Nano to Macro, 2006. 3rd IEEE International Symposium on*, pages 65–68. IEEE, 2006.

[93] Sylvain L. Merlet and Rachid Deriche. Continuous diffusion signal, EAP and ODF estimation via compressive sensing in diffusion MRI. *Medical image analysis*, 17(5):556–572, 2013.

[94] S. Mori, R. Xue, B. Crain, M. Solaiyappan, V. P. Chacko, and PCMv Zijl. 3D reconstruction of axonal fibers from diffusion tensor imaging using fiber assignment by continuous tracking (FACT). In *8th Annual Meeting of the ISMRM, Philadelphia, PA*, volume 320, 1999.

[95] Susumu Mori, Barbara J. Crain, V. P. Chacko, and Peter Van Zijl. Three-dimensional tracking of axonal projections in the brain by magnetic resonance imaging. *Annals of neurology*, 45(2):265–269, 1999.

[96] Susumu Mori, Setsu Wakana, Peter C. M. Van Zijl, and L. M. Nagae-Poetscher. *MRI atlas of human white matter*, volume 16. Am Soc Neuroradiology, 2005.

[97] James Munkres. Algorithms for the assignment and transportation problems. *Journal of the Society for Industrial & Applied Mathematics*, 5(1):32–38, 1957.

[98] Mohammad-Reza Nazem-Zadeh, Kourosh Jafari-Khouzani, Esmaeil Davoodi-Bojd, Quan Jiang, and Hamid Soltanian-Zadeh. Clustering method for estimating principal diffusion directions. *NeuroImage*, 57(3):825–838, 2011.

[99] Lauren O'Donnell, Steven Haker, and Carl-Fredrik Westin. New approaches to estimation of white matter connectivity in diffusion tensor MRI: Elliptic PDEs and geodesics in a tensor-warped space. *Medical Image Computing and Computer-Assisted InterventionâĂŤMICCAI 2002*, pages 459–466, 2002.

[100] Lauren O'Donnell and Carl-Fredrik Westin. White matter tract clustering and correspondence in populations. In *Medical Image Computing and Computer-Assisted Intervention–MICCAI 2005*, pages 140–147. Springer, 2005.

[101] Lauren J. O'Donnell, Alexandra J. Golby, and Carl-Fredrik Westin. Fiber clustering versus the parcellation-based connectome. *NeuroImage*, 80:283–289, 2013.

[102] Lauren J. O'Donnell, William M. Wells, Alexandra J. Golby, and Carl-Fredrik F. Westin. Unbiased group-wise registration of white matter tractography. *Medical image computing and computer-assisted intervention : MICCAI - International Conference on Medical Image Computing and Computer-Assisted Intervention*, 15(Pt 3):123–130, 2012.

[103] Lauren J. O'Donnell and Carl-Fredrik F. Westin. Automatic tractography segmentation using a high-dimensional white matter atlas. *IEEE transactions on medical imaging*, 26(11):1562–1575, November 2007.

[104] E. Olivetti, T. B. Nguyen, E. Garyfallidis, N. Agarwal, and P. Avesani. Fast Clustering for Interactive Tractography Segmentation. In *Pattern Recognition in Neuroimaging (PRNI), 2013 International Workshop on*, pages 42–45. IEEE, June 2013.

[105] Emanuele Olivetti and Paolo Avesani. Supervised segmentation of fiber tracts. In *Proceedings of the First international conference on Similarity-based pattern recognition*, SIMBAD'11, pages 261–274, Berlin, Heidelberg, 2011. Springer-Verlag.

[106] Emanuele Olivetti, Thien B. Nguyen, and Eleftherios Garyfallidis. The Approximation of the Dissimilarity Projection. *IEEE Intl Workshop on Pattern Recognition in NeuroImaging*, 0:85–88, 2012.

[107] Mauricio Orozco-Alzate and César G. Castellanos-Domínguez. Clustering on dissimilarity representations for detecting mislabelled seismic signals at nevado del ruiz volcano. *Earth Sciences Research Journal*, 11(2):135–140, December 2007.

[108] Hae-Jeong Park, Marek Kubicki, Martha E. Shenton, Alexandre Guimond, Robert W. McCarley, Stephan E. Maier, Ron Kikinis, Ferenc A. Jolesz, and Carl-Fredrik Westin. Spatial normalization of diffusion tensor MRI using multiple channels. *Neuroimage*, 20(4):1995–2009, 2003.

[109] Hae-Jeong Park, Carl-Fredrik Westin, Marek Kubicki, Stephan E. Maier, Margaret Niznikiewicz, Aaron Baer, Melissa Frumin, Ron Kikinis, Ferenc A. Jolesz, Robert W. McCarley, and Others. White matter hemisphere asymmetries in healthy subjects and in schizophrenia: a diffusion tensor MRI study. *Neuroimage*, 23(1):213–223, 2004.

[110] Geoffrey J. M. Parker, Claudia A. M. Wheeler-Kingshott, and Gareth J. Barker. Estimating distributed anatomical connectivity using fast marching methods and diffusion tensor imaging. *IEEE transactions on medical imaging*, 21(5):505–512, 2002.

[111] Elzbieta Pekalska and Robert P. W. Duin. *The Dissimilarity Representation for Pattern Recognition: Foundations And Applications (Machine Perception and Artificial Intelligence)*. World Scientific Publishing Company, December 2005.

[112] Franco Pestilli, Jason D. Yeatman, Ariel Rokem, Kendrick N. Kay, and Brian A. Wandell. Evaluation and statistical inference for human connectomes. *Nat Meth*, 11(10):1058–1063, October 2014.

[113] Diana Porro-Muñoz, Emanuele Olivetti, Nusrat Sharmin, ThienBao Nguyen, Eleftherios Garyfallidis, and Paolo Avesani. Tractome: a visual data mining tool for brain connectivity analysis. *Data Mining and Knowledge Discovery*, 29(5):1258–1279, 2015.

[114] Elżbieta PĄŹkalska, Robert P. W. Duin, and Pavel Paclík. Prototype selection for dissimilarity-based classifiers. *Pattern Recognition*, 39(2):189–208, February 2006.

[115] Xiaolin Qin, Juan Tang, Yong Feng, Bernhard Bachmann, and Peter Fritzson. Efficient algorithm for computing large scale systems of differential algebraic equations. *arXiv preprint arXiv:1506.03963*, 2015.

[116] David Raffelt, Tournier, Jurgen Fripp, Stuart Crozier, Alan Connelly, and Olivier Salvado. Symmetric Diffeomorphic Registration of Fibre Orientation Distributions. *NeuroImage*, February 2011.

[117] David Raffelt, J-Donald Tournier, Stephen Rose, Gerard R. Ridgway, Robert Henderson, Stuart Crozier, Olivier Salvado, and Alan Connelly. Apparent fibre density: a novel measure for the analysis of diffusion-weighted magnetic resonance images. *Neuroimage*, 59(4):3976–3994, 2012.

[118] Andre Reichenbach, Mathias Goldau, Christian Heine, and Mario Hlawitschka. V–Bundles: Clustering Fiber Trajectories from Diffusion MRI in Linear Time. In *Medical Image Computing and Computer-Assisted Intervention–MICCAI 2015*, pages 191–198. Springer, 2015.

[119] Torsten Rohlfing, Robert Brandt, Randolf Menzel, and Calvin R. Maurer. Evaluation of atlas selection strategies for atlas-based image segmentation with application to confocal microscopy images of bee brains. *NeuroImage*, 21(4):1428–1442, 2004.

[120] Christian Ros, Daniel Güllmar, Martin Stenzel, Hans-Joachim Mentzel, and Jürgen R. Reichenbach. Atlas-Guided Cluster Analysis of Large Tractography Datasets. *PLoS ONE*, 8(12):e83847+, December 2013.

[121] Juan Ruiz-Alzola, C. F. Westin, Simon K. Warfield, Carlos Alberola, S. Maier, and Ron Kikinis. Nonrigid registration of 3D tensor medical data. *Medical image analysis*, 6(2):143–161, 2002.

[122] D. H. Salat, D. S. Tuch, D. N. Greve, A. J. W. Van Der Kouwe, N. D. Hevelone, A. K. Zaleta, B. R. Rosen, B. Fischl, S. Corkin, H. Diana Rosas, and Others. Age-related alterations in white matter microstructure measured by diffusion tensor imaging. *Neurobiology of aging*, 26(8):1215–1227, 2005.

[123] Daniel Scharstein and Richard Szeliski. A taxonomy and evaluation of dense two-frame stereo correspondence algorithms. *International journal of computer vision*, 47(1-3):7–42, 2002.

[124] Christian Schellewald and Christoph Schnörr. Probabilistic subgraph matching based on convex relaxation. In *International Workshop on Energy Minimization Methods in Computer Vision and Pattern Recognition*, pages 171–186. Springer, 2005.

[125] Julia A. Schnabel, Daniel Rueckert, Marcel Quist, Jane M. Blackall, Andy D. Castellano-Smith, Thomas Hartkens, Graeme P. Penney, Walter A. Hall, Haiying Liu, Charles L. Truwit, and Others. A generic framework for non-rigid registration based on non-uniform multi-level free-form deformations. In *International Conference on Medical Image Computing and Computer-Assisted Intervention*, pages 573–581. Springer, 2001.

[126] Francesc Serratosa. Speeding up fast bipartite graph matching through a new cost matrix. *International Journal of Pattern Recognition and Artificial Intelligence*, 29(02):1550010, 2015.

[127] Nusrat Sharmin, Emanuele Olivetti, and Paolo Avesani. Alignment of Tractograms as Linear Assignment Problem. In Andrea Fuster, Aurobrata Ghosh, Enrico Kaden, Yogesh Rathi, and Marco Reisert, editors, *Computational Diffusion MRI*, Mathematics and Visualization, pages 109–120. Springer International Publishing, 2016.

[128] Joshua S. Shimony, Avi Z. Snyder, Nicholas Lori, and T. E. Conturo. Automated fuzzy clustering of neuronal pathways in diffusion tensor tracking. In *Proc. Intl. Soc. Mag. Reson. Med*, volume 10, page 1, 2002.

[129] Robert E. Smith, Jacques-Donald Tournier, Fernando Calamante, and Alan Connelly. Anatomically-constrained tractography: Improved diffusion MRI streamlines tractography through effective use of anatomical information. *NeuroImage*, 62(3):1924–1938, September 2012.

[130] Robert E. Smith, Jacques-Donald Tournier, Fernando Calamante, and Alan Connelly. SIFT: spherical-deconvolution informed filtering of tractograms. *Neuroimage*, 67:298–312, 2013.

[131] Stamatios N. Sotiropoulos. *Processing of diffusion MR images of the brain: from crossing fibres to distributed tractography*. PhD thesis, University of Nottingham, 2010.

[132] Stamatios N. Sotiropoulos, Saad Jbabdi, Junqian Xu, Jesper L. Andersson, Steen Moeller, Edward J. Auerbach, Matthew F. Glasser, Moises Hernandez, Guillermo Sapiro, Mark Jenkinson, David A. Feinberg, Essa Yacoub, Christophe Lenglet, David C. Van Essen, Kamil Ugurbil, Timothy E. Behrens, and WU-Minn HCP Consortium. Advances in diffusion MRI acquisition and processing in the Human Connectome Project. *NeuroImage*, 80:125–143, October 2013.

[133] Ben Southall, Bernard F. Buxton, John A. Marchant, and Tony Hague. On the performance characterisation of image segmentation algorithms: a case study. In *European Conference on Computer Vision*, pages 351–365. Springer, 2000.

[134] Olaf Sporns. The human connectome: origins and challenges. *Neuroimage*, 80:53–61, 2013.

[135] Olaf Sporns, Giulio Tononi, and Rolf Kötter. The Human Connectome: A Structural Description of the Human Brain. *PLoS Comput Biol*, 1(4):e42+, September 2005.

[136] Colin Studholme, Derek L. G. Hill, and David J. Hawkes. An overlap invariant entropy measure of 3D medical image alignment. *Pattern recognition*, 32(1):71–86, 1999.

[137] Anh P. Ta. *Inexact graph matching techniques: Application to object detection and human action recognition*. PhD thesis, Ph. D. dissertation, INSA de Lyon, 20, rue Albert Einstein, 69621 Villeurbanne Cedex, France, 2010.

[138] Arthur W. Toga. *Brain mapping: An encyclopedic reference*. Academic Press, 2015.

[139] Arthur W. Toga, Kristi A. Clark, Paul M. Thompson, David W. Shattuck, and John D. Van Horn. Mapping the human connectome. *Neurosurgery*, 71(1):1, 2012.

[140] J. Tournier, Fernando Calamante, Alan Connelly, and Others. MRtrix: diffusion tractography in crossing fiber regions. *International Journal of Imaging Systems and Technology*, 22(1):53–66, 2012.

[141] J. D. Tournier, F. Calamante, and A. Connelly. Improved probabilistic streamlines tractography by 2nd order integration over fibre orientation distributions. In *Proc. 18th Annual Meeting of the Intl. Soc. Mag. Reson. Med.(ISMRM)*, page 1670, 2010.

[142] J-Donald Tournier, Fernando Calamante, and Alan Connelly. Robust determination of the fibre orientation distribution in diffusion MRI: Non-negativity constrained super-resolved spherical deconvolution. *NeuroImage*, 35(4):1459–1472, May 2007.

[143] J-Donald Tournier, Fernando Calamante, David G. Gadian, and Alan Connelly. Diffusion-weighted magnetic resonance imaging fibre tracking using a front evolution algorithm. *NeuroImage*, 20(1):276–288, 2003.

[144] J-Donald D. Tournier, Fernando Calamante, David G. Gadian, and Alan Connelly. Direct estimation of the fiber orientation density function from diffusion-weighted MRI data using spherical deconvolution. *NeuroImage*, 23(3):1176–1185, November 2004.

[145] Wen-Hsiang Tsai and King-Sun Fu. Error-correcting isomorphisms of attributed relational graphs for pattern analysis. *IEEE Transactions on systems, man, and cybernetics*, 9(12):757–768, 1979.

[146] Birkan Tunç, William A. Parker, Madhura Ingalhalikar, and Ragini Verma. Automated tract extraction via atlas based adaptive clustering. *Neuroimage*, 102:596–607, 2014.

[147] D. Turnbull and C. Elkan. Fast recognition of musical genres using RBF networks. *Knowledge and Data Engineering, IEEE Transactions on*, 17(4):580–584, April 2005.

[148] Shinji Umeyama. An eigendecomposition approach to weighted graph matching problems. *IEEE transactions on pattern analysis and machine intelligence*, 10(5):695–703, 1988.

[149] D. C. Van Essen, K. Ugurbil, E. Auerbach, D. Barch, T. E. Behrens, R. Bucholz, A. Chang, L. Chen, M. Corbetta, S. W. Curtiss, S. Della Penna, D. Feinberg, M. F. Glasser, N. Harel, A. C. Heath, L. Larson-Prior, D. Marcus, G. Michalareas, S. Moeller, R. Oostenveld, S. E. Petersen, F. Prior, B. L. Schlaggar, S. M. Smith, A. Z. Snyder, J. Xu, E. Yacoub, and WU-Minn HCP Consortium. The Human Connectome Project: a data acquisition perspective. *NeuroImage*, 62(4):2222–2231, October 2012.

[150] David C. Van Essen, Stephen M. Smith, Deanna M. Barch, Timothy E. J. Behrens, Essa Yacoub, and Kamil Ugurbil. The WU-Minn Human Connectome Project: An overview. *NeuroImage*, 80:62–79, October 2013.

[151] Tom Vercauteren, Xavier Pennec, Aymeric Perchant, and Nicholas Ayache. Diffeomorphic demons: Efficient non-parametric image registration. *NeuroImage*, 45(1):S61–S72, 2009.

[152] Dorothée Vercruysse, Daan Christiaens, Frederik Maes, Stefan Sunaert, and Paul Suetens. Fiber Bundle Segmentation Using Spectral Embedding and Supervised Learning. In *Computational Diffusion MRI*, pages 103–114. Springer, 2014.

[153] Eelke Visser, Emil H. J. Nijhuis, Jan K. Buitelaar, and Marcel P. Zwiers. Partition-based mass clustering of tractography streamlines. *Neuroimage*, 54(1):303–312, 2011.

[154] Setsu Wakana, Arvind Caprihan, Martina M. Panzenboeck, James H. Fallon, Michele Perry, Randy L. Gollub, Kegang Hua, Jiangyang Zhang, Hangyi Jiang, Prachi Dubey, and Others. Reproducibility of quantitative tractography methods applied to cerebral white matter. *Neuroimage*, 36(3):630–644, 2007.

[155] Xiaogang Wang, W. Eric Grimson, and Carl-Fredrik F. Westin. Tractography segmentation using a hierarchical Dirichlet processes mixture model. *NeuroImage*, 54(1):290–302, January 2011.

[156] D. Wassermann, L. Bloy, E. Kanterakis, R. Verma, and R. Deriche. Unsupervised white matter fiber clustering and tract probability map generation: applications of a Gaussian process framework for white matter fibers. *NeuroImage*, 51(1):228–241, May 2010.

[157] Demian Wassermann, Nikos Makris, Yogesh Rathi, Martha Shenton, Ron Kikinis, Marek Kubicki, and Carl-Fredrik F. Westin. On describing human white matter anatomy: the white matter query language. *Medical image computing and computer-assisted intervention : MICCAI ... International Conference on Medical Image Computing and Computer-Assisted Intervention*, 16(Pt 1):647–654, 2013.

[158] Demian Wassermann, Nikos Makris, Yogesh Rathi, Martha Shenton, Ron Kikinis, Marek Kubicki, and Carl-Fredrik F. Westin. The white matter query language: a novel approach for describing human white matter anatomy. *Brain structure & function*, January 2016.

[159] Demian Wassermann, Yogesh Rathi, Sylvain Bouix, Marek Kubicki, Ron Kikinis, Martha Shenton, and Carl-Fredrik F. Westin. White matter bundle registration and population analysis based on Gaussian processes. *Information processing in medical imaging : proceedings of the ... conference*, 22:320–332, 2011.

[160] Sandra F. Witelson. Hand and sex differences in the isthmus and genu of the human corpus callosum. *Brain*, 112(3):799–835, 1989.

[161] Pew-Thian Yap, Guorong Wu, Hongtu Zhu, Weili Lin, and Dinggang Shen. F-TIMER: fast tensor image morphing for elastic registration. *IEEE transactions on medical imaging*, 29(5):1192–1203, 2010.

[162] Sang W. Yoo, Pamela Guevara, Yong Jeong, Kwangsun Yoo, Joseph S. Shin, Jean-Francois Mangin, and Joon-Kyung Seong. An Example-Based Multi-Atlas Approach to Automatic Labeling of White Matter Tracts. *PloS one*, 10(7), 2015.

[163] Mikhail Zaslavskiy, Francis Bach, and Jean-Philippe Vert. A Path Following Algorithm for the Graph Matching Problem. *Pattern Analysis and Machine Intelligence, IEEE Transactions on*, 31(12):2227–2242, October 2009.

[164] Ron Zass and Amnon Shashua. Doubly Stochastic Normalization for Spectral Clustering. In *Advances in Neural Information Processing Systems 19, Proceedings of the Twentieth Annual Conference on Neural Information Processing Systems, Vancouver, British Columbia, Canada, December 4-7, 2006*, pages 1569–1576, 2006.

[165] Hui Zhang, Paul A. Yushkevich, Daniel C. Alexander, and James C. Gee. Deformable registration of diffusion tensor MR images with explicit orientation optimization. *Medical image analysis*, 10(5):764–785, 2006.

[166] S. Zhang and D. H. Laidlaw. DTI fiber clustering and cross-subject cluster analysis. In *The International Society for Magnetic Resonance in Medicine*, 2005.

[167] Yajing Zhang, Jiangyang Zhang, Kenichi Oishi, Andreia V. Faria, Hangyi Jiang, Xin Li, Kazi Akhter, Pedro Rosa-Neto, G. Bruce Pike, Alan Evans, and Others. Atlas-guided tract reconstruction for automated and comprehensive examination of the white matter anatomy. *Neuroimage*, 52(4):1289–1301, 2010.

[168] Ulas Ziyan, MertR Sabuncu, Grimson, and Carl-Fredrik Westin. Consistency Clustering: A Robust Algorithm for Group-wise Registration, Segmentation and Automatic Atlas Construction inÂăDiffusion MRI. *International journal of computer vision*, 85(3):279–290, 2009.

[169] Ulas Ziyan, MertR Sabuncu, LaurenJ O'Donnell, and Carl-Fredrik Westin. Nonlinear Registration of Diffusion MR Images Based on Fiber Bundles. In Nicholas Ayache, Sébastien Ourselin, and Anthony Maeder, editors, *Medical Image Computing and Computer-Assisted Intervention âĂŞ MICCAI 2007*, volume 4791 of *Lecture Notes in Computer Science*, pages 351–358. Springer Berlin Heidelberg, 2007.

[170] Orly Zvitia, Arnaldo Mayer, Ran Shadmi, Shmuel Miron, and Hayit K. Greenspan. Co-registration of white matter tractographies by adaptive-mean-shift and Gaussian mixture modeling. *IEEE transactions on medical imaging*, 29(1):132–145, 2010.